Physics of Atomic Nuclei, Vol. 66, No. 12, 2003, pp. 2113–2116. Translated from Yadernaya Fizika, Vol. 66, No. 12, 2003, pp. 2163–2166.

NUCLEI
Theory

On the Duration of the Resonance Absorption and Emission of Nuclear Gamma Rays

A. V. Davydov*

Institute of Theoretical and Experimental Physics,
Bol'shaya Cheremushkinskaya ul. 25, Moscow, 117259 Russia

Received February 20, 2003; in final form, May 29, 2003

Abstract—The Krylov–Fock theorem is applicable to describing the decay of an excited quantum-mechanical system in the case where the time of excited-state formation is much shorter than the characteristic decay time. The results obtained by calculating, on the basis of this theorem, the average lifetime t_{av} of an excited state for nuclei that resonantly scatter γ rays are in serious contradiction with available data on t_{av}, including experimental data. This disproves the assumption that the resonance absorption and emission of γ rays proceeds within times much shorter than $\tau = \hbar/\Gamma$ (Γ is the intrinsic width of a nuclear level). A qualitative explanation of this effect is proposed. © *2003 MAIK "Nauka/Interperiodica".*

Referring to the monograph of Migdal [1], Stepanov and Tsipenyuk [2] indicated that the duration of photon emission from a nucleus [as well as the duration of resonance photon absorption by a nucleus (A.D.)] is about λ_γ/c, where λ_γ is the γ-ray wavelength; for photons of energy 100 keV, this is approximately equal to 3×10^{-20} s. However, there exist theoretical and experimental data that cast some doubt on the validity of the statement that the duration of nuclear gamma-ray resonance absorption (emission) is much shorter than the average lifetime of a nucleus in the state excited upon photon absorption. We now consider the process of "ideal" Mössbauer resonance gamma-ray scattering—that is, a process where gamma-ray-emission and gamma-ray-absorption lines have an intrinsic width Γ and where they are not shifted with respect to each other and are described by a Lorentzian function,

$$F(E) \sim \frac{\Gamma^2/4}{(E-E_0)^2 + \Gamma^2/4}, \qquad (1)$$

where E is the gamma-ray energy and E_0 is the position of the resonance center. In the resonance absorption of such gamma rays, excited nuclei are characterized by an excitation-energy distribution $W(E)$ that is proportional to the product of two functions in (1):

$$W(E) \sim \frac{(\Gamma^2/4)^2}{[(E-E_0)^2 + \Gamma^2/4]^2}. \qquad (2)$$

This function is no longer a Lorentzian function; therefore, the decay of excited nuclei does not obey an exponential law. The spectrum of gamma rays emitted by the excited nuclei of the scatterer has the same form. It can be proven that the FWHM of a γ line described by (2) is approximately 1.5 times less than Γ. Hence, we can expect that the average lifetime t_{av} of nuclei in the excited state that arises upon Mössbauer resonance absorption is about 1.5 times longer than $\tau = \hbar/\Gamma$. Below, it will be shown that the relation $t_{av} = 1.5\tau$ holds exactly under the conditions being considered.

The angular distribution of resonantly scattered γ rays that is perturbed by a magnetic field orthogonal to the scattering plane was analyzed theoretically in [3]. Considering the particular case where the nucleus excited upon photon absorption goes over from the ground state of spin–parity 0^+ to the 2^+ state, the authors of [3] showed that, for $\mu H \ll \Gamma$, where μ is the magnetic moment of the excited nucleus and H is the magnetic-field strength, the angle of rotation $\delta\theta$ of the rosette of the angular distribution of resonantly scattered photons is given by

$$\delta\theta = \Omega\tau\frac{\Delta + 2\Gamma}{\Delta + \Gamma}, \qquad (3)$$

where $\Omega = g\mu_N H/\hbar$ is Larmor frequency for the 2^+ nuclear state, g is the gyromagnetic ratio for this state, μ_N is the nuclear magneton, and Δ is the γ-line width of the exciting radiation. In the case under consideration, $\Delta = \Gamma$ and expression (3) reduces to

$$\delta\theta = 1.5\Omega\tau. \qquad (4)$$

Since the above angle of rotation must be equal to the product of the Larmor frequency Ω and the average

*e-mail: andrey.davydov@itep.ru

duration of nuclear-spin precession (that is, the average lifetime t_{av} of the nucleus in the excited state) it follows from (4) that $t_{av} = 1.5\tau$.

Later on, a similar problem was considered by Eicher [4], who generalized it to the case of an arbitrary multipolarity of the γ transition and showed that expression (4) is valid if the γ-emission line is not shifted with respect to the absorption line. In the study performed by a group from the Institute of Theoretical and Experimental Physics (ITEP, Moscow) and reported in [5], a general expression for the angular distribution of resonantly scattered γ rays that is perturbed by a magnetic field was derived for the case where transitions involve an arbitrary mixture of multipolarities and where no constraints are imposed on the energy of hyperfine interaction. For $\mu H \ll \Gamma$, the following result was obtained in [5] for the angle of rotation of the angular-distribution rosette (see also [6]):

$$\delta\theta = \Omega\hbar \frac{\left\{(\Gamma+\Delta)\left[\frac{(\Gamma+\Delta)(3\Gamma+\Delta)}{4}+s^2\right]-\frac{\Gamma(\Gamma+\Delta)^2}{4}-\Gamma s^2\right\}}{\left[\frac{\Gamma(\Gamma+\Delta)^2}{4}+\Gamma s^2\right](\Gamma+\Delta)}. \quad (5)$$

Here, s is the shift of the source γ line with respect to the absorption line of the scatterer.

Setting $s = 0$, we again arrive at (3) and, hence, at (4). Expression (3) was confirmed by the experiment [6] performed by a group from ITEP with γ rays from ^{191}Ir. In this experiment, use was made of a metallic-osmium γ source, where, after exposure to thermal neutrons in a reactor, ^{191}Os arose. It is well known from the literature that the width of the Mössbauer γ line emitted by this source is $\Delta = (1.351 \pm 0.050)\Gamma$. For this value of Δ, expression (3) yields

$$\delta\theta = (1.425 \pm 0.010)\Omega\tau.$$

The experiment reported in [6] resulted in $\delta\theta = (1.40 \pm 0.11)\Omega\tau$, which confirmed the above theoretical predictions. Thus, there is every reason to believe that the following statement has been proven: in the ideal Mössbauer resonance scattering of γ rays, the scattering nucleus "spends," on average, 1.5τ in an excited state.

Let us now address the following question: What result will quantum-mechanical calculations yield for t_{av} in the case where the time of the nuclear-excitation process (that is, the photon-absorption process) is much shorter than τ. The answer can be obtained by means of the Krylov–Fock theorem [7]. According to this theorem, the probability $L(t)$ that an excited system does not decay within the time t from its formation is controlled by the excitation-energy distribution $W(E)$ formed in the excitation process—that is, over a time much shorter than τ—and is given by

$$L(t) = \left|\int e^{-iEt/\hbar} W(E)dE\right|^2. \quad (6)$$

Adopting expression (2) for $W(E)$, we find that it is then necessary to calculate the squared modulus of the quantity

$$I = \left(\frac{\Gamma^2}{4}\right)^2 \int_{-\infty}^{\infty} \frac{e^{-iEt/\hbar}dE}{[(E-E_0)^2+\Gamma^2/4]^2}. \quad (7)$$

The integral in (7) is calculated by taking the residue at the second-order pole in the lower half-plane. Discarding factors independent of t, we obtain

$$L(t) \sim \left|\left(2+\frac{\Gamma t}{\hbar}\right)e^{-\Gamma t/2\hbar}\right|^2 = \left(2+\frac{\Gamma t}{\hbar}\right)^2 e^{-\Gamma t/\hbar}. \quad (8)$$

The number of decays per unit time at the instant t is determined by the time derivative of $L(t)$,

$$\frac{dL(t)}{dt} = -\frac{\Gamma^2 t}{\hbar^2}\left(2+\frac{\Gamma t}{\hbar}\right)^2 e^{-\Gamma t/\hbar}. \quad (9)$$

The average lifetime of nuclei in an excited state appears to be

$$t_{av} = \frac{\int_0^\infty t\frac{dL(t)}{dt}dt}{\int_0^\infty \frac{dL(t)}{dt}dt} = 2.5\frac{\hbar}{\Gamma} = 2.5\tau \quad (10)$$

instead of the value of 1.5τ, which follows from the width of the γ line emitted by the scatterer; from the theory of magnetic-field-perturbed angular distributions of resonantly scattered γ rays; and, finally, from experimental data on the angle of rotation of the rosette of the angular distribution of resonantly scattered γ rays from ^{191}Ir. For the first time, this was indicated in [8]. It should be noted that the experimental value in question differs by ten standard deviations from the value of t_{av} that results from the Krylov–Fock theorem. In all probability, this result is sufficient for disproving the statement that, in the

process of ideal Mössbauer resonance scattering, the nucleus involved absorbs (and, hence, emits) a photon within a time much shorter than τ. As a matter of fact, this result indicates that the excitation-energy distribution of width $\Gamma/1.5$ cannot be formed within a time less than $1.5\hbar/\Gamma$.

There arises the question of whether the assumption that the photon-absorption (photon-emission) process is long (that is, of duration commensurate with τ) can remedy the situation. We will present a few qualitative arguments in support of this assumption. Measurements of the magnetic-field-perturbed angular distribution of resonantly scattered γ rays show that the nucleus spends, on average, 1.5τ in an excited state, in agreement with the theory. This implies that nuclear transitions from the ground state to an excited state and inverse transitions proceed within a time much shorter than τ. Thus, we arrive at the conclusion that, although nuclear transitions are associated with photon-absorption and photon-emission processes, the respective time scales differ considerably. At the beginning of the γ-wave effect on a nucleus, the nucleus goes over to an excited state; that is, it acquires the spin, parity, and magnetic moment of the excited state. However, the energy of this state has a large uncertainty at the initial instant of γ-wave absorption, since the excitation-energy distribution of nuclei at the instant t must be determined by the frequency spectrum (Fourier integral) of that part of the wave train which has affected the nucleus to this instant. The longer the time within which the wave train affects the nucleus, the narrower the excitation-energy distribution and, accordingly, the smaller the uncertainty in the energy of the excited state. A broad excitation-energy distribution at the initial period of the absorption of the γ wave must be associated with a high probability of photon emission by the excited nucleus at this stage. This very pattern of radiation leads to the value of 1.5τ instead of 2.5τ, which results from the Krylov–Fock theorem. It is worth noting that the initial excitation-energy distribution fixed according to the Krylov–Fock theorem at the initial instant of the decay process retains its shape in the course of time. Within our model of state formation, this distribution must vary (become narrower) in the process of prolonged γ-wave effect on the nucleus. Under these conditions, the Krylov–Fock theorem does not provide a correct description of excited-nucleus decay. It is valid only in the case where the distribution $W(E)$ is formed within a time much shorter than the characteristic time of excited-state decay; moreover, the distribution formed must not undergo, during the entire decay process, changes in shape that are due to any external effects on the nucleus. These conditions are satisfied, for example, in experiments aimed at observing the magnetic-field-perturbed angular distribution of bremsstrahlung photons originating from electrons and undergoing resonance scattering on nuclei. In this case, the wave trains of absorbed radiation are very short, while the photon spectrum is wide, so that, in the nuclear resonance region, it can be treated as an energy-independent constant. As a result, the excitation-energy distribution is described by the Lorentzian function (1) and is formed within a time much shorter than τ. In this case, expression (3) and the Krylov–Fock theorem yield the same value (τ) for the average lifetime of the nucleus in an excited state.

It should be noted that the values of t_{av} that are obtained from experiments measuring the angular distributions of resonantly scattered γ rays and those that are produced by the Krylov–Fock theorem have the same meaning by definition. In both cases, they are averaged over the time dependence of the photon-emission probability. In the first case, there occurs averaging of the angle of rotation of the angular-distribution rosette with respect to its undisturbed position (this angle is equal to $\delta\theta = \Omega t$, where t is the lifetime of a specific nucleus in an excited state), and this is equivalent to the averaging of t. In the second case, t is averaged directly.

There may arise the question of whether the manifestation of the spatial and time extension of γ rays may provide the possibility of pinpointing the origin of photons. Prior to answering this question, we would like to indicate that a detection of a single photon does not reveal its wave properties. In order to observe interference and diffraction patterns and to fix a resonance character of γ-ray interaction with nuclei, it is necessary to detect a large number of photons. At the same time, corpuscular features of photons—such as its momentum and energy and the coordinates of its interaction with a detector material—can be determined by detecting a single photon from either the Compton effect or from photoabsorption. Therefore, we can state that the origin of photons cannot be revealed in those processes where their corpuscular properties manifest themselves. At the same time, different-origin photons differ by their wave properties, this difference being seen only in photon ensembles (it cannot be observed in detecting a single photon). For example, bremsstrahlung from electrons that is absorbed by nuclei generates a natural Lorentzian excitation-energy distribution, and this leads to a intrinsic lifetime of excited nuclei. However, exposure of the same nuclei to Mössbauer photons that are in resonance with them generates, as was shown above, a narrower (by a factor of 1.5) excitation-energy distribution, the average lifetime of excited nuclei being accordingly longer.

ACKNOWLEDGMENTS

I am grateful to V.A. Davydov and Yu.N. Isaev for assistance in work.

REFERENCES

1. A. B. Migdal, *Qualitative Methods in Quantum Theory* (Nauka, Moscow, 1975; Benjamin, Reading, 1977).
2. A. V. Stepanov and Yu. M. Tsipenyuk, Usp. Fiz. Nauk **170**, 83 (2000).
3. C. J. Goebel and K. W. McVoy, Phys. Rev. **148**, 1021 (1966).
4. H. Eicher, Z. Phys. **212**, 176 (1968).
5. I. N. Vishnevsky, A. V. Davydov, G. A. Lobov, and V. I. Povzun, Preprint No. 70, Inst. Teor. Éksp. Fiz. (ITEP, Moscow, 1974).
6. A. V. Davydov, M. M. Korotkov, and P. I. Romasheva, Izv. Akad. Nauk SSSR, Ser. Fiz. **44**, 1778 (1980).
7. N. S. Krylov and V. A. Fok, Zh. Éksp. Teor. Fiz. **17**, 93 (1947); A. S. Davydov, *Quantum Mechanics* (Nauka, Moscow, 1973, 2nd ed.; Pergamon, Oxford, 1976); D. I. Blokhintsev, *Quantum Mechanics* (Nauka, Moscow, 1976, 5th ed.; Reidel, Dordrecht, 1964, transl. 4th ed.).
8. A. V. Davydov and P. I. Romasheva, Izv. Akad. Nauk SSSR, Ser. Fiz. **45**, 1874 (1981).

Translated by O. Chernavskaya

Physics of Atomic Nuclei, Vol. 66, No. 12, 2003, pp. 2117–2127. From Yadernaya Fizika, Vol. 66, No. 12, 2003, pp. 2167–2177.

NUCLEI
Theory

Study of Static and Thermal Properties of Symmetric and Asymmetric Nuclear Matter Using Generalized Density-Dependent M3Y Interaction*

Azza O. El-Shal**

Department of Mathematics and Theoretical Physics, Atomic Energy Authority, Cairo, Egypt

Received April 16, 2002

Abstract—By using the most recent generalized form of the density-dependent nucleon–nucleon DDM3Y interaction, namely, CDM3Yn-Paris interaction, the basic static properties of symmetric and asymmetric nuclear matter such as binding energy per particle, pressure, velocity of sound, and compressibility are calculated. Also, at finite temperature, the thermal properties of nuclear matter are studied, such as the free energy, the pressure, the entropy, and the compressibility. In addition, a comparison using different density-dependent M3Y-Paris interaction (DDM3Y1 and BDM3Y1) is considered. The importance of using the density-dependent term in the M3Y-Paris interaction is to fulfill the saturation requirement for the nuclear matter because M3Y-Paris interaction has an attractive character. Thus, the nuclear matter generated with this interaction is unstable against collapse. This new version of the DDM3Y is the general one, and other previous density-dependent forms can be considered as a special case of this one. Therefore, all the explicit theoretical developments are based on the density-dependent CDM3Yn version. The results obtained are in good agreement with previous theoretical estimates. © *2003 MAIK "Nauka/Interperiodica".*

1. INTRODUCTION

An important subject in theoretical nuclear physics is the study of the properties of dense nuclear matter (NM). These properties are also important for particle physics and astrophysics as well as for nuclear physics. Theoretical calculations of the NM properties, a fully microscopic description of both symmetric and asymmetric NM, remain a challenge for the nuclear many-body theory.

The so-called M3Y effective (in-medium) nucleon–nucleon (NN) interaction based on the G-matrix element of the Paris [1] NN potential is used in our present work. Various effective NN interactions, as well as the adjustments of their parameters to satisfy the constraint imposed by the saturation properties of NM, are described in detail by Khoa *et al.* [2, 3]. Since the original M3Y interaction can be shown to give a wrong description of the saturation properties of normal NM, some realistic density dependences (DDM3Y1 and BDM3Y1) are introduced into this interaction to reproduce the saturation properties of cold, symmetric NM at density $\rho_0 = 0.17$ fm^{-3}. The DDM3Y1 and BDM3Y1 versions of the density-dependent M3Y interaction are shown to give a rather soft equation of state (EOS) for symmetric NM, with the nuclear compressibility K around 200 MeV, within a consistent Hartree–Fock calculation [2]. These versions also are shown to give the most realistic shape for the nucleus–nucleus potential calculated within the double-folding model [3]. It is therefore of considerable interest to use the new version of the M3Y interaction (CDM3Yn, $n = 1$–6) in order to study the symmetric and asymmetric properties of NM. The three different density-dependent versions DDM3Y1, BDM3Y1, and CDM3Yn, which give the nuclear incompressibility $K = 170$–270 MeV, appeared to be the most realistic ones in the folding analysis of refractive α-nucleus and nucleus–nucleus scattering data [4].

In the present work, we use the special version CDM3Y6 of M3Y-Paris interaction to produce the symmetric and asymmetric NM binding energies, pressures, compressibilities, speeds of sound, and entropies at zero and finite temperature. Also, a comparison using the DDM3Y and BDM3Y versions is considered.

2. THEORETICAL FORMALISM

The direct (D) and exchange (EX) parts of the M3Y-Paris NN forces can be written in terms of central component $V_C^{\mathrm{D(EX)}}(r)$ (where the spin–orbit term and the tensor term are not considered) and in terms

*This article was submitted by the author in English.

**e-mail: azshal@hotmail.com

Table

Version	Parameters			
	C	α	β	γ, fm^3
DDM3Y1-Paris	0.2963	3.7231	3.7384, fm^3	–
BDM3Y1-Paris	1.2521	1.7452	1.0	–
CDM3Y6-Paris	0.2658	3.8033	1.4099, fm^3	4.0

of spin–isospin-dependent components $V_\sigma^{\mathrm{D(EX)}}(r)$, $V_\tau^{\mathrm{D(EX)}}(r)$, and $V_{\sigma\tau}^{\mathrm{D(EX)}}(r)$ as

$$V^{\mathrm{D(EX)}}(r) = V_C^{\mathrm{D(EX)}}(r) + V_\sigma^{\mathrm{D(EX)}}(r)(\sigma_1\cdot\sigma_2) \quad (1)$$
$$+ V_\tau^{\mathrm{D(EX)}}(r)(\tau_1\cdot\tau_2) + V_{\sigma\tau}^{\mathrm{D(EX)}}(r)(\sigma_1\cdot\sigma_2)(\tau_1\cdot\tau_2),$$

where

$$V_C^{\mathrm{D}}(r) = 11\,061.625\frac{e^{-4r}}{4r} - 2537.5\frac{e^{-2.5r}}{2.5r}, \quad (2)$$

$$V_C^{\mathrm{EX}}(r) = -1524.25\frac{e^{-4r}}{4r} - 518.75\frac{e^{-2.5r}}{2.5r} \quad (3)$$
$$- 7.8474\frac{e^{-0.7072r}}{0.7072r},$$

$$V_\sigma^{\mathrm{D}}(r) = 938.875\frac{e^{-4r}}{4r} - 36\frac{e^{-2.5r}}{2.5r}, \quad (4)$$

$$V_\sigma^{\mathrm{EX}}(r) = -3492.75\frac{e^{-4r}}{4r} + 795.25\frac{e^{-2.5r}}{2.5r} \quad (5)$$
$$+ 2.615\frac{e^{-0.7072r}}{0.7072r},$$

$$V_\tau^{\mathrm{D}}(r) = 313.625\frac{e^{-4r}}{4r} + 223.5\frac{e^{-2.5r}}{2.5r}, \quad (6)$$

$$V_\tau^{\mathrm{EX}}(r) = -4118.0\frac{e^{-4r}}{4r} + 1054.75\frac{e^{-2.5r}}{2.5r} \quad (7)$$
$$+ 2.6157\frac{e^{-0.7072r}}{0.7072r},$$

$$V_{\sigma\tau}^{\mathrm{D}}(r) = -967.125\frac{e^{-4r}}{4r} + 450\frac{e^{-2.5r}}{2.5r}, \quad (8)$$

$$V_{\sigma\tau}^{\mathrm{EX}}(r) = -2210\frac{e^{-4r}}{4r} + 568.75\frac{e^{-2.5r}}{2.5r} \quad (9)$$
$$- 0.872\frac{e^{-0.7072r}}{0.7072r}.$$

The various density-dependent effective NN interactions are assumed to have the separable form

$$V^{\mathrm{D(EX)}}(\rho, r) = f(\rho)V^{\mathrm{D(EX)}}(r), \quad (10)$$

where $V^{\mathrm{D(EX)}}$ is the direct (exchange) term, derived from the M3Y interaction [5, 6]; r is the interaction separation; and ρ is the density of the surrounding nuclear medium, in which the two nucleons are embedded. The original DDM3Y interaction [7] is assumed to have an exponential dependence on the density,

$$f(\rho) = C[1 + \alpha e^{-\beta\rho}], \quad (11)$$

where the values of the parameters α, β, and C given in [4] are adjusted to satisfy the saturation properties of NM. A more flexible power-law density dependence (DD) is introduced in [2, 3]:

$$f(\rho) = C(1 - \alpha\rho^\beta). \quad (12)$$

These interactions are labeled BDM3Yβ. From this type of DD, the one with a linear density dependence ($\beta = 1$), which yields $K = 270$ MeV when used with the M3Y-Paris interaction, seems to give the best overall description of elastic nucleus–nucleus scattering. It is used extensively in the folding-model analysis as well as in heavy-ion elastic scattering [3, 8]. In a more recent study of the density-dependent effects in refractive nucleus–nucleus scattering [4], a flexible hybrid of the DDM3Y1 and BDM3Y1 forms was introduced to examine the sensitivity of the scattering data on the K value in more detail (at the price of introducing one new parameter),

$$f(\rho) = C[1 + \alpha e^{-\beta\rho} - \gamma\rho]. \quad (13)$$

Parameters of the density dependence in Eqs. (11), (12), and (13) for versions DDM3Y1, BDM3Y1, and CDM3Y6 are given in the table. The density-dependent terms of the M3Y interaction, denoted CDM3Yn ($n = 6$), are used to infer the value of the compressibility coefficient K with more precision [4]. Since the DDM3Y1 and BDM3Y1 types of the DD can be obtained as special cases of the CDM3Yn type, all the explicit theoretical development is based on the CDM3Yn type of the DD.

Polarized nuclear matter is composed of numbers $n\uparrow$ ($n\downarrow$) of spin-up (spin-down) neutrons and $p\uparrow$ ($p\downarrow$) of spin-up (spin-down) protons, with corresponding densities $\rho_{n\uparrow}$, $\rho_{n\downarrow}$, $\rho_{p\uparrow}$, $\rho_{p\downarrow}$, respectively; thus,

$$A = n\uparrow + n\downarrow + p\uparrow + p\downarrow \quad (14)$$

is the total number of particles and the total density ρ is given by

$$\rho = \rho_n + \rho_p = \rho_{n\uparrow} + \rho_{n\downarrow} + \rho_{p\uparrow} + \rho_{p\downarrow}. \quad (15)$$

For polarized nuclear matter, we can define the following parameters [9, 10]. The neutron excess parameter,

$$X = \frac{\rho_n - \rho_p}{\rho}. \quad (16)$$

The neutron spin-up excess parameter,

$$\alpha_n = (\rho_{n\uparrow} - \rho_{n\downarrow})/\rho. \quad (17)$$

The proton spin-up parameter,

$$\alpha_p = (\rho_{p\uparrow} - \rho_{p\downarrow})/\rho. \quad (18)$$

There are four Fermi momenta in this general case, namely, $k_n(\lambda_n)$ for neutrons with spin-up (spin-down) and $k_p(\lambda_p)$ for protons with spin-up (spin-down). These Fermi momenta are related to the excess parameters by the relations

$$k_n^3 = k_{\rm F}^3(1 + X + Y + Z), \quad (19)$$

$$\lambda_n^3 = k_{\rm F}^3(1 + X - Y - Z) \quad (20)$$

and

$$k_p^3 = k_{\rm F}^3(1 - X + Y - Z), \quad (21)$$

$$\lambda_p^3 = k_{\rm F}^3(1 - X - Y + Z), \quad (22)$$

where $k_{\rm F}$ is the Fermi momentum of unpolarized NM,

$$Y = \alpha_n + \alpha_p, \quad (23)$$

$$Z = \alpha_n - \alpha_p. \quad (24)$$

By using the M3Y-Paris interaction [Eqs. (1)–(9)] with the three versions of density dependence [Eqs. (11), (12), and (13)], the energy per nucleon of the NM at zero temperature can be written as

$$E = E_V + X^2 E_X + Y^2 E_Y + Z^2 E_Z, \quad (25)$$

where

$$E_V = \frac{3\hbar^2 k_{\rm F}^2}{10m} + \frac{1}{2}\rho f(\rho)\left[J_D + \int \hat{j}_1^2(\eta) V_C^{\rm EX}(r) d^3r\right], \quad (26)$$

$$E_{X,Y,Z} = \frac{\hbar^2 k_{\rm F}^2}{6m} + \frac{1}{2}\rho f(\rho) \quad (27)$$

$$\times \left\{ -\int j_1^2(\eta) V_C^{\rm EX}(r) d^3r + \int V_{\tau,\sigma,\sigma\tau}^D(r) d^3r \right.$$

$$\left. + \int (\hat{j}_1^2(\eta) - 2\hat{j}_1(\eta) j_2(\eta) + j_2^2(\eta)) V_{\tau,\sigma,\sigma\tau}^{\rm EX}(r) d^3r \right\}.$$

Here,

$$J_D = \int V_C^D(r) d^3r, \quad (28)$$

$$\hat{j}_1(\eta) = \frac{3j_1(\eta)}{\eta}, \quad (29)$$

where $j_n(\eta)$ is the nth-order spherical Bessel function and $\eta = k_{\rm F} r$. In Eq. (25), terms higher than quadratic in X, Y, and Z are neglected. The pressure of a nuclear system is given by

$$P = \rho^2 \frac{\partial E}{\partial \rho}, \quad (30)$$

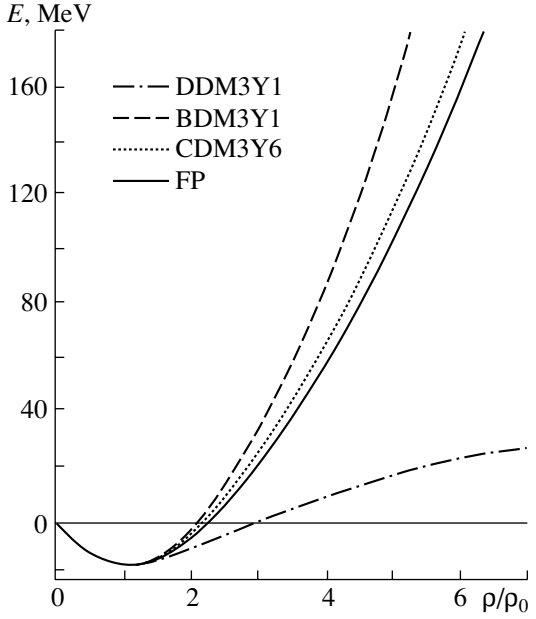

Fig. 1. The energy per particle of nuclear matter as a function of density using different density-dependent M3Y interactions (DDM3Y1, BDM3Y1, and CDM3Y6) in a comparison with FP potential [11].

and the compressibility is given by

$$K = 9\frac{\partial P}{\partial \rho}. \quad (31)$$

By using Eq. (25), we get the pressure and the compressibility at zero temperature as

$$P = P_V + X^2 P_X + Y^2 P_Y + Z^2 P_Z \quad (32)$$

and

$$K = K_V + X^2 K_X + Y^2 K_Y + Z^2 K_Z. \quad (33)$$

Using Eqs. (26) and (27) for E_V, E_X, E_Y, and E_Z, one gets simple analytical equations for $P_V(K_V)$, $P_X(K_X)$, $P_Y(K_Y)$, and $P_Z(K_Z)$.

Also, the speed of sound is given by

$$V_s/c = \left(\frac{\partial P}{\partial \rho}\right)^{1/2}. \quad (34)$$

It is well known from classical thermodynamics that thermal properties of the system are completely determined if the free energy F is known in terms of the density ρ and temperature T,

$$F(\rho, T) = E(\rho, T = 0) - TS(\rho, T), \quad (35)$$

where E is the total energy and S is the entropy. The volume term of the entropy is given by

$$S_V(\rho, T) = \frac{\pi^2 m^*}{\hbar^2 k_{\rm F}^2} k^2 T, \quad (36)$$

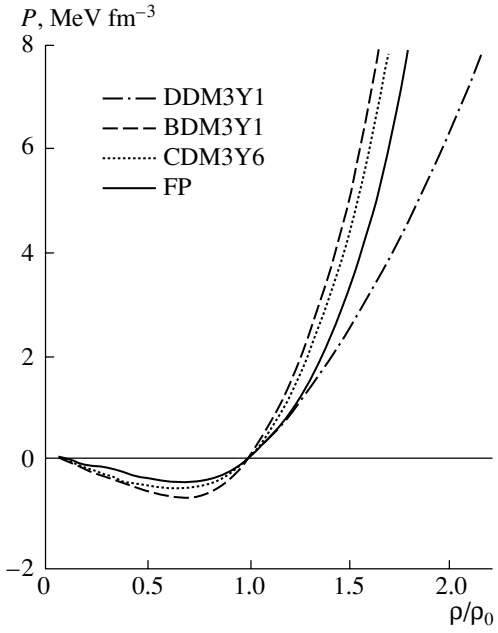

Fig. 2. The pressure of nuclear matter as a function of density at temperature $T = 5$ MeV in comparison with FP potential [11] using the different density-dependent versions of the M3Y interaction.

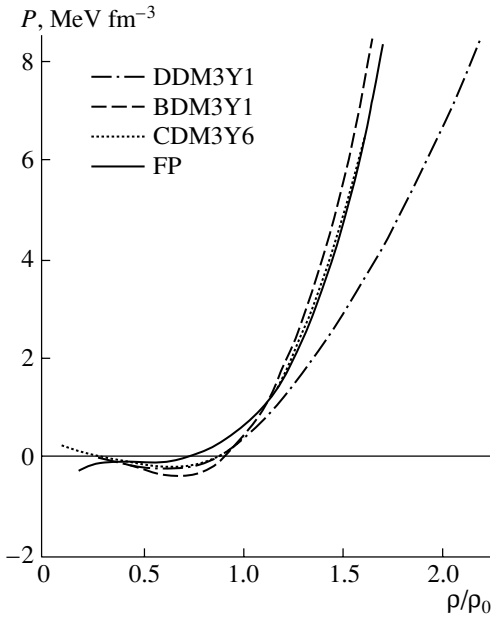

Fig. 3. The same as Fig. 2, but for $T = 10$ MeV.

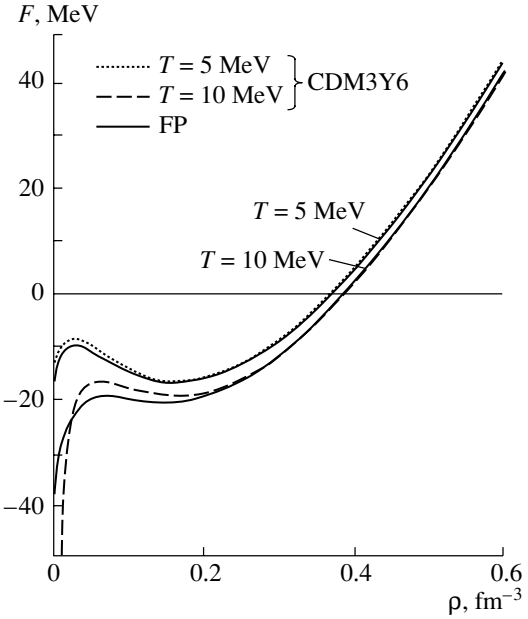

Fig. 4. The free energy of nuclear matter as a function of density using the CDM3Y6 version at $T = 5$ and 10 MeV in comparison with that of FP potential [11].

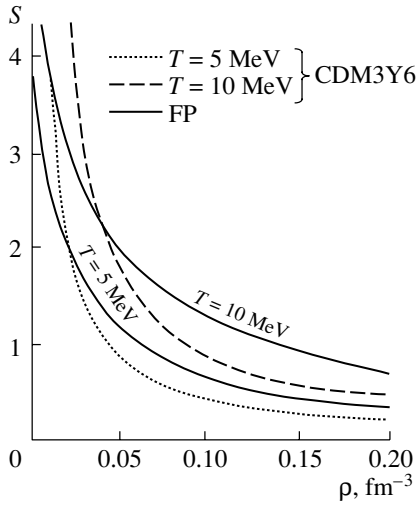

Fig. 5. The entropy of nuclear matter as a function of density using the CDM3Y6 version of M3Y interaction at $T = 5$ and 10 MeV in comparison with that of FP calculations [11].

where k is the Boltzmann constant and is taken to be equal to unity (in the presently considered units), and m^* is the effective mass. The symmetric terms of the free energy at finite temperature are given by

$$F_{X,Y,Z}(\rho, T) = E_{X,Y,Z}(\rho, T = 0) + \frac{\pi^2 T^2}{9\hbar^2 k_{\mathrm{F}}^2} m^*_{X,Y,Z}, \tag{37}$$

where

$$m^*_{X,Y,Z} \tag{38}$$

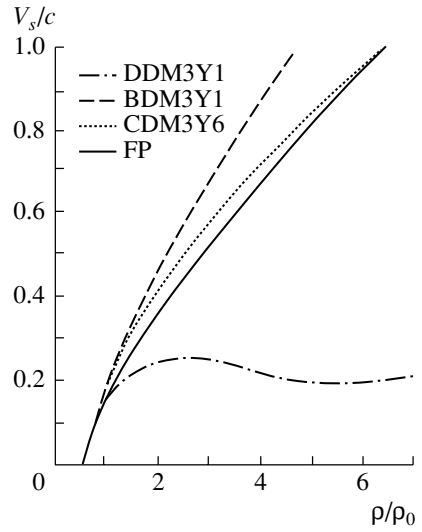

Fig. 6. The speed of sound of nuclear matter as a function of density using different density-dependent M3Y interactions in comparison with results of FP calculations [11].

$$= m\left[1 + \frac{m}{12\hbar^2}\rho f(\rho)\int j_0(\eta) r^2 V^{\rm EX}_{\tau,\sigma,\sigma\tau}(r) d^3r\right],$$

and the pressure of the asymmetric NM at temperature T is given by

$$P^T_{X,Y,Z}(\rho,T) = P_{X,Y,Z}(\rho,T=0) + \frac{\pi^2 T^2}{9\hbar^2} \quad (39)$$
$$\times\left\{\frac{m^2\rho^2}{12\hbar^2 k_{\rm F}^2}\left[\int\left(\left(a(\rho) - \frac{2}{3}f(\rho)\right) j_0(\eta)\right.\right.\right.$$
$$\left.\left.\left. -\frac{1}{3}f(\rho)\eta j_1(\eta)\right) r^2 V^{\rm EX}_{\tau,\sigma,\sigma\tau}(r) d^3r\right] - \frac{2m\rho}{3\hbar^2 k_{\rm F}^2},\right\},$$

where

$$a(\rho) = \rho\frac{df(\rho)}{d\rho} + f(\rho). \quad (40)$$

Also, the compressibility of asymmetric NM at temperature T is given by

$$K^T_{X,Y,Z}(\rho,T) = K_{X,Y,Z}(\rho,T=0) \quad (41)$$
$$+ \frac{\pi^2 T^2 m}{3\hbar^2 k_{\rm F}^2}\left\{\frac{m}{4\hbar^2}\int\left[\left(g(\rho) - \frac{1}{27}\eta^2\rho f\right) j_0(\eta)\right.\right.$$
$$\left. - \frac{2}{3}\eta\rho a(\rho) j_1(\eta) + \frac{2}{27}\eta^2\rho f(\rho) j_2(\eta)\right] r^2$$
$$\left.\times V^{\rm EX}_{\tau,\sigma,\sigma\tau}(r) d^3r - \frac{2}{3}\right\},$$

where

$$g(\rho) = \rho^3\frac{d^2 f}{d\rho^2} + \frac{8}{3}\rho^2\frac{df}{d\rho} + \frac{4}{9}\rho f(\rho). \quad (42)$$

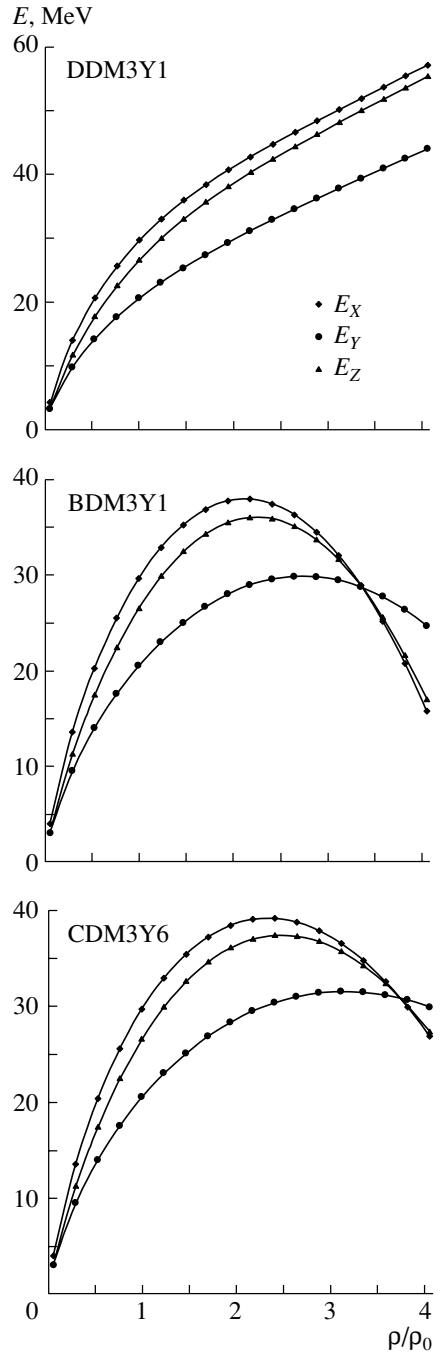

Fig. 7. Symmetry terms of cold NM EOS for the versions DDM3Y1, BDM3Y1, and CDM3Y6 of Paris potential.

3. RESULTS AND DISCUSSION

The formalism described above studies symmetric and asymmetric nuclear matter at zero and finite temperature ($T = 5$ and 10 MeV). In the present analysis, the effect of the density-dependent term introduced into the M3Y-Paris interaction, i.e., the DDM3Y1, BDM3Y1, and CDM3Y6 versions, is also considered. The values of the parameters C, α, β, and γ of $f(\rho)$ are

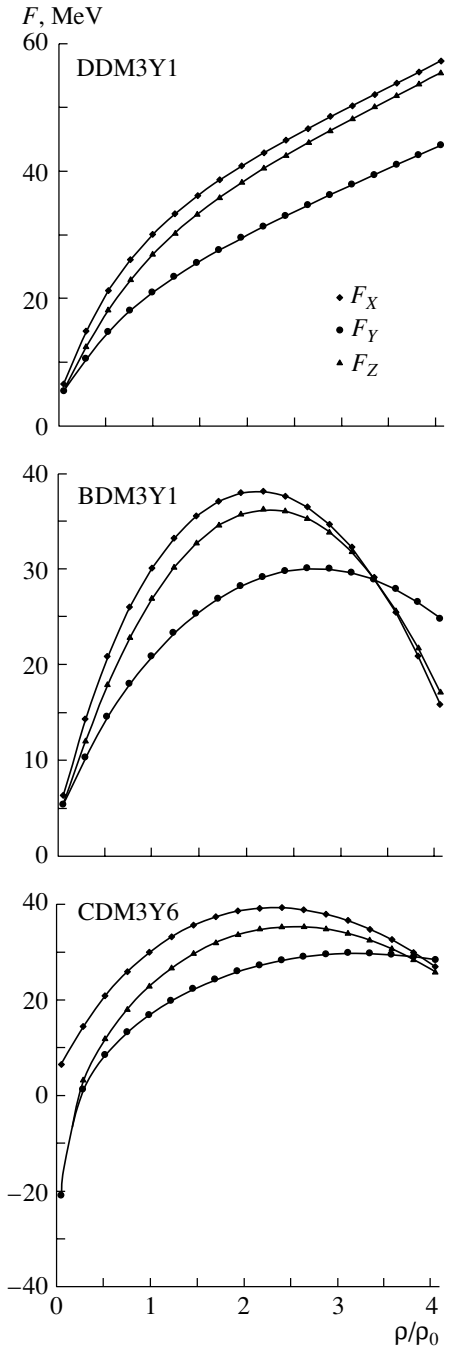

Fig. 8. Symmetry terms of free energy at $T = 5$ MeV for the versions DDM3Y1, BDM3Y1, and CDM3Y6 of Paris potential.

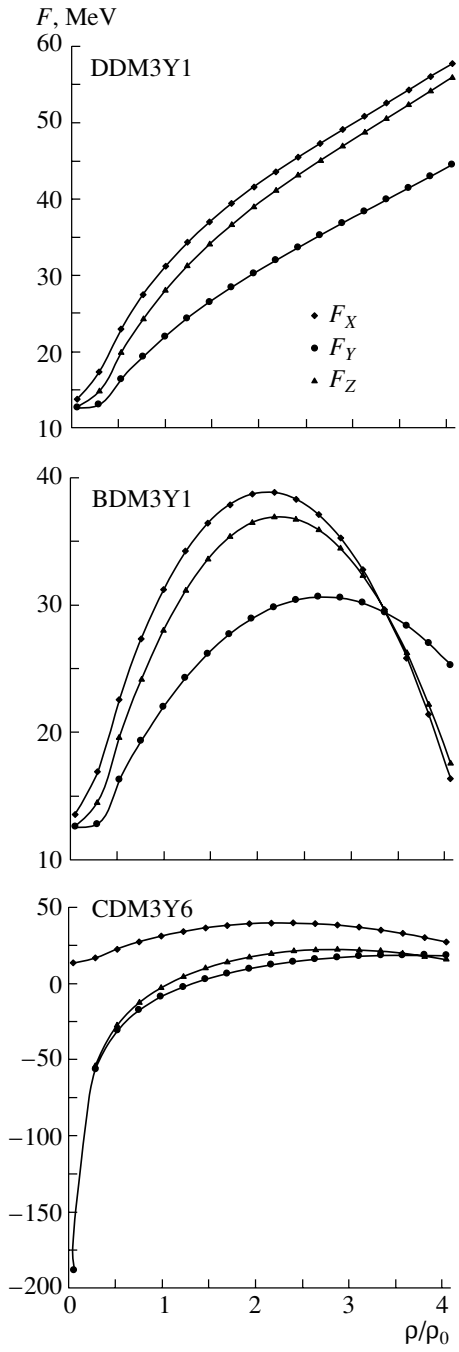

Fig. 9. Symmetry terms of free energy at $T = 10$ MeV for the versions DDM3Y1, BDM3Y1, and CDM3Y6 of Paris potential.

given in the table (see [2] and [4]) for the M3Y-Paris interaction.

In Fig. 1, the EOS is plotted as a function of the density for the DDM3Y1, BDM3Y1, and CDM3Y6 versions and a comparison with the previous work of Friedman and Pandharipande (FP) [11] is shown. The CDM3Y6 version gives a softer EOS than that of BDM3Y1.

The pressure is shown in Figs. 2 and 3 at temperature $T = 5$ and 10 MeV, respectively, with a comparison of FP calculations [11].

The free energy at temperature $T = 5$ and 10 MeV is presented in Fig. 4. The agreement with the previous work of FP [11] is quite good.

The entropy using the CDM3Y6 version is given in Fig. 5, and the speeds of sound of the three versions

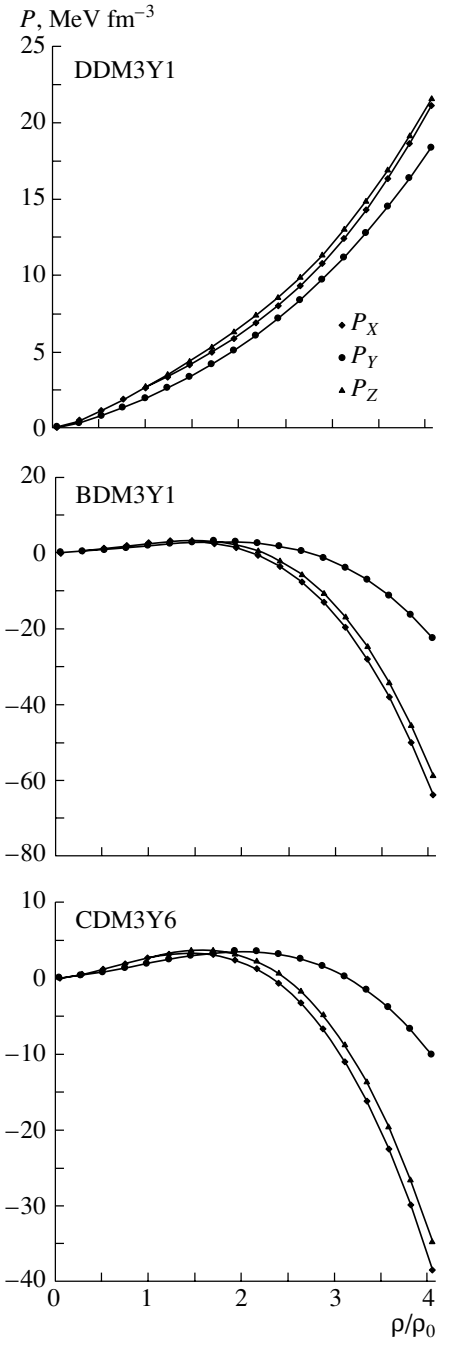

Fig. 10. Symmetry terms of cold NM pressure for the versions DDM3Y1, BDM3Y1, and CDM3Y6 of Paris potential.

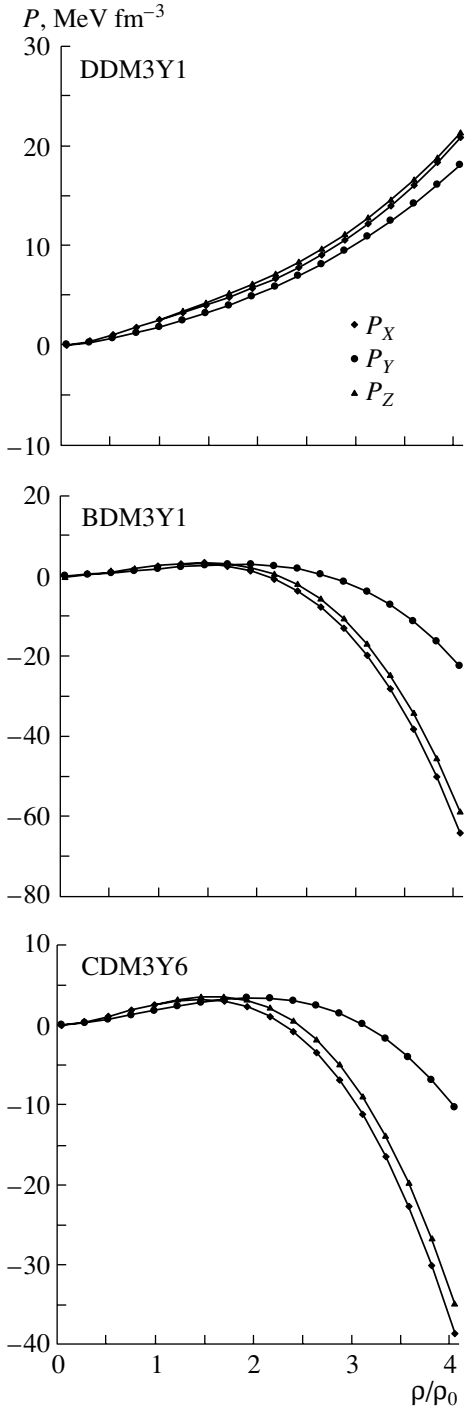

Fig. 11. Symmetry terms of pressure at $T = 10$ MeV for the versions DDM3Y1, BDM3Y1, and CDM3Y6 of Paris potential.

DDM3Y1, BDM3Y1, and CDM3Y6 are illustrated in Fig. 6 with comparison of FP calculations [11]. Here, we can notice that the CDM3Y6 is closer to the FP estimates than the other versions.

According to the present analysis, it is found that the compressibility of normal NM is 176, 270, and 252 MeV for the three versions used, namely, DDM3Y1, BDM3Y1, and CDM3Y6, respectively, which may explain the results obtained.

The symmetry energies E_X, E_Y, and E_Z (for cold NM) as a function of the relative density ρ/ρ_0 are shown in Fig. 7 for the versions DDM3Y1, BDM3Y1, and CDM3Y6.

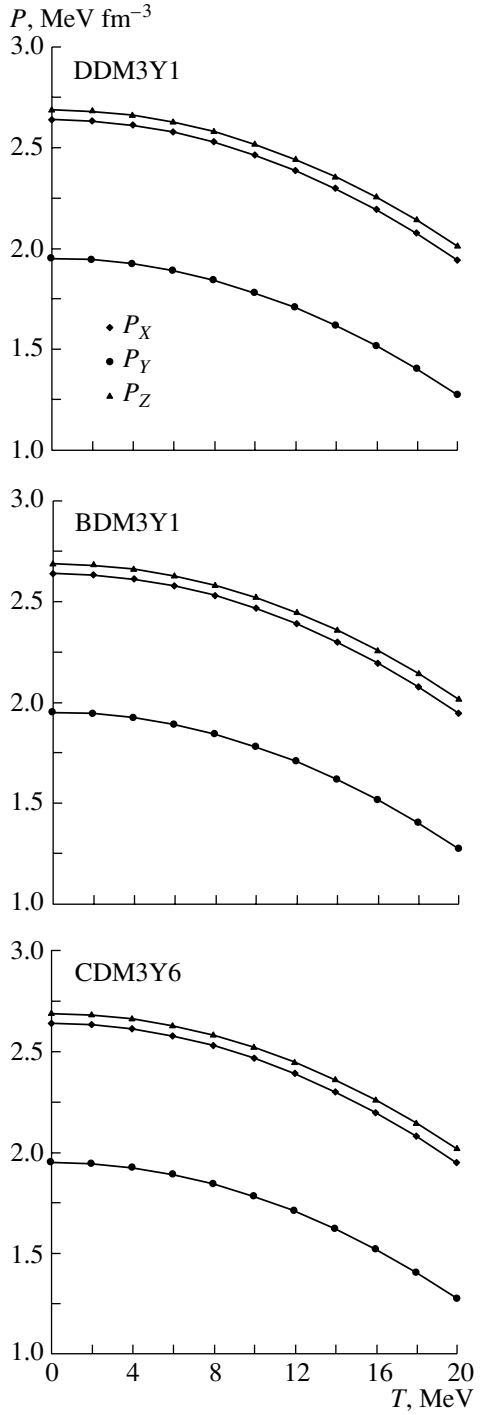

Fig. 12. Symmetry terms of pressure as a function of temperature for the versions DDM3Y1, BDM3Y1, and CDM3Y6 of Paris potential.

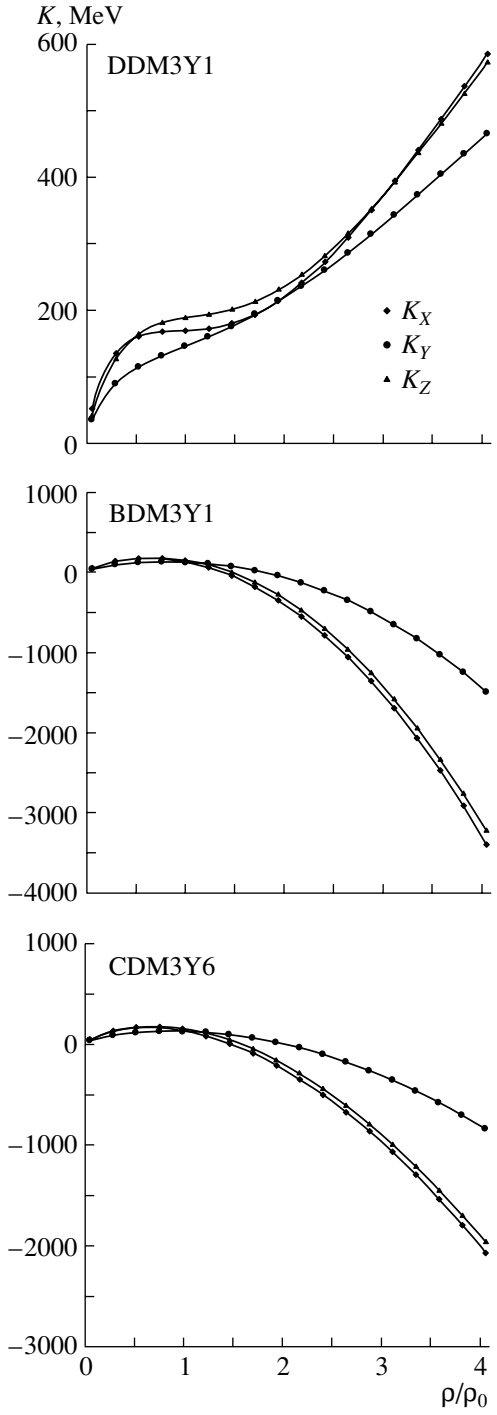

Fig. 13. Symmetry terms of compressibility as a function of relative density at $T = 0$ for the versions DDM3Y1, BDM3Y1, and CDM3Y6 of Paris potential.

Concerning the version DDM3Y1, an increasing behavior of E_X, E_Y, and E_Z is noticed, while for the others (i.e., BDM3Y1 and CDM3Y6) the increase in E_X, E_Y, and E_Z is noticed up to about $2\rho_0$ and then smoothly decreases with increasing density.

The symmetry energy E_X is evaluated for cold NM [12] at neutron–proton asymmetries using different density-dependent M3Y interactions.

An empirical estimate of E_X, E_Y, and E_Z may be obtained with the help of the empirical values of the Landau parameters [13], where $E_X = 27$ MeV, $E_Y = 34.5$ MeV, and $E_Z = 39$ MeV for $k_\mathrm{F} = 1.36$ fm^{-1}.

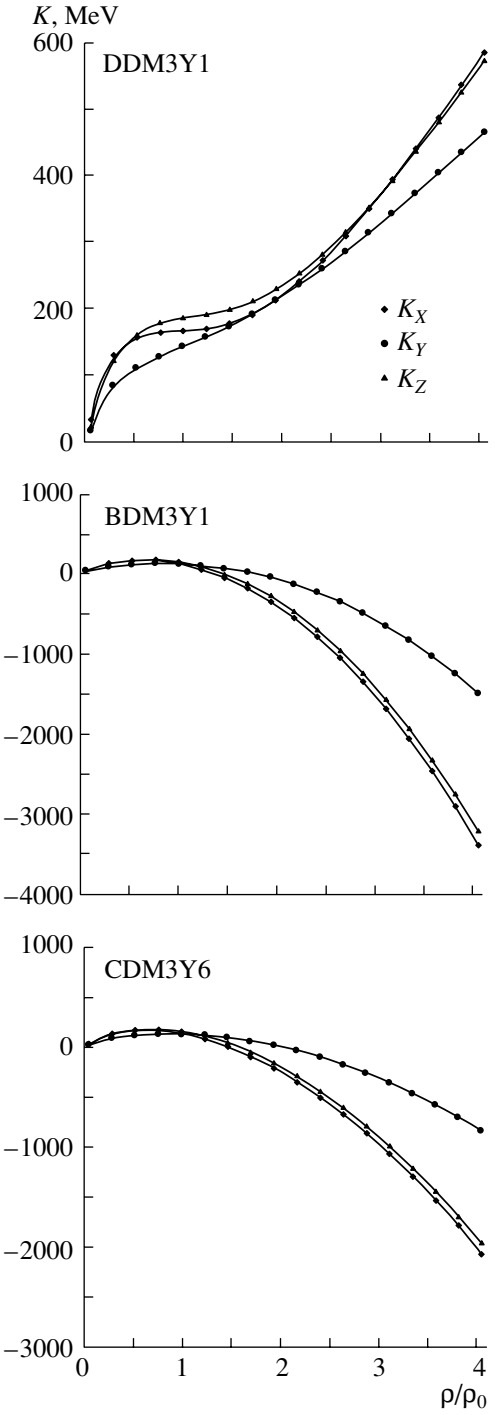

Fig. 14. Symmetry terms of compressibility as a function of relative density at $T = 10$ MeV for the versions DDM3Y1, BDM3Y1, and CDM3Y6 of Paris potential.

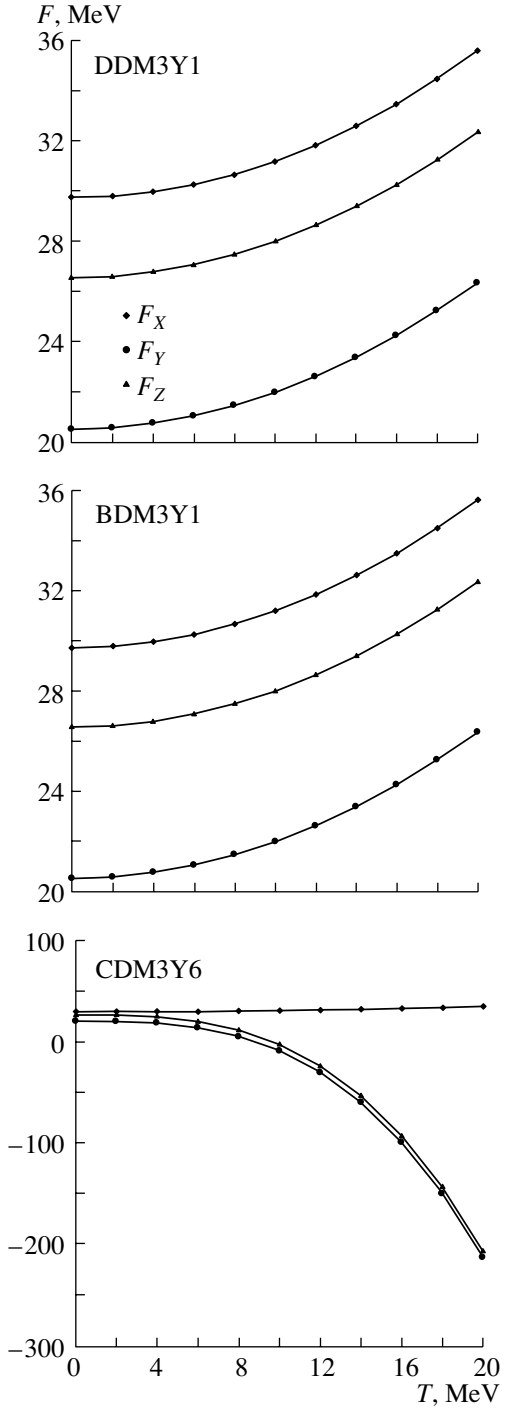

Fig. 15. Symmetry terms of free energy as a function of temperature for the versions DDM3Y1, BDM3Y1, and CDM3Y6 of Paris potential.

Dabrowski [10] calculated E_X, E_Y, and E_Z using the K-matrix theory with the Brueckner–Gammer–Thelar and soft core potential and obtained $E_X = 26.5$ MeV, $E_Y = 32.5$ MeV, and $E_Z = 38$ MeV. According to the generalized hydrodynamics model of Uberall [14], using the Seyler–Blanchard potential (where the calculations are performed with different values of E_Y), it is found that the observed maximum neutron-star mass and surface magnetic field are best explained with $E_X = 33.4$ MeV, $E_Y = 15$ MeV, and $E_Z = 36.5$ MeV. These values are in reasonable agreement with our values.

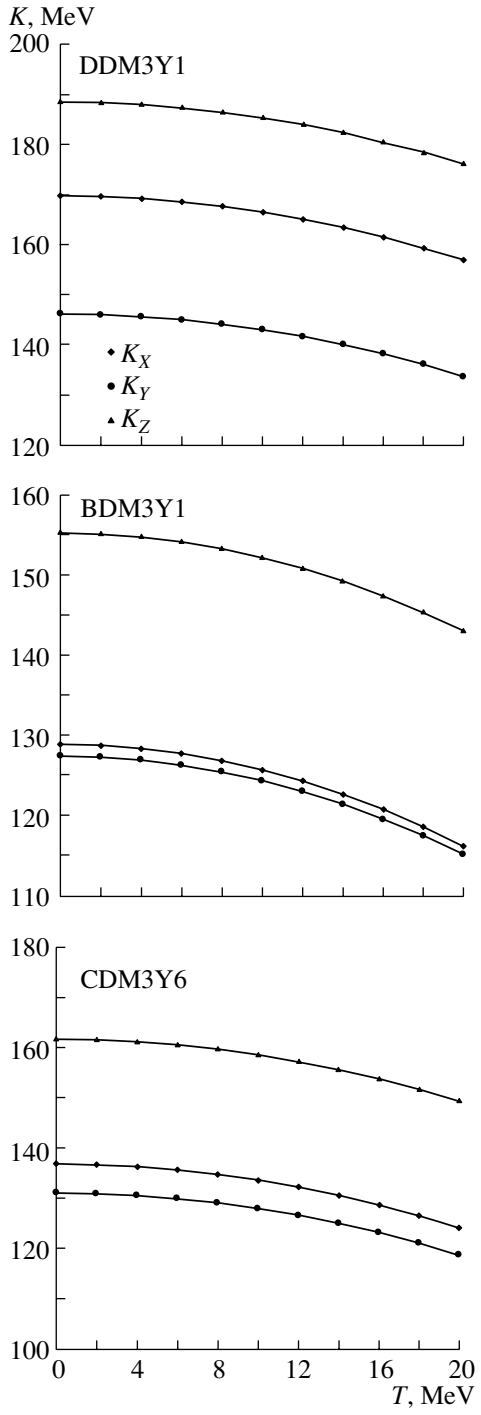

Fig. 16. Symmetry terms of compressibility as a function of temperature for the versions DDM3Y1, BDM3Y1, and CDM3Y6 of Paris potential.

Figures 8 and 9 show the free energy for asymmetric NM as a function of relative density at different temperatures for the three versions.

Concerning the pressure, the effects of the temperature on P_X, P_Y, and P_Z using the three versions are shown in Figs. 10 ($T = 0$ MeV), 11 ($T = 10$ MeV), and 12, where we notice that there is a small effect of the temperature on the pressure of asymmetric NM. A similar dependence on X has been observed by Barranco *et al.* [15]; on X, Y, and Z by Abd-Alla [16, 17]; and by Moharram [18]. The symmetry, spin symmetry, and spin–isospin symmetry compressibilities (K_X, K_Y, and K_Z) are shown in Figs. 13 and 14 as a function of the relative density ρ/ρ_0 for the three versions for $T = 0$ and 10 MeV, respectively. In the version DDM3Y1, K_X, K_Y, and K_Z increase at $T = 0$ and 10 MeV, while in versions BDM3Y1 and CDM3Y6 K_X, K_Y, and K_Z increase slowly until $\rho = \rho_0$ and then decrease rapidly at $T = 0$ and 10 MeV.

The effect of the temperature on the free energy of asymmetric NM is shown clearly in Fig. 15. This illustrates that, for versions DDM3Y1 and BDM3Y1, F_X, F_Y, and F_Z increase smoothly with temperature. For the CDM3Y6 version, the behavior is different; namely, F_X has a very slight increase with the temperature up to $T = 20$ MeV, while F_Y and F_Z are nearly the same as F_X until $T = 5$ MeV and then they decrease rapidly with increasing temperature.

The effect of temperature on the compressibility of asymmetric NM for the three versions is shown in Fig. 16, where K_X, K_Y, and K_Z decrease slowly as the temperature increases.

The importance of the functional form of the density dependence is to facilitate folding calculations of nucleus–nucleus potentials and it can also be used as an effective interaction in a nuclear-structure model. The density dependence CDM3Yβ is somewhat softer than the linear dependence of the BDM3Y1 version with a popular choice of noninteger power, $\beta = 2/3$ (which gives $K = 218$ MeV [13, 19]).

We also note that, even with $K = 270$ MeV, we are still dealing with a quite soft EOS compared with the hard EOS which is sometimes considered in the study of heavy-ion collisions (with $K =$ 400–500 MeV [20]).

We choose the CDM3Y6 version to show that such a version gives a good representation of realistic potential for use in a folding-model analysis of α scattering [21, 22], and it also gives good estimates for static and thermal properties of NM.

REFERENCES

1. H. A. Bethe, Annu. Rev. Nucl. Part. Sci. **38**, 1 (1988).
2. D. T. Khoa and W. von Ortzen, Phys. Lett. B **304**, 8 (1993).
3. D. T. Khoa, W. von Oertzen, and H. G. Bohlen, Phys. Rev. C **49**, 1652 (1994).
4. D. T. Khoa, G. R. Satchler, and W. von Oertzen, Phys. Rev. C **56**, 954 (1997).
5. G. Bertsch, J. Borysowicz, H. McManus, and W. G. Love, Nucl. Phys. A **284**, 399 (1977).

6. N. Anantaraman, H. Toki, and G. F. Bertsch, Nucl. Phys. A **398**, 269 (1983).
7. A. M. Kobos, B. A. Brown, P. E. Hodgson, *et al.*, Nucl. Phys. A **384**, 65 (1982).
8. D. T. Khoa *et al.*, Phys. Rev. Lett. **74**, 34 (1995).
9. J. Dabrowski and P. Hanesel, Phys. Rev. C **7**, 619 (1973).
10. J. Dabrowski, Acta Phys. Pol. B **7**, 657 (1976).
11. B. Friedman and V. R. Pandharipande, Nucl. Phys. A **361**, 502 (1981).
12. D. T. Khoa, W. von Oertzen, and A. A. Ogloblin, Nucl. Phys. A **602**, 98 (1996).
13. S. O. Backman, A. D. Jackson, and J. Speth, Phys. Lett. B **56B**, 209 (1975).
14. H. Uberall, *Electron Scattering from Complex Nuclei* (Academic Press, New York, 1971).
15. M. Barranco and J. R. Buchler, Phys. Rev. C **22**, 1729 (1980).
16. M. Abd-Alla, S. Ramadan, and M. Y. M. Hassan, Phys. Rev. C **36**, 1565 (1987).
17. M. Abd-Alla and S. A. Hager, Phys. Rev. C **61**, 044313 (2000).
18. S. A. Moharram, to be published.
19. D. T. Khoa and W. von Oertzen, Phys. Lett. B **342**, 6 (1995).
20. G. F. Bertsch and S. Das Gupta, Phys. Rep. **160**, 189 (1988).
21. D. T. Khoa, Nucl. Phys. A **668**, 3 (2000).
22. D. T. Khoa, Phys. Rev. C **63**, 034007 (2001).

Physics of Atomic Nuclei, Vol. 66, No. 12, 2003, pp. 2128–2142. From Yadernaya Fizika, Vol. 66, No. 12, 2003, pp. 2178–2192.

NUCLEI
Theory

On the Fermi and Gamow–Teller Strength Distributions in Medium-Heavy Mass Nuclei*

V. A. Rodin[1),2)] and **M. H. Urin[2)]**

Received August 9, 2002; in final form, December 26, 2002

Abstract—An isospin-self-consistent approach based on the continuum-random-phase approximation (CRPA) is applied to describe the Fermi and Gamow–Teller strength distributions within a wide excitation-energy interval. To take into account nucleon pairing in open-shell nuclei, we formulate an isospin-self-consistent version of the proton–neutron-quasiparticle-CRPA (pn-QCRPA) approach by incorporating the BCS model into the CRPA method. The isospin and configurational splittings of the Gamow–Teller giant resonance are analyzed in single-open-shell nuclei. The calculation results obtained for the ^{208}Bi, ^{90}Nb, and Sb isotopes are compared with the available experimental data. © *2003 MAIK "Nauka/Interperiodica".*

1. INTRODUCTION

The Fermi and Gamow–Teller (GT) strength functions in medium-heavy mass nuclei have been studied for a long time. The subject of studies of the GT strength distribution is closely related to the weak probes of nuclei (single and double β decays, neutrino interaction, etc.) as well as to the direct charge-exchange reactions [(p, n), (^{3}He, t), etc.]. The weak probes deal with the low-energy part of the GT strength distribution (see, e.g., [1, 2]). The direct reactions allow one to study the distribution in a wide excitation-energy interval including the region of the GT giant resonance (GTR) (see, e.g., [3–7] and references therein) and also the high-energy region (see, e.g., [8, 9]). The discovery of the isobaric analog resonances (IAR) and the subsequent study of their properties have allowed one to conclude that there is a high degree of isospin conservation in medium-heavy mass nuclei. It means that the IAR exhausts almost the total Fermi strength and the rest is mainly exhausted by the isovector monopole giant resonance (IVMR) [1, 10].

The random-phase-approximation (RPA)-based microscopical studies of the GT strength distribution started from the consideration of a schematic three-level model taking the direct, core-polarization, and back-spin-flip transitions into account [11]. One or two weakly collectivized GT states along with the GTR were found in the model. Realistic continuum-random-phase-approximation (CRPA) calculations for the GT strength distribution were performed in [12, 13]. Some of the states predicted in [11] were found in [13]. Attempts to describe the GT strength distribution in detail within the RPA + Hartree–Fock model have been undertaken recently in [14]. Unfortunately, the authors of [12, 14] did not address the following questions: (i) the GT strength distribution in the high-energy region of the isovector spin-monopole giant resonance (IVSMR); (ii) effects of the nucleon pairing; (iii) the isospin splitting of the GTR.

Having taken the nucleon pairing into consideration in CRPA calculations, the authors of [13] predicted the configurational splitting of the GTR in some nuclei and initiated the respective experimental search for the effect [3]. In [13], however, the influence of the particle–particle interaction in the charge-exchange channel was not taken into account. Along with the pairing interaction in the neutral channel, the proton–neutron interaction is taken into consideration within the proton–neutron-quasiparticle random-phase approximation (pn-QRPA) to describe the double-β-decay rates (see, e.g., [2] and references therein). Unfortunately, most current versions of the pn-QRPA do not treat the single-particle continuum, which hinders the description of both high-lying IVMR and IVSMR. In addition, it seems that the question whether the modern versions of the pn-QRPA comply with the isospin conservation has not been raised yet.

The present paper is stimulated partially by the experimental results of [3–7] and by the intention to overcome (to some extent) the shortcomings of

*This article was submitted by the authors in English.

[1)]Institut für Theoretische Physik der Universität Tübingen, Germany.
[2)]Moscow Engineering Physics Institute (State University), Kashirskoe sh. 31, Moscow, 115409 Russia.
**e-mail: vadim.rodin@uni-tuebingen.de
***e-mail: urin@theor.mephi.ru

previous approaches. As a base, we use the isospin-self-consistent CRPA approach of [15–17], where direct-decay properties of giant resonances have mainly been considered. We pursue the following goals:

(i) application of the isospin-self-consistent CRPA approach to describe the Fermi and GT strength distributions in closed-shell nuclei within a wide excitation-energy interval, including the region of the isovector monopole and spin-monopole giant resonances;

(ii) formulation of an approximate method to deal with the isospin splitting of the GTR;

(iii) taking into account the spin-quadrupole part of the particle–hole interaction for description of GT excitations;

(iv) incorporation of the BCS model into the CRPA method to formulate an isospin-self-consistent version of the proton–neutron-quasiparticle continuum-random-phase-approximation (pn-QCRPA) approach;

(v) application of the pn-QCRPA approach to describe the Fermi and GT strength distributions in single-closed-shell nuclei within a wide excitation-energy interval;

(vi) examination of the GTR configurational splitting effect within the pn-QCRPA and its impact on the total GTR width.

We restrict ourselves to an analysis within the particle–hole subspace and, therefore, do not address the question of the influence of $2p$–$2h$ configurations (see, e.g., [18]) nor the quenching effect (see, e.g., [19]). However, we simulate the coupling of the GT states to many-quasiparticle configurations, using an appropriate smearing parameter.

The above-listed goals could apparently be achieved within the pn-QCRPA approach based on the density-functional method [20]. However, the authors of [20] focused their efforts mainly on the analysis of the low-energy part of the GT strength distribution relevant for astrophysical applications.[3)]

The paper is organized as follows. In Section 2, the basic relationships of the isospin-self-consistent CRPA approach are given. They include description of the model Hamiltonian, its symmetries and the respective sum rules (Sections 2.1 and 2.2), the CRPA equations taking into account the spin-quadrupole part of the particle–hole interaction for description of the GT excitations (Section 2.3), and an approximate description of the isospin splitting of the GTR (Section 2.4). In Section 3, we extend the CRPA approach to incorporate the BCS model to describe both the nucleon pairing in neutral channels and the respective interaction in the charge-exchange particle–particle channels. The generalized model Hamiltonian, its symmetries, and respective sum rules are given in Sections 3.1 and 3.2. The standard pn-QCRPA equations are reformulated in terms of radial parts of the transition density and free two-quasiparticle propagator. That allows us to formulate the coordinate-space representation for the inhomogeneous system of the pn-QRPA equations (Section 3.3). As applied to single-open-shell nuclei, a version of the pn-QCRPA approach is formulated on the basis of the above system (Section 3.4). The choice of the model parameters and calculation results concerned with the Fermi and GT strength distributions in the ^{208}Bi, ^{90}Nb, and Sb isotopes are presented in Section 4. A summary concerning the approach and discussion of the calculation results are given in Section 5.

2. DESCRIPTION OF THE FERMI AND GT STRENGTH FUNCTIONS IN CLOSED-SHELL NUCLEI

2.1. Model Hamiltonian

We use a simple, and at the same time realistic, model Hamiltonian to analyze the Fermi (F), Coulomb (C), and GT strength functions in medium-heavy mass spherical nuclei. The Hamiltonian consists of the mean field $U(x)$ including the phenomenological isoscalar part $U_0(x)$ along with the isovector $U_1(x)$ and the Coulomb $U_{\rm C}(x)$ parts calculated consistently in the Hartree approximation:

$$U(x) = U_0(x) + U_1(x) + U_{\rm C}(x); \qquad (1)$$
$$U_0(x) = U_0(r) + U_{\rm so}(x),$$
$$U_1(x) = \frac{1}{2} v(r) \tau^{(3)},$$
$$U_{\rm C}(x) = \frac{1}{2} U_{\rm C}(r)(1 - \tau^{(3)}).$$

Here, $U_0(r)$ and $U_{\rm so}(x) = U_{\rm so}(r)\boldsymbol{\sigma} \cdot \mathbf{l}$ are the central and spin–orbit parts of the isoscalar mean field, respectively; $v(r)$ is the symmetry potential. The potential $U(x)$ determines the single-particle levels with the energies ε_λ ($\lambda = \pi$ for protons and $\lambda = \nu$ for neutrons, λ being the set of the single-particle quantum numbers, $(\lambda) = \{lj\}$) and the radial wave functions $r^{-1}\chi_\lambda(r)$ along with the radial Green's functions $(rr')^{-1} g_{(\lambda)}(r, r'; \varepsilon)$. On the basis of Eq. (1), one can get expressions relating the matrix elements of the single-particle Fermi ($\tau^{(-)}$) and GT ($\sigma_\mu \tau^{(-)}$) operators (σ_μ are the spherical Pauli matrices):

$$t^{(0)}_{(\pi)(\nu)} \{(\varepsilon_\pi - \varepsilon_\nu)(\chi_\pi \chi_\nu) + v_{\pi\nu} - (U_{\rm C})_{\pi\nu}\} = 0, \quad (2)$$

[3)] We should emphasize the decisive contribution of Prof. S.A. Fayans in developing such a powerful approach. We much regret his too early passing away.

$$t^{(1)}_{(\pi)(\nu)}\{(\varepsilon_\pi-\varepsilon_\nu)(\chi_\pi\chi_\nu)+v_{\pi\nu}-(U_{\rm C})_{\pi\nu} \quad (3)$$
$$-((\boldsymbol{\sigma}\cdot\mathbf{l})_{(\pi)}-(\boldsymbol{\sigma}\cdot\mathbf{l})_{(\nu)})(U_{\rm so})_{\pi\nu}\}=0,$$

with

$$(\chi_\pi\chi_\nu)=\int\chi_\pi(r)\chi_\nu(r)dr,$$

$$f_{\pi\nu}=\int f(r)\chi_\pi(r)\chi_\nu(r)dr,$$

$$t^{(0)}_{(\pi)(\nu)}=\sqrt{2j_\pi+1}\delta_{(\pi)(\nu)},$$

$$t^{(1)}_{(\pi)(\nu)}=\frac{1}{\sqrt{3}}\langle(\pi)||\sigma||(\nu)\rangle.$$

We choose the Landau–Migdal forces to describe the particle–hole interaction [21]. The explicit expression for the forces in the charge-exchange channel is

$$\hat{H}_{p-h}=2\sum_{a>b}(F_0+F_1\boldsymbol{\sigma}_a\cdot\boldsymbol{\sigma}_b)\tau^{(-)}_a\tau^{(+)}_b \quad (4)$$
$$\times\delta(\mathbf{r}_a-\mathbf{r}_b)+\text{h.c.},$$

where the intensities of the non-spin-flip and spin-flip parts of this interaction, F_0 and F_1, respectively, are the phenomenological parameters.

2.2. The Symmetries of the Model Hamiltonian and Sum Rules

The model Hamiltonian $\hat{H}$ complies with the isospin symmetry provided that

$$[\hat{H},\hat{T}^{(-)}]=\hat{U}^{(-)}_{\rm C}, \quad (5)$$

$$\hat{H}=\hat{H}_0+\hat{H}_{p-h},\quad \hat{H}_0=\sum_a(T_a+U(x_a)), \quad (6)$$

$$\hat{T}^{(-)}=\sum_a\tau^{(-)}_a,\quad \hat{U}^{(-)}_{\rm C}=\sum_a U_{\rm C}(r_a)\tau^{(-)}_a.$$

Using the RPA in the coordinate representation for closed-shell nuclei, one can get according to Eqs. (1), (4)–(6) the well-known self-consistency condition [22, 23]

$$v(r)=2F_0n^{(-)}(r); \quad (7)$$

$$n^{(-)}(r)=\langle0|\sum_a\tau^{(3)}_a\delta(\mathbf{r}-\mathbf{r}_a)|0\rangle=n^n(r)-n^p(r),$$

$$n^\beta(r)=\frac{1}{4\pi r^2}\sum_\lambda(2j^\beta_\lambda+1)n^\beta_\lambda(\chi^\beta_\lambda(r))^2, \quad (8)$$

where $n^{(-)}(r)$ is the neutron excess density and n^β_λ are the occupation numbers ($\beta=p,n$). The self-consistency condition relates the symmetry potential to the Landau–Migdal parameter F_0.

The equation of motion for the GT operator $\hat{Y}^{(-)}_\mu=\sum_a(\sigma_\mu)_a\tau^{(-)}_a$ can be derived within the RPA analogously to Eq. (5) [23]:

$$[\hat{H},\hat{Y}^{(-)}_\mu]=\hat{U}^{(-)}_\mu, \quad (9)$$

$$\hat{U}^{(-)}_\mu=\sum_a U_\mu(x_a)\tau^{(-)}_a,\ U_\mu(x) \quad (10)$$
$$=[U_{\rm so}(x),\sigma_\mu]+(2(F_1-F_0)n^{(-)}(r)+U_{\rm C}(r))\sigma_\mu.$$

Equations (5) and (9) allow one to render some relationships useful to check the calculation results for the strength functions within the RPA. The strength function corresponding to the single-particle probing operator $\hat{V}^{(\mp)}=\sum_a V(x_a)\tau^{(\mp)}_a$ is defined as

$$S^{(\mp)}_V(\omega)=\sum_s|\langle s|\hat{V}^{(\mp)}|0\rangle|^2\delta(\omega-\omega_s), \quad (11)$$

with $\omega_s=E_s-E_0$ being the excitation energy of the corresponding isobaric nucleus measured from the ground state of the parent nucleus. Using Eqs. (5) and (11), one gets the relationship

$$S^{(\mp)}_{\rm F}(\omega)=\omega^{-2}S^{(\mp)}_{\rm C}(\omega). \quad (12)$$

Here, the F and C strength functions correspond to the probing operators $\hat{T}^{(\mp)}$ and $\hat{U}^{(\mp)}_{\rm C}$, respectively.

The model-independent non-energy-weighted sum rule (NEWSR) for F(0^+) and GT(1^+) excitations is well known [24]:

$$(\text{NEWSR})_J=\langle0|\left[\hat{G}^{(-)+}_{J\mu},\hat{G}^{(-)}_{J\mu}\right]|0\rangle=(N-Z); \quad (13)$$

$$\hat{G}^{(-)}_{00}=\hat{T}^{(-)},\quad \hat{G}^{(-)}_{1\mu}=\hat{Y}^{(-)}_\mu.$$

The energy-weighted sum rules (EWSR)

$$(\text{EWSR})_J=\langle0|\left[\hat{G}^{(-)+}_{J\mu},\left[\hat{H},\hat{G}^{(-)}_{J\mu}\right]\right]|0\rangle \quad (14)$$

are rather model-dependent and according to Eqs. (5), (9), and (10) are equal to

$$(\text{EWSR})_0=\int U_{\rm C}(r)n^{(-)}(r)d^3r, \quad (15)$$

$$(\text{EWSR})_1=(\text{EWSR})_0-\frac{4}{3}\langle0|\hat{U}_{\rm so}|0\rangle \quad (16)$$
$$+2(F_1-F_0)\int(n^{(-)}(r))^2d^3r,$$

with

$$\langle0|\hat{U}_{\rm so}|0\rangle=4\sum_\beta\sum_\lambda n^\beta_\lambda(j^\beta_\lambda-l^\beta_\lambda)l^\beta_\lambda(l^\beta_\lambda+1)(U_{\rm so})_{\lambda\lambda}.$$

According to Eqs. (5), (13), and (15), the exact (within the RPA) isospin $SU(2)$ symmetry is realized for the model Hamiltonian in question in the limit

$$U_{\rm C} \to \Delta_{\rm C} = (N-Z)^{-1}\int U_{\rm C}(r)n^{(-)}(r)d^3r.$$

In this limit, the energy E_A and the wave function $|A\rangle$ of the "ideal" isobaric analog state (IAS) are $E_A = E_0 + \Delta_{\rm C}$ and $|A\rangle = (N-Z)^{-1/2}\hat{T}^{(-)}|0\rangle$, respectively. The "ideal" IAS exhausts 100% of $(\mathrm{NEWSR})_0$. In the calculations with the use of a realistic Coulomb mean field, the IAS exhausts almost 100% of $(\mathrm{NEWSR})_0$ (with the rest exhausted mainly by the IVMR). Therefore, one can approximately use the isospin classification of the nuclear states. Redistribution of the Fermi strength is caused mainly by the Coulomb mixing of the IAS and the states having the "normal" isospin $T_0 - 1$ ($T_0 = (N-Z)/2$ is the isospin of both the parent-nucleus ground state and its analog state). In the present model, the mixing is due to the difference $U_{\rm C}(r) - \Delta_{\rm C}$. The Wigner $SU(4)$ symmetry is realized in the limit $U_{\rm so} \to 0$, $F_1 \to F_0$, $U_{\rm C} \to \Delta_{\rm C}$. In this limit the energy E_G and the wave function $|G\mu\rangle$ of the "ideal" Gamow–Teller state (GTS) are $E_G = E_A$ and $|G\mu\rangle = (N-Z)^{-1/2}\hat{Y}^{(-)}_\mu|0\rangle$, respectively. Redistribution of the GT strength is mainly due to the spin–orbit part of the mean field.

2.3. The Strength Functions within the Continuum-RPA

The distribution of the particle–hole strength can be calculated within the continuum-RPA making use of the full basis of the single-particle states. Being based on the above-described model Hamiltonian, the CRPA equations for calculations of the F(C) and GT strength functions can be derived using the methods of finite Fermi system theory [21]. Let $\hat{V}^{(\mp)}_{JLS\mu} = \sum_a V_{JLS\mu}(x_a)\tau^{(\mp)}_a$ be the multipole charge-exchange probing operator leading to excitations with angular momentum J and parity $\pi = (-1)^L$. Here, $V_{JLS\mu}(x) = V_{JLS}(r)T_{JLS\mu}(\mathbf{n})$, where $T_{JLS\mu}(\mathbf{n}) = \sqrt{4\pi}\sum_{M'M} C^{J\mu}_{LM'SM}Y_{LM'}\sigma_{SM}$ is the irreducible spin-angular tensor operator with $\sigma_{00} = 1$, $\sigma_{1\mu} = \sigma_\mu$. In particular, we have $V_{000}(r) = 1(U_{\rm C}(r))$, $T_{0000} = 1$ and $V_{101}(r) = 1$, $T_{101\mu} = \sigma_\mu$ for description of F(C) and GT excitations, respectively. After separation of the isospin and spin-angular variables, the strength functions corresponding to the probing operators $\hat{V}^{(\mp)}_{JLSM}$ are determined by the following equations:

$$S^{(\mp)}_{JLS}(\omega) = -\frac{1}{\pi}\mathrm{Im}\sum_{L'S'}\int V_{JLS}(r) \times A^{(\mp)}_{JLS,JL'S'}(r,r';\omega)\tilde{V}^{(\mp)}_{JL'S'}(r',\omega)drdr', \quad (17)$$

$$\tilde{V}^{(\mp)}_{JL'S'}(r,\omega) = V_{JLS}(r)\delta_{LL'}\delta_{SS'} + \frac{2F_{S'}}{4\pi r^2} \times \sum_{L''S''}\int A^{(\mp)}_{JL'S',JL''S''}(r,r';\omega)\tilde{V}^{(\mp)}_{JL''S''}(r',\omega)dr'. \quad (18)$$

Here, $\tilde{V}^{(\mp)}_{JLS}(r,\omega)$ are the effective radial probing operators, $F_{S=0,1}$ are the interaction intensities of Eq. (4), and $(4\pi rr')^{-2}A^{(\mp)}_{JLS,JL'S'}(r,r';\omega)$ are the radial free-particle–hole propagators:

$$A^{(-)}_{JLS,JL'S'}(r_1,r_2;\omega) = 4\pi\sum_{\nu\pi}\frac{\langle(\pi)||T_{JLS}||(\nu)\rangle\langle(\pi)||T_{JL'S'}||(\nu)\rangle^*}{2J+1} \times\{n_\nu\chi_\nu(r_1)\chi_\nu(r_2)g_{(\pi)}(r_1,r_2;\varepsilon_\nu+\omega) + n_\pi\chi_\pi(r_1)\chi_\pi(r_2)g_{(\nu)}(r_1,r_2;\varepsilon_\pi-\omega)\}. \quad (19)$$

The expression for $A^{(+)}$ can be obtained from Eq. (19) by the substitution $\pi \leftrightarrow \nu$ with ω being the excitation energy of the daughter nucleus in the β^+ channel measured from the ground state of the parent nucleus. For $J^\pi = 0^+$ excitations ($L = S = 0$), there is only one nonzero propagator $A^{(\mp)}_{000,000}$ and, therefore, Eqs. (17), (18) have the simplest form. Such a form has been used explicitly in [16] for describing IAR and IVMR. For $J^\pi = 1^+$ excitations ($S = 1$), propagators $A^{(\mp)}_{1L1,1L'1}$ are diagonal with respect to S and, therefore, Eq. (18) is the system of equations for effective operators $\tilde{V}^{(\mp)}_{101}$ and $\tilde{V}^{(\mp)}_{121}$. As a result, the spin-quadrupole part of the particle–hole interaction contributes to the formation of the GT strength function, as follows from Eqs. (17), (18). The use of only diagonal (with respect to L) propagators $A^{(\mp)}_{JL1,JL1}$ corresponds to the so-called "symmetric" approximation. In particular, this approximation was used in [15, 17] to describe the monopole and dipole spin-flip charge-exchange excitations. As a rule, the use of the "symmetric" approximation leads just to small errors in calculations of the strength functions $S^{(\mp)}_{JLS}$ in the vicinity of the respective giant resonance (see, e.g., [25]). Nevertheless, the detailed description of the low-energy part of the GT strength distribution appeals to the "nonsymmetric" approximation.

The Fermi and GT strength functions $S^{(\mp)}_J(\omega)$ (hereafter, indices $L = 0, S = J$ are omitted) calculated within the CRPA for not overly high excitation energies (including the region of IAR and GTR) reveal narrow resonances corresponding to the particle–hole-type doorway states. Therefore, the

following parametrization holds in the vicinity of each doorway state:

$$S_J^{(\mp)}(\omega) \simeq -\frac{1}{\pi}\mathrm{Im}\frac{(r_J^{(\mp)})_s}{\omega-\omega_s+\frac{i}{2}\Gamma_s}. \qquad (20)$$

Here, $(r_J^{(\mp)})_s$, ω_s, and Γ_s are the strength, energy, and escape width of the doorway state, respectively. The values of $x_J^{\mathrm{tot}} = x_J^{(-)} - x_J^{(+)} = (\int S_J^{(-)}(\omega)d\omega - \int S_J^{(+)}(\omega)d\omega)/(\mathrm{NEWSR})_J$, $y_J^{\mathrm{tot}} = y_J^{(-)} + y_J^{(+)} = (\int \omega S_J^{(-)}(\omega)d\omega + \int \omega S_J^{(+)}(\omega)d\omega)/(\mathrm{EWSR})_J$ are useful for comparison with unity to check the quality of the calculation results. Due to the relations given in Eqs. (11) and (20), the ratio of the C to the F strengths has to be ω_s^2 for each doorway state.

2.4. Isospin Splitting of the GT Strength Distribution

Due to the high degree of the isospin conservation in nuclei, the GT states are classified with the isospin T_0-1, T_0, T_0+1. In particular, T_0 components of the GT strength function can be considered as the isobaric analog of the isovector $M1$ states in the respective parent nucleus:

$$|M,T_0\rangle = (2T_0)^{-1/2}\hat{T}^{(-)}|M1,T_0\rangle. \qquad (21)$$

According to the definition (11), the strength function of the T_0 components is proportional to the strength function of the isovector $M1$ giant resonance in the parent nucleus:

$$S_{T_0}^{(-)}(\omega) = (2T_0)^{-1}S_{M1}^{(0)}(\omega' = \omega - \Delta_{\mathrm{C}}). \qquad (22)$$

Here, $S_{M1}^{(0)}(\omega')$ is the $M1$ strength function corresponding to the probing operator $\hat{M}_\mu^{(0)} = \sum_a (\sigma_\mu)_a \tau_a^{(3)}$ and depending on the excitation energy in the daughter nucleus. Within the CRPA, the $M1$ strength function is calculated using relations that are similar to those of Eqs. (17), (18) and can be found, e.g., in [26].

According to Eq. (22), a noticeable effect of the isospin splitting of the GT strength function takes place only for nuclei with not too large a neutron excess. The suppression of the T_0 and T_0+1 components is the reason why the GT states $|s\rangle$, obtained within the RPA, are usually assigned the isospin T_0-1, although the RPA GT states do not have a definite isospin. In fact, the states $|s\rangle$ and $|M,T_0\rangle$ are nonorthogonal:

$$\langle M,T_0|s\rangle = (2T_0)^{-1/2} \qquad (23)$$
$$\times \langle M1,T_0|\left[\hat{T}^{(+)},\hat{Q}_s^{(-)}\right]|0\rangle = b_M^s,$$

where $\hat{Q}_s^{(-)}$ is an RPA boson-type operator corresponding to the creation of a collective GT state $|s\rangle$. Therefore, one has to project $|s\rangle$ states onto the space of the GT states with the isospin $T_0-1=T_<$ by means of subtraction of the admixtures of T_0 states to force the relevant orthogonality condition:

$$|s,T_0-1\rangle = \left(1-\sum_M (b_M^s)^2\right)^{-1/2} \qquad (24)$$
$$\times\left(|s\rangle - \sum_M b_M^s|M,T_0\rangle\right).$$

This equation is valid under the assumption that the integral relative strength $x_> = \sum_M x_M$ of the $T_0 = T_>$ component is small compared to unity. In this case, taking into account the T_0+1 component is even more unimportant. We restrict the further analysis to the approximation that there is only the GT state in the respective RPA calculations exhausting 100% of the NEWSR and, therefore, this state can be considered as the "ideal" GTS. Under these assumptions, one has

$$b_M^s = (2T_0)^{-1/2}\langle M,T_0|\hat{Y}^{(-)}|0\rangle = x_M^{1/2}, \qquad (25)$$
$$x_< = 1 - x_>.$$

Having averaged the exact nuclear Hamiltonian over the state $|s,T_0\rangle$ in the form of Eq. (24), one gets

$$\omega_< = x_<^{-1}\left(x_s\omega_s - \sum_M x_M\omega_M\right). \qquad (26)$$

According to the approximate relations (25) and (26), the relative strength and the energy of the T_0-1 GTS diminish as compared with the respective RPA values. The decrease is determined by the zeroth and first moments of the strength function of the isovector $M1$ GR in the parent nucleus:

$$x_> = (N-Z)^{-2}\int S_{M1}^{(0)}(\omega')d\omega', \qquad (27)$$
$$\sum_M \omega_M x_M = (N-Z)^{-2}\int S_{M1}^{(0)}(\omega')\omega' d\omega'.$$

These relations again lead to the conclusion that the value $x_> \simeq 2A^{1/3}(N-Z)^{-2}$ is rather small even if the value $(N-Z)$ is not large. Only for nuclei with a minimal neutron excess (a few units) could all three isospin components of the GT strength have comparable strengths.

3. THE STRENGTH FUNCTIONS IN OPEN-SHELL NUCLEI

3.1. The Model Hamiltonian

The interaction $\hat{H}_{p-p}$ in the particle–particle channels has to be included in the model Hamiltonian

for nuclei with open shells, in order to take the effects of nucleon pairing into consideration. We choose the interaction in the following separable form (as is used in the BCS model) in both the neutral and the charge-exchange particle–particle channels with the total angular momentum and parity of the nucleon pair being $J^\pi = 0^+, 1^+$ ($L = 0, S = J$):

$$\hat{H}_{p-p} = -\frac{1}{2}\sum_{J\mu} G_J \sum_{\substack{\beta=p,n\\ \beta'=p,n}} (\hat{P}^{J\mu}_{\beta\beta'})^+ \hat{P}^{J\mu}_{\beta\beta'}. \quad (28)$$

Here, $G_{J=0,1}$ are the intensities of the particle–particle interaction, and $P^{J\mu}$ is the annihilation operator for the nucleon pair:

$$\hat{P}^{J\mu}_{\beta\beta'} = \sum_{\lambda\lambda'} (\chi^\beta_\lambda \chi^{\beta'}_{\lambda'}) P^{J\mu}_{\beta\beta',\lambda\lambda'}, \quad (29)$$

$$P^{J\mu}_{\beta\beta',\lambda\lambda'} = t^{(J)}_{(\lambda)(\lambda')} \sum_{mm'} (J\mu | j^\beta_\lambda m j^{\beta'}_{\lambda'} m') a^{\beta'}_{\lambda' m'} a^\beta_{\lambda m},$$

where $a_{\lambda m}(a^+_{\lambda m})$ is the annihilation (creation) operator of the nucleon in the state with the quantum numbers λm (m is the projection of the particle angular momentum). The interaction (28) preserves the isospin symmetry of the model Hamiltonian.

We use the Bogolyubov transformation to describe the nucleon pairing in the neutral channels in terms of quasiparticle creation (annihilation) operators $\alpha^+_{\lambda m}(\alpha_{\lambda m})$ (see, e.g., [27]). As a result, we get the following model Hamiltonian to describe F(C) and GT excitations in the β^- channel within the quasiboson version of the pn-QRPA:

$$\hat{H} = \hat{H}_0 + \hat{H}_{p-h} + \hat{H}_{p-p}; \quad (30)$$

$$\hat{H}_0 = \sum_{\beta=p,n}\sum_{\lambda m} E^\beta_\lambda (\alpha^\beta_{\lambda m})^+ \alpha^\beta_{\lambda m} - \frac{1}{2}(\mu_p - \mu_n)\hat{T}^{(3)}.$$

Here, $E^\beta_\lambda = \sqrt{(\xi^\beta_\lambda)^2 + \Delta^2_\beta}$ is the quasiparticle energy; $\xi^\beta_\lambda = \varepsilon^\beta_\lambda - \mu_\beta$; and μ_β and Δ_β are the chemical potential and the energy gap, respectively, which are determined from the BCS-model equations:

$$N_\beta = \sum_\lambda (2j^\beta_\lambda + 1)(v^\beta_\lambda)^2, \quad (31)$$

$$\Delta_\beta = G_0 \sum_\lambda (2j^\beta_\lambda + 1) u^\beta_\lambda v^\beta_\lambda$$

with N_β being the corrsponding particle number, $v^2_\lambda = (1 - \xi_\lambda/E_\lambda)/2$, and $u^2_\lambda = 1 - v^2_\lambda$.

The total interaction Hamiltonian in both particle–hole (4) and particle–particle (28) channels can be expressed in terms of the quasiparticle pn-pair creation and annihilation operators which obey approximately the bosonic commutation rules:

$$A^{J\mu}_{\pi\nu} = \sum_{mm'} (J\mu | j_\pi m j_\nu m') \alpha_{\nu m'} \alpha_{\pi m}, \quad (32)$$

$$[A^{J'\mu'}_{\pi'\nu'}, (A^{J\mu}_{\pi\nu})^+] = \delta_{\pi\pi'}\delta_{\nu\nu'}\delta_{JJ'}\delta_{\mu\mu'}.$$

The explicit expressions for the interactions are

$$\hat{H}_{p-h} = \sum_{J\mu} \frac{2F_J}{4\pi} \sum_{\pi\nu\pi'\nu'} (\chi_\pi \chi_\nu \chi_{\pi'} \chi_{\nu'}) (Q^{J\mu}_{\pi\nu})^+ Q^{J\mu}_{\pi'\nu'}, \quad (33)$$

$$\hat{H}_{p-p} = -\sum_{J\mu} G_J \sum_{\pi\nu\pi'\nu'} (\chi_\pi \chi_\nu)(\chi_{\pi'}\chi_{\nu'}) (P^{J\mu}_{\pi\nu})^+ P^{J\mu}_{\pi'\nu'}, \quad (34)$$

where

$$Q^{J\mu}_{\pi\nu} = t^{(J)}_{(\pi)(\nu)} (u_\pi v_\nu A^{J\mu}_{\pi\nu} + v_\pi u_\nu (\tilde{A}^{J\mu}_{\pi\nu})^+),$$

$$P^{J\mu}_{\pi\nu} = t^{(J)}_{(\pi)(\nu)} (u_\pi u_\nu A^{J\mu}_{\pi\nu} - v_\pi v_\nu (\tilde{A}^{J\mu}_{\pi\nu})^+),$$

$$\tilde{A}^{J\mu}_{\pi\nu} = (-1)^{J+\mu} A^{J\,-\mu}_{\pi\nu},$$

$$(\chi_\pi \chi_\nu \chi_{\pi'} \chi_{\nu'}) = \int \chi_\pi \chi_\nu \chi_{\pi'} \chi_{\nu'} r^{-2} dr.$$

3.2. The Symmetries of the Model Hamiltonian and Sum Rules

Due to the isobaric invariance of the particle–particle interaction (28), Eq. (5) still holds and leads exactly to the same self-consistency condition of Eq. (7) with the only difference that the proton and neutron densities are determined with account of the particle redistribution caused by the nucleon pairing:

$$n^\beta(r) = \frac{1}{4\pi r^2} \sum_\lambda (2j^\beta_\lambda + 1)(v^\beta_\lambda)^2 (\chi^\beta_\lambda(r))^2. \quad (35)$$

The direct realization of Eq. (5) within the pn-QRPA with use made of Eqs. (30)–(34) and $\hat{T}^{(-)} = \sum_{\pi\nu}(\chi_\pi\chi_\nu)(Q^{00}_{\pi\nu})^+$ also leads to the self-consistency condition of Eq. (7), provided that the full basis of the single-particle states for neutron and proton subsystems is used along with Eq. (2) for the radial overlap integrals for the proton and neutron wave functions. The consistent mean Coulomb field $U_C(r)$ and $(EWSR)_0$ of Eq. (15) are determined by the proton and neutron excess densities of Eq. (35), respectively.

Equation (12), relating the F and C strength functions, also holds within the pn-QRPA if all the above-mentioned conditions are fulfilled. In particular, the use of a truncated basis of the single-particle states within the BCS model leads to an unphysical violation of the isospin symmetry. In such a case the degree

of violating Eq. (12) can be considered as a measure of the violation.

The equation of motion for the GT operator $\hat{Y}_\mu^{(-)}$ with the nucleon pairing taken into consideration is somewhat modified as compared to Eqs. (9), (10). According to Eqs. (30)–(34) and making use of the full basis of the single-particle states along with Eq. (2) for the radial overlap integrals, we get within the pn-QRPA ($\hat{Y}_\mu^{(-)} = \sum_{\pi\nu}(\chi_\pi\chi_\nu)(Q_{\pi\nu}^{1\mu})^+$)

$$[\hat{H}, \hat{Y}_\mu^{(-)}] = (\hat{U}_\mu^{(-)})_{p-h} + (\hat{U}_\mu^{(-)})_{p-p}. \qquad (36)$$

The operator $(\hat{U}_\mu^{(-)})_{p-h}$ is defined by expression (10), in which both the neutron excess and the proton densities are used according to Eq. (35). The expression for $(\hat{U}_\mu^{(-)})_{p-p}$ has the form

$$(\hat{U}_\mu^{(-)})_{p-p} = \frac{G_0 - G_1}{G_0}(\Delta_n(\hat{P}_{pn}^{1\mu})^+ - \Delta_p\tilde{\hat{P}}_{pn}^{1\mu}). \quad (37)$$

According to Eqs. (10), (36), and (37) the expression for $(\mathrm{EWSR})_1$ consists of two terms, the former, $(\mathrm{EWSR})_1^{p-h}$, coinciding with Eq. (16) with the nucleon densities and the occupation numbers appropriately modified by the nucleon pairing, and the latter being due to the nucleon pairing only:

$$(\mathrm{EWSR})_1^{p-p} = \frac{G_0 - G_1}{G_0}\frac{\Delta_n^2 + \Delta_p^2}{G_0}. \qquad (38)$$

In the $SU(4)$-symmetry limit, one has the equality $(\mathrm{EWSR})_1 = (\mathrm{EWSR})_0$, which also holds for double-closed-shell nuclei.

3.3. The pn-QRPA Equations

The system of the homogeneous equations for the forward and backward amplitudes $X_{\pi\nu}^J(s) = \langle s, J\mu|(A_{\pi\nu}^{J\mu})^+|0\rangle$ and $Y_{\pi\nu}^J(s) = \langle s, J\mu|\tilde{A}_{\pi\nu}^{J\mu}|0\rangle$, respectively, is usually solved to calculate the energies ω_s and the wave functions $|s, J\mu\rangle$ of the isobaric nucleus within the quasiboson version of the pn-QRPA (see, e.g., [2]). In particular, the system of equations for the amplitudes follows from the equations of motion for the operators A^+ and $\tilde{A}$ making use of the Hamiltonian (30), (33), (34). Instead, we rewrite the system in equivalent terms of the elements $r^{-2}\varrho_i^J(s,r)$ of the radial transition density. The elements are determined by the amplitudes $X(s)$ and $Y(s)$ as follows:

$$\varrho_i^J(s,r) = \sum_{\pi\nu} t_{(\pi)(\nu)}^{(J)}\chi_\pi(r)\chi_\nu(r)\langle s, J\mu|\left(R_{\pi\nu}^{J\mu}\right)_i|0\rangle, \qquad (39)$$

$$i = 1, 2, 3, 4,$$

$$\left(R_{\pi\nu}^{J\mu}\right)_1 = \left(Q_{\pi\nu}^{J\mu}\right)^+, \quad \left(R_{\pi\nu}^{J\mu}\right)_2 = \tilde{Q}_{\pi\nu}^{J\mu}, \qquad (40)$$
$$\left(R_{\pi\nu}^{J\mu}\right)_3 = \tilde{P}_{\pi\nu}^{J\mu}, \quad \left(R_{\pi\nu}^{J\mu}\right)_4 = \left(P_{\pi\nu}^{J\mu}\right)^+,$$

where the operators P and Q are defined after Eqs. (33), (34). According to the definition (39), the elements ϱ_1, ϱ_2, ϱ_3, ϱ_4 can be called, respectively, the particle–hole, hole–particle, hole–hole, and particle–particle components of the transition density, which can generally be considered as a four-dimensional vector $\{\varrho_i^J\}$. In particular, the particle–hole strength of the state $|s, J\mu\rangle$ corresponding to a probing operator $\hat{V}_{J\mu}^{(-)}$ is determined by the element ϱ_1^J:

$$(r_J^{(-)})_s = \left(4\pi\int \varrho_1^J(s,r)V_J(r)dr\right)^2$$

[compare to Eq. (20)]. The pn-QRPA system of equations for the elements ϱ_i^J is the following (hereafter only the "symmetric" approximation is considered):

$$\varrho_i^J(s,r) = \frac{1}{4\pi}\sum_k \int A_{J,ik}^{(-)}(r, r_1; \omega = \omega_s) \qquad (41)$$
$$\times F_k^J(r_1, r_2)\varrho_k^J(s, r_2)dr_1dr_2,$$

$$F_1^J(r_1, r_2) = F_2^J(r_1, r_2) = 2F_J\frac{\delta(r_1 - r_2)}{r_1 r_2}, \qquad (42)$$
$$F_3^J(r_1, r_2) = F_4^J(r_1, r_2) = -4\pi G_J,$$

$$A_{J,ik}^{(-)}(r_1, r_2; \omega) = \sum_{\pi\nu}\left(t_{(\pi)(\nu)}^{(J)}\right)^2\chi_\pi(r_1) \qquad (43)$$
$$\times \chi_\nu(r_1)\chi_\pi(r_2)\chi_\nu(r_2)A_{\pi\nu,ik}^{(-)}(\omega),$$

$$A_{\pi\nu,11}^{(-)} = \frac{u_\pi^2 v_\nu^2}{\{-\}} - \frac{u_\nu^2 v_\pi^2}{\{+\}},$$
$$A_{\pi\nu,12}^{(-)} = u_\pi v_\pi v_\nu u_\nu\left(\frac{1}{\{-\}} - \frac{1}{\{+\}}\right),$$
$$A_{\pi\nu,14}^{(-)} = u_\pi v_\pi\left(\frac{v_\nu^2}{\{-\}} + \frac{u_\nu^2}{\{+\}}\right),$$
$$A_{\pi\nu,13}^{(-)} = u_\nu v_\nu\left(\frac{u_\pi^2}{\{-\}} + \frac{v_\pi^2}{\{+\}}\right),$$
$$A_{\pi\nu,22}^{(-)} = \frac{v_\pi^2 u_\nu^2}{\{-\}} - \frac{v_\nu^2 u_\pi^2}{\{+\}},$$
$$A_{\pi\nu,23}^{(-)} = u_\pi v_\pi\left(\frac{u_\nu^2}{\{-\}} + \frac{v_\nu^2}{\{+\}}\right),$$
$$A_{\pi\nu,24}^{(-)} = u_\nu v_\nu\left(\frac{v_\pi^2}{\{-\}} + \frac{u_\pi^2}{\{+\}}\right),$$
$$A_{\pi\nu,33}^{(-)} = \frac{u_\pi^2 u_\nu^2}{\{-\}} - \frac{v_\nu^2 v_\pi^2}{\{+\}},$$

$$A^{(-)}_{\pi\nu,44} = \frac{v^2_\pi v^2_\nu}{\{-\}} - \frac{u^2_\nu u^2_\pi}{\{+\}},$$
$$A^{(-)}_{\pi\nu,ik} = A^{(-)}_{\pi\nu,ki}, \quad A^{(-)}_{\pi\nu,34} = A^{(-)}_{\pi\nu,12},$$

where $\{-\} = \omega^{(-)} - E_\pi - E_\nu$, $\{+\} = \omega^{(-)} + E_\pi + E_\nu$, $\omega = \omega^{(-)} + \mu_p - \mu_n$ gives the excitation energy with respect to the mother-nucleus ground-state energy. All actual calculations in the present work are performed in terms of ω, whereas the experimental energy difference between the ground states of daughter and mother nuclei is used to represent the results in terms of the daughter-nucleus excitation energy E_x.

According to Eq. (41), schematically represented as $\varrho^J_i = \sum_k A^{(-)}_{J,ik}(\omega = \omega_s) F^J_k \varrho^J_k$, the 4×4 matrix $(4\pi r^2_1 r^2_2)^{-1} A^{(-)}_{J,ik}(r_1, r_2; \omega)$ is the radial part of the free two-quasiparticle propagator, whereas the quantities $v^J_k(s, r_1) = \int F^J_k(r_1, r_2)\varrho^J_k(s, r_2)dr_2$ are the elements of the radial transition potential. To describe the excitations in the β^+ channel, one should use the same system (41) with $A^{(-)}$ superseded by $A^{(+)}$. The expression for the particle–hole propagator $A^{(+)}$ can be obtained from Eqs. (43) by the substitutions $\nu \leftrightarrow \pi$, $n \leftrightarrow p$. In the case of neglecting nucleon pairing ($G_J = 0$), the system of Eqs. (41) decouples and $A^{(-)}_{J,11}$ becomes determined by Eq. (19) taken in the "symmetric" approximation (it can be shown easily using the spectral expansion for the radial Green's functions $g_{(\lambda)}(r, r'; \varepsilon)$).

The expression for the elements of the free two-quasiparticle propagator (43) can be obtained by making use of the regular and anomalous single-particle Green's functions for Fermi systems with nucleon pairing in an analogous way as was done in monograph [21] to describe the Fermi system response to a single-particle probing operator acting in the neutral channel. Namely, the matrix A can be depicted as a set of diagrams shown in Fig. 1. To illustrate this statement, let us consider the system of equations for the elements of the transition potential v_i. The system follows from Eq. (41) and can be schematically represented as $v_i = \sum_k F_i A^{(-)}_{ik}(\omega = \omega_s)v_k$.

Using expression (43) for the free two-quasiparticle propagator, one can obtain a system of inhomogeneous equations of the pn-QRPA to calculate the strength functions (11) with the full basis of the single-particle states taken into consideration for the particle–hole channel. The system has a form similar to that of Eqs. (17), (18) taken in the "symmetric" approximation:

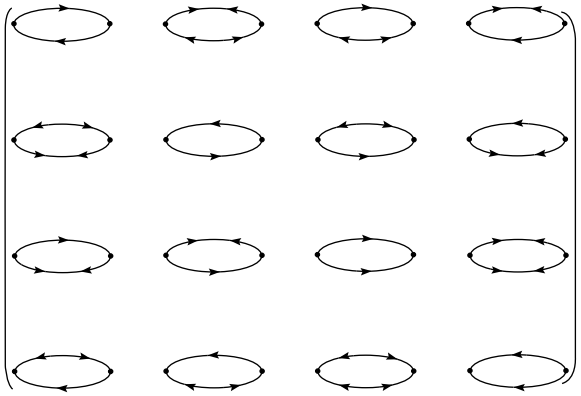

Fig. 1. Diagrams corresponding to elements $A^{(-)}_{\pi\nu,ik}$ of the free two-quasiparticle propagator of Eq. (43). Upper (lower) lines correspond to propagation of proton (neutron) quasiparticles.

$$S^{(\mp)}_J(\omega) = -\frac{1}{\pi}\mathrm{Im}\sum_i \int V_J(r) \tag{44}$$
$$\times A^{(\mp)}_{J,1i}(r, r'; \omega)\tilde{V}^{(\mp)}_{J,i}(r', \omega)drdr',$$
$$\tilde{V}^{(\mp)}_{J,i}(r, \omega) = V_J(r)\delta_{i1} + \frac{1}{4\pi r^2} \tag{45}$$
$$\times \sum_k \int F^J_i(rr_1)A^{(\mp)}_{J,ik}(r_1, r_2; \omega)\tilde{V}^{(\mp)}_{J,k}(r_2, \omega)dr_1dr_2.$$

The same as in the case without pairing, the residues $(r^{(\mp)}_J)_s$ in poles of the strength functions [see Eq. (20)] coincide with the particle–hole strengths of the pn-QRPA excitations corresponding to the probing operators $\hat{V}^{(\mp)}_{J\mu}$.

3.4. Strength Functions in Single-Open-Shell Nuclei

We restrict further consideration to the case of single-open-shell nuclei. For this case, the system of Eqs. (45) for the radial effective operators $\tilde{V}^{(\mp)}_{J,i}(r, \omega)$ is noticeably simplified. Let us consider for definiteness the excitations in the β^- channel for a nucleus in which only the proton pairing is realized ($\Delta_n = 0$). Then, according to Eq. (43), the elements $A^{(-)}_{J,12}, A^{(-)}_{J,13}, A^{(-)}_{J,24}, A^{(-)}_{J,34}$ of the free two-quasi-particle propagator equal zero and the system (45) reduces to a system of equations for only two radial effective operators $\tilde{V}^{(-)}_{J,1}$ and $\tilde{V}^{(-)}_{J,4}$. The elements $A^{(-)}_{J,11}, A^{(-)}_{J,14}, A^{(-)}_{J,44}$ entering this system can be rewritten in a form that allows one to take the

full basis of the single-particle states in the particle–hole channel for both subsystems. To get this form, one should set $E_\pi = |\varepsilon_\pi - \mu_\pi|$ for $E_\pi > k\Delta_p$ ($k \gg 1$) and use the spectral expansion for the radial single-particle Green's functions in Eq. (43). As a result, we come to the following representation for $A^{(-)}_{J,11}$:

$$A^{(-)}_{J,11}(r_1, r_2; \omega) \tag{46}$$
$$= \sum_{\nu(\pi)} \left(t^{(J)}_{(\pi)(\nu)}\right)^2 n_\nu \chi_\nu(r_1)\chi_\nu(r_2)$$
$$\times g_{(\pi)}(r_1, r_2; \varepsilon_\nu + \omega) + \sum_{(\nu)\pi} \left(t^{(J)}_{(\pi)(\nu)}\right)^2 v^2_\pi \chi_\pi(r_1)$$
$$\times \chi_\pi(r_2) g_{(\nu)}(r_1, r_2; \mu_\pi - E_\pi - \omega)$$
$$+ \sum_{\nu\pi}{}' \left(t^{(J)}_{(\pi)(\nu)}\right)^2 n_\nu \chi_\nu(r_1)\chi_\nu(r_2)\chi_\pi(r_1)\chi_\pi(r_2)$$
$$\times \left\{ \frac{u^2_\pi}{\omega - \mu_p - E_\pi + \varepsilon_\nu} + \frac{v^2_\pi}{\omega - \mu_p + E_\pi + \varepsilon_\nu} \right.$$
$$\left. - \frac{1}{\omega - \varepsilon_\pi + \varepsilon_\nu} \right\},$$

where $\sum'_{\nu\pi}$ denotes the sum taken over the proton states with $E_\pi < k\Delta_p$ only. For the consistency of the consideration, the same truncation should be used in realization of the BCS model according to the second of Eqs. (31). The corresponding expressions for the elements $A^{(-)}_{J,14}$ and $A^{(-)}_{J,44}$ are

$$A^{(-)}_{J,14}(r_1, r_2; \omega) \tag{47}$$
$$= -\sum_{(\nu)\pi}{}' \left(t^{(J)}_{(\pi)(\nu)}\right)^2 u_\pi v_\pi \chi_\pi(r_1)\chi_\pi(r_2)$$
$$\times g_{(\nu)}(r_1, r_2; \mu_\pi - E_\pi - \omega)$$
$$+ \sum_{\nu\pi}{}' \left(t^{(J)}_{(\pi)(\nu)}\right)^2 n_\nu \chi_\nu(r_1)\chi_\nu(r_2)\chi_\pi(r_1)\chi_\pi(r_2)$$
$$\times \left\{ \frac{1}{\omega - \mu_p - E_\pi + \varepsilon_\nu} - \frac{1}{\omega - \mu_p + E_\pi + \varepsilon_\nu} \right\},$$
$$A^{(-)}_{J,44}(r_1, r_2; \omega) \tag{48}$$
$$= \sum_{(\nu)\pi}{}' \left(t^{(J)}_{(\pi)(\nu)}\right)^2 u^2_\pi \chi_\pi(r_1)\chi_\pi(r_2)$$
$$\times g_{(\nu)}(r_1, r_2; \mu_\pi - E_\pi - \omega)$$
$$+ \sum_{\nu\pi}{}' \left(t^{(J)}_{(\pi)(\nu)}\right)^2 n_\nu \chi_\nu(r_1)\chi_\nu(r_2)\chi_\pi(r_1)\chi_\pi(r_2)$$
$$\times \left\{ \frac{v^2_\pi}{\omega - \mu_p - E_\pi + \varepsilon_\nu} + \frac{u^2_\pi}{\omega - \mu_p + E_\pi + \varepsilon_\nu} \right\}.$$

Equations (44)–(48) realize a continuum version of the pn-QRPA (pn-QCRPA) on the truncated basis of the BCS problem in proton-open-shell nuclei.

To go to the case where only the neutron pairing is realized, Eqs. (46)–(48) should be changed by the substitution $\pi \leftrightarrow \nu$, $p \leftrightarrow n$, $\omega \to -\omega$. As before, the expression for the elements of the free two-quasiparticle propagator $A^{(+)}$ can be obtained from the corresponding elements $A^{(-)}$ by the substitution $\pi \leftrightarrow \nu$, $p \leftrightarrow n$.

4. CALCULATION RESULTS

4.1. Choice of Model Parameters

Parametrization of the isoscalar part of the mean field $U_0(x)$, along with the values of the parameters used in the calculations, has been described in detail in [28]. The dimensionless intensities f_J of the Landau–Migdal forces of Eq. (4) are chosen as usual: $F_J = f_J \cdot 300$ MeV fm^3. The value $f_0 = f' = 1.0$ of the parameter f' determining the symmetry potential according to Eq. (7) is also taken from [28], where the experimental nucleon separation energies have been satisfactorily described for closed-shell subsystems in a number of nuclei. The value of the dimensionless intensity $f_1 = g'$ of the spin-isovector part of the Landau–Migdal forces $g' = 0.8$ is chosen to reproduce within the CRPA the experimental energy of the GTR in the ^{208}Pb parent nucleus [15].

The strength of the monopole particle–particle interaction G_0 is chosen to reproduce the experimental pairing energies [actually, we identify the pairing energy with Δ, obtained by solving the BCS-model Eqs. (31)]. The summation in the second of the equations is limited to an interval of 7 MeV above and below the Fermi level. The same truncation is used in the expressions like (46)–(48) for the elements of the free two-quasiparticle propagator. Comparing the calculated value of the nucleon separation energy $B^{\rm calc}_\beta \simeq -\mu_\beta + \Delta_\beta$ with the corresponding experimental one can be considered as a test of the version of the BCS model used. The parameters of the BCS model, along with $B^{\rm calc}_\beta$ and $B^{\rm exp}_\beta$, are listed in Table 1. Note also that the strength of the spin–spin particle–particle interaction G_1 is chosen equal to G_0, which seems close to the realistic ones used in the literature. Such a choice allows us to simplify the calculation control using the $(\mathrm{EWSR})_1$, because the "particle–particle" part of this sum rule goes to zero in accordance with Eq. (38). Another reason for the choice is the "soft" spin–isospin $SU(4)$ symmetry, which is roughly realized in nuclei (see, e.g., [29]).

Table 1. Calculated values of the pairing gap Δ_β along with the calculated and experimental proton and neutron separation energies $B_{p,n}^{\mathrm{calc,\,exp}}$. The monopole pairing strength G_0 is also given (all values are given in MeV)

Nucleus	G_0A	Δ_β	B^{calc}		B^{exp}	
			n	p	n	p
^{90}Zr	14.0	1.15	11.5	8.2	11.98	8.36
^{112}Sn	11.5	1.3	10.9	7.5	10.79	7.56
^{114}Sn	11.5	1.4	10.7	8.3	10.30	8.48
^{116}Sn	11.5	1.3	9.9	9.1	9.56	9.28
^{118}Sn	11.5	1.4	9.7	9.9	9.33	10.00
^{120}Sn	11.5	1.4	9.4	10.7	9.11	10.69
^{122}Sn	11.5	1.4	9.1	11.5	8.81	11.4
^{124}Sn	11.5	1.2	8.7	12.3	8.49	12.10

Table 2. Calculated characteristics of the Fermi strength distribution along with respective experimental data [3, 4, 7] (see the text for details)

Parent nucleus	x, %			y, %			E_{IAR}, MeV		$\bar{E}_{\mathrm{IVMR}}$, MeV
	IAR	high	(+)	IAR	high	(+)	calc.	exp.	
^{90}Zr	98.6	1.5	0.5	94.2	4.2	0.9	4.6	5.0	27.1
^{112}Sn	97.8	2.4	0.6	92.9	5.6	0.7	5.6	6.2	25.0
^{114}Sn	98.0	2.4	0.5	93.5	5.5	0.7	6.8	7.3	25.3
^{116}Sn	97.3	2.4	0.4	93.2	5.4	0.5	7.8	8.4	25.5
^{118}Sn	97.7	2.4	0.3	93.9	5.3	0.5	8.8	9.3	26.0
^{120}Sn	97.6	2.4	0.3	93.9	5.2	0.4	9.7	10.2	26.4
^{122}Sn	97.5	2.4	0.2	94.0	5.2	0.3	10.7	11.2	26.8
^{124}Sn	96.8	2.5	0.2	93.4	5.2	0.3	11.7	12.2	27.3
^{208}Pb	94.4	6.2	0.2	89.8	6.2	0.2	14.4	15.1	32.5

4.2. F(C) Strength Functions

The F(C) strength functions have been calculated within the CRPA for the ^{208}Pb parent nucleus according to Eqs. (17), (18) and within the *pn*-QCRPA for ^{90}Zr and tin isotopes according to Eqs. (44), (45) or their modifications. The "cutoff" parameter $k = 3$ was used in calculations of the radial propagators of Eqs. (46)–(48). All the above-mentioned equations have been taken for $J = 0$. The following characteristics of the F strength distribution have been deduced from the calculated F strength functions: the IAR energy E_{IAR}; the mean energy $\bar{E}^{(-)}_{\mathrm{IVMR}}$ of the IVMR$^{(-)}$; relative Fermi strength x for three energy intervals: the vicinity of the IAR, IVMR$^{(-)}$, and IVMR$^{(+)}$; relative energy-weighted Fermi strength y for these three energy regions. As for the low-energy interval, for all nuclei in question, the values of x are below 0.1% (except for ^{90}Zr, where $x \simeq 0.2\%$). The value of $(\mathrm{EWSR})_0$ entering the definition of y has been calculated according to Eq. (15) with the nucleon densities modified by the nucleon pairing. All the characteristics of the Fermi strength distribution are listed in Table 2 along with the experimental IAR energies. To check the self-consistency of the model, the parameter

$$z = \left| \frac{\int S_{\mathrm{C}}^{(-)}(\omega) d\omega}{\int S_{\mathrm{F}}^{(-)}(\omega)\omega^2 d\omega} - 1 \right|$$

has also been calculated.

Table 3. Calculated characteristics of the Gamow–Teller strength distribution along with respective experimental data [3, 4, 7] (see the text for details)

Parent nucleus	x, %				y, %				E_{GTR}, MeV		$\bar{\Gamma}_{\mathrm{GTR}}$, MeV	
	low	GTR	high	(+)	low	GTR	high	(+)	calc.	exp.	calc.	exp.
^{90}Zr	14.8	76.5	9.1	4.1	6.7	79.3	8.2	2.4	8.8 (8.4)	8.8 ± 0.1	3.1 (2.7)	4.8 ± 0.2
^{112}Sn	21.5	77.1	7.5	2.1	13.1	72.6	11.8	1.9	9.2 (9.2)	8.94 ± 0.25	3.4 (2.8)	4.8 ± 0.3
^{114}Sn	20.6	75.6	6.9	3.8	12.4	72.8	11.3	1.6	9.9 (9.5)	9.39 ± 0.25	4.4 (2.8)	5.6 ± 0.3
^{116}Sn	17.6	74.8	7.1	0.9	10.3	73.0	11.8	1.1	10.7 (10.3)	10.04 ± 0.25	5.2 (3.0)	5.5 ± 0.3
^{118}Sn	17.1	75.6	7.0	2.0	9.3	74.1	11.6	1.3	11.9 (11.5)	10.61 ± 0.25	4.9 (3.3)	5.7 ± 0.3
^{120}Sn	28.6	61.4	7.8	1.2	19.5	63.4	12.8	1.3	13.0 (12.5)	11.45 ± 0.25	4.5 (3.4)	6.4 ± 0.3
^{122}Sn	22.3	65.6	8.5	0.6	14.1	67.4	13.8	0.8	13.8 (13.5)	12.25 ± 0.25	3.9 (3.5)	5.6 ± 0.3
^{124}Sn	21.6	66.9	9.0	0.6	12.5	68.5	14.3	0.8	14.4 (14.3)	13.25 ± 0.25	3.6 (3.5)	5.2 ± 0.3
^{208}Pb	17.0	65.8	18.7	0.7	9.1	63.8	25.0	0.7	15.6	15.6 ± 0.2	3.7	3.54 ± 0.25

4.3. GT Strength Functions

The GT strength functions have been calculated within the CRPA for the ^{208}Pb parent nucleus according to Eqs. (17), (18) and within the pn-QCRPA for ^{90}Zr and tin isotopes according to Eqs. (44), (45) or their modifications taken for $J = 1$. From the calculated GT strength functions, the relative GT strength x and relative energy-weighted GT strength y for four energy intervals (low-energy, the vicinity of the GTR, high-energy, and the vicinity of the IVSMR$^{(+)}$) have been deduced. The value of $(\mathrm{EWSR})_1^{p-h}$ entering the definition of y has been calculated according to Eq. (16) with the nucleon densities and the occupation numbers modified by the nucleon pairing. The value of $(\mathrm{EWSR})_1^{p-p}$ defined according to Eq. (38) equals zero because of setting $G_1 = G_0$ in our calculations. The values of the parameters x and y are listed in Table 3 along with the calculated energies of the GTR. The values of the relative strengths $x_s = r_s/(N - Z)$ of the GT doorway states calculated according to Eq. (20) with and without the nucleon pairing taken into consideration are shown in Figs. 2 and 3 (solid and dotted vertical lines, respectively) for ^{90}Zr and tin isotopes. The values of x_s calculated within the CRPA for ^{208}Pb are shown in Fig. 4 (solid vertical lines).

The coupling of the GT doorway states to many-quasiparticle configurations is taken into consideration phenomenologically and is described on average over the energy in terms of the smearing parameter $I(\omega)$ simulating the mean spreading width of the doorway states. Following [15], we choose $I(E_x)$ to be a universal function revealing saturation at rather high excitation energies:

$$I(E_x) = \alpha \frac{E_x^2}{1 + E_x^2/B^2}, \qquad (49)$$

where α and B are adjustable parameters and E_x is the excitation energy in the daughter nucleus. Equation (49) is close to the parametrization of the intensity of the optical-potential imaginary part obtained within the modern version of an optical model. The choice of parameters $\alpha = 0.09$ MeV^{-1} and $B = 7$ MeV has allowed us to describe satisfactorily the total widths of a number of the isovector giant resonances (including GTR) in the ^{208}Pb parent nucleus [17]. In this work, the energy-averaged GT strength function $\bar{S}_1^{(-)}$ is calculated as $\bar{S}_1^{(-)}(\omega) = S_1^{(-)}(\omega + iI(E_x)/2)$ using the same parametrization of I, where $S_1^{(-)}$ is the GT strength function calculated according to the CRPA or pn-QCRPA equations. The calculation results are shown in Figs. 2–4 (thin solid curve). The calculated energy dependence in the vicinity of the GTR is approximated by the Breit–Wigner formulas to get both the GTR energy E_{GTR} and the width $\bar{\Gamma}_{\mathrm{GTR}}$. The values of E_{GTR} obtained thereby and $\bar{\Gamma}_{\mathrm{GTR}}$ along with the values calculated without the nucleon pairing taken into consideration (in brackets) are listed in Table 3 in comparison with the corresponding experimental data.

We analyze the effect of the isospin splitting according to Eqs. (24), (26) without taking the nucleon pairing into consideration, because this effect turns out to be weak even for such a rather light parent nucleus as ^{90}Zr. In this case, there is only the T_0 component of the GT strength function in ^{90}Nb (due to the $g_{9/2} \to g_{7/2}$ $M1$ transition in the proton subsystem).

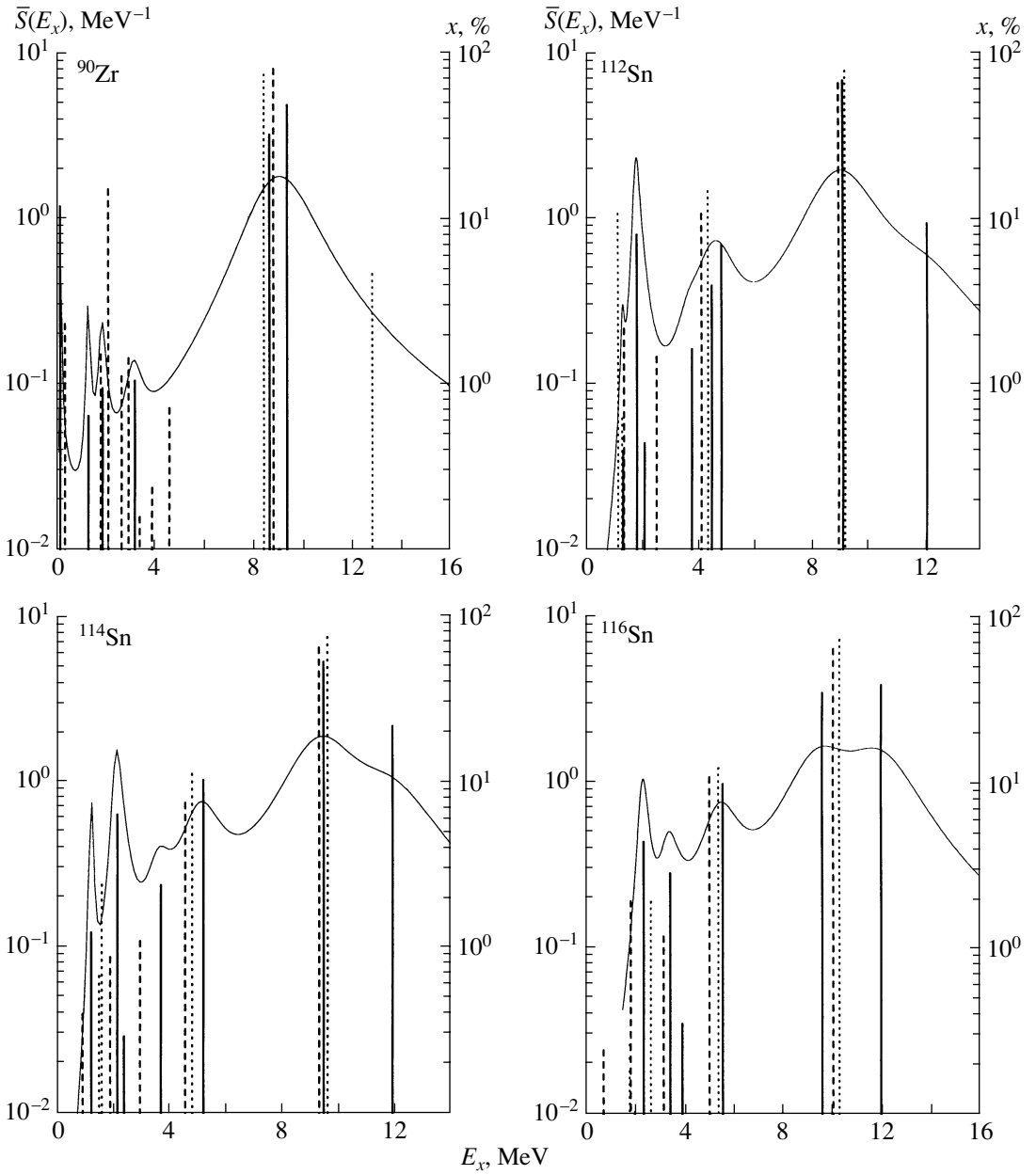

Fig. 2. The relative GT strengths x in ^{90}Nb and $^{112-116}$Sb calculated within the pn-QCRPA (solid vertical line) and CRPA (dotted vertical lines) in comparison with the respective experimental data [3, 7] (dashed vertical lines). The smeared pn-QCRPA GT-strength distribution $\bar{S}$ is also shown (thin solid curves).

Its relative strength and energy are $x_> = 4.7\%$ and $E_> = 12.8$ MeV, respectively. It leads to a decrease in the relative strength and energy of the GTR equal to $x_>$ and $x_>(E_> - E_<)/x_< = 0.3$ MeV, respectively, as compared with the values found within the CRPA.

5. DISCUSSION OF THE RESULTS

5.1. Summary Concerning the Approach

We have extended the CRPA approach, used previously in [15–17] for describing the GTR and the IAR in closed-shell nuclei, and have formulated a version of the pn-QCRPA approach for describing the GT and F strength distributions in open-shell nuclei. The common ingredients of both approaches are the following: the phenomenological isoscalar part of the nuclear mean field; the isovector part of the Landau–Migdal particle–hole interaction; the isospin self-consistency condition being used to calculate the symmetry potential; the mean Coulomb field calculated in the Hartree approximation; the use of the full basis of the single-particle states in the particle–hole

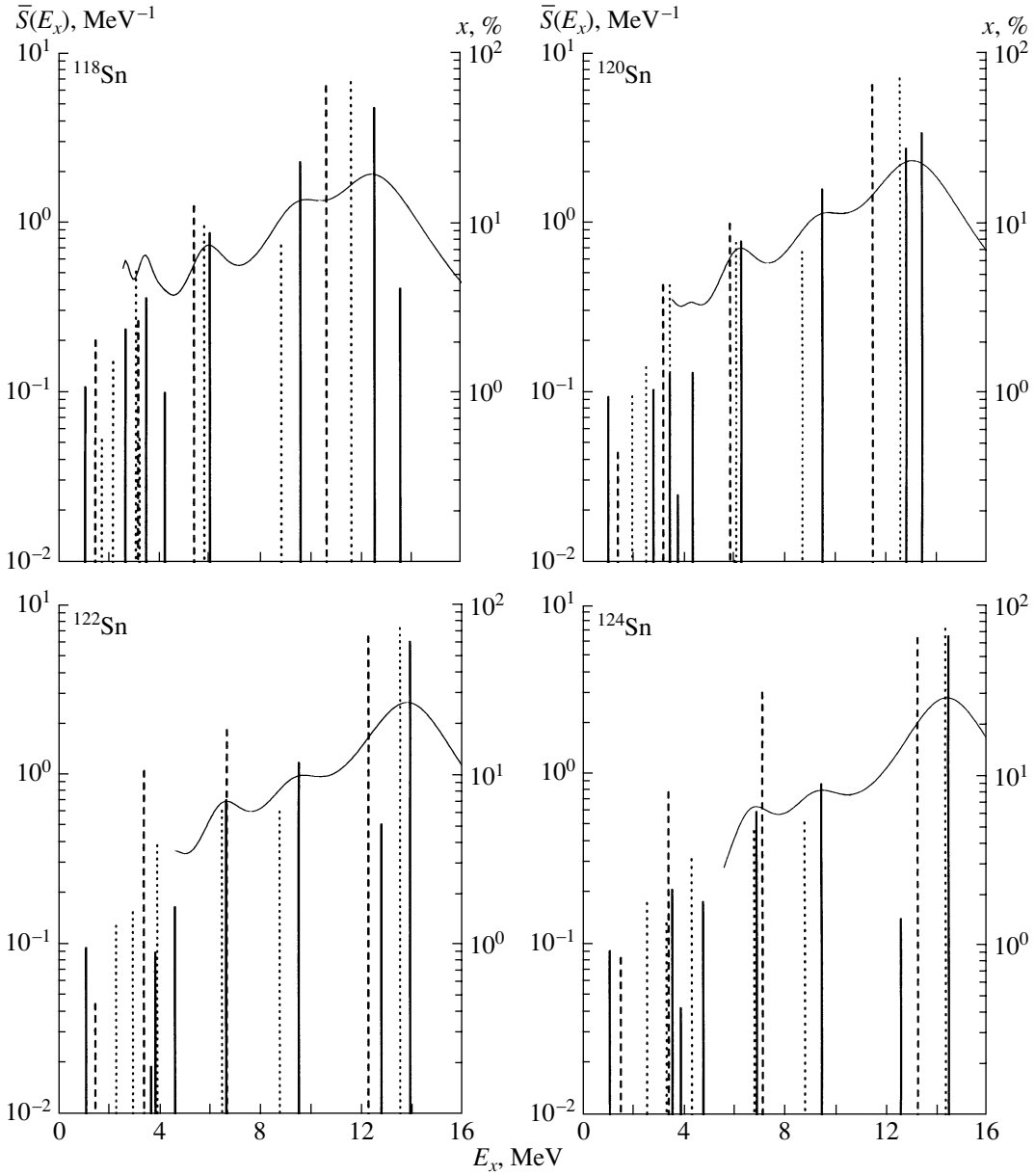

Fig. 3. The same as in Fig. 2 but for $^{118-124}$Sb (the experimental data are taken from [3]).

channel and, as a result, formulation of the continuum versions of the RPA; a phenomenological description of the coupling of the particle–hole doorway states to many-quasiparticle configurations in terms of the mean doorway-state spreading width (the smearing parameter).

The specific feature of the developed *pn*-QCRPA approach is the use of an isospin-invariant particle–particle interaction to describe both the nucleon pairing phenomenon in neutral channels and the particle–particle interaction in charge-exchange channels. The method to check the isospin self-consistency, which could be violated by the use of a truncated basis of single-particle states in the particle–particle channel within the approach, is also used.

5.2. F(C) Strength Distribution

The present results (Table 2) show at the microscopic level that the isospin is a good quantum number for medium-heavy mass nuclei. In particular, the IAR exhausts almost all the Fermi strength. The rest is mainly exhausted by the IVMR. The heavier the nucleus, the more the relative F strength of the IVMR becomes. Similar results have also been obtained for the energy-weighted F strength distribution.

The appropriate choice of the particle–particle interaction, along with the use of the same truncated basis of single-particle states in the neutral and charge-exchange channels, ensures the isospin self-consistency of the approach (the calculated values of z are found to be less than 0.1%). For the same reason, the effect of the nucleon pairing on the Fermi strength distribution is small.

The systematic lowering of the IAR energy compared with the experimental value is a shortcoming of the approach, possibly caused by the absence of the full self-consistency.

5.3. GT Strength Distribution

For all nuclei in question, the calculated GT strength function splits into three main regions (see Table 3 and Figs. 2–4). The main part of the GT strength (70–80%) is exhausted by the GTR. In the case of ^{208}Bi, the calculated GTR relative strength is found to be in reasonable agreement with the respective experimental value $x_{\mathrm{GTR}}^{\mathrm{exp}} = (60 \pm 15)\%$ [4]. The spin-quadrupole part of the particle–hole interaction is taken into account only for ^{208}Bi. As a result, the calculated GTR relative strength is decreased from 68 to 66% and the low-energy GT strength is noticeably redistributed. In the case of ^{90}Nb, the difference between experimental and calculated results is somewhat larger: $x_{\mathrm{GTR}}^{\mathrm{exp}} = (39 \pm 4)\%$ [6]; $x_{\mathrm{GTR}}^{\mathrm{exp}} = (61 \pm 8)\%$ ($x^{\mathrm{exp}} = (66^{+20}_{-10})\%$ up to 20 MeV in excitation energy) [5]. This could be partly due to the well-known quenching effect that has been discussed during the last two decades. This effect is still not established experimentally, and its discussion is beyond the scope of this work.

The calculated high-energy part of the GT strength distribution is mainly exhausted by the IVSMR and its satellites. This part is relatively large for ^{208}Bi (about 19%) and decreases to about 9% for ^{90}Nb (4.6% due to the IVSMR and 4.5% due to the $T_>$ component of the GTR). The low-energy part contains the weakly collectivized GT states, which can be related to those found in [11, 13, 14]. The nucleon pairing leads to noticeable enriching of the calculated low-energy part of the GT strength distribution in open-shell nuclei. This fact is in qualitative agreement with respective experimental data (shown in Figs. 2–4). The calculated values $x_{low}/x_{\mathrm{GTR}} =$ 19.2 and 25.8% are found to agree reasonably with the corresponding experimental values of 28.2 and 30.4% [7] for ^{90}Nb and ^{208}Bi, respectively. Bearing in mind also the above-mentioned calculated and experimental values of x_{GTR}, we can expect that the quenching effect is not as noticeable as is usually assumed.

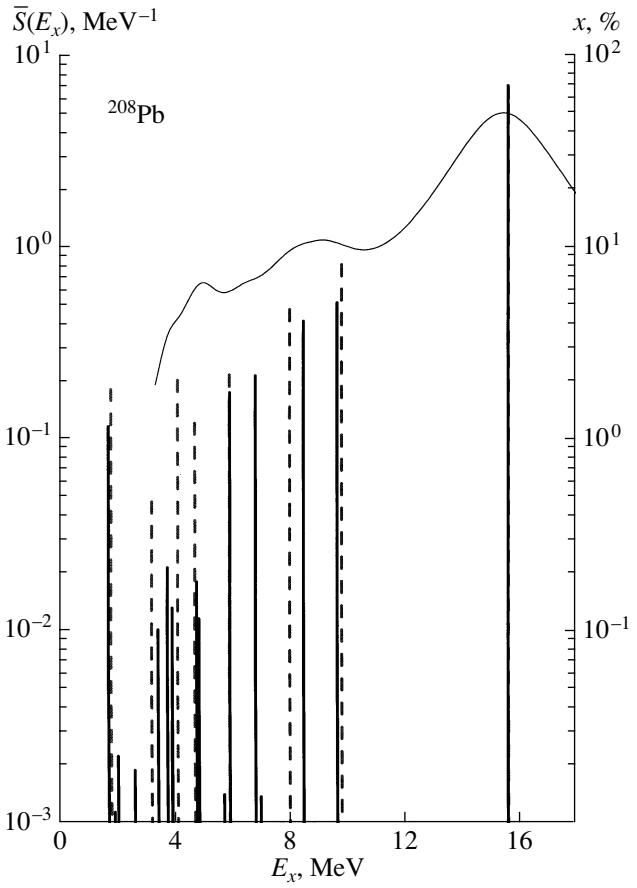

Fig. 4. The relative GT strengths x in ^{208}Bi calculated within the CRPA (solid vertical lines) along with the respective smeared distribution $\bar{S}$ (thin solid curve). The experimental data are taken from [7] (dashed vertical lines).

The configurational splitting of the main GT state is found for some single-open-shell nuclei (Figs. 2, 3). In the case of the ^{90}Zr parent nucleus, the splitting is caused by the direct spin-flip transition $1f^n_{7/2} \to 1f^p_{5/2}$, which becomes possible due to the proton pairing and whose energy is close to the GTR energy calculated without this transition taken into account. The value of the splitting (about 0.5 MeV) is found to be rather small. For this reason, the total GTR width is only slightly increased. In the case of the Sn isotopes, the strongest effect caused by the $1h^n_{11/2} \to 1h^p_{9/2}$ transition is found for the ^{120}Sn parent nucleus. The splitting energy is found to be rather large and leads to a noticeable increase in the total GTR width. The calculated isospin splitting energy

for ^{90}Nb (4.0 MeV) is found to be in good agreement with the respective experimental one (4.4 MeV [6]).

In conclusion, we incorporate the BCS model in the CRPA method to formulate a version of the partially self-consistent *pn*-QCRPA approach for describing the multipole particle–hole strength distributions in open-shell nuclei. The approach is applied to describe the F and GT strength functions in a wide excitation-energy interval for a number of single- and double-closed-shell nuclei. A reasonable description of the available experimental data is obtained.

ACKNOWLEDGMENTS

We are grateful to Prof. M. Fujiwara and Prof. A. Faessler for thoroughly reading the manuscript and many valuable remarks. V.A.R. would like to thank the Graduiertenkolleg "Hadronen in Vakuum, in Kernen und Sternen" (GRK683) for supporting his stay in Tübingen and Prof. A. Faessler for hospitality.

REFERENCES

1. A. Bohr and B. R. Mottelson, *Nuclear Structure* (Benjamin, New York, 1969), Vol. 1.
2. J. Suhonen and O. Civitarese, Phys. Rep. **300**, 123 (1998).
3. J. Jänecke *et al.*, Phys. Rev. C **48**, 2828 (1993); K. Pham *et al.*, Phys. Rev. C **51**, 526 (1995); M. Fujiwara *et al.*, Nucl. Phys. A **599**, 223 (1996).
4. H. Akimune *et al.*, Phys. Rev. C **52**, 604 (1995).
5. M. Moosburger *et al.*, Phys. Rev. C **57**, 602 (1998).
6. J. Jänecke *et al.*, Nucl. Phys. A **687**, 270c (2001).
7. A. Krasznahorkay *et al.*, Phys. Rev. C **64**, 067302 (2001).
8. T. Wakasa *et al.*, Phys. Rev. C **55**, 2909 (1997).
9. T. Wakasa *et al.*, Nucl. Phys. A **687**, 26c (2001).
10. N. Auerbach, Phys. Rep. **98**, 273 (1983).
11. Yu. V. Gaponov and Yu. S. Lyutostanskii, Yad. Fiz. **19**, 62 (1974); Fiz. Élem. Chastits At. Yadra **12**, 1234 (1981) [Sov. J. Part. Nucl. **12**, 528 (1981)].
12. N. Auerbach and A. Klein, Phys. Rev. C **30**, 1032 (1984).
13. V. G. Guba, M. A. Nikolaev, and M. G. Urin, Phys. Lett. B **218**, 283 (1989); Yad. Fiz. **51**, 937 (1990) [Sov. J. Nucl. Phys. **51**, 622 (1990)].
14. T. Suzuki, H. Sagawa, and N. Van Giai, Phys. Rev. C **57**, 139 (1998); T. Suzuki and H. Sagawa, Eur. Phys. J. A **9**, 49 (2000).
15. E. A. Moukhai, V. A. Rodin, and M. H. Urin, Phys. Lett. B **447**, 8 (1999).
16. M. L. Gorelik and M. H. Urin, Phys. Rev. C **63**, 064312 (2001).
17. V. A. Rodin and M. H. Urin, Nucl. Phys. A **687**, 276c (2001).
18. G. F. Bertsch and I. Hamamoto, Phys. Rev. C **26**, 1323 (1982); N. D. Dang, A. Arima, T. Suzuki, and S. Yamaji, Phys. Rev. Lett. **79**, 1638 (1997); S. Drożdż, V. Klempt, J. Speth, and J. Wambach, Phys. Lett. B **166B**, 18 (1986); S. Drożdż, S. Nishizaki, J. Speth, and J. Wambach, Phys. Rep. **197**, 1 (1990).
19. A. Arima, T. Cheon, K. Shimizu, *et al.*, Phys. Lett. B **122B**, 126 (1983); T. Suzuki and H. Sakai, Phys. Lett. B **455**, 25 (1999); A. Arima, W. Bentz, T. Suzuki, and T. Suzuki, Phys. Lett. B **499**, 104 (2001).
20. I. N. Borzov, E. L. Trykov, and S. A. Fayans, Yad. Fiz. **52**, 985 (1990) [Sov. J. Nucl. Phys. **52**, 627 (1990)]; Nucl. Phys. A **584**, 335 (1995); I. N. Borzov and S. Goriely, Phys. Rev. C **62**, 035501 (2000).
21. A. B. Migdal, *Theory of Finite Fermi-Systems and Properties of Atomic Nuclei* (Nauka, Moscow, 1983) [in Russian].
22. B. L. Birbrair and V. A. Sadovnikova, Yad. Fiz. **20**, 645 (1974) [Sov. J. Nucl. Phys. **20**, 347 (1975)].
23. O. A. Rumyantsev and M. H. Urin, Phys. Lett. B **443**, 51 (1998).
24. K. Ikeda, S. Fujii, and J. I. Fujita, Phys. Lett. **3**, 271 (1963).
25. M. H. Urin and O. N. Vyazankin, Nucl. Phys. A **537**, 534 (1992).
26. V. A. Rodin and M. H. Urin, Part. Nucl. **31**, 490 (2000).
27. V. G. Soloviev, *Theory of Complex Nuclei* (Pergamon, Oxford, 1976).
28. M. L. Gorelik, S. Shlomo, and M. H. Urin, Phys. Rev. C **62**, 044301 (2000).
29. D. M. Vladimirov and Y. V. Gaponov, Yad. Fiz. **55**, 1824 (1992) [Sov. J. Nucl. Phys. **55**, 1010 (1992)].

Physics of Atomic Nuclei, Vol. 66, No. 12, 2003, pp. 2143–2148. From Yadernaya Fizika, Vol. 66, No. 12, 2003, pp. 2193–2198.

ELEMENTARY PARTICLES AND FIELDS
Theory

Process $\gamma^*\gamma \to \sigma$ at Large Virtuality of γ^{**}

M. K. Volkov[**], **A. E. Radzhabov, and V. L. Yudichev**

Joint Institute for Nuclear Research, Dubna, Moscow oblast, 141980 Russia

Received November 19, 2002; in final form, March 4, 2003

Abstract—The process $\gamma^*\gamma \to \sigma$ is investigated in the framework of the $SU(2) \times SU(2)$ chiral NJL model. The form factor of the process is derived for arbitrary virtuality of γ^* in the Euclidean kinematic domain. The asymptotic behavior of this form factor resembles the asymptotic behavior of the $\gamma^*\gamma \to \pi$ form factor.

A recent analysis of the experimental data on the pseudoscalar meson production in the transition process $\gamma^*\gamma \to P$ [1] (where γ^*, γ are photons with large and small virtuality, respectively, and P is a pseudoscalar meson) revealed satisfactory agreement with the perturbative QCD (pQCD) predictions [2–6] for the asymptotic behavior of the $\gamma^*\gamma \to P$ form factor at large negative virtuality of one of the photons. However, for a correct description of the asymptotic behavior of the transition form factor, it is not enough to apply only the pQCD technique, and it is necessary to use the nonperturbative sector for determining a distribution amplitude (DA) of quarks in a meson. In the lowest order of pQCD, the light-cone operator product expansion (OPE) predicts the high Q^2 behavior of the form factor as follows [2, 3]:

$$F_P(q_1^2, q_2^2, p^2 = 0)\big|_{Q^2\to\infty} = J_P(\omega)\,\frac{f_P}{Q^2} + O\left(\frac{\alpha_s}{\pi}\right) + O\left(\frac{1}{Q^4}\right), \quad (1)$$

with the asymptotic coefficient given by

$$J_P(\omega) = \frac{4}{3}\int_0^1 \frac{dx}{1-\omega^2(2x-1)^2}\varphi_P^A(x). \quad (2)$$

Here, $\varphi_P^A(x)$ is the leading-twist meson light-cone DA normalized by

$$\int_0^1 dx\,\varphi_P^A(x) = 1; \quad (3)$$

α_s is the strong coupling constant; Q^2 and ω are, respectively, the total virtuality of the photons and the asymmetry in their distribution:

$$Q^2 = -(q_1^2 + q_2^2) \geqslant 0, \quad \text{and} \quad \omega = (q_1^2 - q_2^2)/(q_1^2 + q_2^2), \quad |\omega| \leqslant 1, \quad (4)$$

where q_1, q_2 are the momenta of photons; f_P is the meson weak decay constant (for the pion, $f_\pi = 93$ MeV).

Unfortunately, the determination of $\varphi_P^A(x)$ is a rather nontrivial problem and cannot be performed in the framework of only pQCD. At asymptotically high Q^2, the DA is $\varphi_P^{A,\text{asympt}}(x) = 6x(1-x)$ and $J_P^{\text{asympt}}(|\omega| = 1) = 2$. The fit of the CLEO data [1] for the pion corresponds to $J_\pi^{\text{CLEO}}(|\omega| \approx 1) = 1.6 \pm 0.3$, indicating that, already at moderately high momenta ($Q^2 = 8$ GeV^2), this value is not too far from its asymptotic limit.

In our previous work [7], it was shown that the calculation of the $\gamma^*\gamma \to P$ amplitude in the framework of the chiral quark model of the NJL type [8] is free from difficulties connected with the necessity of determining the DA. Our results for the form-factor asymptotics agreed with experiment [1] and with the predictions made in QCD sum rules [4–6] and the instanton-induced quark model (IQM) [9]. Also, both the NJL and IQM model allow one to derive the meson DA.

Here, we continue the investigation started in [7] and consider the scalar–isoscalar-meson production through the process $\gamma^*\gamma \to \sigma$, where σ is associated with the lightest scalar–isoscalar state $f_0(400–1200)$ [10], and the photon γ^* is off-shell. Direct observation of σ is hardly possible; however, in the low-mass region, it can show itself as a resonance in the pion pair production [11].

In our paper, all the calculations are performed in the framework of the $SU(2) \times SU(2)$ NJL model.

[*] This article was submitted by the authors in English.

[**] e-mail: volkov@thsun1.jinr.ru

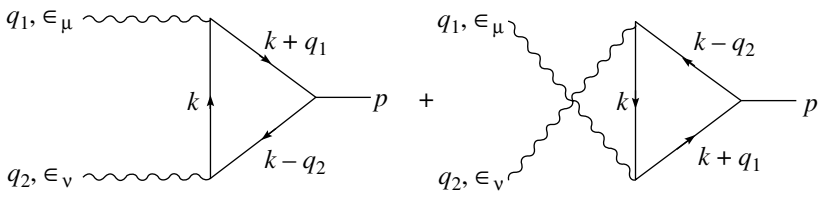

Fig. 1. Diagrams contributing to the amplitude of the process $\gamma^*\gamma \to \sigma$.

We derive a gauge-invariant expression for the amplitude of $\gamma^*\gamma \to \sigma$ and determine the form factor of the process, for which the asymptotic behavior is studied at large virtualities of γ^*. Notice that the asymptotic behavior of the $\gamma^*\gamma \to \sigma$ and $\gamma^*\gamma \to \pi$ form factors is similar.

The interaction of mesons with u and d quarks is described by the following quark–meson Lagrangian:

$$L(\bar{q}, q, A, \sigma, \pi) = \bar{q}(x)[i\hat{\partial} - M \qquad (5)$$
$$- eQ\hat{A}(x) + g(\sigma(x) + i\gamma_5 \boldsymbol{\tau} \cdot \boldsymbol{\pi}(x))]q(x),$$

where $\bar{q}$ and q are the u and d quark fields

$$q(x) = \begin{pmatrix} u(x) \\ d(x) \end{pmatrix}; \qquad (6)$$

M is the constituent mass matrix, $M = \mathrm{diag}(m_u, m_d)$ $(m_u \approx m_d \approx m)$; $\hat{A} = A_\mu \gamma^\mu$ is the photon field; σ stands for the scalar–isoscalar meson; $\boldsymbol{\pi}$ is the pion triplet, $\boldsymbol{\tau}$ are the Pauli matrices; e is FM charge, $e^2/4\pi = 1/137$; $Q = 1/6(1 + 3\tau_3)$ is the charge operator; and g is the constant of quark–meson interaction[1)] defined by the relation $g^{-2} = 4I_2$, where

$$I_2 = \frac{3}{(2\pi)^4} \int \frac{d^4_{\mathrm{E}} k \; \theta(\Lambda^2 - k^2)}{(k^2 + m^2)^2}. \qquad (7)$$

The subscript "E" in $d^4_{\mathrm{E}} k$ means that the integration is performed for momenta in the Euclidean metric. The cutoff Λ eliminates the UV divergence.

Using the Goldberger–Treiman relation $g = m/f_\pi$ and the relation $g_\rho = \sqrt{6}g$ [8], where $g_\rho \approx 6.1$ is the constant describing the decay $\rho \to 2\pi$, we determine the constituent quark mass $m = 234$ MeV and $\Lambda = 1050$ MeV.

Let us note that the $\gamma^*\gamma \to \sigma$ amplitude also describes a two-photon decay of σ. The amplitudes for radiative decays of scalar mesons (S) were obtained in [12]. The amplitude of the process $S \to \gamma\gamma$ has the form

$$A = e^2 T^{\mu\nu}_{S\to\gamma\gamma} \epsilon_\mu(q_1) \epsilon_\nu(q_2), \qquad (8)$$

where ϵ are polarization vectors, and q_1 and q_2 are photon momenta.

Up to the one-loop, the process is described by the diagrams in Fig. 1, which give for the tensor $T^{\mu\nu}_{S\to\gamma\gamma}$ [2)]

$$T^{\mu\nu}_{S\to\gamma\gamma} = T^{(1)\mu\nu}_{S\to\gamma\gamma} + T^{(2)\mu\nu}_{S\to\gamma\gamma}, \qquad (9)$$

where

$$T^{(1)\mu\nu}_{S\to\gamma\gamma} = C_S \left(q_1^\nu q_2^\mu - g^{\mu\nu}(q_1 \cdot q_2)\right) J_m(q_1, q_2), \quad (10)$$

$$T^{(2)\mu\nu}_{S\to\gamma\gamma} = C_S B^{\mu\nu}(q_1, q_2), \qquad (11)$$

and the transversality condition $\epsilon_\mu(q_1) q_1^\mu = \epsilon_\nu(q_2) \times q_2^\nu = 0$ is taken into account. Here,

$$J_m(q_1, q_2) = -\frac{i}{(2\pi)^4} \int d^4k \frac{1}{D(0)D(q_1)D(-q_2)}, \qquad (12)$$

$$B^{\mu\nu}(q_1, q_2) = -\frac{i}{(2\pi)^4} \qquad (13)$$
$$\times \int d^4k \frac{g^{\mu\nu}(m^2 - k^2) + 4k^\mu k^\nu}{D(0)D(q_1)D(-q_2)},$$

$$D(q) = m^2 - (k + q)^2. \qquad (14)$$

The constant C_S is to be specified for each type of scalar meson. In the case of σ, it is

$$C_\sigma = \frac{40}{3} gm. \qquad (15)$$

The term $T^{(1)\mu\nu}_{\sigma\to\gamma\gamma}$ has a gauge-invariant form. The Pauli–Villars regularization is necessary to restore the gauge invariance of $T^{(2)\mu\nu}_{\sigma\to\gamma\gamma}$, which leads to the following form of $B^{\mu\nu}$ (see Appendix for details) for $q_1^2 = q_2^2 = 0$:

$$B^{\mu\nu}(q_1, q_2) = 2\left(\frac{q_1^\nu q_2^\mu}{(q_1 \cdot q_2)} - g^{\mu\nu}\right) m^2 \qquad (16)$$
$$\times (J_m(0, 0) - J_m(q_1, q_2)).$$

[1)] Following [7], we do not take into account $\pi - a_1$ transitions. Therefore, $g_\pi = g_\sigma = g$.

[2)] Here, the first part of $T^{\mu\nu}_{S\to\gamma\gamma}$ can be obtained in the gauge-invariant form immediately. In order to obtain the gauge-invariant form for second part of $T^{\mu\nu}_{S\to\gamma\gamma}$, it is necessary to use intermediate Pauli–Villars regularization.

In our paper, we apply the Pauli–Villars regularization with one subtraction for an arbitrary function $Y(m^2)$ as follows:

$$Y^{PV}(m^2) = Y(m^2) - Y(M^2). \quad (17)$$

Formally, as all integrals we calculate here converge, the regularization can be lifted off by reaching the $M^2 \to \infty$ limit. In our particular case, the regularized expression will, however, differ from the nonregularized one; the constant term, which violates gauge invariance, is thereby canceled.

In the case of σ production through $\gamma^*\gamma \to \sigma$, the amplitude can also be divided into two parts:

$$T^{\mu\nu}_{\gamma^*\gamma\to\sigma} = T^{(1)\mu\nu}_{\gamma^*\gamma\to\sigma} + T^{(2)\mu\nu}_{\gamma^*\gamma\to\sigma}, \quad (18)$$

where the first term is again gauge-invariant,

$$T^{(1)\mu\nu}_{\gamma^*\gamma\to\sigma} = C_\sigma \left(q_1^\nu q_2^\mu - g^{\mu\nu}(q_1\cdot q_2)\right) J_m(q_1,q_2), \quad (19)$$

whereas the second one becomes gauge-invariant after the Pauli–Villars regularization is implemented and then lifted off. Moreover, as one of the photons is off-shell, $B^{\mu\nu}$ acquires an additional term proportional to q_1^2 (see Appendix):

$$T^{(2)\mu\nu}_{\gamma^*\gamma\to\sigma} = C_\sigma \left(\frac{q_1^\nu q_2^\mu}{(q_1\cdot q_2)} - g^{\mu\nu}\right) \quad (20)$$
$$\times \left[2m^2\left(J_m(0,0) - J_m(q_1,q_2)\right) - \frac{q_1^2}{2(q_1\cdot q_2)}\right.$$
$$\left.\times \frac{i}{(2\pi)^4}\int d^4k \frac{1}{D(q_1)}\left(\frac{1}{D(-q_2)} - \frac{1}{D(0)}\right)\right].$$

After the gauge invariance of the amplitude is restored, we define the process form factor $F(q_1,q_2)$:

$$T^{\mu\nu}_{\gamma^*\gamma\to\sigma} = (q_1^\nu q_2^\mu - (q_1\cdot q_2)g^{\mu\nu})F(q_1,q_2), \quad (21)$$

where

$$F(q_1,q_2) = \frac{40 f_\pi g^2}{3}\left[J_m(q_1,q_2) - \frac{2m^2}{(q_1\cdot q_2)}\right. \quad (22)$$
$$\times \left(J_m(q_1,q_2) - J_m(0,0)\right) - \frac{q_1^2}{2(q_1\cdot q_2)^2}\frac{i}{(2\pi)^4}$$
$$\left.\times \int d^4k \frac{1}{D(q_1)}\left(\frac{1}{D(-q_2)} - \frac{1}{D(0)}\right)\right].$$

After the change of variable $k = k' - (q_1 - q_2)/2$ (in the following, we omit the prime symbol), the form factor takes the form

$$F(q_1,q_2) = \frac{5 f_\pi g^2}{6\pi^2}\int \frac{d^4k}{i\pi^2} \quad (23)$$
$$\times \left[\frac{1 - 2m^2/(q_1\cdot q_2)}{D(-p/2)D(p/2)D(-(q_1-q_2)/2)}\right.$$
$$\left. + \frac{2m^2}{(q_1\cdot q_2)}\frac{1}{D(0)^3} + \frac{q_1^2}{2(q_1\cdot q_2)^2}\frac{1}{D(p/2)}\right.$$
$$\left.\times\left(\frac{1}{D(-p/2)} - \frac{1}{D(-(q_1-q_2)/2)}\right)\right],$$

where $p = q_1 + q_2$. It is convenient to consider $F(q_1,q_2)$ in terms of p^2 (notice that $p^2 = M_\sigma^2$), q_1^2, and q_2^2. Further, we restrict ourselves to the case of $q_2^2 = 0$; thus, we have two independent variables p^2 and q_1^2. The kinematics of the process under investigation corresponds to large negative q_1^2, and we introduce, for convenience, a positive magnitude Q^2 defined as $Q^2 = -q_1^2$. After that, the form factor $F(q_1,q_2)$ can be considered as depending on p^2 and Q^2:

$$\tilde{F}(p^2,Q^2) = F(q_1,q_2)|_{q_2^2=0;q_1^2<0}, \quad (24)$$

$$\tilde{F}(p^2,Q^2) = \frac{5 f_\pi g^2}{6\pi^2} \quad (25)$$
$$\times \left[\left(1 - \frac{4m^2}{p^2+Q^2}\right)K_\Lambda(p^2,Q^2) + \frac{4m^2}{p^2+Q^2}L_\Lambda\right.$$
$$\left. - \frac{2Q^2}{(p^2+Q^2)^2}\left(M_\Lambda(p^2) - N_\Lambda(p^2,Q^2)\right)\right],$$

where

$$K_\Lambda(p^2,Q^2) = \int^\Lambda \frac{d^4k}{i\pi^2} \quad (26)$$
$$\times \frac{1}{D(-p/2)D(p/2)D(-(q_1-q_2)/2)},$$

$$L_\Lambda = \int^\Lambda \frac{d^4k}{i\pi^2}\frac{1}{D(0)^3}, \quad (27)$$

$$M_\Lambda(p^2) = \int^\Lambda \frac{d^4k}{i\pi^2}\frac{1}{D(-p/2)D(p/2)}, \quad (28)$$

$$N_\Lambda(p^2,Q^2) = \int^\Lambda \frac{d^4k}{i\pi^2}\frac{1}{D(-(q_1-q_2)/2)D(p/2)}. \quad (29)$$

In all integrals, we implement the UV cutoff Λ that constrains quark momenta to the domain where chiral symmetry is spontaneously broken and the bosonization of quarks takes place [see (7)].

An analogous method was used in [7]. One can compare (25) with the pion form factor obtained in [7] for $q_1^2 \neq 0$, $q_2^2 \neq 0$,

$$F_\pi(p^2,q_1^2,q_2^2) = C_\pi \int \frac{d^4k}{i\pi^2} \quad (30)$$
$$\times \frac{1}{D(-p/2)D(p/2)D(-(q_1-q_2)/2)},$$

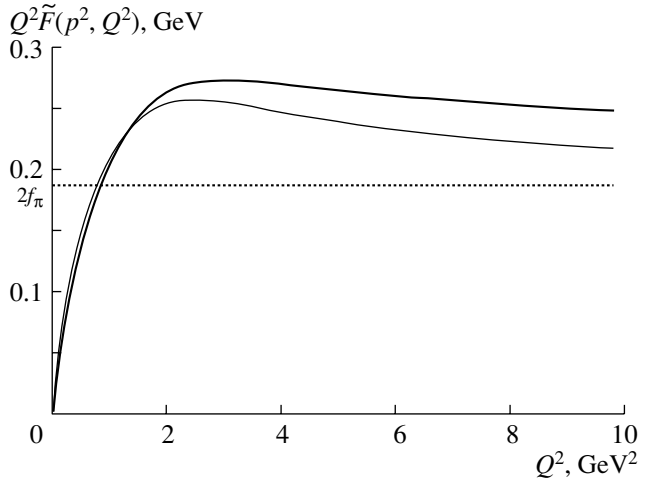

Fig. 2. The form factor of the process $\gamma^*\gamma \to \sigma$ multiplied by Q^2 at Q^2 from 0 to 10 GeV^2. The thick curve is for $p^2 = (0.45\ \text{GeV})^2$ and the thin one is for $p^2 = 0$. We compare these curves with the theoretical limit for the pion transition form factor: $2f_\pi$.

where C_π is a constant. In [7], the following expression was obtained for $K_\Lambda(p^2, Q^2)$ after introducing Feynman parameters, integrating over the angles, and changing the variables $k^2 = u$:

$$K_\Lambda(p^2, Q^2) = \int_0^{\Lambda^2} \frac{du\,u}{m^2 + u - p^2/4} \tag{31}$$
$$\times \int_0^1 dx \left[\frac{1}{\sqrt{b^2 - a_+}\left(b + \sqrt{b^2 - a_+}\right)} + \frac{1}{\sqrt{b^2 - a_-}\left(b + \sqrt{b^2 - a_-}\right)} \right].$$

Here,

$$b = m^2 + u + \frac{1}{2}xQ^2 - \frac{1}{4}(1 - 2x)\,p^2, \tag{32}$$
$$a_\pm = 2uxQ^2\,(x \pm (1 - x)) - (1 - 2x)\,up^2.$$

Analogously, one can write the integrals $N_\Lambda(p^2, Q^2)$ and $M_\Lambda(p^2)$ as follows:

$$N_\Lambda(p^2, Q^2) \tag{33}$$
$$= 2\int_0^{\Lambda^2} du\,u \int_0^1 dx \frac{1}{\sqrt{b^2 - a_+}\left(b + \sqrt{b^2 - a_+}\right)},$$

$$M_\Lambda(p^2) = 2\int_0^{\Lambda^2} \frac{du\,u}{b_0\left(b_0 + \sqrt{b_0^2 - a_{+0}}\right)}. \tag{34}$$

Here,

$$b_0 = b|_{x\to 0} = m^2 + u - \frac{1}{4}p^2, \tag{35}$$
$$a_{+0} = a_+|_{x\to 0} = -up^2.$$

Now, we can calculate the asymptotics for $\tilde{F}(p^2, Q^2)$ when $Q^2 \to \infty$. Using the approximation described in [7] and expanding in a series of $1/Q^2$, we obtain the following asymptotics for the form factor $\tilde{F}(p^2 = 0, Q^2)$ in the leading order [the last term in (25) is of the order of $1/Q^4$]:

$$\tilde{F}(p^2 = 0, Q^2) = \frac{5f_\pi g^2}{6\pi^2}\frac{1}{Q^2}(6.21 + 1.81 - 4.2) \tag{36}$$
$$+ O\left(\frac{1}{Q^4}\right) = J_S\frac{f_\pi}{Q^2} + O\left(\frac{1}{Q^4}\right),$$
$$J_S \approx 3.28 + 0.96 - 2.22 = 2.02. \tag{37}$$

We also calculate numerically $Q^2\tilde{F}(p^2, Q^2)$ for intermediate values of Q^2 and for a different choice of p^2. The curves drawn for $p^2 = 0$ and $p^2 = M_\sigma^2 = (0.45\ \text{GeV})^2$ are shown in Fig. 2. The value $M_\sigma = 450$ MeV is consistent with recent experimental [13] and theoretical [14] data. A comparison of the results for the function $Q^2\tilde{F}(p^2, Q^2)$ with an analogous function for the pion [7] shows similarity in their asymptotic behavior. However, some differences occur at intermediate values of Q^2. Indeed, the pion function grows monotonically in the whole region of Q^2. At the beginning, it grows rapidly, and for $Q^2 > 2$ GeV^2, it slowly approaches the asymptotic value. In the case of the σ meson, the function $Q^2\tilde{F}(p^2, Q^2)$ also experiences a rapid growth up to approximately 2 GeV^2; after that, it slowly decreases to an asymptotic value. Asymptotic values for these functions are practically equal to each other.

In this work, we have shown that, in the framework of the $SU(2) \times SU(2)$ chiral quark model of the NJL type, it is possible to describe the behavior of the $\gamma^*\gamma \to \sigma$ form factor in a wide region of Q^2. The exact expression for the form factor of the process is obtained, and its asymptotic behavior is investigated. A comparison of the π (see [7]) and σ form factors reveals similarity in their asymptotic behavior, which can be understood as a consequence of chiral symmetry.

Our results can be useful in investigations of the processes where pion pairs in the S wave are produced in two-photon collisions [15]. Indeed, in these processes, as a rule, the σ-pole diagram plays the dominant role [8, 11]. Some data on the pair-pion

production is already available [16]. Also, one can find a discussion on this topic in [17].

Note also that the information concerning the amplitudes $\gamma^*\gamma \to \pi$, $\gamma^*\gamma \to \sigma$ can allow us to calculate corrections to the muon anomalous magnetic moment from the processes $\gamma^*\gamma \to \pi \to \gamma^*\gamma^*$, $\gamma^*\gamma \to \sigma \to \gamma^*\gamma^*$, where γ^* interact with the muon. Last year, this topic was discussed in various papers (see [18]).

Further, we plan to calculate the transition form factor for two off-shell photons with arbitrary virtualities in the framework of both the NJL and IQM model, and it will allow us also to define the DA.

ACKNOWLEDGMENTS

We thank A.E. Dorokhov, S.B. Gerasimov, and E.A. Kuraev for fruitful discussions.

The work was supported by the Russian Foundation for Basic Research, project no. 02-02-16194.

APPENDIX

Expression (12) for $J_m(q_1, q_2)$ can be rewritten in the following form:

$$J_m(q_1,q_2) = -\frac{i}{(2\pi)^4} \tag{A.1}$$
$$\times \int d^4k \frac{1}{D(0)D(q_1)D(-q_2)} = -\frac{1}{(4\pi)^2}\frac{1}{2(q_1\cdot q_2)}$$
$$\times \int_0^1 \frac{dx}{x} \ln\left(\frac{m^2 - p^2x(1-x)}{m^2 - q_1^2x(1-x)}\right).$$

Let us rewrite the expression for $B^{\mu\nu}$ [see (13)] using the Feynman parameters:

$$B^{\mu\nu}(q_1,q_2) = -\frac{i}{(2\pi)^4} \tag{A.2}$$
$$\times \int d^4k \frac{g^{\mu\nu}(m^2-k^2) + 4k^\mu k^\nu}{D(0)D(q_1)D(-q_2)}$$
$$= \frac{g^{\mu\nu}(q_1\cdot q_2) - q_1^\nu q_2^\mu}{(4\pi)^2}\int_0^1 dx \int_0^{1-x} dy \frac{4xy}{Z}$$
$$+ \frac{g^{\mu\nu}}{(4\pi)^2}\int_0^1 dx \int_0^{1-x} dy \left(1 + \frac{q_1^2x(1-2x)}{Z}\right),$$

where

$$Z = m^2 - q_1^2x(1-x) - 2(q_1\cdot q_2)xy. \tag{A.3}$$

The first term in (A.2) is gauge-invariant, while the other is noninvariant and can also be divided into two terms

$$\frac{1}{(4\pi)^2}\int_0^1 dx \int_0^{1-x} dy \tag{A.4}$$
$$+ \frac{q_1^2}{(4\pi)^2}\int_0^1 dx \int_0^{1-x} dy \frac{x(1-2x)}{Z}.$$

The first term in (A.4) is a constant and is canceled by the Pauli–Villars regularization. Integrating over y in the second term and making substitution $1-2x = z$, one can see that this part equals zero:

$$-\frac{1}{(4\pi)^2}\frac{q_1^2}{4(q_1\cdot q_2)}\int_{-1}^1 dz z \ln\left(\frac{4m^2 + (q_1^2 + 2(q_1\cdot q_2)(1-z^2))}{4m^2 + q_1^2(1-z^2)}\right) = 0. \tag{A.5}$$

Therefore, the expression for $B^{\mu\nu}$ becomes gauge-invariant after the Pauli–Villars regularization is implemented and then lifted off:

$$B^{\mu\nu}(q_1,q_2) \tag{A.6}$$
$$= (q_1^\nu q_2^\mu - (q_1\cdot q_2)g^{\mu\nu})(I(m^2) - I(M^2))|_{M^2\to\infty},$$

$$I(m^2) = -\frac{1}{(4\pi)^2}\int_0^1 dx \int_0^{1-x} dy \frac{4xy}{Z}. \tag{A.7}$$

Integrating over y in $I(m^2)$, we obtain

$$I(m^2) = \frac{1}{(4\pi)^2}\frac{1}{(q_1\cdot q_2)} + \frac{1}{(4\pi)^2}\frac{m^2}{(q_1\cdot q_2)^2} \tag{A.8}$$
$$\times \int_0^1 \frac{dx}{x} \ln\left(\frac{m^2 - p^2x(1-x)}{m^2 - q_1^2x(1-x)}\right)$$
$$- \frac{1}{(4\pi)^2}\frac{q_1^2}{(q_1\cdot q_2)^2}$$
$$\times \int_0^1 dx(1-x) \ln\left(\frac{m^2 - p^2x(1-x)}{m^2 - q_1^2x(1-x)}\right).$$

Now, let us show that $I(m^2)$ can be expressed through the integral

$$\frac{i}{(2\pi)^4}\int d^4k \frac{D(0) - D(-q_2)}{D(0)D(q_1)D(-q_2)} \tag{A.9}$$

$$= \frac{1}{(4\pi)^2}\int\limits_0^1 dx \ln\left(\frac{m^2 - p^2x(1-x)}{m^2 - q_1^2x(1-x)}\right)$$

$$= \frac{2}{(4\pi)^2}\int\limits_0^1 dx(1-x)\ln\left(\frac{m^2 - p^2x(1-x)}{m^2 - q_1^2x(1-x)}\right).$$

Using (A.1) and (A.9), we rewrite $I(m^2)$ as follows:

$$I(m^2) = \frac{1}{(4\pi)^2}\frac{1}{(q_1\cdot q_2)} \tag{A.10}$$
$$- \frac{2m^2}{(q_1\cdot q_2)}J_m(q_1,q_2) - \frac{q_1^2}{2(q_1\cdot q_2)^2}\frac{i}{(2\pi)^4}$$
$$\times \int d^4k \frac{D(0) - D(-q_2)}{D(0)D(q_1)D(-q_2)}.$$

Formally, the first term in (A.10) can be rewritten as

$$\frac{2m^2}{(q_1\cdot q_2)}J_m(0,0), \tag{A.11}$$

because

$$J_m(0,0) = -\frac{i}{(2\pi)^4}\int \frac{d^4k}{D(0)^3} = \frac{1}{2(4\pi)^2m^2}. \tag{A.12}$$

Finally, the regularized expression for $B^{\mu\nu}(q_1,q_2)$ has the form

$$B^{\mu\nu}(q_1,q_2) = (q_1^\nu q_2^\mu - (q_1\cdot q_2)g^{\mu\nu}) \tag{A.13}$$
$$\times\left(-\frac{2m^2}{(q_1\cdot q_2)}J_m(q_1,q_2) + \frac{2m^2}{(q_1\cdot q_2)}J_m(0,0)\right.$$
$$\left. - \frac{q_1^2}{2(q_1\cdot q_2)^2}\frac{i}{(2\pi)^4}\int d^4k\frac{D(0) - D(-q_2)}{D(0)D(q_1)D(-q_2)}\right).$$

Equation (A.13) is expressed in terms of formal integrals. This gives us an advantage of further implementing a regularization different from the Pauli–Villars scheme.

REFERENCES

1. J. Gronberg *et al.* (CLEO Collab.), Phys. Rev. D **57**, 33 (1998).
2. S. J. Brodsky and G. P. Lepage, Phys. Lett. B **87B**, 359 (1979); Phys. Rev. D **22**, 2157 (1980).
3. V. L. Chernyak and A. R. Zhitnitsky, Phys. Rep. **112**, 173 (1984).
4. S. V. Mikhailov and A. V. Radyushkin, Yad. Fiz. **52**, 1095 (1990) [Sov. J. Nucl. Phys. **52**, 697 (1990)].
5. S. V. Mikhailov and A. V. Radyushkin, Pis'ma Zh. Éksp. Teor. Fiz. **43**, 712 (1986) [JETP Lett. **43**, 712 (1986)]; Yad. Fiz. **49**, 794 (1989) [Sov. J. Nucl. Phys. **49**, 494 (1989)]; Phys. Rev. D **45**, 1754 (1992).
6. A. V. Radyushkin and R. T. Ruskov, Nucl. Phys. B **481**, 625 (1996); hep-ph/9706518.
7. A. E. Dorokhov, M. K. Volkov, and V. L. Yudichev, Preprint No. E4-2001-162 (Joint Inst. Nucl. Res., Dubna, 2001); Yad. Fiz. **66**, 973 (2003) [Phys. At. Nucl. **66**, 941 (2003)]; hep-ph/0203136.
8. M. K. Volkov, Fiz. Élem. Chastits At. Yadra **17**, 433 (1986) [Sov. J. Part. Nucl. **17**, 186 (1986)].
9. I. V. Anikin, A. E. Dorokhov, and Lauro Tomio, Phys. Lett. B **475**, 361 (2000); A. E. Dorokhov and Lauro Tomio, Phys. Rev. D **62**, 014016 (2000); I. V. Anikin, A. E. Dorokhov, and L. Tomio, Part. Nucl. **31**, 509 (2000); I. V. Anikin and O. V. Teryaev, Phys. Lett. B **509**, 95 (2001).
10. D. E. Groom *et al.*, Eur. Phys. J. C **15**, 1 (2000).
11. A. E. Dorokhov, M. K. Volkov, J. Hüfner, *et al.*, Z. Phys. C **75**, 127 (1997); M. K. Volkov, E. A. Kuraev, D. Blaschke, *et al.*, Phys. Lett. B **424**, 235 (1998); M. K. Volkov, A. E. Radzhabov, and N. L. Russakovich, Yad. Fiz. **66**, 1030 (2003) [Phys. At. Nucl. **66**, 997 (2003)]; hep-ph/0203170.
12. M. K. Volkov, Theor. Math. Phys. **101**, 1473 (1994).
13. E. M. Aitala *et al.* (E791 Collab.), Phys. Rev. Lett. **86**, 770 (2001).
14. M. K. Volkov and V. L. Yudichev, Eur. Phys. J. A **10**, 223 (2001).
15. M. Diehl, T. Gousset, B. Pire, and O. Teryaev, Phys. Rev. Lett. **81**, 1782 (1998); hep-ph/9805380; Ph. Hagler, B. Pire, L. Szymanowski, and O. V. Teryaev, Phys. Lett. B **535**, 117 (2002); **540**, 324 (Erratum) (2002); hep-ph/0202231.
16. J. Dominik *et al.* (CLEO Collab.), Phys. Rev. D **50**, 3027 (1994).
17. C. Vogt, hep-ph/0207077.
18. E. Bartos, A. Z. Dubnickova, S. Dubnicka, *et al.*, Nucl. Phys. B **632**, 330 (2002); hep-ph/0106084; M. Knecht and A. Nyffeler, Phys. Rev. D **65**, 073034 (2002); hep-ph/0111058.

Physics of Atomic Nuclei, Vol. 66, No. 12, 2003, pp. 2149–2158. Translated from Yadernaya Fizika, Vol. 66, No. 12, 2003, pp. 2199–2208.

ELEMENTARY PARTICLES AND FIELDS
Theory

New Possibilities for Studying Nucleon Resonances on the Basis of an Analysis of Polarization Observables and Off-Scattering-Plane Angular Distributions in the Reaction $\gamma_v p \to \pi^+\pi^- p$

V. Burkert[1], V. I. Mokeev, M. Ripani[2], M. Anghinolfi[2], M. Battaglieri[2], A. A. Boluchevskii[3], E. N. Golovach, R. De Vita[2], L. Elouadrhiri[1], B. S. Ishkhanov, M. V. Osipenko[2], N. S. Markov[3], G. Ricco[2,4], M. Taiuti[4], and G. V. Fedotov

Institute of Nuclear Physics, Moscow State University, Vorob'evy gory, Moscow, 119899 Russia

Received April 30, 2002; in final form, October 9, 2002

Abstract—A model for describing the double charged-pion production by real and virtual photons in the energy region of nucleon-resonance excitation is further developed for calculating the angular distributions of reaction products off the scattering plane and the beam asymmetry. It is shown that investigation of these observables has a rich potential for extracting the first data on the Coulomb excitation of many nucleon resonances and for separating the contributions of various helicity amplitudes to the excitation of nucleon resonances by transverse photons. © *2003 MAIK "Nauka/Interperiodica".*

1. INTRODUCTION

Presently, extensive investigations of electromagnetic form factors for nucleon resonances (N^*) are being performed in the experiments of the CLAS Collaboration [1] by using the entire set of observables in various channels of real- and virtual-photon interaction with nucleons. At total c.m. energies W above 1.7 GeV, the exclusive channel of double charged-pion production ($\pi^+\pi^-$), along with channels involving the emission of pion pairs that contain neutral particles ($\pi^+\pi^0 n$, $\pi^0\pi^0 p$), makes a dominant contribution to the cross section for real- and virtual-photon interaction with nucleons. This channel is very promising for extracting data on electromagnetic form factors for high-lying nucleon resonances ($M_{N^*} > 1.6$ GeV), since the majority of the decays of such nucleon resonances lead to final multipion states; it is also of great interest for seeking baryon resonances that are predicted within general principles of quark models [2–6], but which have not yet been discovered experimentally (missing baryon resonances). According to model predictions, missing baryon resonances are much more strongly coupled to final two-pion states than to states resulting from the emission of a single pion; at the same time, the electomagnetic form factors for discovered and missing resonances of this type are commensurate.

A strong overlap of many high-lying nucleon resonances and a significant contribution from nonresonance mechanisms, which decreases as the square Q^2 of the photon 4-momentum grows, are features peculiar to reactions that involve the production of $\pi^+\pi^-$ pairs by real and virtual photons. These features entail serious difficulties in applying model-independent approaches to extracting electromagnetic form factors for nucleon resonances—for example, an expansion in terms of partial waves that is followed by a determination of form factors for each partial wave.

A phenomenological model was developed in [7–10] for describing double charged-pion production by real and virtual photons over a region in which one can employ meson and baryon degrees of freedom—to be more specific, this is a region where $W < 4.0$ GeV and where the Mandelstam variables u and t, as well as Q^2, do not exceed a few GeV^2 units. The model faithfully reproduces the entire body of data obtained worldwide for processes involving double charged-pion production by photons. This model was used to analyze the first data of the CLAS Collaboration on the production of $\pi^+\pi^-$ pairs by virtual photons over the region $0.65 < Q^2 < 1.3$ GeV^2 [10]. That analysis was aimed at a determination of first data on electromagnetic form factors for the majority of nucleon resonances of mass higher than 1.6 GeV, as well as at searches for missing baryon states.

[1] Jefferson Laboratory, 12000 Jefferson Avenue, Newport News, VA 23606, USA.
[2] Istituto Nazionale di Fisica Nucleare, Sezione di Genova, Genova, Italy.
[3] Department of Physics, Moscow State University, Vorob'evy gory, Moscow, 119899 Russia.
[4] Universitá di Genova, via Dodecaneso 33, I-16146 Genova, Italy.

1063-7788/03/6612-2149$24.00

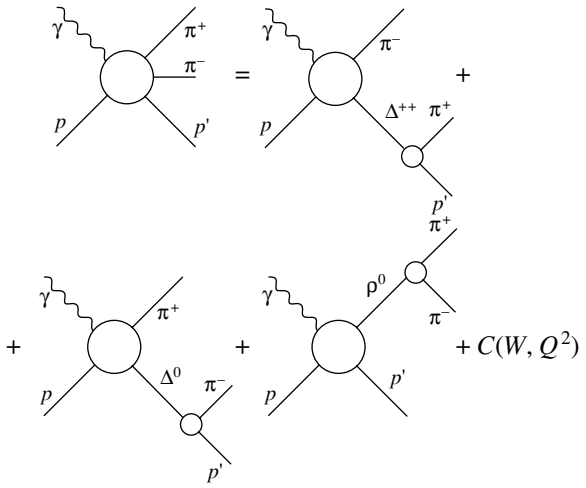

Fig. 1. Diagrams for quasi-two-body processes leading to the production of $\pi^+\pi^-$ pairs on a proton.

In view of a phenomenological character of the description of nonresonance mechanisms and the amplitudes of nucleon-resonance decays off the mass shell, reliable information about the electromagnetic form factors for nucleon resonances can be deduced only from a simultaneous analysis of many exclusive channels and of the entire body of observables, including differential cross sections, the polarization asymmetry of the beam or the target, and the double beam–target polarization asymmetry. A model for describing the differential cross sections for the production of $\pi^+\pi^-$ pairs by photons was presented in [7–9]. In [11], the model was extended to describe the double beam–target polarization asymmetry

$$A = \frac{\sigma_{1/2} - \sigma_{3/2}}{\sigma_{1/2} + \sigma_{3/2}}, \qquad (1)$$

where $\sigma_{1/2}$ and $\sigma_{3/2}$ are the cross sections for double charged-pion production for the cases where the total helicity of the system formed by a primary photon and a primary proton is 1/2 and 3/2, respectively. New information about the structure of nucleon resonances can be obtained by studying so-called off-scattering-plane angular distributions, which are defined as single-differential cross sections with respect to the angle between the momentum of one of the particles and the electron-scattering plane, $d\sigma/d\varphi$, in the reaction $\gamma_v p \to \pi^+\pi^- p$. (Here and below, γ_v stands for a virtual photon.) This differential cross section is controlled by the interference between the matrix elements corresponding to different helicity states of the photons involved: (i) between $\lambda_\gamma = +1$ and $\lambda_\gamma = -1$ and (ii) between $\lambda_\gamma = 0$ and $\lambda_\gamma = \pm 1$ [12–14]. Thus, measurement of these cross sections furnishes additional information about the interference between the transverse form factors $A_{1/2}$ and $A_{3/2}$ for nucleon resonances, as well as about the interference between the longitudinal form factor $C_{1/2}$ and the transverse form factors for nucleon resonances. The asymmetry of a polarized electron beam receives a contribution from the interference between the matrix elements of the amplitudes for the photon helicities of $\lambda_\gamma = 0$ and $\lambda_\gamma = \pm 1$ [13, 14]. It should be noted that, while off-scattering-plane angular distributions depend on the real parts of the aforementioned interference terms, the beam asymmetry depends on the imaginary parts of those terms. Therefore, information about the interference between the longitudinal and transverse amplitudes from measurements of the beam asymmetry may be supplementary to that from measurements of off-scattering-plane angular distributions. It should be emphasized that, in studying cross sections that are determined by the sum of the squared moduli of helicity amplitudes, it is impossible separate the form factors $A_{1/2}$ and $C_{1/2}$ because they manifest themselves identically in observables; thus, a global analysis of data on off-scattering-plane angular distributions and on the beam asymmetry would make it possible to obtain data on the experimentally unexplored Coulomb electromagnetic form factors $C_{1/2}(Q^2)$ for nucleon resonances. In this study, we present a further development of the model describing double charged-pion production on protons. In particular, we derive expressions for off-scattering-plane angular distributions of final particles and for the polarization asymmetry of the beam in the case of double pion production. We also investigate the possibility of extracting the form factor $C_{1/2}$ for the $P_{11}(1440)$ resonance.

2. DESCRIPTION OF THE OFF-SCATTERING-PLANE ANGULAR DISTRIBUTIONS OF THE PRODUCTS OF THE REACTION $\gamma_v p \to \pi^+\pi^- p$ AND OF THE POLARIZATION ASYMMETRY OF THE BEAM

Within the model proposed in [7, 8], the production of $\pi^+\pi^-$ pairs on a proton is described in terms of a superposition of the mechanisms represented by the tree diagrams in Fig. 1. All the remaining mechanisms contributing to the cross section are parametrized by using a complex-valued amplitude $C(W, Q^2)$ whose choice will be discussed below. Each of the quasi-two-body mechanisms represented by the diagrams in Fig. 1 is described by a superposition of nonresonance processes and nucleon-resonance excitations in the s channel in a photon–proton collision followed by a decay into $\pi^-\Delta^{++}$ and $\rho^0 p$ states. The model includes all nucleon resonances

having a mass below 2.0 GeV and a **** status by the Particle Data Group and experimentally manifesting themselves by decays through the $\pi^-\Delta^{++}$ or the $\rho^0 p$ channel. Nonresonance mechanisms in the $\pi^-\Delta^{++}$ channel are described by a set of Reggeized Born terms whose gauge invariance is restored upon Reggeization. A special approach is developed for describing effects of initial- and final-state interaction in the quasi-two-body channels $\gamma_v p \to \pi^-\Delta^{++}$ and $\gamma_v p \to \pi^+\Delta^0$ [9]. Nonresonance processes in the quasi-two-body channel $\gamma_v p \to \rho^0 p$ are described in the diffraction approximation [8]. The model developed in [7–9] relates the electromagnetic form factors for nucleon resonances to the measured differential cross sections for the reaction $\gamma_v p \to \pi^+\pi^- p$ and makes it possible to extract these electromagnetic form factors from the best fit to the measured cross sections. A detailed description of resonance and nonresonance mechanisms in the processes shown in Fig. 1 is given in [7–9]. In the present study, we restrict our consideration to the use of this model in describing the off-scattering-plane angular distributions of negatively charged pions, $d\sigma/d\varphi_{\pi^-}$, and the polarization asymmetry of the beam, $d\sigma_h/d\varphi_{\pi^-}$ (the definition of σ_h is given below).

The differential cross section for the reaction $\gamma_v p \to \pi^+\pi^- p$ in the absence of incident-electron polarization can be represented in the form [7, 8, 12, 13]

$$\frac{d^5\sigma}{d\tau} = \frac{4\pi\alpha}{4K_L M_N}\left\{\left(\frac{J_x J_x^* + J_y J_y^*}{2} + \varepsilon_L J_z J_z^*\right) + \varepsilon\frac{J_x^* J_x - J_y^* J_y}{2} + \sqrt{2\varepsilon_L(1+\varepsilon)}\frac{J_z^* J_x + J_x^* J_z}{2}\right\}\frac{1}{32W^2}\frac{1}{(2\pi)^5}, \quad (2)$$

where $d\tau$ is a phase-space element, $d\tau = dS_{\pi^+\pi^-} dS_{\pi^+ p} d\Omega_{\pi^-} d\alpha$; $S_{\pi^+\pi^-}$ is the squared invariant mass of the $\pi^+\pi^-$ system; $S_{\pi^+ p}$ is the squared invariant mass of the $\pi^+ p$ system; $d\Omega_{\pi^-}$ is an element of the solid angle of π^--meson emission, $d\varphi_{\pi^-}\sin\vartheta_{\pi^-} d\vartheta_{\pi^-}$; and α is the angle between the reaction plane and the plane spanned by the 3-momenta of the π^+ and p particles.

All kinematical variables are defined in the c.m. frame of the colliding photon and proton. The quantity W is the sum of the photon and primary-proton energies; $\alpha = 1/137$ is the fine-structure constant; and

$$K_L = \frac{W^2 - M_N^2}{2M_N}, \quad (3)$$

where M_N is the nucleon mass. The degrees of the longitudinal (ε_L) and transverse (ε) polarizations of a virtual photon are given by

$$\varepsilon = \left(1 + \left(\frac{2\bar{q}^2}{Q^2}\right)\tan^2\frac{\vartheta_e}{2}\right)^{-1}, \qquad \varepsilon_L = \frac{Q^2}{\nu}\varepsilon, \quad (4)$$

where ν and $\bar{q}^2$ are, respectively, the energy of this photon and the squared modulus of its 3-momentum; ϑ_e is the electron scattering angle in the laboratory frame; and Q^2 is the sign-reversed square of the virtual-photon 4-momentum. The hadron currents J_μ ($\mu = x, y, z$) appearing in (2) and the helicity amplitudes $\langle\pi\pi\lambda_{p'}|T|\lambda_p\lambda_\gamma\rangle$ of the reaction $\gamma_v p \to \pi^+\pi^- p$ are related by the equations

$$J_x(\lambda_p, \lambda_{p'}) = -\frac{1}{\sqrt{2}}(\langle\lambda_{p'}\pi\pi|T|\lambda_\gamma = +1, \lambda_p\rangle - \langle\lambda_{p'}\pi\pi|T|\lambda_\gamma = -1, \lambda_p\rangle), \quad (5)$$

$$J_y(\lambda_p, \lambda_{p'}) = \frac{i}{\sqrt{2}}(\langle\lambda_{p'}\pi\pi|T|\lambda_\gamma = +1, \lambda_p\rangle + \langle\lambda_{p'}\pi\pi|T|\lambda_\gamma = -1, \lambda_p\rangle),$$

$$J_z(\lambda_p, \lambda_{p'}) = \frac{\nu}{\sqrt{Q^2}}\langle\lambda_{p'}\pi\pi|T|\lambda_\gamma = 0, \lambda_p\rangle.$$

The angular distribution of negatively charged pions off the electron-scattering plane, $d\sigma/d\varphi_{\pi^-}$, can be obtained by integrating the fivefold-differential cross section (2) over all variables, with the exception of φ_{π^-}; that is,

$$\frac{d\sigma}{d\varphi_{\pi^-}} = \int\frac{d^5\sigma}{d\tau}d\tau', \quad (6)$$

where $d\tau' = dS_{\pi^+\pi^-} dS_{\pi^+ p}\sin\vartheta_{\pi^-} d\vartheta_{\pi^-} d\alpha$.

Within the model used here, the dependence of the helicity amplitudes on the angle φ_{π^-} is controlled by the equation

$$\langle\lambda_{p'}\pi\pi|T|\lambda_\gamma\lambda_p\rangle = \langle\lambda_{p'}\pi\pi|T|\lambda_\gamma\lambda_p\rangle|_{\varphi_{\pi^-}=0}\cdot e^{i(\lambda_\gamma - \lambda_p)\varphi_{\pi^-}}, \quad (7)$$

where $\langle\lambda_{p'}\pi\pi|T|\lambda_\gamma\lambda_p\rangle|_{\varphi_{\pi^-}=0}$ is the helicity amplitude calculated at zero emission angle of the negatively charged pion, $\varphi_{\pi^-} = 0$. Substituting (7) into (5) and evaluating the bilinear combinations of the hadron currents in (2), we find that the first term in the parenthetical expression on the right-hand side of (2) is independent of φ_{π^-}; it is merely the sum of the quantities obtained by averaging, over the initial spin states of the photon and proton, and summing, over the final helicity states, the squared moduli of the matrix elements of the helicity amplitudes and yields

the cross sections for the reaction $\gamma_v p \to \pi^+\pi^- p$ that are integrated over the angle φ_{π^-}. The second term on the right-hand side of (2) is broken down into the sum of terms that are proportional to $\cos 2\varphi_\pi$ and $\sin 2\varphi_\pi$, while the third term in this expression is given by the sum of terms that are proportional to $\cos\varphi$ and $\sin\varphi$. Upon integration in (6), the differential cross section $d\sigma/d\varphi_{\pi^-}$ reduces to the form

$$d\sigma/d\varphi_{\pi^-} = A + B\cos 2\varphi_\pi + \tilde{B}\sin 2\varphi_\pi + C\cos\varphi_\pi + \tilde{C}\sin\varphi_\pi. \quad (8)$$

The coefficient A in (8) is determined by the sum of the squared moduli of the matrix elements of the helicity amplitudes in the parenthetical expression on the right-hand side of (2):

$$A = \int \frac{4\pi\alpha}{4K_L M_N} \times \left(\frac{1}{4} \sum_{\lambda_\gamma = \pm 1, \lambda_p \lambda_{p'}} \langle \lambda_{p'} \pi\pi | T | \lambda_\gamma, \lambda_p \rangle^* \times \langle \lambda_{p'} \pi\pi | T | \lambda_\gamma, \lambda_p \rangle + \varepsilon_L \frac{1}{2} \sum_{\lambda_p \lambda_{p'}} \langle \lambda_{p'} \pi\pi | T | \lambda_\gamma = 0, \lambda_p \rangle^* \times \langle \lambda_{p'} \pi\pi | T | \lambda_\gamma = 0, \lambda_p \rangle \right) \frac{1}{32W^2} \frac{1}{(2\pi)^5} d\tau'. \quad (9)$$

The coefficients B and $\tilde{B}$ are controlled by the second term in the braced expression on the right-hand side of (2) and are due to the interference between the amplitudes for transverse photons of helicity $\lambda_\gamma = +1$ and -1:

$$B = \int \frac{(4\pi\alpha)\varepsilon}{4K_L M_N} \left(-2\mathrm{Re} \left(\frac{1}{4} \times \sum_{\lambda_\gamma = \pm 1, \lambda_p \lambda_{p'}} \langle \lambda_{p'} \pi\pi | T | \lambda_\gamma = -1, \lambda_p \rangle^* \times \langle \lambda_{p'} \pi\pi | T | \lambda_\gamma = +1, \lambda_p \rangle \right) \right) \frac{1}{32W^2} \frac{1}{(2\pi)^5} d\tau', \quad (10)$$

$$\tilde{B} = \int \frac{(4\pi\alpha)\varepsilon}{4K_L M_N} \left(2\mathrm{Im} \left(\frac{1}{4} \times \sum_{\lambda_\gamma = \pm 1, \lambda_p \lambda_{p'}} \langle \lambda_{p'} \pi\pi | T | \lambda_\gamma = -1, \lambda_p \rangle^* \times \langle \lambda_{p'} \pi\pi | T | \lambda_\gamma = +1, \lambda_p \rangle \right) \right) \frac{1}{32W^2} \frac{1}{(2\pi)^5} d\tau'.$$

The coefficients C and $\tilde{C}$ are determined by the third term in the aforementioned braced expression and are due to the interference between the $\lambda_\gamma = 0$ and $\lambda_\gamma = \pm 1$ amplitudes:

$$C = \int \frac{4\pi\alpha}{4K_L M_N} \frac{\nu}{\sqrt{Q^2}} \frac{1}{\sqrt{2}} \sqrt{2\varepsilon_L(1+\varepsilon)} \times \left(-2\mathrm{Re} \frac{1}{4} \sum_{\lambda_p \lambda_{p'}} \langle \lambda_{p'} \pi\pi | T | \lambda_\gamma = 0, \lambda_p \rangle^* \times \left(\langle \lambda_{p'} \pi\pi | T | \lambda_\gamma = +1, \lambda_p \rangle - \langle \lambda_{p'} \pi\pi | T | \lambda_\gamma = -1, \lambda_p \rangle \right) \right) \frac{1}{32W^2} \frac{1}{(2\pi)^5} d\tau', \quad (11)$$

$$\tilde{C} = \int \frac{4\pi\alpha}{4K_L M_N} \frac{\nu}{\sqrt{Q^2}} \frac{1}{\sqrt{2}} \sqrt{2\varepsilon_L(1+\varepsilon)} \times \left(2\mathrm{Im} \frac{1}{4} \sum_{\lambda_p \lambda_{p'}} \langle \lambda_{p'} \pi\pi | T | \lambda_\gamma = 0, \lambda_p \rangle^* \times \left(\langle \lambda_{p'} \pi\pi | T | \lambda_\gamma = +1, \lambda_p \rangle + \langle \lambda_{p'} \pi\pi | T | \lambda_\gamma = -1, \lambda_p \rangle \right) \right) \frac{1}{32W^2} \frac{1}{(2\pi)^5} d\tau'.$$

We note that, upon the integration of the expression in (8) with respect to the angle φ_{π^-}, all terms featuring the dependence on the angle φ_{π^-} vanish. For the reaction $\gamma_v p \to \pi^+\pi^- p$, the approach developed in [7, 8] describes the cross section integrated with respect to the angle φ_{π^-}.

In the case where a polarized electron of helicity λ_e is scattered by an unpolarized proton, the cross section (2) develops an additional term that is proportional to λ_e [13, 14]; that is,

$$\frac{d^5\sigma_h}{d\tau} = \frac{4\pi\alpha}{4K_L M_N} \left\{ h\sqrt{2\varepsilon_L(1-\varepsilon)} \frac{i(J_y^* J_z - J_z^* J_y)}{2} + h\sqrt{(1-\varepsilon^2)} \frac{i(J_x^* J_y - J_y^* J_x)}{2} \right\} \frac{1}{32W^2} \frac{1}{(2\pi)^5}, \quad (12)$$

$$h = 2\lambda_e,$$

where λ_e is the incident-electron helicity. Substituting expression (5) for the currents J_μ into (12) with the phases in (7) for the helicity amplitudes and integrating the cross sections (12) with respect to all variables, with the exception of φ_{π^-}, we obtain $d\sigma_h/d\varphi_{\pi^-}$ in the form

$$d\sigma_h/d\varphi_{\pi^-} = h(\tilde{A}_h + C_h \sin\varphi_{\pi^-} + \tilde{C}_h \cos\varphi_{\pi^-}). \quad (13)$$

The coefficient $\tilde{A}_h$ emerges from the second term in (12) and has the form

$$\tilde{A}_h = \int \frac{4\pi\alpha}{4K_L M_N}\frac{1}{4}\sqrt{1-\varepsilon^2} \quad (14)$$
$$\times \left(\sum_{\lambda_p\lambda_{p'}} |\langle\lambda_{p'}\pi\pi|T|\lambda_\gamma = +1, \lambda_p\rangle|^2 \right.$$
$$\left. - \sum_{\lambda_p\lambda_{p'}} |\langle\lambda_{p'}\pi\pi|T|\lambda_\gamma = -1, \lambda_p\rangle|^2\right)\frac{1}{32W^2}\frac{1}{(2\pi)^5}d\tau'.$$

The coefficients C_h and $\tilde{C}_h$ are given by

$$C_h = \int \frac{4\pi\alpha}{4K_L M_N}\sqrt{2\varepsilon_L(1-\varepsilon)}\frac{1}{4}\frac{\nu}{\sqrt{Q^2}}\frac{1}{\sqrt{2}} \quad (15)$$
$$\times \left(2\mathrm{Im}\left(\sum_{\lambda_p\lambda_{p'}} \langle\lambda_{p'}\pi\pi|T|\lambda_\gamma = 0, \lambda_p\rangle^* \right.\right.$$
$$\times (\langle\lambda_{p'}\pi\pi|T|\lambda_\gamma = +1, \lambda_p\rangle$$
$$\left.\left. - \langle\lambda_{p'}\pi\pi|T|\lambda_\gamma = -1, \lambda_p\rangle)\right)\right)\frac{1}{32W^2}\frac{1}{(2\pi)^5}d\tau',$$

$$\tilde{C}_h = \int \frac{4\pi\alpha}{4K_L M_N}\sqrt{2\varepsilon_L(1-\varepsilon)}\frac{1}{4}\frac{\nu}{\sqrt{Q^2}}\frac{1}{\sqrt{2}}$$
$$\times \left(-2\mathrm{Re}\left(\sum_{\lambda_p\lambda_{p'}} \langle\lambda_{p'}\pi\pi|T|\lambda_\gamma = 0, \lambda_p\rangle^* \right.\right.$$
$$\times (\langle\lambda_{p'}\pi\pi|T|\lambda_\gamma = +1, \lambda_p\rangle$$
$$\left.\left. + \langle\lambda_{p'}\pi\pi|T|\lambda_\gamma = -1, \lambda_p\rangle)\right)\right)\frac{1}{32W^2}\frac{1}{(2\pi)^5}d\tau'.$$

The helicity amplitudes appearing in Eqs. (9)–(11), (14), and (15) are calculated at $\varphi_{\pi^-} = 0$. From the results obtained by measuring the differential cross sections (2) for the exclusive channel $\gamma_v p \to \pi^+\pi^- p$ at two opposite helicities of the incident electron, $h = \pm 1$, one can deduce the differential cross section (12): the difference of the differential cross sections (2) at $h = +1$ and $h = -1$ is equal to the doubled cross section in (12). The resulting structure of expressions (8) and (13) for the φ_{π^-} dependence of the cross sections $d\sigma/d\varphi_{\pi^-}$ and $d\sigma_h/d\varphi_{\pi^-}$ is coincident with that presented in [14] for the production of more than two particles in the final state. The requirement that the amplitude of the reaction $\gamma_v p \to \pi^+\pi^- p$ be invariant under a space inversion leads to the vanishing of the tilde-labeled coefficients in Eqs. (10), (11), and (13)–(15) upon integration with respect to τ', whereupon relations (8) and (13) reduce to the well-known relations presented in [13] for the production of two particles in the final state. The vanishing of the tilde-labeled coefficients is of a dynamical character, and its verification is a good test of the description of various mechanisms within the present model—above all, of the choice of the relative phases of the quasi-two-body processes illustrated in Fig. 1 and the phases between the resonance and nonresonance components of these processes, as well as of the parametrization of the remaining mechanisms in terms of the complex-valued quantity $C(W, Q^2)$. Upon taking into account the vanishing of the tilde-labeled coefficients, the cross section $d\sigma_h/d\varphi_{\pi^-}$ proves to be proportional to $\sin\varphi_{\pi^-}$; therefore, the integral of this cross section with respect to the angle φ_{π^-} is equal to zero. As follows from expressions (11) and (15), the coefficients C and C_h appearing in (8) and (13) carry information about the interference between the Coulomb form factors for nucleon resonances and the transverse form factors $A_{1/2}$ and $A_{3/2}$. It should be noted that measurement of the off-scattering-plane angular distributions of negatively charged pions yields information about the real part of the interference term [coefficient C in Eq. (8)], while measurement of the polarization asymmetry of the beam furnishes information about the imaginary part of this interference term [coefficient C_h in Eq. (13)]. The coefficient B in expression (8) for the off-scattering-plane angular distribution carries information about the interference between the transverse form factors $A_{1/2}$ and $A_{3/2}$ for nucleon resonances.

In order to describe observables that contain terms associated with the interference between different helicity states of the photon—for example, the off-scattering-plane angular distributions and the polarization asymmetry of the beam—it is necessary to introduce the amplitude $C(W, Q^2)$ correctly. A parametrization of $C(W, Q^2)$ by a real-valued function of W and Q^2 is illegitimate, since a real-valued amplitude that does not feature a dependence on the helicities of initial- and final-state particles does not satisfy the requirement that the amplitude be invariant under the transformation of space inversion; as a result, the tilde-labeled coefficients in expressions (8) and (13) would prove to be nonvanishing in that case.

We have tested the correctness of two parametrizations for $C(W, Q^2)$: (i) The first was a parametrization with the aid of the contact term

$$C(W, Q^2) = C'(W, Q^2)\varepsilon_\mu(\lambda_\gamma)\bar{u}_{p'}\gamma_\mu u_p, \quad (16)$$

where $\varepsilon_\mu(\lambda_\gamma)$ is the wave vector of the photon whose helicity is λ_γ; $\bar{u}_{p'}$ and u_p are Dirac spinors that describe, respectively, the initial- and the final-state proton; and $C'(W, Q^2)$ is a real-valued factor that is determined from the best fit to experimental data on the cross sections for the production of $\pi^+\pi^-$ pairs in

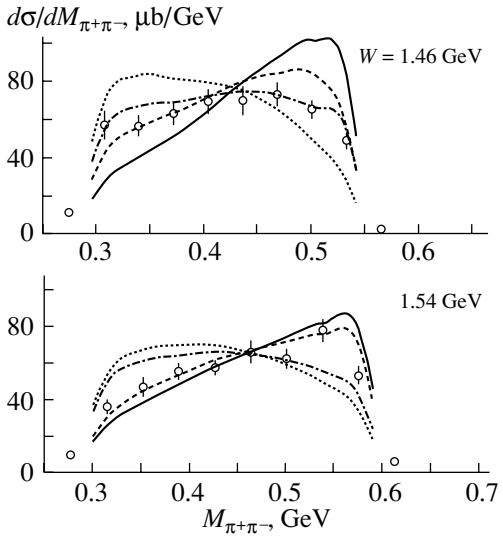

Fig. 2. Invariant-mass distributions of $\pi^+\pi^-$ pairs according to calculations employing the parametrization in (16), along with data of the CLAS Collaboration [10]. The data are presented at $Q^2 = 0.95$ GeV^2 in two W bins. Different curves correspond to different values of the relative phase of the amplitude associated with the diagrams in Fig. 1 and the phase-space amplitude: (solid curve) 0°, (dashed curve) 90°, (dotted curve) 180°, (dash-dotted curve) 270°.

each (W, Q^2) bin. (ii) The second was a parametrization of the form

$$C(W, Q^2) = C'(W, Q^2)e^{i\varphi_{3b}}, \qquad (17)$$

where φ_{3b} is the phase of the sum of the amplitudes of the tree diagrams in Fig. 1. The absolute value $C'(W, Q^2)$ of the amplitude in (17) corresponds to the phase-space approximation. With the phase φ_{3b} chosen as was indicated above, we were able to describe the transformation of the amplitude under a space inversion correctly. The calculations performed for the kinematical region of the E-93-006 experiment of the CLAS Collaboration [10] ($1.44 < W < 1.89$ GeV at $Q^2 = 0.65$ and 0.95 GeV^2 and $1.41 < W < 2.09$ GeV at $Q^2 = 1.3$ GeV^2) revealed that the parametrizations in (16) and (17) both lead to the vanishing of the tilde-labeled coefficients in (8) and (13); therefore, each of them makes it possible to describe the properties of the total amplitude under the transformations of space inversion adequately.

In Fig. 2, the invariant-mass distribution $d\sigma/dM_{\pi^+\pi^-}$ calculated with the parametrization in (16) for $C(W, Q^2)$ is compared with its counterparts measured in the E-93-006 experiment of the CLAS Collaboration [10] for $Q^2 = 0.95$ GeV^2 at $W = 1.46$ and 1.54 GeV. The different curves in this figure correspond to different values of the relative phase of the amplitude associated with the diagrams in Fig. 1 and the amplitude of the contact term (16): 0°, 90°, 180°, and 270°. This phase was additionally introduced since the measured distributions $d\sigma/dM_{\pi^+\pi^-}$ could not be reproduced with zero phase. One can see that the calculated cross sections are greatly dependent on the relative phase of the contact term. This strong dependence stems from the fact that, if one chooses five independent kinematical variables ($S_{\pi^+\pi^-}$, S_{π^+p}, ϑ_{π^-}, φ_{π^-}, α), a change in the invariant mass of the $\pi^+\pi^-$ system at fixed values of the remaining variables leads to a change in the emission angle of the final proton, which is described by the spinor $\bar{u}_{p'}$ in (16); this in turn leads to a pronounced change in the contact term. We note that the parametrization in (16) is purely phenomenological, its choice not being dictated by any basic physical principles. Therefore, the choice between the parametrizations in Eqs. (16) and (17) must rely on the possibility of obtaining the best fit to available data. Our calculations have revealed that, in the case of a contact term in the form (16), it is impossible to choose, for this term, a W-independent phase that would lead to a good description of data for $W < 1.6$ GeV. In view of this, the parametrization in (17) is used everywhere below for the phase-space amplitude.

3. EFFECT OF NUCLEON RESONANCES ON OFF-SCATTERING-PLANE ANGULAR DISTRIBUTIONS OF NEGATIVELY CHARGED PIONS AND ON THE POLARIZATION ASYMMETRY OF THE BEAM

Within the approach outlined above, we have calculated the W dependence of the coefficients B and C in (8), which control the off-scattering-plane angular distributions of negatively charged pions, and the W dependence of the coefficients C_h in (13), which characterize the beam asymmetry at $Q^2 = 0.95$ GeV^2. The calculations were performed for 12 nucleon resonances presented in [7, 8], the nucleon-resonance form factors and model parameters used in these calculations being chosen on the basis of the best fit to the data of the CLAS Collaboration at $Q^2 = 0.95$ GeV^2 [15]. In order to verify the sensitivity of the coefficients C_h and C as functions of W to variations in the Coulomb form factors for nucleon resonances, the calculations were performed at three values of the Coulomb form factor $C_{1/2}$ for the $P_{11}(1440)$ state: the value of $C_{1/2} = -0.157$ GeV$^{-1/2}$, which corresponds to the best fit to the data of the CLAS Collaboration [15]; the sign-reversed value of $C_{1/2} = 0.157$ GeV$^{-1/2}$; and zero value, $C_{1/2} = 0$, which corresponds to the assumption that the $P_{11}(1440)$ state undergoes no Coulomb excitation.

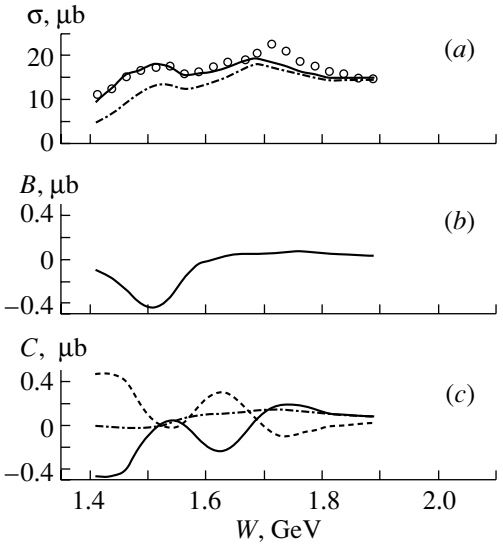

Fig. 3. (a) Total cross sections for the production of $\pi^+\pi^-$ pairs and coefficients (b) B and (c) C versus W according to calculations employing various values of the Coulomb form factor for the $P_{11}(1440)$ state: (solid curves) $C_{1/2} = -0.157$ GeV$^{-1/2}$, (dashed curves) $C_{1/2} = 0.157$ GeV$^{-1/2}$, and (dash-dotted curves) $C_{1/2} = 0$.

The results obtained by calculating the integrated cross sections and the coefficient C versus W are shown in Figs. 3a and 3c, respectively, by the solid curves for $C_{1/2} = -0.157$ GeV$^{-1/2}$, the dashed curve for $C_{1/2} = 0.157$ GeV$^{-1/2}$, and the dash-dotted curves for $C_{1/2} = 0$. As follows from the data presented in Fig. 3a, which displays the integrated cross sections for the reaction $\gamma_v p \to \pi^+\pi^- p$ at two opposite values of $C_{1/2}$, this integrated cross section as a function of W exhibits but a relatively weak dependence on the sign of the form factor $C_{1/2}$. At the same time, a strong dependence on the sign of the form factor $C_{1/2}$ for the $P_{11}(1440)$ state is observed in the coefficients C as a function of W, variations in C versus $C_{1/2}$ being the most pronounced in the region of W around $P_{11}(1440)$; however, the effect of $C_{1/2}$ is sizable at high values of W, up to $W \sim 1.7$ GeV.

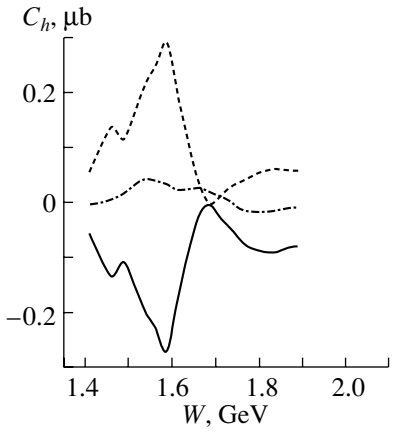

Fig. 4. Coefficient C_h in (13) versus W according to calculations employing various values of the Coulomb form factor for the $P_{11}(1440)$ state: (solid curve) $C_{1/2} = -0.157$ GeV$^{-1/2}$, (dashed curve) $C_{1/2} = 0.157$ GeV$^{-1/2}$, and (dash-dotted curve) $C_{1/2} = 0$.

In analyzing data reported in [10, 15], the Coulomb form factor for the $P_{11}(1440)$ state was introduced as an adjustable parameter in describing the cross section for the reaction $\gamma_v p \to \pi^+\pi^- p$ as a function of W for $W < 1.7$ GeV. From data presented in [15], which contain the differential cross sections $d\sigma/d\Omega_{\pi^-}$, $d\sigma/d\Omega_{\pi^+\pi^-}$, and $d\sigma/d\Omega_{\pi^+ p}$ defined in terms of the sum of the squared moduli of helicity amplitudes, it is impossible to separate the nucleon-resonance form factors $A_{1/2}$ and $C_{1/2}$, since all of the aforementioned cross sections depend on these form factors only through the combination $A^2_{1/2} + \varepsilon_L C^2_{1/2}$. On the other hand, the coefficients C in (8) are determined by the products of electromagnetic form factors, $A_{1/2}C_{1/2}$, and that is why the coefficient C greatly depends on the form factor $C_{1/2}$ for the $P_{11}(1440)$ state, as is predicted by the present calculation. In view of this, an analysis of the off-scattering-plane distributions of negatively charged pions with

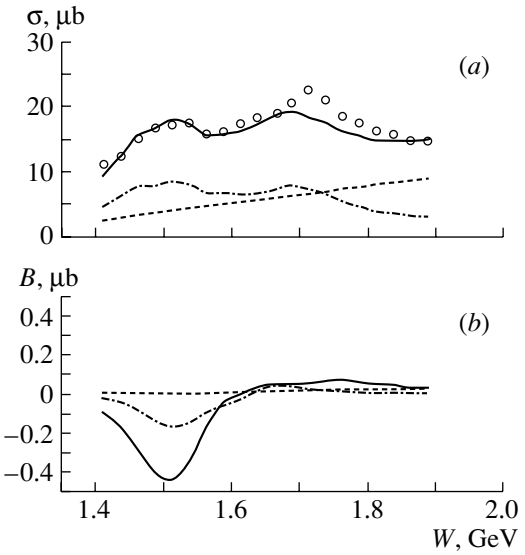

Fig. 5. (a) Integrated cross sections for the reaction $\gamma_v p \to \pi^+\pi^- p$ and (b) coefficients B (solid curves in Figs. 1a and 1b) versus W, along with the contributions to these quantities from (dash-dotted curves) nucleon-resonance excitations and (dashed curves) nonresonance mechanisms.

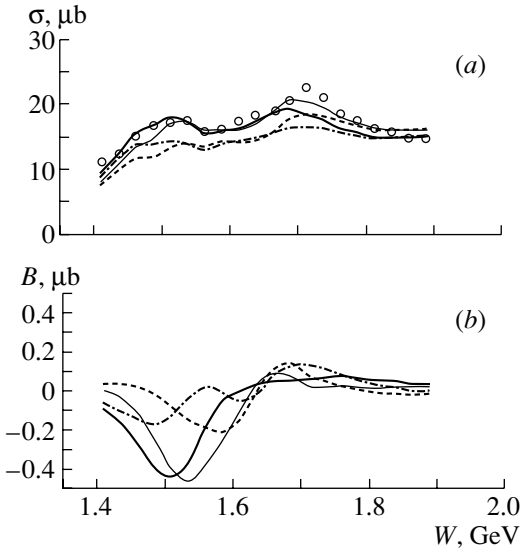

Fig. 6. (*a*) Integrated cross sections for the reaction $\gamma_v p \to \pi^+\pi^- p$ and (*b*) coefficients B versus W according to calculations employing various values of the relative phase of resonance and nonresonance processes in the quasi-two-body channel $\gamma_v p \to \pi^-\Delta^{++}$: (thick solid curves) 0°, (dashed curves) 90°, (thin solid curves) 180°, and (dash-dotted curves) 270°.

respect to the angle φ_π has a very high potential for a determination of the Coulomb form factor for the $P_{11}(1440)$ state. Experimental data on the Coulomb form factor for this state are of particular interest for obtaining deeper insight into its structure—in particular, such data may furnish information about the presence of a gluon-component admixture [16].

Figure 4 shows the calculated coefficients C_h for the asymmetry of the beam versus W. The calculations were performed for the above values of the form factor $C_{1/2}$ for the $P_{11}(1440)$ state. It turns out that the magnitude and the sign of the form factor $C_{1/2}$ for the $P_{11}(1440)$ state affect the W dependence of the coefficients C_h significantly. At $C_{1/2} = 0$, the coefficients C_h are also close to zero, which is indicative of a dominant contribution of the Coulomb excitation of nucleon resonances to the beam asymmetry. The interference between the longitudinal and transverse amplitudes for photon interaction generates the only contribution to the beam asymmetry; owing to this, the Coulomb form factors for nucleon resonances can be determined, in this case, via a more straightforward procedure in relation to an analysis of angular distributions off the scattering plane, since, in the latter case, there are a contribution from the interference between the longitudinal and transverse amplitudes and a contribution from the interference between transverse amplitudes for different photon-helicity values. At the same time, a global analysis of angular distributions off the scattering plane and of the asymmetry of the beam will make it possible to improve the reliability of extracting the Coulomb form factors.

At present, there are virtually no data on the Coulomb form factors for nucleon resonances heavier than $P_{11}(1440)$. An analysis of JJNAF data on angular distributions off the scattering plane and on the beam asymmetry within the approach proposed in the present study will make it possible to obtain the first experimental information about the Coulomb form factors for most nucleon resonances.

The solid curve in Fig. 5*b* depicts the calculated W dependences of the coefficients B in (8), which characterize the off-scattering-plane distribution of negatively charged pions with respect to the angle φ. In the same panel, the dashed and the dash-dotted curve represent the contributions of, respectively, nonresonance and resonance mechanisms. The results of the calculations performed within the same approach for the integrated cross section and for its resonance and nonresonance components are displayed in Fig. 5*a*. The contribution of nonresonance mechanisms to the integrated cross section ranges between 20 and 60%, while the contribution of nonresonance processes to the coefficient B is less than the nucleon-resonance contribution by more than one order of magnitude. A comparison of the calculated W dependence of the coefficient B and the resonance contribution to it reveals that the structure observed at $W = 1.5$ GeV is formed owing predominantly to the interference between nucleon resonances and nonresonance mechanisms.

The formation of the structure at 1.5 GeV in the W dependence of the coefficient B is due to the following circumstances. As follows from Eq. (10), the coefficient B is sensitive to variations in the product of the helicity electromagnetic amplitudes $A_{1/2}$ and $A_{3/2}$ for nucleon resonances. At $Q^2 = 0.95$ GeV^2, this product is greater for the $D_{13}(1520)$ state than for all other states included in the model. Moreover, it was shown in [17] that a significant interference with nonresonance Born terms is characteristic of this state. These are the circumstances that lead to the emergence of a structure at $W = 1.5$ GeV in the W dependence of the coefficients B.

A strong suppression of the contribution from nonresonance processes and a significant contribution from the interference between nucleon resonances and nonresonance mechanisms to the W dependence of the coefficient B may open the possibility for extracting, from data on the W dependence of the coefficient B, the relative phase of the interference between resonance and nonresonance mechanisms. It is rather difficult to estimate this phase on the basis of theoretical models, and its determination from

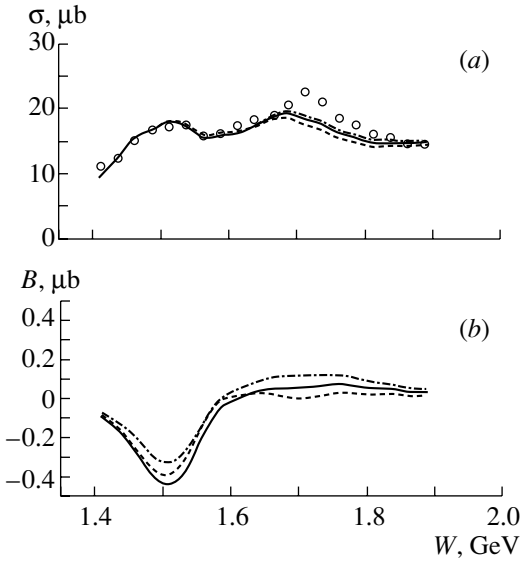

Fig. 7. (*a*) Integrated cross sections for the reaction $\gamma_v p \to \pi^+\pi^- p$ and (*b*) coefficients B versus W according to calculations performed with the $\sqrt{A_{1/2}^2 + A_{3/2}^2}$ value for $D_{13}(1520)$ from a fit to data of the CLAS Collaboration and under the assumption that the contribution of $A_{1/2}$ is (dashed curves) 10% or (dash-dotted curves) 90% of $\sqrt{A_{1/2}^2 + A_{3/2}^2}$. Also shown in both panels are the results of the calculations employing the values of $A_{1/2}$ and $A_{3/2}$ from a fit to the data (solid curves).

experimental data is therefore of considerable interest. Providing additional information compared to the total cross section, measurement of the coefficient B may help to separate the contributions of the helicity amplitudes $A_{1/2}$ and $A_{3/2}$ more accurately.

In order to explore these possibilities, we have calculated the coefficients B at four values of the relative phase of the resonance and nonresonance mechanisms in the channel $\gamma_v p \to \pi^-\Delta^{++}$: 0°, 90°, 180°, and 270°. For the various values of this relative phase, Fig. 6*b* displays the calculated W dependences of the coefficients B. In the region $W < 1.7$ GeV, one can see a significant effect of the relative phase of the resonance and nonresonance mechanisms in the $\pi\Delta$ channel on the W dependence of the coefficients B. At the same time, the effect of this relative phase on the W dependence of either the integrated cross sections or the coefficients B is quite modest in the region $W > 1.7$ GeV. Thus, it may prove to be possible to extract the relative phase of resonance and nonresonance mechanisms from the W dependence of the coefficient B for $W < 1.7$ GeV.

For the value of $\sqrt{A_{1/2}^2 + A_{3/2}^2}$ for the $D_{13}(1520)$ state from a fit to data of the E-93-006 experiment at JLAB [10, 15], we have calculated the W dependence of the coefficients B for (i) the case where the contribution of $A_{1/2}$ is 10% of the contribution of $\sqrt{A_{1/2}^2 + A_{3/2}^2}$, (ii) the case where $A_{1/2}$ and $A_{3/2}$ are set to the values from a fit to data given in [10, 15], and (iii) the case where the contribution of $A_{1/2}$ is 90% of the contribution of $\sqrt{A_{1/2}^2 + A_{3/2}^2}$. The results of these calculations are given in Fig. 7. The prospects for separating the form factors $A_{1/2}$ and $A_{3/2}$ are not optimistic here. At the same time, a simultaneous analysis of the ϑ distributions of negatively charged pions (ϑ is the emission angle of these particles with respect to the virtual-photon 3-momentum), their off-scattering-plane distribution with respect to φ, and the double beam–target polarization asymmetry [11] opens new possibilities for separating the contributions of $A_{1/2}$ and $A_{3/2}$ to the electromagnetic excitations of nucleon resonances.

4. CONCLUSION

A further development of the model proposed in [7–10] and intended for describing double charged-pion production by photons on a proton has been presented. Within the approach formulated in the present study, we have calculated off-scattering-plane angular distributions of pions and the beam asymmetry.

Our model calculations have revealed that off-scattering-plane angular distributions and the polarization asymmetry of the beam are highly sensitive to the Coulomb excitation of the $P_{11}(1440)$ state. Analyzing, within the approach developed in the present study, data of the CLAS Collaboration on polarization beam asymmetries and on off-scattering-plane angular distributions would make it possible to obtain the first information about the Coulomb excitation of nucleon resonances.

A global analysis of the angular distributions of negatively charged pions with respect to the photon momentum, their off-scattering-plane distributions, and the double beam–target polarization asymmetry would provide additional possibilities for distributing the electromagnetic strength of the nucleon resonance between the amplitudes $A_{1/2}$ and $A_{3/2}$. Moreover, it may prove to be possible to determine, from experimental data, the relative phase of the resonance and nonresonance mechanisms in $\pi\Delta$ production; this would be of importance since it is rather difficult to estimate this phase theoretically.

REFERENCES

1. V. Burkert, Nucl. Phys. A **684**, 16 (2001).
2. R. Koniuk and N. Isgur, Phys. Rev. D **21**, 1868 (1980).
3. M. M. Giannini, Rep. Prog. Phys. **54**, 453 (1990).
4. S. Capstick and W. Roberts, Phys. Rev. D **49**, 4570 (1994).
5. F. Stancu and P. Stassart, Phys. Rev. D **47**, 2140 (1993).
6. K. F. Liu and C. W. Wong, Phys. Rev. D **28**, 170 (1983).
7. V. Mokeev, M. Ripani, M. Anghinolfi, *et al.*, Yad. Fiz. **64**, 1368 (2001) [Phys. At. Nucl. **64**, 1292 (2001)].
8. M. Ripani, V. Mokeev, M. Battaglieri, *et al.*, Yad. Fiz. **63**, 2036 (2000) [Phys. At. Nucl. **63**, 1943 (2000)].
9. V. Mokeev, M. Ripani, M. Anghinolfi, *et al.*, Nucl. Phys. A **672**, 220 (2000).
10. V. Mokeev, M. Ripani, M. Anghinolfi, *et al.*, in *Proceedings of the Workshop on the Physics of Excited Nucleons (NSTAR 2001), Mainz, Germany, 2001,* Ed. by D. Drechsel and L. Tiator (World Sci., 2001), p. 181.
11. M. Ripani, V. Mokeev, M. Anghinolfi, *et al.*, Yad. Fiz. **66**, 1322 (2003) [Phys. At. Nucl. **66**, 1282 (2003)].
12. E. Amaldi, S. Fubini, and G. Furlan, Springer Trac. Mod. Phys. **83**, 1 (1979).
13. D. Drechsel and L. Tiator, J. Phys. G **18**, 449 (1992).
14. T. W. Donnelly, *New Vistas in Electro-Nuclear Physics*, Ed. by E. L. Tomusiak and H. S. Coplon; NATO ASI Series **142**, 151 (1991).
15. V. I. Mokeev, M. Ripani, M. Anghinolfi, *et al.*, AIP, accepted for publication.
16. V. Burkert, in *Proceedings of the Conference NSTAR 2000, Newport News, USA, 16–19 Feb. 2000,* Ed. by V. Burkert, L. Elouadrhiri, J. J. Kelly, and R. C. Minehart (World Sci., 2000), p. 1.
17. J. C. Nacher and E. Oset, Nucl. Phys. A **674**, 205 (2000).

Translated by A. Isaakyan

Physics of Atomic Nuclei, Vol. 66, No. 12, 2003, pp. 2159–2168. From Yadernaya Fizika, Vol. 66, No. 12, 2003, pp. 2209–2218.

ELEMENTARY PARTICLES AND FIELDS
Theory

Observation of Coherent π^0 Electroproduction on Deuterons at Large Momentum Transfer*

E. Tomasi-Gustafsson[1),2)], L. Bimbot[3)], S. Danagoulian[4),5)], K. Gustafsson[6)], D. Mack[5)], H. Mkrtchyan[7)], and M. P. Rekalo[1),8),9)]

Received September 6, 2002; in final form, March 11, 2003

Abstract—The first experimental results for the coherent π^0 electroproduction on a deuteron, $e + d \to e + d + \pi^0$, at large momentum transfer, are reported. The experiment was performed at Jefferson Laboratory at an incident electron energy of 4.05 GeV. A large pion production yield has been observed in the kinematical region $1.1 < Q^2 < 1.8$ GeV^2, from the threshold to 200-MeV excitation energy in the $d\pi^0$ system. The Q^2 dependence is compared with theoretical predictions. © *2003 MAIK "Nauka/Interperiodica".*

1. INTRODUCTION

After elastic scattering, the reaction $e + d \to e + d + \pi^0$ is the simplest coherent process for ed collisions that contains information on the deuteron structure and on the elementary nucleon amplitudes. This reaction has characteristics that make it a very good source of knowledge on the deuteron structure, complementary to other probes. The presence of a deuteron with zero isospin in the initial and final states leads to a specific isotopic structure for the corresponding amplitudes. The elastic ed scattering is essentially determined by an isoscalar combination of nucleon electromagnetic form factors, whereas the coherent pion electroproduction on the deuteron allows both a scan of the full isospin structure of the nucleon electromagnetic current in the resonance region and a separation of isoscalar and isovector contributions. This increases the degree of complexity, but simultaneously opens a unique way to progress in the understanding of the deuteron and nucleon structure.

Besides the calculation of static hadronic properties like masses or magnetic moments, the description of elastic and inelastic form factors (which contain dynamical information on the hadron structure) represents a powerful test for theoretical models. In particular, in the intermediate energy region, the electromagnetic form factors should be a helpful signature of the transition from the confinement regime to perturbative QCD [1].

The experimental determination of the three form factors of the deuteron requires the measurement of polarization observables. The most recent elastic scattering ed data at large values of momentum transfer squared, $Q^2 \leq 6$ GeV^2 [2], have been successfully compared to pQCD predictions, whereas polarization measurements [3] lead to the conclusion that, up to $Q^2 \simeq 2$ GeV^2, the deuteron structure can be described by conventional models based on nucleon and meson degrees of freedom. It seems very difficult to extend such measurements to higher momentum transfer with existing techniques [4]. However, inelastic processes, such as $e + d \to e + d + \pi^0$ (accessible with existing beams and polarimeters), probe the deuteron at smaller distances than the elastic scattering at the same value of Q^2. An appropriate choice of kinematics can lead to new and interesting information. Two $d\pi^0$-excitation-energy regions seem particularly promising: the threshold region and the Δ-excitation region.

Considerable experimental activity has been going on in the field of near-threshold pion production in γp collisions [5, 6], ep collisions [7], and γd collisions [8], but the data on pion production in ed collisions are scarce. The experimental study of this reaction is now possible at Mainz and at Jefferson Laboratory

*This article was submitted by the authors in English.

[1)]LNS-Saclay, Gif-sur-Yvette, France.
[2)]DAPNIA/SPhN, CEA/Saclay, Gif-sur-Yvette, France.
[3)]IPNO, IN2P3, BP 1, Orsay, France.
[4)]North Carolina State University, Greensboro, NC 27411, USA.
[5)]Thomas Jefferson National Accelerator Facility, Newport News, VA 23606, USA.
[6)]Helsinki Institute of Physics, University of Helsinki, Helsinki, Finland.
[7)]Yerevan Physics Institute, Yerevan, 375036 Armenia.
[8)]Middle East Technical University, Physics Department, Ankara, Turkey.
[9)]National Science Center: KFTI, Kharkov, 310108 Ukraine.

1063-7788/03/6612-2159$24.00

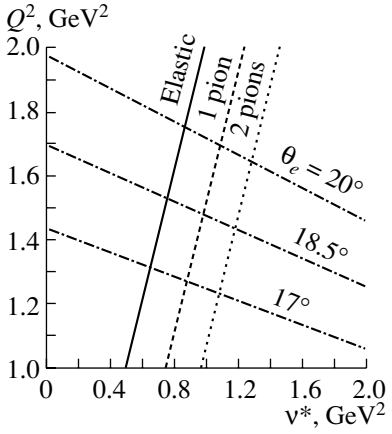

Fig. 1. Kinematical lines of *ed* interaction in the Q^2-vs.-ν^* plane calculated for a beam energy $E_1 = 4.05$ GeV. The elastic line (solid line) and the threshold lines for one-pion (dashed line) and two-pion production (dotted line) are indicated. The angular range covered by the kinematics of the electron is also indicated (dash-dotted lines).

(JLab), due to the high duty cycle of the electron machines. Threshold π^0 electroproduction on protons and deuterons has been investigated by the A1 collaboration at Mainz [9] at small momentum transfer squared $Q^2 \leq 0.1$ GeV^2.

At this low momentum transfer, different, nonperturbative QCD, approaches, in particular, Chiral Perturbation Theory (ChPT), can be applied. Phenomenological approaches such as effective Lagrangian models, isobar models, quark models, and hybrid models are widely applicable. A general theoretical study of pion electroproduction on deuterons was first developed in [10]. An adequate dynamical approach to pion electroproduction has to take into account all previous theoretical findings related to other electromagnetic processes on the deuteron, such as elastic *ed* scattering, π^0 photoproduction $\gamma + d \to d + \pi^0$ [11], and deuteron photodisintegration $\gamma + d \to n + p$ [12]. Like these processes, the reaction $e + d \to e + d + \pi^0$ involves the study of the deuteron structure and of the reaction mechanism and the determination of the neutron elementary amplitudes, $\gamma^* + n \to n + \pi^0$, where γ^* is a virtual photon. Note that the exact cancellation of rescattering effects, due to the processes $\gamma^* + d \to p + p + \pi^-(n + n + \pi^+) \to d\pi^0$ in the near-threshold region [13], allows one to extract the neutron amplitudes from the data on $e + d \to e + d + \pi^0$, in the framework of the impulse approximation.

Here, the first experimental observation of π^0 electroproduction on deuterons is reported at large values of the momentum transfer squared and at relatively small excitation energy of the produced $d\pi^0$ system. This kinematical region is only accessible at JLab.

The data were collected during the t_{20} experiment, the primary aim of which was the measurement of the deuteron tensor polarization in elastic *ed* scattering [3]. We have reconstructed the dependence on the kinematical variables that contain the physical information for the process $e + d \to e + d + \pi^0$, taking into account the difficulties related to limited experimental acceptance and to low detection efficiency. With a complete measurement of the fivefold differential cross section, the comparison to the theory would have been straightforward. Here, the detection of the deuteron, due to limited resolution and statistics, does not allow a complete and precise reconstruction of the physical event. We derive from the experiment the Q^2 dependence of the yield, which can be directly compared to theoretical models, such as an effective Lagrangian model and pQCD predictions.

Our paper is organized as follows. In Section 2, we present kinematical and dynamical characteristics of the process $e + d \to e + d + \pi^0$. The description of the experiment is presented in Section 3. Section 4 is devoted to the discussion of the experimental results and to the comparison with theoretical predictions. The main results are summarized in the Conclusions. The Appendix contains a detailed scheme of the experimental analysis in the case of incomplete event reconstruction.

2. THE PROCESS $e + d \to e + d + \pi^0$

2.1. The Kinematics

In the framework of the one-photon mechanism, the process $e + d \to e + X$ is equivalent to $\gamma^* + d \to X$, where X is a hadronic system, and this gives the most convenient choice of kinematical variables for the electroproduction processes. The detection of the recoil deuteron in coincidence with the scattered electron allows a full reconstruction of the kinematics for $\gamma^* + d \to d + \pi^0$.

In the limit of zero electron mass, the momentum transfer squared from the incident to the outgoing electron, Q^2, is defined as

$$Q^2 = 4E_1E_2 \sin^2 \frac{\theta_e}{2},$$

where E_1 (E_2) is the energy of the incident (scattered) electron and θ_e is the electron scattering angle (in the laboratory system). As defined here, Q^2 is positive in the spacelike region.

The energy and the angle of the scattered electron enable the determination of the momentum transfer

squared Q^2 and of the invariant mass of the produced hadronic system W:

$$W = \sqrt{M^2 - Q^2 + 2\nu^*},$$

where M is the deuteron mass and the quantity $\nu^* = M(E_1 - E_2)$ is related to the energy transferred from the electron to the hadronic system X.

Events from elastic scattering and electroproduction of one and two pions follow straight lines in a plane defined by Q^2 vs. ν^* (Fig. 1), corresponding to a definite value of the invariant mass W. Fixed values of θ_e also correspond to straight lines in the Q^2–ν^* plane. In Fig. 1, the lines corresponding to $\theta_e = 18.5°(\pm 1.5°)$ are drawn to emphasize the kinematical limits of the experimental setup.

For the analysis of the π^0-production data near threshold, instead of the invariant variable $t = (p_1 - p_2)^2$ (p_1 and p_2 are the 4-momenta of the target and of the outgoing deuteron, respectively), it is preferable to use $\cos\tilde{\theta}_\pi$, where $\tilde{\theta}_\pi$ is the pion production angle in the center-of-mass system (c.m.s.) of the final $d\pi^0$ system.

At a given value of W, the final deuteron energy in the laboratory system, E_d, can be expressed as a quadratic function of the cosine of the deuteron scattering angle, $\cos\theta_d$, which is drawn in Fig. 2 for different values of ΔW. In this figure, the threshold point for π^0 electroproduction and the point for elastic ed kinematics, at a fixed value of incident electron energy and electron scattering angle, are also indicated.

These considerations are valid for coplanar kinematics, where all momenta of the final particles in $e + d \to e + d + \pi^0$ are in the same plane. This corresponds to two values of the azimuthal angle of the final deuteron, $\phi = 0$ and $\phi = \pi$, relative to the electron scattering plane, defined by the directions of the 3-momenta of the initial and final electrons $\mathbf{k}_1$ and $\mathbf{k}_2$. The left-hand side of each ellipse in Fig. 2 (with respect to the center, i.e., the threshold point) corresponds to $\phi = \pi$ (the deuteron scattering angle is smaller than the threshold value) and the right-hand side of the ellipses corresponds to $\phi = 0$ (the deuteron scattering angle is larger than the threshold value).

Note, in conclusion, that the measurement of E_d allows the determination of $\cos\tilde{\theta}_\pi$ as a function of E_d, W, and Q^2 through the following expression:

$$2M^2 - 2ME_d = -Q^2 + m_\pi^2 - \frac{(W^2 - Q^2 - M^2)(W^2 + m_\pi^2 - M^2)}{2W^2} + 2\cos\tilde{\theta}_\pi \sqrt{\left[\frac{(W^2 - Q^2 - M^2)^2}{4W^2} + Q^2\right]\left[\frac{(W^2 + m_\pi^2 - M^2)^2}{4W^2} - m_\pi^2\right]}. \quad (1)$$

The knowledge of the $\cos\tilde{\theta}_\pi$ dependence for the differential cross section of $\gamma^* + d \to d + \pi^0$ is essential in order to perform a multipole analysis.

2.2. The Dynamics

In the framework of the one-photon mechanism, the differential cross section for $e + d \to e + d + \pi^0$ can be written as [14]

$$\sigma(\phi) = \frac{d^5\sigma}{dE_2 d\Omega \widetilde{d\Omega}} = \mathcal{N}\big[\mathcal{H}_T + \epsilon\mathcal{H}_L + \epsilon\mathcal{H}_P \cos 2\phi + \sqrt{2\epsilon(1+\epsilon)}\mathcal{H}_I \cos\phi\big], \quad (2)$$

where $\mathcal{N}$ is a normalization kinematical coefficient,

$$\mathcal{N} = \frac{\alpha^2}{64\pi^3}\frac{E_2}{E_1}\frac{q_\pi}{MW}\frac{1}{(1-\epsilon)}\frac{1}{Q^2}, \quad (3)$$

and ϵ is the degree of linear polarization of the virtual photon,

$$\epsilon^{-1} = 1 + 2\frac{\mathbf{k}_{\gamma^2}}{Q^2}\tan^2\frac{\theta_e}{2}. \quad (4)$$

Here, $\mathbf{k}_\gamma^2 = (\mathbf{k}_1 - \mathbf{k}_2)^2 = E_1^2 + E_2^2 - 2E_1E_2\cos\theta_e$, $\mathbf{q}_\pi$ is the pion 3-momentum in the c.m.s. of the reaction $\gamma^* + d \to d + \pi^0$ with $\mathbf{q}_\pi^2 = E_\pi^2 - m_\pi^2$, $E_\pi = (W^2 + m_\pi^2 - M^2)/(2W)$, and $\alpha = e^2/(4\pi) \simeq 1/137$.

The terms $\mathcal{H}_a$ ($a = T, L, P, I$) are related to the four standard contributions to the differential cross section for $\gamma^* + d \to d + \pi^0$, corresponding to the different polarizations of the virtual photon: T and P are the transverse components, L is the longitudinal component, and I is the interference between the longitudinal and transversal components. The element of solid angle for the scattered electron (deuteron) in the laboratory (c.m.) system is $d\Omega$ ($\widetilde{d\Omega}$). Note that $\widetilde{d\Omega} = d\cos\tilde{\theta}_\pi d\phi_\pi$.

The different contributions $\mathcal{H}_a$ depend on Q^2, W, and $\cos\tilde{\theta}_\pi$. The azimuthal dependence is explicit in the cosine terms [Eq. (2)]. The three kinematical quantities ϵ, $\mathcal{N}$, and ϕ depend on the electron kinematics.

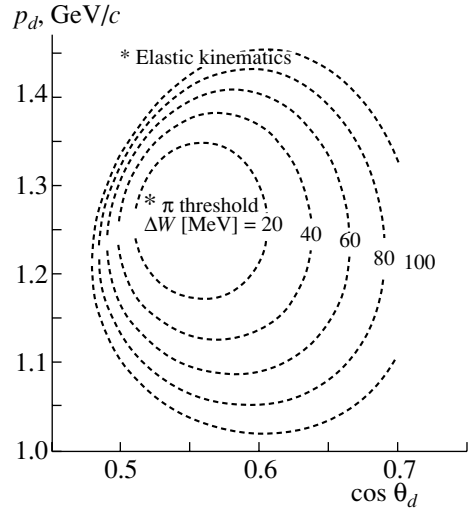

Fig. 2. The deuteron momentum as a function of the deuteron scattering angle, in coplanar kinematics, for different values of ΔW, the excess of invariant $d\pi$ mass over the pion-production threshold. The initial electron energy is $E_1 = 4.05$ GeV and $\theta_e = 18.5°$.

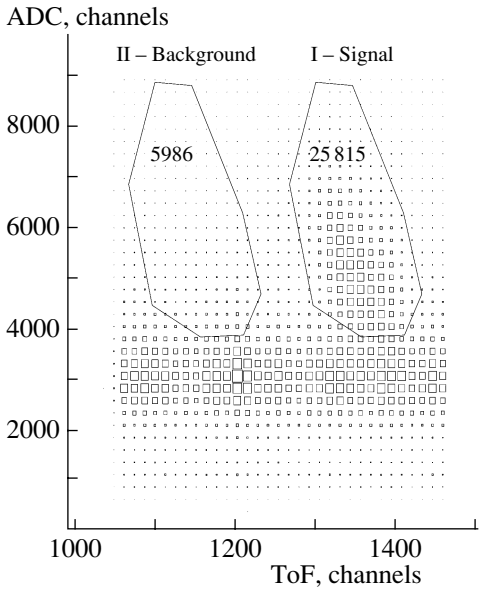

Fig. 3. Two-dimensional plot of the events in the ADC-vs.-time-of-flight plane. The contours are used to select the deuterons from $e + d \to e + d + \pi^0$ events (contour I, labeled "Signal") and to estimate the background (contour II, labeled "Background"). The events at ADC values around 3000 correspond to random electron–protons coincidences.

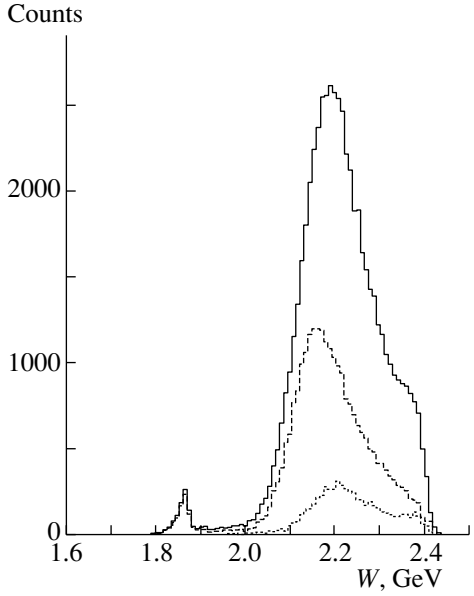

Fig. 4. Experimental distribution of the invariant mass W corresponding to events in the range of time of flight 1280–1440 (solid line) and to events selected, according to Fig. 3, by contour I (dashed line) or by contour II (dotted line).

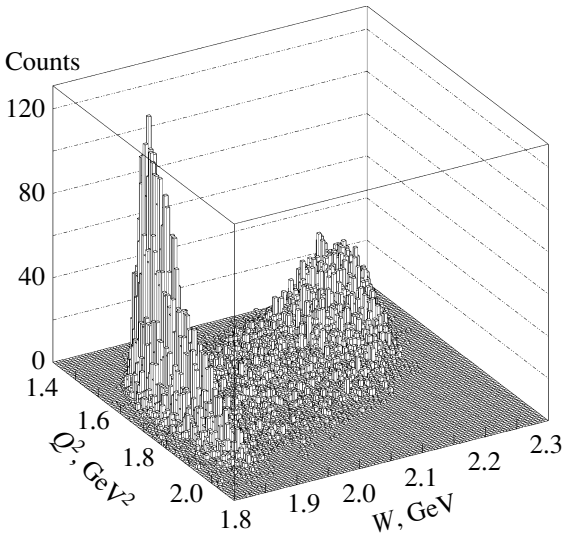

Fig. 5. Two-dimensional plot of the number of counts as a function of momentum transfer squared Q^2 and invariant mass of the hadronic system W for the $e + d \to e + X$ reaction in the near-elastic kinematics. The beam energy is 4.05 GeV and the $\theta_e = 20.3°$. Events corresponding to the elastic peak are centered around $W = M$.

A measurement of $\sigma(\phi)$ for three values of ϕ (for example, $\phi = 0,\ \pi/2$, and π) and for two values of the parameter ϵ allows a complete and unique separation of all four contributions to the cross section. Note that Eq. (2) can be considered a generalization of the Rosenbluth formula for a three-body reaction, in which only two particles are detected in the final state.

In the near-threshold region, in the framework of the S- and P-wave pion production, the four contributions to the differential cross section of

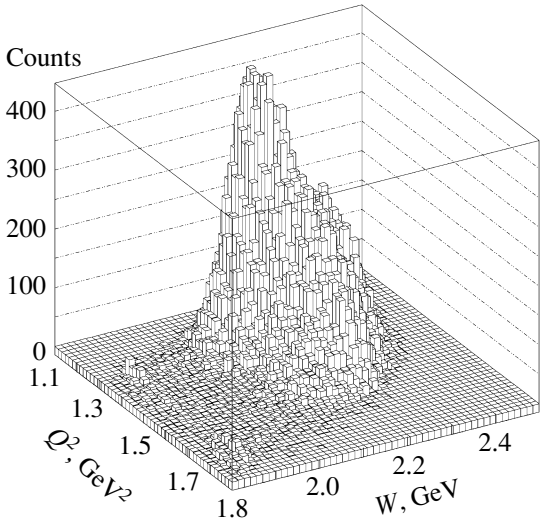

Fig. 6. Two-dimensional plot of the number of counts as a function of momentum transfer Q^2 and invariant mass of the hadronic system W for the $e + d \to e + X$ reaction in the pion kinematics. The beam energy is 4.05 GeV and $\theta_e = 18.5°$. Events corresponding to pion production are visible for $W > M + m_\pi$.

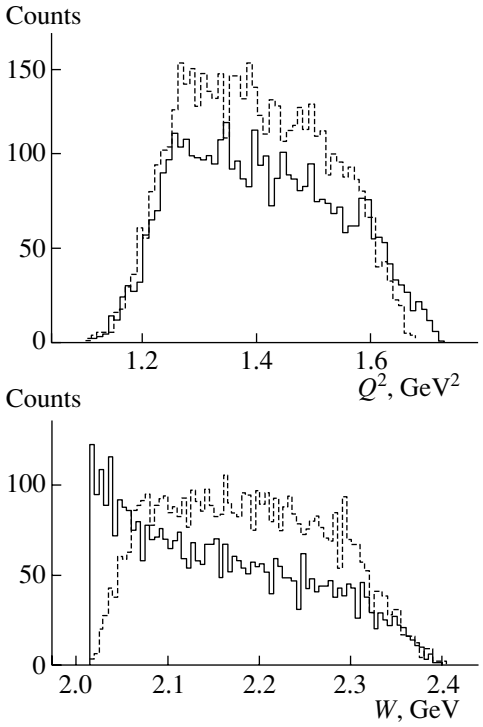

Fig. 7. Q^2 distribution and W distribution, following a Monte Carlo simulation. The solid line corresponds to a uniform input cross section and the dashed line corresponds to an input distribution corrected by the kinematical factor $\mathcal{N}$ (Eq. 3).

$e + d \to e + d + \pi^0$ can be parametrized as functions of $\cos\tilde{\theta}_\pi$ as follows (omitting, for simplicity, the deuteron form factors):

$$\mathcal{H}_T = a_0 + a_1 \cos\tilde{\theta}_\pi + a_2 \cos^2\tilde{\theta}_\pi, \qquad (5)$$

$$\mathcal{H}_P = b_0 \sin^2\tilde{\theta}_\pi,$$

$$\mathcal{H}_L = c_0 + c_1 \cos\tilde{\theta}_\pi + c_2 \cos^2\tilde{\theta}_\pi,$$

$$\mathcal{H}_I = \sin\tilde{\theta}_\pi (d_0 + d_1 \cos\tilde{\theta}_\pi),$$

where the real coefficients a_i, b_i, c_i, and d_i are well-defined quadratic combinations of multipole amplitudes for $\gamma^* + d \to d + \pi^0$, which are functions of only two variables, Q^2 and W. All the dynamical information about this process is contained in these multipole amplitudes. The experimental determination of the Q^2 and W dependences of the multipole amplitudes would allow a direct comparison with the theory. In the framework of the S- and P-wave contributions, the fivefold cross section has to be measured for at least nine points (for different $\cos\tilde{\theta}_\pi$, ϕ, and ϵ) in order to determine fully the multipole amplitudes (the moduli and relative phases).

In the case of limited acceptance or of partial information on one or both of the final particles, one can extract from the experiment—and compare to theoretical predictions—only some combinations of the above-mentioned coefficients. For example, near threshold, the pions are emitted in a narrow cone around the virtual photon direction (in the laboratory system) and the experimental resolution may not allow a precise determination of the azimuthal angle, or, on the contrary, far above threshold the detection acceptance may not cover the full phase space. We derive in the Appendix a rigorous method for the data analysis, in the case of limited kinematical information.

3. THE EXPERIMENT

From Figs. 1 and 2, it appears that the kinematical characteristics of the outgoing particles (the scattered electron and deuteron) in the process $e + d \to e + d + \pi^0$ in the threshold region are close to those of the elastic process $e + d \to e + d$. Therefore, the experimental setup of the t_{20} experiment at JLab, which had a double-arm detection for elastic ed scattering, could be used to study the inelastic process of π^0 production. The experiment was performed in Hall C. With small changes in the spectrometer settings, it was possible to reach near-threshold kinematics in which π^0 events were detected. The typical luminosity was about 2×10^{38} cm^2 s^{-1} obtained with a 40-μA continuous electron beam and a 12-cm-long liquid deuterium target. The electrons were detected in a large-solid-angle (6 msr) spectrometer (HMS) with an energy resolution $\Delta E/E = 10^{-3}$. The deuterons were focused on the polarimeter

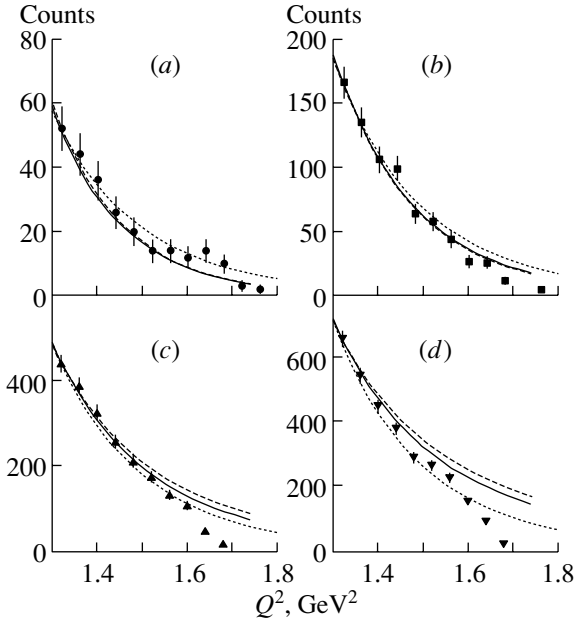

Fig. 8. Q^2 dependence of the counting rates, corrected by the kinematical factor $\mathcal{N}$ (3), for different bins of the invariant mass excess $\Delta W = W - W_{\rm th}$: (*a*) $0 \le \Delta W \le 40$ MeV; (*b*) $40 \le \Delta W \le 80$ MeV; (*c*) $80 \le \Delta W \le 120$ MeV; (*d*) $120 \le \Delta W \le 160$ MeV. The solid curve and dashed curves correspond to different ranges of ϕ integration from [10] (see the text). The dotted curve is the pQCD prediction, with $N = 14$ and $m^2 = 1.41$ GeV^2; see Eq. (6). All curves are normalized to data at $Q^2 = 1.3$ GeV^2.

POLDER [15] through a magnetic transport line located at a fixed angle, θ_d, of 60.5°. For the initial electron energy, $E_e = 4.05$ GeV, the scattered electrons were detected at an angle $\theta_e = 18.5°$ corresponding to a range of 4-momentum squared $1.1 < Q^2 < 1.8$ GeV^2. The coincidence between electrons and deuterons reduced the high background. A more detailed description of the experimental setup can be found in [3, 16].

The deuterons were identified in the two-dimensional spectrum corresponding to the time-of-flight-versus-the-ADC signal related to the energy loss in the POLDER start detectors. The deuterons were selected by the contour shown in Fig. 3 (contour I, labeled "Signal"). An estimation of the background, done by displacing the contour (contour II, labeled "Background"), is about 20%. The largest part of the background, corresponding to protons coming from deuteron breakup, does not appear in the figure, as it corresponds to a different region of the time-of-flight spectrum.

The spectrum of the invariant mass W is shown in Fig. 4 for different selection criteria of events. Above the pion threshold, $W_{\rm th} = M + m_\pi$, a significant number of events were observed. The transition between the elastic and the pion production regions is illustrated in Figs. 5 and 6. The number of counts is plotted as a two-dimensional function of Q^2 and W, for the $e + d \to e + X$ reaction, for spectrometer settings corresponding to elastic kinematics (Fig. 5) and to pion kinematics (Fig. 6), where a tail from elastic scattering is still visible. The experimental resolutions are $\Delta W/W = 0.3\%$ and $\Delta Q^2/Q^2 = 0.7\%$.

In this measurement, in four hours of beam on target, 25 815 pion events were counted in contour I, 330 of which correspond to the near-threshold region in an invariant mass range $\Delta W = W - W_{\rm th} = 40$ MeV. This total number is comparable to the number of events for elastic *ed* scattering in similar experimental conditions.

4. THE RESULTS

The deuteron magnetic channel has large angular acceptance and low momentum resolution. The deuteron momentum and scattering angle could not be reconstructed with precision. For this reason, the information presented here concerns the kinematical variables calculated from the electron channel. We focus here on the Q^2 dependence of the differential cross section of the process $e + d \to e + d + \pi^0$, for which theoretical predictions are available.

In Fig. 7, we show the Monte Carlo expectation [17] for the Q^2 and the W distributions, calculated for a uniform input distribution (solid line) and for a distribution weighted by the kinematical factor $\mathcal{N}$ (Eq. 3). The figure shows the range of detection where the acceptance of the apparatus is reasonably flat: $1.3 \le Q^2 \le 1.6$ GeV^2 and W from threshold up to 2.3 GeV.

In order to extract the Q^2 distribution, quite conservative cuts were applied in order to select events well inside the acceptance of the deuteron channel. We assumed that the efficiency is constant in this central region. This is reasonably supported by the Monte Carlo simulations.

Systematic errors due to event selection were estimated with the help of a parallel analysis, where the selection of events was done by a window in the time-of-flight and electron-momentum bidimensional plot. Background subtraction was done by displacing a window in the time-of-flight spectrum. The final distributions were consistent within the error bars.

In Fig. 8, the Q^2 dependence of the counting rates integrated over the experimental acceptance is given for different region of W, in bins of 40 MeV, from threshold to the Δ-excitation region. The data are corrected by the kinematical factor $\mathcal{N}$ [see Eq. (3)] in order to make an easier comparison with the theoretical predictions. We did not attempt to apply an

absolute normalization of the data due to a large uncertainty on the reconstruction of the deuteron kinematics, although the $d\pi^0$ events were unambiguously identified.

Moreover, the radiative corrections are necessary to extract absolute values of the cross section. For the considered process, at relatively large momentum transfer, radiative corrections are, in principle, far from being negligible. Their calculation is complicated from a theoretical point of view, and to the best of our knowledge, no calculation exists for pion coherent electroproduction on the deuteron. Furthermore, the acceptance has to be taken into account precisely. But if we consider relative yields, this problem can be neglected, mainly due to the logarithmic, i.e., weak, dependence of radiative corrections on Q^2 and relatively small Q^2 interval in the present experiment.

The four spectra show a similar steep decreasing behavior.[10] In general, the acceptance in one variable is a complicated function of other variables and it is usually estimated through sophisticated simulations. But if the ϕ acceptance is small or constant, or in the case of full 2π ϕ acceptance, a rigorous treatment of the data is possible, even without full information on the azimuthal angle (see Appendix). The relative Q^2 dependence of the yields can be compared with theoretical calculations, such as the impulse approximation or pQCD scaling laws [18].

Predictions available from a classical (mesonic) model on coherent pion electroproducion [10], where the reaction mechanism is described within the impulse approximation (the deuteron is described by the Paris wave function) and the $\gamma^* + N \to N + \pi$ interaction is treated in the framework of an effective Lagrangian model [10], are shown in Fig. 8. The solid and dashed curves correspond, respectively, to ϕ integration over 2π and to the limit for small $\Delta\phi$, which is closer to the experimental conditions. For 2π acceptance, only $\mathcal{H}_T$ and $\mathcal{H}_L$ contribute to the cross section, whereas, in the case of small ϕ acceptance, all contributions to the exclusive cross section are present (see Appendix).

The theoretical curves are normalized to the highest experimental point, for the smallest value of Q^2. After normalization, the results are not very sensitive to the opening of the azimuthal angle. Such behavior can be interpreted as an indication of a weak ϕ dependence of the $d(e, e'\pi^0)d$ cross section. Another possibility is that the different contributions induce a similar Q^2 dependence of the cross section, integrated in this kinematical region. The theoretical model [10] indeed predicts a large ϕ dependence in the Δ region.

Following the quark counting rule of pQCD [1], the asymptotic behavior of the electromagnetic (elastic and inelastic) form factors of hadrons follows a $(1/Q^2)^{(n_1+n_2)/2-1}$ dependence, where $n_1(n_2)$ is the number of quarks in the initial (final) state. For pion electroproduction on the deuteron (at relatively large momentum transfer and small excitation energies, where the electroproduction process is determined by the inelastic electromagnetic current, $\gamma^* + d \to d + \pi^0$, with $n_1 = 6$ and $n_2 = 6 + 2 = 8$), we expect a value of $n_1 + n_2 = 14$, which corresponds to a steeper decrease in the cross section compared to elastic ed scattering, where $n_1 + n_2 = 12$.

The Q^2 behavior for the coherent inelastic deuteron cross section is illustrated in Fig. 8, where we show the results of the parametrization

$$\sigma_{d\pi^0}(Q^2) = \frac{\sigma_{d\pi^0}(0)}{(1 + Q^2/m^2)^N} \qquad (6)$$

for $N = 14$ (dotted curve) and for $m^2 = 1.41$ GeV^2, according to [1].

The results from these two approaches are consistent with the present data. As for elastic ed scattering [2], the measurement of the cross section alone does not allow us to disentangle predictions given by different models of the deuteron structure.

5. CONCLUSIONS

Coherent π^0 electroproduction on the deuteron, $e + d \to e + d + \pi^0$, at relatively large momentum transfer has been detected for the first time. The specific conditions of this experiment covered coherent π^0 production in the near-threshold region and in the region of excitation of the Δ resonance. A steep decrease with Q^2 in the counting rate has been observed at different values of W.

The present results show that it is possible to foresee a research program based on the experimental study of coherent pion electroproduction on the deuteron at relatively large momentum transfer, at threshold, and in the Δ region, to access

the relative contributions of S and P waves for different values of Q^2;

the Q^2-scaling behavior of S- and P-wave excitation for $\gamma^* + d \to d + \pi^0$;

the specific mass parameter, m^2, which enters into the Q^2 dependence of the different contributions to the differential cross section to be compared to meson and nucleon form-factor values;

the Δ-isobar excitation on the deuteron, $\gamma^* + d \to \Delta + N \to d + \pi^0$.

[10] The deviation from a monotonic decrease for $Q^2 \geq 1.6$ GeV^2 may reflect a limitation in the acceptance (see Fig. 7).

We have established the feasibility of such an experimental study, since counting rates are similar to elastic scattering. More complete results could be obtained at the Jefferson Laboratory in a dedicated experiment, which would stimulate parallel efforts from the theoretical side in developing specific calculations adapted to this newly accessible region. In particular, in addition to the differential cross section, measurements of the vector and tensor polarization of the outgoing deuteron are possible in this energy domain [19].

Finally, we would like to recall that, after several decades of experimental and theoretical studies of *ed* elastic scattering, the situation with the deuteron models (choices of nucleon form factors, deuteron wave functions, corrections to impulse approximation, etc.) is not yet disentangled. In this respect, a detailed study of $e + d \to e + d + \pi^0$ will bring new important pieces of information.

ACKNOWLEDGMENTS

We would like to thank all the members of the t_{20} Collaboration for help in taking the data, and, in particular, J. Arvieux, E. Beise, R. Gilman, C. Glashausser, and S. Kox for useful discussions.

APPENDIX

We present here a possible scheme for the analysis of $e^- + d \to e^- + d + \pi^0$ data, taking into account the case of partial information of the detected particles.

For the estimation of the ϕ acceptance, it is necessary to know the relative angle between the 3-momentum of the virtual photon, $\mathbf{k}_\gamma$, and the momentum of the scattered deuteron. This angle depends on the variable W and can be calculated using the following expression for the production angle of the virtual photon θ_γ relative to the electron scattering angle:

$$\cos\theta_\gamma = \frac{E_2\cos\theta_e + E_1}{k_\gamma}.$$

Limited ϕ acceptance. If we approximate the ϕ acceptance for the emitted deuteron as

$$-\frac{\Delta\phi}{2} \le \phi \le \frac{\Delta\phi}{2},$$

then, for $\Delta\phi \ll 1$, all possible contributions in Eq. (2), namely, 1, $\cos 2\phi$, and $\cos\phi$, will give the same results:

$$\int\limits_{-\Delta\phi/2}^{\Delta\phi/2} 1 d\phi = \Delta\phi,$$

$$\int\limits_{-\Delta\phi/2}^{\Delta\phi/2} \cos 2\phi d\phi = \sin\Delta\phi \simeq \Delta\phi,$$

$$\int\limits_{-\Delta\phi/2}^{\Delta\phi/2} \cos\phi d\phi = \sin\Delta\phi \simeq \Delta\phi.$$

Thus, we can write the ϕ-integrated cross section as follows:

$$\frac{d^4\sigma}{dE_2 d\Omega d\cos\tilde{\theta}_\pi} = \Delta\phi\mathcal{N}\sigma(Q^2, W, \cos\tilde{\theta}_\pi, E_1),$$

with the following dependence for $\cos\tilde{\theta}_\pi$:

$$\sigma(Q^2, W, \cos\tilde{\theta}_\pi, E_1) = A_0 + A_1\cos\tilde{\theta}_\pi + A_2\cos^2\tilde{\theta}_\pi + A_3\sin\tilde{\theta}_\pi + A_4\sin\tilde{\theta}_\pi\cos\tilde{\theta}_\pi, \quad \text{(A.1)}$$

where the five coefficients A_i are definite linear combinations of the coefficients (5):

$$\begin{aligned} A_0 &= a_0 + \epsilon(c_0 + b_0), \quad \text{(A.2)}\\ A_1 &= a_1 + \epsilon c_1,\\ A_2 &= a_2 + \epsilon(c_2 - b_0),\\ A_3 &= \sqrt{2\epsilon(1+\epsilon)}d_0,\\ A_4 &= \sqrt{2\epsilon(1+\epsilon)}d_1. \end{aligned}$$

The E_1 dependence of all these coefficients A_i is contained only in the parameter ϵ.

If we can measure the cross section $d^4\sigma/dE_2 d\Omega d\cos\tilde{\theta}_\pi$ at five different values of $\tilde{\theta}_\pi$, we will determine all five coefficients $A_i(Q^2, W, \cos\tilde{\theta}_\pi, E_1)$, which can be compared to theoretical predictions.

Full 2π acceptance. In this case only the L and T components of the cross section contribute to the integral of (2) in the interval $0 \le \phi \le 2\pi$:

$$\frac{d^4\sigma}{dE_2 d\Omega d\cos\tilde{\theta}_\pi} = 2\pi\mathcal{N}\sigma(Q^2, W, \cos\tilde{\theta}_\pi, E_1),$$

with the following dependence on $\cos\tilde{\theta}_\pi$:

$$\sigma(Q^2, W, \cos\tilde{\theta}_\pi, E_1) = A_0 + A_1\cos\tilde{\theta}_\pi + A_2\cos^2\tilde{\theta}_\pi \quad \text{(A.3)}$$

and the three coefficients A_i are definite linear combinations of the coefficients (5):

$$\begin{aligned} A_0 &= a_0 + \epsilon c_0, \quad \text{(A.4)}\\ A_1 &= a_1 + \epsilon c_1,\\ A_2 &= a_2 + \epsilon c_2. \end{aligned}$$

The Rosenbluth fit in ϵ is very useful for the separation of the different contributions to the coefficients A_0–A_2.

$\cos\tilde{\theta}_\pi$ integration. This integration has to be done if the deuteron energy (in the laboratory system) is not properly measured.

The representation (5) is well adapted to $\cos\tilde{\theta}_\pi$ integration over the energy acceptance of the deuteron channel. We can use the one-to-one correspondence between the deuteron energy E_d (in laboratory system) and $\cos\tilde{\theta}_\pi$. From Eq. (2), we find

$$\cos\tilde{\theta}_\pi = \frac{T_0 - E_d}{T_1},$$

where T_0 and T_1 are

$$T_0 = \frac{1}{4M}\left[W^2 - Q^2 - m_\pi^2 + \frac{(M^2 - Q^2)(M^2 - m_\pi^2)}{W^2}\right],$$

$$T_1 = \frac{1}{M}\left[\left(\frac{(W^2 + Q^2 - M^2)^2}{4W^2} - Q^2\right)\left(\frac{(W^2 + m_\pi^2 - M^2)^2}{4W^2} - m_\pi^2\right)\right]^{1/2},$$

i.e., the energies T_0 and T_1 are functions of Q^2 and W only.

The final result can be written as

$$\frac{d^3\sigma}{dE_2 d\Omega} = \Delta\phi\mathcal{N}\tilde{\sigma}(Q^2, W, E_1),$$

where

$$\tilde{\sigma}(Q^2, W, E_1) = A_0 I_0 + A_1 I_1 + A_2 I_2 + A_3 I_3 + A_4 I_4.$$

The coefficients I_0–I_4 are the integrals over the acceptance of the deuteron channel:

$$I_0 = \int_\Delta d\cos\tilde{\theta}_\pi = \frac{1}{T_1}\int_{E_d^{\min}}^{E_d^{\max}} dE_d, \qquad \text{(A.5)}$$

$$I_1 = \int_\Delta \cos\tilde{\theta}_\pi d\cos\tilde{\theta}_\pi = -\frac{1}{T_1^2}\int_{E_d^{\min}}^{E_d^{\max}} (T_0 - E_d)dE_d,$$

$$I_2 = \int_\Delta \cos^2\tilde{\theta}_\pi d\cos\tilde{\theta}_\pi = -\frac{1}{T_1^3}\int_{E_d^{\min}}^{E_d^{\max}} (T_0 - E_d)^2 dE_d,$$

$$I_3 = \int_\Delta \sin\tilde{\theta}_\pi d\cos\tilde{\theta}_\pi = -\frac{1}{T_1}\int_{E_d^{\min}}^{E_d^{\max}} dE_d\sqrt{1 - \frac{(T_0 - E_d)^2}{T_1^2}},$$

$$I_4 = \int_\Delta \sin\tilde{\theta}_\pi\cos\tilde{\theta}_\pi d\cos\tilde{\theta}_\pi = -\frac{1}{T_1^2}\times\int_{E_d^{\min}}^{E_d^{\max}} dE_d(T_0 - T_1)\sqrt{1 - \frac{(T_0 - E_d)^2}{T_1^2}},$$

where $E_d^{\min}$ and $E_d^{\max}$ are the minimal and maximal energies of the deuteron (in the laboratory system). The coefficients I_0–I_4 are functions of Q^2 and W for each initial energy of the electron beam E_1.

The calculation of the coefficients A_0–A_4, in the framework of a definite model for $\gamma^* + d \to d + \pi^0$, together with numerical values for I_0–I_4, allows a straightforward comparison of the measured cross section $d^2\tilde{\sigma}/dQ^2dW$ with theoretical predictions.

REFERENCES

1. S. J. Brodsky and G. R. Farrar, Phys. Rev. Lett. **31**, 1153 (1973); S. J. Brodsky and B. T. Chertok, Phys. Rev. D **14**, 3003 (1976); Phys. Rev. Lett. **37**, 269 (1976).
2. L. C. Alexa *et al.*, Phys. Rev. Lett. **82**, 1374 (1999).
3. D. Abbott *et al.*, Phys. Rev. Lett. **84**, 5053 (2000); K. Hafidi, PhD Thesis (University of Paris XI, 1999); Report DAPNIA/SPhN-99-05T; W. Zhao, PhD Thesis (MIT, 1999); K. Gustafsson, PhD Thesis (University of Maryland, 2000).
4. F. Gross and R. Gilman, nucl-th/0110015.
5. M. Fuchs *et al.*, Phys. Lett. B **368**, 20 (1996); A. M. Bernstein, E. Shuster, R. Beck, *et al.*, Phys. Rev. C **55**, 1509 (1997).
6. J. C. Bergström *et al.*, Phys. Rev. C **53**, R1052 (1996); J. C. Bergström, R. Igarashi, and J. M. Vogt, Phys. Rev. C **55**, 2016 (1997).
7. H. B. van der Brink *et al.*, Nucl. Phys. A **612**, 391 (1997).
8. J. C. Bergström *et al.*, Phys. Rev. C **57**, 3203 (1998).
9. M. O. Distler *et al.*, Phys. Rev. Lett. **80**, 2294 (1998); I. Ewald *et al.*, Phys. Lett. B **499**, 238 (2001).
10. M. P. Rekalo, E. Tomasi-Gustafsson, and J. Arvieux, LNS/Ph/97-20; Ann. Phys. (N. Y.) **295**, 1 (2002).
11. D. G. Meekins *et al.*, Phys. Rev. C **60**, 052201 (1999).

12. C. W. Bochna *et al.*, Phys. Rev. Lett. **81**, 4576 (1998); E. C. Schulte *et al.*, Phys. Rev. Lett. **86**, 2975 (2001); K. Wijesooriya *et al.*, Phys. Rev. Lett. **87**, 102302 (2001).
13. M. P. Rekalo and E. Tomasi-Gustafsson, Phys. Rev. C **66**, 015203 (2002).
14. A. Akhiezer and M. P. Rekalo, *Hadron Electrodynamics* (Naukova Dumka, Kiev, 1977).
15. S. Kox *et al.*, Nucl. Instrum. Methods Phys. Res. A **346**, 527 (1994); S. Real, PhD Thesis (University of Grenoble 1, 1994), Report No. ISN-94-04; L. Eyraud, PhD Thesis (University of Grenoble 1, 1998), Report No. ISN-98-101.
16. D. Abbott *et al.*, Phys. Rev. Lett. **82**, 1379 (1999); A. Honegger, PhD Thesis (University of Basel, 1999); D. Pitz, PhD Thesis (University of Paris XI, 2000); Report DAPNIA/SPhN-99-05T.
17. D. Pitz, t_{20} Collab. Int. Report 25/2/1999; private communication.
18. V. A. Matveev, R. M. Muradian, and A. N. Tavkhelidze, Lett. Nuovo Cimento **7**, 719 (1973).
19. E. Tomasi-Gustafsson *et al.*, Nucl. Instrum. Methods Phys. Res. A **420**, 90 (1999).

Physics of Atomic Nuclei, Vol. 66, No. 12, 2003, pp. 2169–2177. From Yadernaya Fizika, Vol. 66, No. 12, 2003, pp. 2219–2227.

ELEMENTARY PARTICLES AND FIELDS
Theory

Z Lineshape Versus Fourth-Generation Masses*

S. S. Bulanov[**], **V. A. Novikov**[***], **L. B. Okun**[****],
A. N. Rozanov[1)*****], and **M. I. Vysotsky**[******]

Institute for Theoretical and Experimental Physics,
Bol'shaya Cheremushkinskaya ul. 25, Moscow, 117259 Russia

Received March 5, 2003

Abstract—The dependence of the Z-resonance shape on the location of the threshold of the $N\bar{N}$ production (N is the fourth-generation neutrino) is analyzed. The bounds on the existence of the fourth generation are derived from the comparison of the theoretical expression for the Z lineshape with the experimental data. The fourth generation is excluded at 95% C.L. for $m_N < 46.7 \pm 0.2$ GeV. © *2003 MAIK "Nauka/Interperiodica".*

1. INTRODUCTION

The straightforward generalization of the Standard Model through the inclusion of extra chiral generations of heavy leptons (N, E) and quarks (U, D) was studied in a number of papers [1–10]. In [1–3], the analysis of deviations from the Standard Model due to the fourth-generation contribution was carried out in terms of S, T, and U parameters for fourth-generation particles much heavier than m_Z. The case of new light physics was investigated in [4, 5], using modified S, T, and U parameters, in order to take into account the effects of relatively light new particles. Particle and astroparticle implications of the fourth-generation neutrinos were studied in [7]. A more thorough investigation of the properties of the fourth generation in the framework of GUT models was carried out in [8]. It was shown in [9] that, unifying spins and charges in the framework of $SO(1, 13)$ group, one gets four families of leptons and quarks. Possible manifestations of fourth-generation particles at hadron colliders were studied in [10].

The bounds on the existence of the fourth generation from the analysis of an electroweak data fit were obtained in [6, 11–14]. However, the dependence of the Z resonance shape on the contribution of the fourth generation and, in particular, on the location of the threshold of $N\bar{N}$ production was not considered in [11–14] because the results were obtained in the Breit–Wigner approximation. This approximation is valid for the thresholds of the fourth-generation particle production being far from m_Z. If the threshold location approaches m_Z ($m_N \to m_Z/2$), then one gets a fast worsening of the fit (see Fig. 4 of [13]). It is due to the fact that the standard approach to the radiative corrections to the electroweak observables, used in [6, 11–14], does not work in the presence of a heavy neutrino (N) with $m_N - m_Z/2 < \Gamma_Z$. After Taylor expansion over $(p^2 - m_Z^2)$, the expression for the polarization operator tends to infinity for $m_N \to m_Z/2$ because the point at which the Taylor expansion is performed becomes the branch point of the polarization operator.

According to the results of [11–14], the best fit corresponds to $m_N \approx 50$ GeV, which is why careful analysis of the region $m_N \approx m_Z/2$ is undertaken in this paper. We study the dependence of the Z lineshape on the location of the threshold of $N\bar{N}$ production. We analyze the energy dependence of the $e^+e^- \to Z \to hadrons$ cross section near Z resonance and find that it exhibits a characteristic behavior near the threshold, a cusp.[2)] The cusp is caused by the square root $\sqrt{s - 4m_N^2}$ appearing in the contribution of the fourth-generation neutrino to the po-

*This article was submitted by the authors in English.

[1)]CPPM, IN2P3, CNRS, Universite Mediteranee, Marseilles, France; ITEP, Moscow, Russia.
[**]e-mail: bulanov@heron.itep.ru
[***]e-mail: novikov@heron.itep.ru
[****]e-mail: okun@heron.itep.ru
[*****]e-mail: rozanov@cppm.in2p3.fr
[******]e-mail: vysotsky@heron.itep.ru

[2)]Such behavior of the cross section in quantum mechanics was discovered by Wigner, Baz, and Breit and is discussed in [15]. In particle physics, an analogous phenomenon was considered in [16]. Unlike cases analyzed previously, Z-boson physics is purely perturbative, allowing one to get explicit formulas for cross section. However, being perturbative, the variations of cross section because of the cusp are small. Nevertheless, high precision of experimental data on Z production allows us to limit N mass from below.

1063-7788/03/6612-2169$24.00

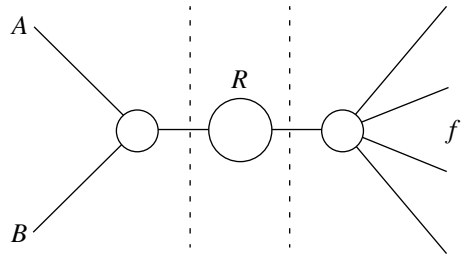

Fig. 1. The reaction $A + B \to R \to f$.

larization operator of Z boson. The form of the cusp is determined by the location of the threshold with respect to m_Z.

Then, we compare the theoretical expression for the Z lineshape with the experimental data presented in [17] using ZFITTER [18] in order to take into account the electromagnetic corrections and find that the fourth generation is excluded at 95% C.L. for $m_N < 46.7 \pm 0.2$ GeV. This bound depends on the masses of the charged fourth-generation particles and on the mass of the Higgs. Using the results of [14], we fix the mass of the charged lepton (E) and take into account that the splittings of quark masses and Higgs mass are not independent. This leaves us with one free parameter—the splitting of quark masses, which we vary from 0 to 50 GeV. This variation is the source of the theoretical uncertainty in the bound on N mass, as well as the uncertainties of the input parameters of ZFITTER. Note that $\chi^2/n_{\text{d.o.f.}}$ for the Z lineshape with the fourth generation is even better for certain region of mass values than $\chi^2/n_{\text{d.o.f.}}$ for the SM prediction.

The paper is organized as follows. In Section 2, we discuss the general behavior of the cross sections near threshold. In Section 3, the exact formulas for the contributions of the fourth-generation particles to the cross section of $e^+e^- \to hadrons$ are presented. We study the behavior of the $e^+e^- \to hadrons$ cross section near the threshold of $N\bar{N}$ production in Section 4. Using the result of Section 3, we compare our prediction for the Z lineshape in the presence of the fourth generation with the experimental data in Section 5. The conclusions are presented in Section 6.

2. THE CROSS SECTIONS NEAR THRESHOLD

Let us consider the interaction of two particles A and B, which form some resonance R, which in turn decays into a system of particles f (see Fig. 1). The behavior of the cross section of this process near the R peak can be calculated in the general case, regardless of the exact form of interaction. We need only the partial width of particle R. The cross section near the resonance is described by the Breit–Wigner formula [18]

$$\sigma = \frac{4\pi s^2}{I^2}\frac{2S_R+1}{(2S_A+1)(2S_B+1)} \times \frac{\Gamma_{R\to A+B}\Gamma_{R\to f}}{(s-M^2)^2+\Gamma^2 s^2/M^2}\frac{s}{M^2}, \quad (1)$$

where $s = (p_A + p_B)^2$; M and Γ are mass and total width of R, respectively; $I = (1/2) \times \sqrt{(s-(m_A+m_B)^2)(s-(m_A-m_B)^2)}$; and S_R, S_A, and S_B are spins of particles R, A, and B, respectively.

Let us consider the case when the reaction occurs not only near the resonance, but also near the threshold of $N\bar{N}$ production. In order to study this effect, we write explicitly the contribution of the $N\bar{N}$ loop to the propagator of particle R:

$$\frac{1}{s - M^2 + i\Gamma s/M + \Sigma_R^{(N)}(s)}; \quad (2)$$

the imaginary part of polarization operator $\Sigma_R^{(N)}(s)$ is connected with the $R \to N\bar{N}$ decay probability by the unitarity relation. The decay probability is proportional to $\sqrt{s-4m_N^2}$, the factor that arises from the integration over phase space. Then, if we rewrite the polarization operator as $\Sigma_R^{(N)}(s) = a + ib\sqrt{s-4m_N^2}$ and expand the expression for the propagator near $s = 4m_N^2$, it will take the following form:

$$T_0 + iT_1\sqrt{s-4m_N^2}, \quad (3)$$

where T_0 and T_1 are some functions of a, b, s, m_Z^2, and Γ_Z. Then, the cross section is proportional to [15]

$$\sigma \sim |T_0|^2 + 2\sqrt{s-4m_N^2}\,\mathrm{Im}[T_0T_1^*], s > 4m_N^2; \quad (4)$$

$$\sigma \sim |T_0|^2 - 2\sqrt{4m_N^2-s}\,\mathrm{Re}[T_0T_1^*], s < 4m_N^2.$$

The form of the cross-section energy behavior near threshold is defined by the value of the angle $\arg(T_0) - \arg(T_1)$ (see Fig. 2) [15]. In all cases, there are two branches lying on both sides of a common vertical tangent. Thus, the existence of the reaction threshold leads to the appearance of the characteristic energy dependence of the cross section. The cross section near threshold is a linear function of $\sqrt{s-4m_N^2}$ with different slopes under and above threshold. The existence of the square root branch point, $s = 4m_N^2$, prevents the amplitude expansion near the branch point in the Taylor series.

Below, we will consider the case when $R \equiv Z$.

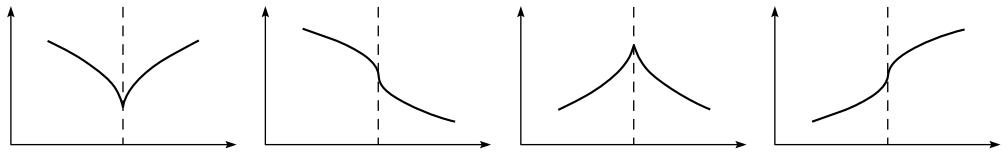

Fig. 2. Different cases of cross-section behavior near threshold. The vertical axis is σ, while the horizontal one is s; the dashed line crosses the horizontal axis at $4m_N^2$.

3. POLARIZATION OPERATOR

The cross section of $e^+e^- \to Z \to hadrons$ near Z resonance is well described by the Breit–Wigner formula [18]

$$\sigma_h^{\rm SM} = \frac{12\pi\Gamma_e\Gamma_h}{|p^2 - m_Z^2 + i\Gamma_Z^{\rm SM}p^2/m_Z|^2}\frac{p^2}{m_Z^2}, \qquad (5)$$

where $p = p_1 + p_2$, p_1 and p_2 are momenta of initial electron and positron, m_Z is the mass of Z boson, Γ_e is the width of $Z \to e^+e^-$ decay, Γ_h is the width of $Z \to hadrons$, and $\Gamma_Z^{\rm SM}$ is the total width of Z in the SM.

The fourth generation contributes to the Z-boson polarization operator. This contribution can be accounted for in expression (5) by replacing the denominator:

$$|p^2 - m_Z^2 + i\Gamma_Z^{\rm SM}p^2/m_Z|^2 \to |p^2 - m_Z^2 + i\Gamma_Z p^2/m_Z + \Sigma_Z^{(4\rm th)}(p^2) - {\rm Re}[\Sigma_Z^{(4\rm th)}(m_Z^2)]|^2, \qquad (6)$$

where the subtraction is performed due to the fact that we follow the approach of [11–13] and use experimental values for m_Z, α, and Fermi coupling constant G_μ. Thus, the renormalization scheme is an on-shell one. The real part of the polarization operator at $s = m_Z^2$ is subtracted in order to avoid the shifting of Z boson mass. It is due to the fact that the real part of the polarization operator contributes to m_Z;

$$\Sigma_Z^{(4\rm th)}(p^2) = \Sigma_Z^{(N)}(p^2) + \Sigma_Z^{(E)}(p^2) + \Sigma_Z^{(U)}(p^2) + \Sigma_Z^{(D)}(p^2) \qquad (7)$$

is the contribution of the fourth generation to Z polarization operator. The contribution of the $N\bar{N}$ channel to Z width is taken into account by the imaginary part of $\Sigma_Z^{(N)}(p^2)$.

Note that Γ_Z in (6) includes decays of Z into particles of the first three generations. The fourth generation also influences Γ_Z in a nondirect way. It is due to the fact that the polarization operators of gauge bosons enter the radiative corrections for g_A and g_V, which in turn enter the amplitude of the Z-boson decay into a fermion–antifermion pair:

$$M(Z \to f\bar{f}) = \frac{1}{2}\bar{f}Z_\alpha\bar{\psi}_f(\gamma_\alpha g_{Vf} + \gamma_\alpha\gamma_5 g_{Af})\psi_f, \qquad (8)$$

where $\bar{f}^2 = 4\sqrt{2}G_\mu m_Z^2 = 0.54866(4)$. In the case of Z decay into $\nu\bar{\nu}$, the contribution of final-state interaction equals zero and

$$\Gamma_\nu = 4\Gamma_0(g_{V\nu}^2 + g_{A\nu}^2), \qquad (9)$$

where $\Gamma_0 = G_\mu m_Z^3/(24\sqrt{2}\pi)$ is the so-called "standard" width. If we neglect the masses of neutrinos, then $g_{V\nu} = g_{A\nu} = g_\nu$. For the decay into any pair of charged leptons, we get

$$\Gamma_l = 4\Gamma_0 \times \left[g_{Vl}^2\left(1 + \frac{3\bar{\alpha}}{4\pi}\right) + g_{Al}^2\left(1 + \frac{3\bar{\alpha}}{4\pi} - 6\frac{m_l^2}{m_Z^2}\right)\right], \qquad (10)$$

where m_l is the mass of the lepton and $\bar{\alpha} \equiv \alpha(m_Z^2) = [128.896(90)]^{-1}$. The situation changes slightly in the case of $Z \to q\bar{q}$. There appear the radiative corrections (R_{Vq} and R_{Aq}) due to gluon exchange and emission in the final state:

$$\Gamma_q = 12\Gamma_0\left(g_{Vq}^2 R_{Vq} + g_{Aq}^2 R_{Aq}\right). \qquad (11)$$

According to the results of [19], the one-loop expressions for g_{Al} and $R_l = g_{Vl}/g_{Al}$ are

$$g_{Al} = -\frac{1}{2} - \frac{3\bar{\alpha}}{64\pi s^2c^2}V_A, \qquad (12)$$

$$R_l = 1 - 4s^2 + \frac{3\bar{\alpha}}{4\pi(c^2 - s^2)}V_R,$$

$$g_\nu = \frac{1}{2} + \frac{3\bar{\alpha}}{64\pi s^2c^2}V_\nu, \qquad (13)$$

and in the case of quarks

$$g_{Aq} = T_{3q}\left[1 + \frac{3\bar{\alpha}}{32\pi s^2c^2}V_{Aq}\right], \qquad (14)$$

$$R_q = 1 - 4|Q_q|s^2 + \frac{3\bar{\alpha}|Q_q|}{4\pi(c^2 - s^2)}V_{Rq},$$

where $c \equiv \cos\theta_{\text{eff}}$ and $s \equiv \sin\theta_{\text{eff}}$.

The exact expressions for V_A, V_R, V_{Aq}, and V_{Rq} in the SM can be found in [19].

The fourth-generation particles contribute to physical observables through polarization operators of gauge bosons, as was mentioned above. This gives corrections δV_i to the functions V_i $(i = A, R)$ [11],

$$\frac{3\bar{\alpha}}{16\pi s^2 c^2}\delta V_A = \Pi_Z^{(4\text{th})}(m_Z^2) - \Pi_W^{(4\text{th})}(0) - \Sigma_Z^{(4\text{th})\prime}(m_Z^2), \quad (15)$$

$$\frac{3\bar{\alpha}}{16\pi s^2 c^2}\delta V_R = \left[\Pi_Z^{(4\text{th})}(m_Z^2) - \Pi_W^{(4\text{th})}(0) - \Sigma_\gamma^{(4\text{th})\prime}(0)\right] - \frac{sc(c^2-s^2)}{s^2c^2}\Pi_{\gamma Z}^{(4\text{th})}(m_Z^2),$$

where $\Pi_Z(m_Z^2) = \Sigma_Z(m_Z^2)/m_Z^2$. Note that all singular terms, proportional to $1/\varepsilon$ ($\varepsilon = D - 4$), on the right hand sides of Eqs. (15), arising from polarization operators, cancel, as was shown in [19]. Thus, expressions (15) are finite. However, these formulas work well for new particles much heavier than the Z boson. If $m_N \to m_Z/2$, then $\Sigma_Z^{(4\text{th})\prime}(m_Z^2)$ tends to infinity. $\Sigma_Z^{(4\text{th})\prime}(m_Z^2)$ comes from the Taylor expansion of the Z boson polarization operator near m_Z. In order to get rid of this unphysical infinity, which arises due to the fact that the expansion is performed at the branch point of the polarization operator, we use the exact expression for the contribution of fourth-generation particles to the Z boson polarization operator.

For the contribution of the fourth-generation particles, we get

$$\Pi_Z^{(\phi)}(p^2) = \frac{N_c\bar{\alpha}}{8\pi s^2c^2}\left[\Delta_\phi + 4g_{A\phi}^2\frac{m_\phi^2}{p^2}F\left(\frac{m_\phi^2}{p^2}\right) - \frac{2(g_{A\phi}^2+g_{V\phi}^2)}{3}\left(\left(1+2\frac{m_\phi^2}{p^2}\right)F\left(\frac{m_\phi^2}{p^2}\right)+\frac{1}{3}\right)\right]. \quad (16)$$

Here, $\phi = N, E, U, D$; $N_c = 3$ for quarks and $N_c = 1$ for leptons; $\Sigma_Z^{(\phi)}(p^2) = p^2\Pi_Z^{(\phi)}(p^2)$;

$$F(x) = \left[-2 + 2\sqrt{4x-1}\arctan\frac{1}{\sqrt{4x-1}}\right]; \quad (17)$$

Δ_ϕ are singular parts,

$$\Delta_\phi = 2\left(\frac{1}{3}(g_{A\phi}^2+g_{V\phi}^2) - 2g_{A\phi}^2\frac{m_\phi^2}{p^2}\right) \times \left(\frac{1}{\varepsilon} - \gamma + \ln 4\pi - \ln\frac{m_\phi^2}{\mu^2}\right), \quad (18)$$

where $\varepsilon \to 0$, $\gamma = -\Gamma'(1) = 0.577\ldots$, and μ is a parameter with dimension of mass, which is needed to preserve the dimensionality of the initial integral.

Let us consider the contribution of N to g_A and g_V. $\Sigma_Z'(m_Z^2)$ arises in g_A due to the renormalization of the Z boson wave function. In order to avoid infinities, we will expand near m_Z only the singular part of the polarization operator, i.e.,

$$p^2 - m_Z^2 + \Sigma_Z(p^2) = (1 + \Sigma_Z'(m_Z^2)\big|_s) \times \left[p^2 - m_Z^2\left(1 - \Pi_Z(m_Z^2)\Big|_s - \frac{p^2}{m_Z^2}\Pi_Z(p^2)\Big|_{\text{FP}}\right)\right],$$

where index "s" denotes the singular part and index "FP" denotes the finite part. Then, in Eqs. (15), we should replace $\Sigma_Z'(m_Z^2)$ by $\Sigma'(m_Z^2)\big|_s$ and $\Pi_Z(m_Z^2)$ by $\Pi_Z(m_Z^2)\big|_s + (p^2/m_Z^2)\,\Pi_Z(p^2)\big|_{\text{FP}}$. The combination of singular terms in the resulting expression is the same as in (15) and that is why they cancel each other.

Let us consider the expression for the $e^+e^- \to$ *hadrons* cross section in the presence of the fourth generation. The singular part of the polarization operator is absorbed in partial widths Γ_e and Γ_h and also in total width of Z, Γ_Z:

$$\frac{\Gamma_e^0\Gamma_h^0}{|p^2 - m_Z^2 + i\Gamma_Z^0 p^2/m_Z + \Sigma^{(4\text{th})}(p^2) - \text{Re}[\Sigma^{(4\text{th})}(m_Z^2)]|^2} = \frac{\Gamma_e^0\Gamma_h^0}{(1+\Sigma'|_s)^2|p^2 - m_Z^2 + i\Gamma_Z^0 p^2/[(1+\Sigma'|_s)m_Z] + (\Sigma^{(4\text{th})}(p^2) - \text{Re}[\Sigma^{(4\text{th})}(m_Z^2)])|_{\text{FP}}|^2} = \frac{\Gamma_e\Gamma_h}{|p^2 - m_Z^2 + i\Gamma_Z p^2/m_Z + (\Sigma^{(4\text{th})}(p^2) - \text{Re}[\Sigma^{(4\text{th})}(m_Z^2)])|_{\text{FP}}|^2}, \quad (19)$$

where $\Gamma_e = \Gamma_e^0/(1+\Sigma'|_s)$, $\Gamma_h = \Gamma_h^0/(1+\Sigma'|_s)$, $\Gamma_Z = \Gamma_Z^0/(1+\Sigma'|_s)$, and we used the decomposition

$$\Sigma^{(4\text{th})}(p^2) - \text{Re}[\Sigma^{(4\text{th})}(m_Z^2)] = (\Sigma^{(4\text{th})}(p^2) - \text{Re}[\Sigma^{(4\text{th})}(m_Z^2)]|_s + (\Sigma^{(4\text{th})}(p^2) - \text{Re}[\Sigma^{(4\text{th})}(m_Z^2)])|_{\text{FP}} = \Sigma'(m_Z^2)\big|_s(p^2 - m_Z^2) + (\Sigma^{(4\text{th})}(p^2) - \text{Re}[\Sigma^{(4\text{th})}(m_Z^2)])|_{\text{FP}}.$$

The cancellation of the singularities is due to the fact that Γ_e, Γ_h, and Γ_Z are proportional to $\bar{f}_0^2$, which can be rewritten in terms of G_μ, m_Z, and polarization operators as in [19]:

$$\bar{f}_0^2 = 4\sqrt{2}G_\mu m_Z^2[1 - \Pi_W(0) + \Pi_Z(m_Z^2) - D], \tag{20}$$

where D comes from the radiative corrections to G_μ [19]. If we divide $\bar{f}_0^2$ by $(1 + \Sigma'|_s)$, then the resulting expression will be finite, due to the fact that all singular terms cancel. Thus, in the expression for the cross section of $e^+e^- \to hadrons$, there are no singular terms.

We should note that there is an ambiguity in the definition of singular and finite parts of the polarization operator. The constant term, proportional to $\bar{\alpha}$, can be added to the singular part and subtracted from the finite part:

$$\Pi_Z(p^2) = \left(\Pi_Z(p^2)\big|_s + a\bar{\alpha}\right) + \left(\Pi_Z(p^2)\big|_{\rm FP} - a\bar{\alpha}\right).$$

However, this ambiguity does not affect the expression for the cross section. It is obvious from the following expressions:

$$\frac{\Gamma_e^0\Gamma_h^0}{(1+\Sigma'|_s + a\bar{\alpha})^2|p^2 - m_Z^2 + i\Gamma_Z^0 p^2/[(1+\Sigma'|_s)m_Z] + \hat{\Sigma} - a\bar{\alpha}(p^2 - m_Z^2)|^2}$$
$$= \frac{\Gamma_e'\Gamma_h'}{|(p^2 - m_Z^2)(1 - a\bar{\alpha}) + i\Gamma_Z' p^2/m_Z + \hat{\Sigma}|^2} = \frac{\Gamma_e'\Gamma_h'/(1-a\bar{\alpha})^2}{|(p^2 - m_Z^2) + i\Gamma_Z' p^2/[(1-a\bar{\alpha})m_Z] + \hat{\Sigma}|^2}$$
$$= \frac{\Gamma_e\Gamma_h}{|(p^2 - m_Z^2) + i\Gamma_Z p^2/m_Z + \hat{\Sigma}|^2},$$

where $\hat{\Sigma} = (\Sigma^{(4\text{th})}(p^2) - \mathrm{Re}[\Sigma^{(4\text{th})}(m_Z^2)])|_{\rm FP}$;

$$\Gamma_i = \frac{\Gamma_i'}{1 - a\bar{\alpha}} = \frac{\Gamma_i^0}{(1+\Sigma'|_s + a\bar{\alpha})(1 - a\bar{\alpha})}$$
$$= \frac{\Gamma_i^0}{1 + \Sigma'|_s + a\bar{\alpha} - a\bar{\alpha}} = \frac{\Gamma_i^0}{1 + \Sigma'|_s},$$

where $i = e, h, Z$.

4. Z LINESHAPE IN THE PRESENCE OF FOURTH GENERATION

According to the results of the previous section, the amplitude of $e^+e^- \to hadrons$ is proportional to

$$A_h \sim \Big[p^2 - m_Z^2 + i\Gamma_Z^0 p^2/m_Z + \Sigma_Z^{(4\text{th})}(p^2) - \mathrm{Re}(\Sigma_Z^{(4\text{th})}(m_Z^2))\Big]^{-1}. \tag{21}$$

In order to study the behavior of the cross section near the threshold qualitatively, we shall neglect the contributions of U, D, and E to $\Sigma_Z^{(4\text{th})}(p^2)$, as well as the contribution of all fourth-generation particles to g_A and g_V. Then, expression (21) takes the following form:

$$A_h \sim \Big[p^2 - m_Z^2 + i\Gamma_Z p^2/m_Z + (\Sigma_Z^{(N)}(p^2) - \mathrm{Re}[\Sigma_Z^{(N)}(m_Z^2)])|_{\rm FP}\Big]^{-1}. \tag{22}$$

Expanding this expression near the threshold of $N\bar{N}$ production ($p^2 = 4m_N^2$, $A_h \sim T_0 + iT_1\sqrt{p^2 - 4m_N^2}$), we obtain the following behavior for the cross section:

$$\sigma_{p^2<4m_N^2} \sim \frac{1}{\gamma}\left(1 + \frac{\bar{f}^2 m_Z^2}{64\pi}\frac{(4m_N^2 - m_Z^2)\sqrt{4m_N^2/p^2 - 1}}{\gamma}\right), \tag{23}$$

$$\sigma_{p^2>4m_N^2} \sim \frac{1}{\gamma}\left(1 - \frac{\bar{f}^2 m_Z^2}{64\pi}\frac{m_Z\Gamma_Z\sqrt{1 - 4m_N^2/p^2}}{\gamma}\right), \tag{24}$$

where $\gamma = (4m_N^2 - m_Z^2)^2 + (m_Z\Gamma_Z)^2$ and the second terms in the brackets in Eqs. (23), (24) are proportional to $\mathrm{Re}[T_0T_1^*]$ and $\mathrm{Im}[T_0T_1^*]$, respectively. As was mentioned in Section 2, the form of the p^2 dependence of the cross section near the threshold is determined by the relative phase of T_0 and T_1. In our case, we have two types of cusps (see Fig. 3), which correspond to $\arg T_0 - \arg T_1$ lying in the fourth quadrant for $4m_N^2 < m_Z^2$ and in the third quadrant for $4m_N^2 > m_Z^2$, or to $\mathrm{Re}[T_0T_1^*]$ and $\mathrm{Im}[T_0T_1^*]$ being negative for $4m_N^2 < m_Z^2$ and $\mathrm{Re}[T_0T_1^*]$ being positive and $\mathrm{Im}[T_0T_1^*]$ being negative for $4m_N^2 > m_Z^2$. It can also be seen from Fig. 3 that the cross section of $e^+e^- \to hadrons$ decreases above the threshold in accordance with the unitarity.

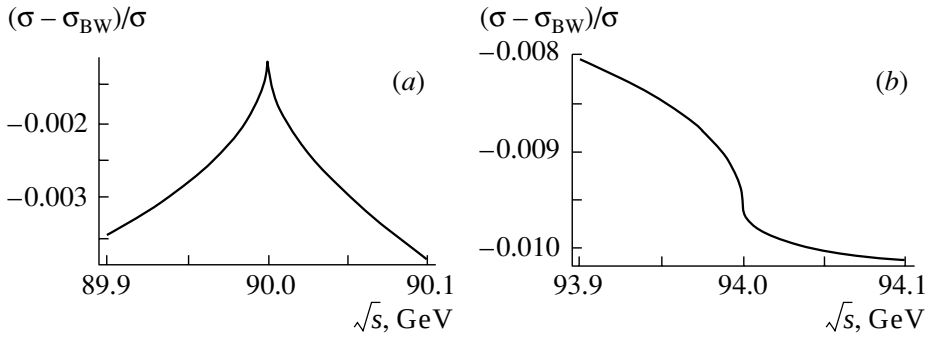

Fig. 3. The dependence of relative departure of the $e^+e^- \to hadrons$ cross section in the presence of the fourth generation from the SM prediction on the c.m. energy of e^+e^- for $m_N = 45$ (*a*) and 47 GeV (*b*).

Though the change in Z lineshape due to these cusps is very small compared to the pure Breit–Wigner curve, as is shown in Fig. 3, this effect may manifest itself, when the theoretical predictions are compared with the experimental data. This is due to the fact that the Z lineshape is measured with very high precision. In the next section, we will compare the theoretical cross section with the experimental data.

5. COMPARISON WITH THE EXPERIMENT

The experimental data on the cross section of $e^+e^- \to hadrons$ reaction is usually presented in the form that includes the electromagnetic corrections, i.e., initial- and final-state interactions and photon emission [17]. In order to compare our formulas for the cross section with experimental ones, we use the ZFITTER code [18], which takes into account these corrections. We use the following inputs:

$$m_Z = 91.1882(22)\ \text{GeV}, \quad m_t = 175(4.4)\ \text{GeV},$$
$$\bar{\alpha} = 1/128.918(45), \quad \alpha_s = 0.1182(27),$$
$$m_H = 120\ \text{GeV}.$$

With the reasonable assumption that the initial- and final-state radiation effects are not significantly modified by the fourth generation, we can calculate the cross section

$$\sigma_h^{\text{th}} = \sigma_h \frac{\sigma_h^{\text{ZF}}}{\sigma_h^{\text{SM}}}, \tag{25}$$

where σ_h^{ZF} is the result of the ZFITTER code and

$$\sigma_h = \frac{12\pi\Gamma_e\Gamma_h}{|p^2 - m_Z^2 + i\Gamma_Z p^2/m_Z + (\Sigma^{(4\text{th})}(p^2) - \text{Re}[\Sigma^{(4\text{th})}(m_Z^2)])_{\text{FP}}|^2}\frac{p^2}{m_Z^2} \tag{26}$$

at values of c.m. energy at which the experimental values of cross section were measured [17]. There are 35 experimental points from 1993 data, which we use.[3)] These points are extracted from Fig. 2 of [17] and presented in the table. We took only the points corresponding to the 1993–1995 set, due to the fact that they are measured with higher precision than the 1991–1993 set. Then, we calculate $\chi^2/n_{\text{d.o.f.}}$, where $n_{\text{d.o.f.}} = 35 - N$, N being the number of fitted parameters,[4)] and

$$\chi^2 = \sum_{i=1}^{35}\left(\frac{\sigma_h^{\text{th}} - \sigma_h^{\text{exp}}}{\delta\sigma_h^{\text{exp}}}\right)^2, \tag{27}$$

σ_h^{exp} being the experimental value of the cross section and $\delta\sigma_h^{\text{exp}}$ being its error, in order to determine at what confidence level the fourth generation is excluded by the experimental data. However, the bound on N mass from below depends on the Higgs mass and mass splittings between U and D quarks and between E and N leptons. The effects of varying m_H, $|m_U - m_D|$, and $|m_E - m_N|$ are not independent. As was shown in [14], the increase in $|m_U - m_D|$ or $|m_E -$

[3)] If we also fit the value of m_Z together with m_N using these 35 experimental points, it will lead to the new value of $m_Z = 91.1901$ GeV. However, this value and the SM value 91.1882(22) coincide within the accuracy of calculation. The bound of m_N is only slightly affected ($m_N < 46.6 \pm 0.2$ GeV).

[4)] In our case $N = 1$, because only heavy-neutrino mass is a free parameter; all other parameters are fixed.

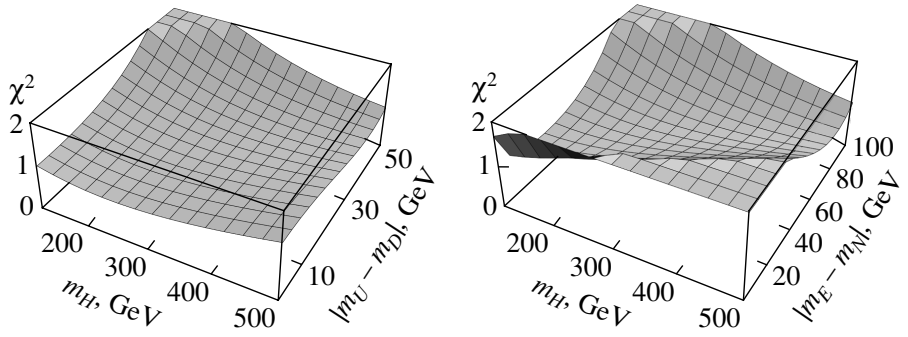

Fig. 4. The dependence of χ^2 on m_H, $|m_U - m_D|$ and on m_H, $|m_E - m_N|$.

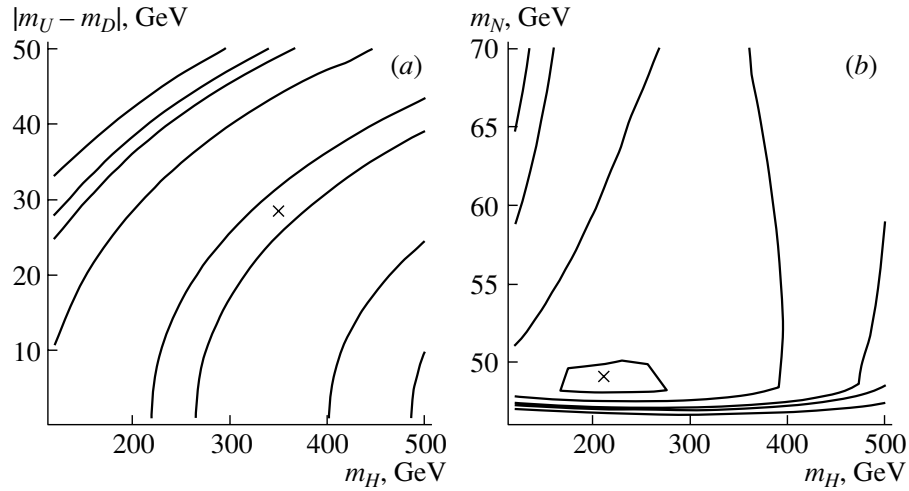

Fig. 5. Exclusion plots (a) on the plane m_H–$|m_U - m_D|$ for $m_N = 49$ GeV and (b) on the plane m_H–m_N for $|m_U - m_D| = 10$ GeV; $\chi^2_{\min} = 0.85$ denoted by crosses. Solid curves represent the borders of 1σ, 2σ, 3σ, 4σ, and 5σ regions.

$m_N|$ can be compensated by the increase in Higgs mass. This leads to the appearance of $\chi^2_{\min}$ valleys. It can be seen from Fig. 4, where the dependences of χ^2 on $m_H, |m_U - m_D|$ and $m_H, |m_E - m_N|$ are shown for $m_N = 49$ GeV.

If we then use the LEP II bound $m_E > 100$ GeV and the results of [14] that the best fit of electroweak data corresponds to the light E near the bound and $m_N \approx 50$ GeV, then we have only two parameters, m_H and $|m_U - m_D|$, that affect the bound on m_N. As can be seen from Fig. 5a, the best fit is acquired for $0.11m_H - 19.7\ \text{GeV} < |m_U - m_D| < 0.12m_H - 9.2$ GeV. In this region of masses, we calculate χ^2 and find that the fourth generation is excluded at 95% C.L. for $m_N < 46.7 \pm 0.2$ GeV. The theoretical uncertainty is caused by the variation of $|m_U - m_D|$ from 0 to 50 GeV, as well as by the uncertainties of the input parameters of ZFITTER, which were also used in the calculation of σ_h and σ_h^{SM}. The main contribution to the theoretical uncertainty comes from m_t and α_s. The variation from 0 to 50 GeV is chosen because the quality of the fit is fast worsening for $|m_U - m_D| > 50$ GeV.

In order to illustrate the dependence of the fit quality on the Higgs mass, we study $\chi^2(m_N, m_H)$ (see Fig. 5b). From this figure, it is seen that the 95%-C.L. bound lies below 50 GeV and varies slightly with the increase in the Higgs mass near $m_N = 47$ GeV. In this figure, we take $|m_U - m_D| = 10$ GeV. It can be seen from Fig. 5 that, for a certain region of the fourth-generation particles and Higgs masses, the quality of the fit can be even better than in the SM. According to the results of [17], $\chi^2/n_{\text{d.o.f.}}(\text{SM}) = 1.09$, which corresponds to the 2σ level, while in the presence of the fourth generation it is $\chi^2_{\min}/n_{\text{d.o.f.}} = 0.88$, which is inside the 1σ region.

We should note that the direct search for heavy neutrinos in e^+e^- annihilation into a pair of heavy

The experimental values of the $e^+e^- \to hadrons$ cross section, obtained by ALEPH, DELPHI, L3, and OPAL Collaborations, extracted from Fig. 2 of [17] ($\sqrt{s}$ is presented in GeV; σ_h, in nb; the 1993–1995 data set)

ALEPH			DELPHI			L3			OPAL		
$\sqrt{s}$	σ_h	$\delta\sigma_h$	$\sqrt{s}$	σ_h	$\delta\sigma_h$	$\sqrt{s}$	σ_h	$\delta\sigma_h$	$\sqrt{s}$	σ_h	$\delta\sigma_h$
89.4316	9.891	0.043	89.4307	9.87	0.044	89.447	10.088	0.034	89.4415	9.980	0.044
89.4400	9.980	0.044	89.4378	9.93	0.056	89.4515	10.08	0.034	89.45	10.044	0.034
91.1806	30.500	0.078	91.186	30.392	0.065	91.206	30.358	0.067	91.207	30.445	0.053
91.1980	30.43	0.032	91.2	30.50	0.044	91.222	30.547	0.034	91.222	30.46	0.025
91.2200	30.458	0.067	91.203	30.46	0.19	91.297	30.525	0.087	91.285	30.64	0.098
91.2840	30.555	0.13	91.28	30.65	0.13	91.309	30.545	0.067	92.973	14.27	0.046
91.2950	30.678	0.078	91.292	30.67	0.098	92.983	14.231	0.046	93.035	13.85	0.046
91.3030	30.660	0.090	91.304	30.46	0.086	99.035	13.91	0.053			
92.9685	14.300	0.060	92.966	14.35	0.044						
93.0140	14.04	0.056	93.014	13.89	0.045						

neutrinos with the emission of an initial-state bremsstrahlung photon ($e^+e^- \to \gamma +$ nothing) could result in the bound $m_N \geq 50$ GeV [12, 13] if all four LEP experiments were to make a combined analysis [20].

Though this bound on m_N would be slightly better than the one obtained in the present paper, the data and the procedure used to extract the bounds are completely different and independent.

6. CONCLUSIONS

In the present paper, we analyzed the dependence of Z lineshape on the location of the threshold of $N\bar{N}$ production. We studied the behavior of the $e^+e^- \to hadrons$ cross section near the threshold of $N\bar{N}$ production and determined how this threshold changes the Z lineshape. In order to find the bound on m_N, we compared the theoretical predictions for the Z lineshape with the experimental data, using the exact formulas for Z polarization operator, instead of expanding it in a Taylor series near m_Z.

We found that the bound on N mass depends on the Higgs mass and the splittings of fourth-generation quark and lepton masses ($|m_U - m_D|$ and $|m_E - m_N|$). However, the effects caused by them are not independent, because the increase in mass splittings can be compensated by the increase in the Higgs mass, as was shown in [14]. Using the results of [14], we fixed $m_E = 100$ GeV. Then, we used the fact that $|m_U - m_D|$ and m_H are not independent. Thus, we had one free parameter left: $|m_U - m_D|$. We varied $|m_U - m_D|$ from 0 to 50 GeV and found that the fourth generation is excluded by the experimental data at 95% C.L. for $m_N < 46.7 \pm 0.2$ GeV. The theoretical uncertainty is caused by the variation of $|m_U - m_D|$, as well as by the uncertainties of the input parameters of ZFITTER, which were also used in the calculation of σ_h and σ_h^{SM}.

ACKNOWLEDGMENTS

We are grateful to M.Yu. Khlopov and N. Mankoc-Borstnik for correspondence.

This work was partially supported by the Russian Foundation for Basic Research (project no. 00-15-96562) and by the Federal Scientific Technical Program of the Ministry of Science and Technology of the Russian Federation under contract no. 40.052.1.1.1112.

REFERENCES

1. J. Erler and P. Langacker, Eur. Phys. J. C **15**, 95 (2000).
2. A. Masiero *et al.*, Phys. Lett. B **355**, 329 (1995).
3. T. Inami *et al.*, Mod. Phys. Lett. A **10**, 1471 (1995).
4. N. Evans, Phys. Lett. B **340**, 81 (1994).
5. P. Bamert and C. P. Burgess, Z. Phys. C **66**, 495 (1995).
6. V. A. Novikov *et al.*, Mod. Phys. Lett. A **10**, 1915 (1995).
7. D. Fargion *et al.*, Phys. Rev. D **52**, 1828 (1995); **54**, 4684 (1996); K. Belotsky *et al.*, hep-ph/0210153; D. Fargion *et al.*, Pis'ma Zh. Éksp. Teor. Fiz. **68**, 657 (1998) [JETP Lett. **68**, 685 (1998)]; JETP Lett. **69**, 434 (1999); K. M. Belotsky *et al.*, Yad. Fiz. **65**, 407 (2002) [Phys. At. Nucl. **65**, 382 (2002)]; Phys. Lett. B **529**, 10 (2002).

8. C. D. Froggatt and J. E. Dubicki, in *Proceedings of the Workshops "What Comes beyond the Standard Model," 2000, 2001,* Vol. 1.
9. A. Borstnik-Bracic and N. Mankoc-Borstnik, in *Proceedings of the Workshops "What Comes beyond the Standard Model," 2000, 2001, 2002,* Vol. 2; D. Lukman, A. Kleppe, and N. Mankoc-Borstnik, in *Proceedings of the Workshops "What Comes beyond the Standard Model," 2000, 2001, 2002,* Vol. 2.
10. E. Arik *et al.*, Phys. Rev. D **66**, 033003, 116006 (2002).
11. M. Maltoni, V. A. Novikov, L. B. Okun, *et al.*, Phys. Lett. B **476**, 107 (2000).
12. V. A. Ilyin *et al.*, Phys. Lett. B **503**, 126 (2001); hep-ph/0006324; V. A. Ilyin *et al.*, in *Proceedings of the ICHEP2000 Osaka Conference*; hep-ph/0009167.
13. V. A. Novikov *et al.*, Phys. Lett. B **529**, 111 (2002); hep-ph/0111028.
14. V. A. Novikov *et al.*, JETP Lett. **76**, 127 (2002); hep-ph/0203132.
15. L. D. Landau and E. M. Lifshitz, *Quantum Mechanics* (Nauka, Moscow, 1974), Para. 147 [in Russian].
16. A. I. Baz and L. B. Okun, Zh. Éksp. Teor. Fiz. **35**, 757 (1959) [Sov. Phys. JETP **8**, 526 (1959)].
17. LEP Collab., CERN-EP/2000-153; hep-ex/0101027.
18. D. Bardin *et al.*, Comput. Phys. Commun. **133**, 229 (2001).
19. V. A. Novikov *et al.*, Rep. Prog. Phys. **62**, 1275 (1999).
20. ALEPH Collab., ALEPH 2001-010; CONF 2001-007 (2001); P. Abreu *et al.* (DELPHI Collab.), Eur. Phys. J. C **16**, 53 (2000); M. Acciari *et al.* (L3 Collab.), Phys. Lett. B **470**, 268 (1999); G. Abbiendi *et al.* (OPAL Collab.), Eur. Phys. J. C **14**, 73 (2000).

Physics of Atomic Nuclei, Vol. 66, No. 12, 2003, pp. 2178–2182. From Yadernaya Fizika, Vol. 66, No. 12, 2003, pp. 2228–2232.

ELEMENTARY PARTICLES AND FIELDS
Theory

Neutron–Antineutron Oscillations in the Trapping Box*

B. O. Kerbikov

Institute for Theoretical and Experimental Physics,
Bol'shaya Cheremushkinskaya ul. 25, Moscow, 117259 Russia

Received December 25, 2002; in final form, April 9, 2003

Abstract—The problem of n–$\bar{n}$ oscillations for ultracold neutrons confined within a trap is reexamined. It is shown that the growth of the $\bar{n}$ component with time is to a decent accuracy given by $P(\bar{n}) = \varepsilon_{n\bar{n}}^2 t_L t$, where $\varepsilon_{n\bar{n}}$ is the mixing parameter and $t_L \sim 1$ s is the neutron propagation time between subsequent collisions with the trap walls. Possible corrections to this law and open questions are discussed.

1. INTRODUCTION

For several decades, the problem of nucleon instability has been a subject of intense and diversified theoretical and experimental studies. An interesting facet of this fundamental problem is a hypothetical process of neutron–antineutron oscillations [1]. Such oscillations have been thoroughly discussed in the free-space regime and inside nuclei (see, e.g., [1–5] and references therein). The third and very interesting possibility of searching for n–$\bar{n}$ oscillations is to use ultracold neutrons (UCN) confined in a trap. This subject was discussed by several authors [2, 3, 6], but, in contrast to the first two regimes, the picture of n–$\bar{n}$ oscillations of UCN remains rather obscure. On the other hand, several experiments of this kind are in preparation now. Therefore, it is appropriate to address this subject again. We shall follow two complementary lines of arguments. The first one is based on simple qualitative estimates, while the second makes use of the time evolution equation focusing on the interaction of the two-component n–$\bar{n}$ system with the walls of the trap. Both approaches lead to a conclusion that the $\bar{n}$ component grows (approximately) linearly with observation time contrary to quadratic time dependence in the free-space regime.

2. RELEVANT PARAMETERS

We start by introducing a set of definitions and parameters. Our treatment will be somewhat schematic in the sense that we do not consider any specific geometry of the trap, concrete UCN spectrum, or a variety of trap materials. All these points can be easily accounted for as soon as one sticks to a given experimental setup.

First, we recall that neutrons with energy $E < 10^{-7}$ eV $= 100$ neV are called ultracold. A useful relation connecting the neutron velocity v in cm/s and E in neV reads

$$v \simeq 10^2 (E/5.22)^{1/2}. \quad (1)$$

In particular, the velocity corresponding to $E = 100$ neV is $v \simeq 4.4 \times 10^2$ cm/s.

A less formal definition of UCN involves a notion of the real part of the optical potential corresponding to the trap material. Namely, neutrons with energies less than the height of this potential are called ultracold. The two definitions are essentially equivalent since for most materials the optical potential is on the order of 100 neV (see below).

Our main interest concerns strongly absorptive interaction of the antineutron component with the trap wall. Therefore, very weak absorption of neutrons on the wall will be neglected. Interesting by itself, this problem is beyond the scope of the present work. According to the second definition of UCN (i.e., $E < U_{nA}$), they undergo complete reflection from the trap walls and may be stored for about 10^3 s (β-decay time), as was first pointed out by Zeldovich [7]. For each material, the limiting neutron velocity is given by (1) with E replaced by U_{nA}.

To be concrete, we consider neutrons with energy $E = 80$ neV, which, according to (1), corresponds to $v = 3.9 \times 10^2$ cm/s. Such neutrons have momenta $k \simeq 12.3$ eV and de Broglie wavelengths $\lambda \simeq 10^{-5}$ cm. As for the wall material, we take ^{12}C with the density $\rho = 2.25$ g/cm^3, or $N \simeq 1.13 \times 10^{-16}$ fm^{-3}. The coherent n^{12}C scattering length is $a_n = 6.65$ fm [8] (the imaginary part of the scattering length is at least three orders of magnitude smaller

*This article was submitted by the author in English.

and is ignored, as was already stated). The corresponding n^{12}C optical potential reads

$$U_n = \frac{2\pi}{m} N a_n \simeq 195 \text{ neV}, \quad (2)$$

with m being the neutron mass. The limiting velocity corresponding to $E = U_n$ is $v_n^{(0)} \simeq 6.1 \times 10^2$ cm/s. Thus, neutrons under consideration with $v_n = 3.9 \times 10^2$ cm/s are certainly ultracold with respect to ^{12}C trap walls.

Experimental data on antineutron–nucleus scattering lengths at ultralow energies are absent. Only some indirect information may be gained from the level shifts of antiprotonic atoms. The energy behavior of the $\bar{n}A$ annihilation cross section is governed by the well-known $1/v$ law:

$$\sigma_a = -4\pi \frac{\mathrm{Im} a_{\bar{n}A}}{k}. \quad (3)$$

Several fits to the $\bar{n}A$ scattering lengths have been proposed in the literature. We consider as the most reliable that of [9] based on the internuclear cascade model. Even within this particular model, one finds several solutions for $\bar{n}^{12}$C scattering length. Therefore, the one we have chosen for our analysis may be called "motivated" by [9] and reads

$$a_{\bar{n}} = (3 - i \cdot 1) \text{ fm}. \quad (4)$$

Then, according to (2), the $\bar{n}^{12}$C optical potential is equal to

$$V_{\bar{n}} = U_{\bar{n}} - iW_{\bar{n}} \simeq (90 - i \cdot 30) \text{ neV}. \quad (5)$$

The limiting $\bar{n}$ velocity corresponding to $U_{\bar{n}}$ from (5) is, according to (1), $v_{\bar{n}}^{(0)} \simeq 4.15 \times 10^2$ cm/s. Now, our choice $E = 80$ neV$< U_{\bar{n}} < U_n$ is clear since we want to deal with ultracold $\bar{n}$ as well. The case $U_{\bar{n}} < E < U_n$ will be considered in the next publication. Needless to say, due to strong $\bar{n}$ absorption, the condition $E_{\bar{n}} < U_{\bar{n}}$ in no way provides complete reflection of $\bar{n}$ from the wall (see below).

Next, we recall that the lower limit on n–$\bar{n}$ oscillation time $\tau_{n\bar{n}}$ has been obtained from experimental study of n–$\bar{n}$ transitions in free space and inside nuclei (see [4, 9–11] and references therein). For our purposes, it is enough to keep in mind a crude value

$$\tau_{n\bar{n}} > 10^8 \text{ s}. \quad (6)$$

Correspondingly, the value of the mixing parameter is

$$\varepsilon_{n\bar{n}} = \frac{1}{\tau_{n\bar{n}}} < 10^{-23} \text{ eV}. \quad (7)$$

The dynamical meaning of $\varepsilon_{n\bar{n}}$ will be clear from the evolution equation that will be presented below. To give some perception of the value of $\varepsilon_{n\bar{n}}$, we may say that, if one considers a neutron confined in a one-dimensional 5-m-long box, then the level splitting will be just 10^{-23} eV.

Finally, we introduce the parameter $t_L \sim 1$ s—the time which neutrons need to cross the trapping box, or the time between two subsequent collisions with the walls. We also recall that both the β-decay time and the UCN storage time are on the order of 10^3 s.

3. HITTING THE TRAP WALL: SIMPLE ESTIMATES

Now, with relevant parameters at hand, we can analyze what happens with an admixture of neutrons and possible antineutrons when they interact with the wall of the trap. In this section, we present simple estimates.

Treatment based on the time evolution equation will be postponed until the next section. A third approach based on the wave packet formulation will only be touched on in the present paper and will be discussed in detail in the next publication.

First, we consider the collision of neutrons with the wall. As compared to antineutrons, this problem is much simpler due to the lack of absorption (see remarks on the previous pages).

In our illustrative example, a neutron with $v = 3.9 \times 10^2$ cm/s hits the ^{12}C wall of the trap. Such a velocity is well below the limiting ^{12}C value $v_n^{(0)} \simeq 6.1 \times 10^2$ cm/s and, hence, the neutron undergoes a complete reflection, $R = 1$. Being absolutely correct, the statement that the reflection coefficient $R = 1$ does not constitute the whole story. First, even at $v < v_n^{(0)}$, the tail of the neutron wave function penetrates inside the wall. On general grounds, the penetration depth is $l_w(n) \sim \lambda \simeq 10^{-5}$ cm, with λ being the de Broglie wavelength. Second, collision with the wall is not an instantaneous act, but is characterized by a certain collision time. The rigorous derivation of this time should be based on the wave packet formalism [12–14]. However, simple estimates presented below yield the same results.

Inside the wall, the neutron wave function has the form

$$\psi_n(x) \propto \exp\{-\kappa_n x\}, \quad \kappa_n = \sqrt{2m(U_n - E)}. \quad (8)$$

From (8), it is natural to identify

$$l_w(n) \simeq 1/\kappa_n \simeq 0.14 \times 10^{-5} \text{ cm}, \quad (9)$$

which is a few times less than the naive expectation $l_w(n) \sim \lambda = 10^{-5}$ cm. The collision time may be estimated as[1)]

$$\tau_{\rm coll}(n) \simeq \frac{2l_w(n)}{v} \simeq 0.7 \times 10^{-8}\ {\rm s}. \qquad (10)$$

This result is in perfect agreement with what is predicted from collision theory formulated in terms of the wave packets. Namely, if one describes the incident neutron by a wave packet

$$\psi_n(x,t) = \sqrt{\frac{a}{\pi}} \exp\left(ikx - \frac{k^2 t}{2m}\right) \frac{\sin[(x-vt)/a]}{x-vt}, \qquad (11)$$

where a is its width in x space, then

$$\tau_{\rm coll} = [E(U_0 - E)]^{-1/2} \simeq 0.7 \times 10^{-8}\ {\rm s} \qquad (12)$$

for $E = 80$ neV and $U_0 = 195$ neV. At this point, we note that

$$\tau_{\rm coll} v \simeq 2l_w \ll a = \frac{\lambda}{\pi}\left(\frac{\Delta\lambda}{\lambda}\right)^{-1}.$$

We shall return to this remark in connection with possible decoherence of n and $\bar{n}$ due to the difference in their collision times.

Now, we turn to $\bar{n}$ with the same velocity $v = 3.9 \times 10^2$ cm/s hitting the ^{12}C wall.

Due to absorption (annihilation), the $\bar{n}$ wave function inside the wall has the form

$$\psi_{\bar{n}}(x) \propto \exp(ik_{\bar{n}}x - \kappa_{\bar{n}}x), \qquad (13)$$

$$(ik_{\bar{n}} - \kappa_{\bar{n}})^2 = 2m(U_{\bar{n}} - iW_{\bar{n}} - E), \qquad (14)$$

where E is the energy of the incident $\bar{n}$. Equations (13) and (14) yield

$$l_w(\bar{n}) \simeq \frac{1}{\kappa_{\bar{n}}} \qquad (15)$$

$$= m^{-1/2}\left\{U_{\bar{n}} - E + [(U_{\bar{n}} - E)^2 + W^2]^{1/2}\right\}^{-1/2}$$

$$\simeq 0.32 \times 10^{-5}\ {\rm cm}.$$

Then, $\bar{n}$ collision time is

$$\tau_{\rm coll}(\bar{n}) \simeq \frac{2l_w(\bar{n})}{v} \simeq 1.6 \times 10^{-8}\ {\rm s}, \qquad (16)$$

which is about 2 times larger than the neutron collision time given by Eq. (10).[2)]

The crucial parameter that determines the fate of $\bar{n}$ hitting the wall is the ratio of the collision time (16) to the absorption (annihilation) time. The latter quantity is velocity independent by virtue of the $1/v$ law (3) and is expressed through the $\bar{n}$ mean free path Λ according to

$$\tau_{\rm abs}(\bar{n}) \sim \frac{\Lambda}{v} \simeq \frac{m}{4\pi N|{\rm Im}a_{\bar{n}A}|} \simeq 1.1 \times 10^{-8}\ {\rm s} \qquad (17)$$

for the ^{12}C trap wall. Thus,

$$\tau_{\rm coll}(\bar{n})/\tau_{\rm abs}(\bar{n}) > 1, \qquad (18)$$

which implies the collapse of the possible $\bar{n}$ component on the wall.

Already at this point, it is clear that this, in turn, leads to the time dependence of the probability of finding the $\bar{n}$ component stated in the Abstract, namely, $P(\bar{n}) = \varepsilon_{n\bar{n}}^2 t_L t$. A rigorous derivation of this equation is given in the next section.

Still, one may argue that the above estimates should be taken with caution and a certain fraction of $\bar{n}$ may still be reflected from the wall. Then, Eqs. (10) and (16) enable one to estimate the splitting between the centers of the n and $\bar{n}$ wave packets [see (11)] after the reflection. One has

$$\delta x \simeq v(\tau_{\rm coll}(\bar{n}) - \tau_{\rm coll}(n)) \qquad (19)$$

$$\simeq 0.35 \times 10^{-5}\ {\rm cm} \sim \lambda \ll a.$$

Whether this retardation influences the n–$\bar{n}$ mixing in free space between collisions with the trap walls will be discussed elsewhere.

The main point to be improved on in the above estimates is mentioned in the footnote to Eq. (10). Certain guidance in this direction may be found in [15].

Finally, we note that the treatment presented above seems physically more transparent than formal calculations of the reflection coefficient from the complex potential.

4. HITTING THE TRAP WALL: TIME-DEPENDENT APPROACH

As a "warming up" exercise we consider n–$\bar{n}$ oscillations in free space with β decay neglected. This is a standard two-level problem treated in any serious textbook on quantum mechanics. The phenomenological Hamiltonian is a 2×2 matrix in the basis of the two-component n–$\bar{n}$ wave function

$$H = E_i\delta_{ij} + \varepsilon\sigma_x, \qquad (20)$$

with $i, j = n, \bar{n}$. The evolution equation reads

$$i\frac{\partial}{\partial t}\begin{pmatrix}\psi_n\\ \psi_{\bar{n}}\end{pmatrix} = \begin{pmatrix}E_n & \varepsilon\\ \varepsilon & E_{\bar{n}}\end{pmatrix}\begin{pmatrix}\psi_n\\ \psi_{\bar{n}}\end{pmatrix}. \qquad (21)$$

Assuming that $\psi_n(t=0) = 1$, $\psi_{\bar{n}}(t=0) = 0$, and diagonalizing the Hamiltonian (20), one arrives at the

[1)] Strictly speaking, neutron velocity inside the wall is different from v.

[2)] The wave packet formalism, as was shown by V.A. Lensky, leads to a somewhat smaller value (see our next publication).

following expression for the probability of finding $\bar{n}$ at time t [2–6]:

$$|\psi_{\bar{n}}(t)|^2 = \frac{4\varepsilon^2}{\omega^2+4\varepsilon^2}\sin^2\left(\frac{1}{2}\sqrt{\omega^2+4\varepsilon^2}t\right), \quad (22)$$

where $\omega = E_{\bar{n}} - E_n$. In free space, the difference between $E_{\bar{n}}$ and E_n may be due to the Earth's magnetic field. In this case,

$$\omega = 2\mu_n B \simeq 6\times 10^{-12}\ \text{eV}, \quad (23)$$

where μ_n is the neutron magnetic moment. Without a magnetic field, i.e., at $\omega = 0$, and at $t \ll \tau_{n\bar{n}} \simeq 10^8$ s, one has

$$|\psi_{\bar{n}}(t)|^2 \simeq \varepsilon_{n\bar{n}}^2 t^2, \quad (24)$$

while with the Earth's magnetic field Eq. (24) is valid only at extremely short times, $t \ll (\mu_n B)^{-1} \simeq 2\times 10^{-4}$ s, while at larger times

$$|\psi_{\bar{n}}(t)|^2 \simeq \frac{4\varepsilon^2}{\omega^2}\sin^2(t/\tau_B) \simeq 10^{-23}\sin^2(t/\tau_B), \quad (25)$$

where $\tau_B = (\mu_n B)^{-1} \simeq 2\times 10^{-4}$ s.

The use of (22) to test fundamental symmetries is discussed in [5].

Next, we consider the general Hamiltonian of the n–$\bar{n}$ system inside the wall with annihilation and β decay included. The problem is reminiscent of strangeness oscillations in the $K\bar{K}$ system. With annihilation and β decay included, the Hamiltonian (20) is replaced by

$$H = \begin{pmatrix} E_n - i\dfrac{\Gamma_\beta}{2} & \varepsilon_{n\bar{n}} \\ \varepsilon_{n\bar{n}} & E_{\bar{n}} - i\dfrac{\Gamma_a}{2} - i\dfrac{\Gamma_\beta}{2} \end{pmatrix}, \quad (26)$$

where $\Gamma_\beta^{-1} \sim 10^3$ s and $\Gamma_a \simeq 2W_n \simeq 60$ neV for ^{12}C.

In arriving at (22), diagonalization of the Hamiltonian (20) has been done exactly. Performing a similar procedure with (26), use can be made of a small parameter $4\varepsilon^2 \ll |H_{11}-H_{22}|^2$. Indeed, inside the wall, effective fields acting on n and $\bar{n}$ differ by tens of neV [see (2) and (5)], while $\varepsilon_{n\bar{n}} \sim 10^{-14}$ neV. Expanding $\{(H_{11}-H_{22})^2 + 4\varepsilon_{n\bar{n}}^2\}^{1/2}$ with respect to this small parameter, one finds the two eigenvalues of the Hamiltonian (26)

$$\mu_1 \simeq E_n' - i\frac{\Gamma_\beta}{2} - i\frac{\Gamma_\varepsilon}{2}, \quad (27)$$

$$\mu_2 \simeq E_{\bar{n}}' - i\frac{\Gamma_a}{2} - i\frac{\Gamma_\beta}{2} + i\frac{\Gamma_\varepsilon}{2}. \quad (28)$$

Here, $E_n' = E_n - E_\varepsilon$, $E_{\bar{n}}' = E_{\bar{n}} + E_\varepsilon$, and

$$E_\varepsilon + i\frac{\Gamma_\varepsilon}{2} = \frac{\varepsilon_{n\bar{n}}^2}{E_{\bar{n}} - E_n - i\Gamma_a/2}. \quad (29)$$

The "wrong" sign of the last term in (28) is an artifact of the square root expansion, but this is physically irrelevant since $\Gamma_\varepsilon \ll \Gamma_\beta \ll \Gamma_a$ ($\Gamma_\varepsilon \sim 10^{-39}$ eV, $\Gamma_\beta \sim 10^{-18}$ eV, $\Gamma_a \sim 10^{-7}$ eV).

In terms of eigenvalues μ_1 and μ_2, the general solution of the two-component evolution equation has the form [16]

$$\psi(t) = \begin{pmatrix} \psi_n(t) \\ \psi_{\bar{n}}(t) \end{pmatrix} \quad (30)$$
$$= \left(\frac{H-\mu_2}{\mu_1-\mu_2}e^{-i\mu_1 t} + \frac{H-\mu_1}{\mu_2-\mu_1}e^{-i\mu_2 t}\right)\psi(0).$$

Again, we start with a solution corresponding to initial conditions $\psi_n(t=0)=1$, $\psi_{\bar{n}}(t=0)=0$. Then, from (26)–(30), one gets

$$|\psi_{\bar{n}}(t)|^2 = \frac{\varepsilon_{n\bar{n}}^2}{\omega^2+\Gamma_a^2/4}e^{-(\Gamma_\beta+\Gamma_\varepsilon)t} \quad (31)$$
$$\times\left\{1 + e^{-\Gamma_a' t} - 2e^{-\Gamma_a' t/2}\cos\omega t\right\},$$

where $\omega = E_{\bar{n}} - E_n$, $\Gamma_a' = \Gamma_a - 2\Gamma_\varepsilon$, and Γ_ε is defined by (29). Since $\Gamma_\varepsilon \ll \Gamma_\beta$ and $\Gamma_\varepsilon \ll \Gamma_a$, one can rewrite (31) in a simpler form without noticeable lost of accuracy, namely,

$$|\psi_{\bar{n}}(t)|^2 = \frac{\varepsilon_{n\bar{n}}^2}{\omega^2+\Gamma_a^2/4}e^{-\Gamma_\beta t} \quad (32)$$
$$\times\left\{1 + e^{-\Gamma_a t} - 2e^{-\Gamma_a t/2}\cos\omega t\right\}.$$

This equation resembles that giving the probability of finding $\bar{K}^0$ in an initially pure K^0 beam. Notice that, instead of the overall factor $1/4$ for the $K^0\bar{K}^0$ system, we find in (32) an extremely small factor $\varepsilon_{n\bar{n}}^2(\omega^2+\Gamma_a^2/4)^{-1} \sim 10^{-32}$(!) reflecting the fact that mixing is very small as compared to the complex splitting of n and $\bar{n}$ eigenvalues in the medium.

Consider (32) at $t = \tau_{\text{coll}}(\bar{n}) \simeq 1.6\times 10^{-8}$ s [see (16)]. Then, $\Gamma_\beta\tau_{\text{coll}}(\bar{n}) \sim 10^{-11}$, $\Gamma_a\tau_{\text{coll}}(\bar{n}) \simeq 1.5$, $\cos\omega\tau_{\text{coll}}(\bar{n}) \simeq 0.7$, and (32) yields

$$|\psi_{\bar{n}}(\tau_{\text{coll}}(\bar{n}))|^2 \lesssim 10^{-32}. \quad (33)$$

Physically, this means that, if a pure n beam collides with a wall made of ^{12}C, the tiny admixture of $\bar{n}$ which would have emerged during the collision time is completely damped by annihilation and n–$\bar{n}$ energy splitting.

The free-space regime (24) is "hidden" in (32) at the limit of very short times, $t \ll 1/\Gamma_a \sim 10^{-8}$ s. Then,

$$|\psi_{\bar{n}}(t)|^2 \simeq \frac{\varepsilon_{n\bar{n}}^2}{\omega^2+\Gamma_a^2/4}\sin^2\frac{\omega t}{2} \quad (34)$$

$$\simeq \frac{\varepsilon_{n\bar{n}}^2 t^2}{1+\Gamma_a^2/(4\omega^2)} \simeq 0.9\varepsilon_{n\bar{n}}^2 t^2,$$

where, at the last step, use has been made of the values of Γ_a and ω for ^{12}C.

Next, consider Eq. (30) at initial conditions that are closer to the real experimental situation. Namely, suppose that a UCN beam collides with the wall after crossing the trap. The Earth's magnetic field is assumed to be shielded, so that the free-space Eq. (24) is valid inside the trap. Then initial conditions in (30) read

$$\psi_{\bar{n}}(t=0) = \varepsilon_{n\bar{n}} t_L, \quad \psi_n(t=0) = \sqrt{1-\varepsilon_{n\bar{n}}^2 t_L^2}, \tag{35}$$

where $t_L \simeq 1$ s. Then, at $t = \tau_{\rm coll}(\bar{n}) \simeq 1.6\times 10^{-8}$ s, i.e., just after the collision with the wall, one gets

$$|\psi_{\bar{n}}(\tau_{\rm coll})|^2 \simeq \varepsilon_{n\bar{n}}^2 t_L^2 e^{-(\Gamma_a+\Gamma_\beta)\tau_{\rm coll}}\left[1+O\left(1/t_L\Gamma_a\right)\right]. \tag{36}$$

This result is again physically transparent. During the collision, the $\bar{n}$ component is depleted by annihilation, while antineutrons "newly born" inside the wall are damped according to our previous result (32).

Now, $\tau_{\rm coll}(\bar{n}) \simeq 1.6\times 10^{-8}$ s and $\Gamma_a \simeq 60$ neV, so that $\exp(-\Gamma_a\tau_{\rm coll}) \simeq 0.2$. This means that only 1 per $\simeq 5\bar{n}$ survives after the collision.

This result is in line with estimates presented in Section 3, but here we are on a somewhat more qualitative footing.

If one considers the fraction 1/5 as a small parameter, then the probability of antineutron detection at time t will be

$$|\psi_{\bar{n}}(t)|^2 = \varepsilon_{n\bar{n}}^2 t_L t, \tag{37}$$

instead of $\varepsilon_{n\bar{n}}^2 t^2$ free-space law (24). Indeed, the probability of n–$\bar{n}$ transition between the two subsequent collisions with the walls is $\varepsilon_{n\bar{n}}^2 t_L^2$, while the number of collisions during the observation time is t/t_L. The extrapolation between the laws (24) and (37) will be discussed in the next publication.

ACKNOWLEDGMENTS

I am deeply grateful to Yu.A. Kamyshkov for grabbing him into the subject and presenting a clear introduction. Discussion of the oscillation problem with M.I. Vysotsky was very enlightening. Useful remarks and information were gained from V.A. Lensky, L.A. Kondratyuk, A.E. Kudryavtsev, and the members of the ITEP seminar.

Special thanks for essential financial support go to V.A. Novikov, L.B. Okun, and the Russian Foundation for Basic Research (project nos. 00-02-17836 and 00-15-96786).

REFERENCES

1. V. A. Kuzmin, Pis'ma Zh. Éksp. Teor. Fiz. **12**, 335 (1970) [JETP Lett. **13**, 335 (1970)].
2. K. G. Chetyrkin *et al.*, Phys. Lett. B **99B**, 358 (1981).
3. M. Baldo-Ceolin, in *Festischrift for Val Telegdi*, Ed. by K. Winter (Elsevier, Amsterdam, 1988), p. 17.
4. A. Gal, Phys. Rev. C **61**, 028201 (2000).
5. Yu. G. Abov, F. S. Dzheparov, and L. B. Okun, Pis'ma Zh. Éksp. Teor. Fiz. **39**, 493 (1984) [JETP Lett. **39**, 599 (1984)].
6. R. Golub, in *Proceedings of the International Workshop on Future Prospects of Baryon Instability Search, Oak Ridge, 1996*, Ed. by S. J. Ball and Y. A. Kamyshkov, p. 329.
7. Ya. B. Zeldovich, Zh. Éksp. Teor. Fiz. **36**, 1952 (1959).
8. V. K. Ignatovich, *The Physics of Ultracold Neutrons* (Nauka, Moscow, 1986) [in Russian], p. 228.
9. Ye. S. Golubeva and L. A. Kondratyuk, Nucl. Phys. B (Proc. Suppl.) **56**, 103 (1997).
10. M. Baldo-Ceolin *et al.*, Z. Phys. C **63**, 409 (1994).
11. J. Chung *et al.*, Phys. Rev. D **66**, 032004 (2002).
12. A. Messiah, *Quantum Mechanics* (North-Holland, Amsterdam, 1962), Vol. 1.
13. M. L. Goldberger and K. M. Watson, *Collision Theory* (Wiley, New York, 1964).
14. V. M. Galitsky, B. M. Karnakov, and V. I. Kogan, *Problems in Quantum Mechanics* (Nauka, Moscow, 1992) [in Russian].
15. I. M. Frank, Usp. Fiz. Nauk **161** (11), 109 (1991).
16. I. Yu. Kobzarev, N. N. Nikolaev, and L. B. Okun, Yad. Fiz. **10**, 864 (1969).

Physics of Atomic Nuclei, Vol. 66, No. 12, 2003, pp. 2183–2188. Translated from Yadernaya Fizika, Vol. 66, No. 12, 2003, pp. 2233–2238.

ELEMENTARY PARTICLES AND FIELDS
Theory

Quasielastic Kaon Knockout from a Proton and Momentum Distribution of Virtual Kaons in the Proton

I. T. Obukhovsky, L. L. Sviridova, and V. G. Neudatchin

Institute of Nuclear Physics, Moscow State University, Vorob'evy gory, Moscow, 119899 Russia

Received January 8, 2003

Abstract—The momentum distribution of kaons in the proton and the coupling-constant ratio $f_{K\Lambda N}/f_{K\Sigma N}$ are determined on the basis of the $^3P_0$ quark model of meson–baryon coupling. The longitudinal cross section for kaon electroproduction is calculated. The results of the present study are compatible with available experimental data, but more detailed data on the longitudinal cross section would make it possible to refine the absolute values of the coupling constants $f_{K\Lambda N}$ and $f_{K\Sigma N}$. © *2003 MAIK "Nauka/Interperiodica".*

1. INTRODUCTION

The problem of studying the strange component $s\bar{s}$ in nucleons with the aid of processes involving the photo- and electroproduction of ϕ [1] and K [2, 3] mesons at beam energies of a few GeV is being extensively discussed in the literature. However, vector dominance and Pomeron exchange, which are by no means related to the strange component, play a key role in the production of a vector ϕ meson. For this reason, it is necessary to overcome serious difficulties [1] in order to extract the contribution of the t-channel pole diagram corresponding to the emission of a virtual ϕ meson (which is present in a nucleon owing precisely to the strange component $s\bar{s}$) into a continuum upon photon emission or electron impact. There are no such problems in the knockout of a pseudoscalar K meson if the strange component is studied in the channels $p(e,e'K)Y$, where $Y=\Sigma,\Lambda$.

Previously, the knockout of a π meson was considered in [4], where it was shown that direct experimental information about the momentum distributions of pions in nucleons in various channels of virtual $N\to B+\pi$ decays [$B=N,\Delta,N^*(3/2^-1/2^-)$, $N^{**}(1/2^+)\ldots$] or of ρ (ω) mesons in the same channels can be obtained if use is made of the kinematics of quasielastic pion knockout by high-energy electrons, $N(e,e'\pi)B$, at rather high values of the squared 4-momentum of a virtual photon, $Q^2\simeq 2$–$5\,(\mathrm{GeV}/c)^2$. In this case, the contribution of the t-channel pole diagram in Fig. 1 featuring a virtual pion (for longitudinal photons, $\pi+\gamma_L\to\pi$) or a virtual ρ meson (for transverse photons, $\rho+\gamma_T\to\pi$) is absolutely dominant, which makes it possible to extract the above momentum distributions directly from experimental data.

The pion momentum distribution $\overline{|\Psi_N^{B\pi}(\mathbf{k})|^2}$ and the free-scattering cross section $d\sigma(e+\pi\to e'+\pi)/d\Omega_\pi^*$ enter into the expression for the differential cross section

$$\frac{d^5\sigma_L}{dE_{e'}d\Omega_{e'}d\Omega_\pi^*}=E_{e'}\frac{\overline{|\Psi_N^{B\pi}(\mathbf{k})|^2}}{(4\pi)^3E_NE_BE_\pi}$$
$$\times\left(1-\frac{E_\pi}{|k_\pi|}\cos\theta_\pi\right)\frac{d\sigma(e+\pi\to e'+\pi)}{d\Omega_\pi^*};$$

therefore, there does not arise the problem of gauge invariance [4]. We perform our analysis in the laboratory frame, taking into account the pole z-diagram that represents the virtual production of a $\pi^+\pi^-$ pair. It is worth noting that the situation is completely different in the case of pion photoproduction ($Q^2=0$), where tree diagrams (that is, s-channel pole diagrams) also play a significant role [5].

In [6], the ideas outlined above were combined with the quark microscopic approach and the pic-

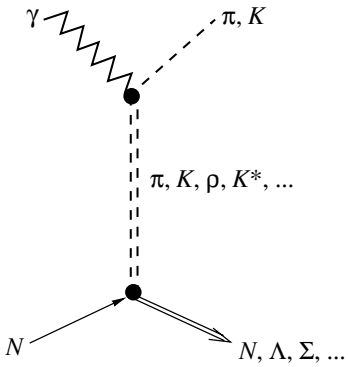

Fig. 1. Pole diagram corresponding to the quasielastic-knockout reaction.

1063-7788/03/6612-2183$24.00

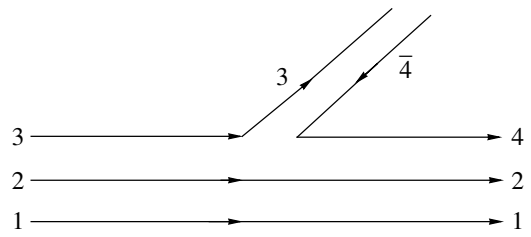

Fig. 2. Quark picture of K-meson production.

ture of meson production from a scalar $q\bar{q}$ fluctuation in the polarized QCD vacuum. This polarization–fluctuation picture is employed in the present study as a conceptual framework for describing the contributions of various types of mesons to the meson cloud of a nucleon (in all probability, it may serve as a basis for obtaining deeper insight into microscopic physics behind such approaches as Regge pole theory). To be more specific, use was made of the popular model of a scalar $^3P_0$ fluctuation ($u\bar{u} + d\bar{d} + s\bar{s}$) [7]. The pion wave functions in the aforementioned pion–baryon channels of virtual $N \to B + \pi$ decays [$B = N$, Δ, $N^*(3/2^-, 1/2^-)$, $N^{**}(1/2^+)\ldots$] were determined by projecting the multiparticle $q^4\bar{q}$ wave function onto these channels [6]. For $B = N$, the agreement with the momentum distribution extracted earlier in [4] from experimental data reported in [8] was rather good (the momentum distributions in other channels have not yet been measured).

In the present study, we extend this microscopic approach to $Y + K$ channels ($Y = \Lambda, \Sigma$). We extract the amplitude of the strange component $s\bar{s}$ directly from the kaon spectroscopic factor S_N^{KY} in some of the channels being considered.

2. DESCRIPTION OF THE FORMALISM

Within the $^3P_0$ model, the Hamiltonian for K^+-meson production in the transition $u \to s + K^+$ has the same form as that for π^+ production in the transition $u \to d$ (see, for example, [9]), but we must replace there the isospin τ matrix by the corresponding λ matrix of the $SU(3)_F$ flavor group; that is,

$$H^{(3)}_{u\to s+K^+} = -i\frac{f_{Kqq}}{m_K}\frac{\exp(i\frac{2}{3}\mathbf{k}\cdot\boldsymbol{\rho}')}{(2\pi)^{2/3}(2\omega_K(\mathbf{k}))^{1/2}}\lambda^{(3)}_{u\to s} \quad (1)$$
$$\times \hat{O}^{(3)}(\boldsymbol{\rho}', \boldsymbol{\rho})\left(\boldsymbol{\sigma}^{(3)}\left[\frac{\omega_K(\mathbf{k})}{2m_{sq}}\left(\frac{2}{i}\boldsymbol{\nabla}_\rho + \frac{2}{3}\mathbf{k}\right) + \left(1 + \frac{\omega_K(\mathbf{k})}{6m_{sq}}\right)\mathbf{k}\right]\right),$$

where f_{Kqq} is the Kqq coupling constant (we emphasize that, in the case of pion production, the amplitude of a $q\bar{q}$ fluctuation was normalized to the effective πqq coupling constant $f_{\pi qq} = \frac{3}{5}f_{\pi NN}$, while, in the case of K-meson production, f_{Kqq} is a free parameter); m_K is the K-meson mass; $\mathbf{k}$ and $\omega_K(\mathbf{k})$ are the K-meson momentum and energy, respectively, $\omega_K(\mathbf{k}) = \sqrt{\mathbf{k}^2 + m_K^2}$; $\lambda^{(3)}_{u\to s}$ is the Gell-Mann matrix corresponding to the transition $u \to s$, the superscript (3) corresponding to the third quark (see Fig. 2); $\boldsymbol{\sigma}^{(3)}$ stands for the spin Pauli matrices for the third quark; $m_{sq} = (m_s + m_q)/2$, $m_s \approx 500$ MeV and $m_q = 313$ MeV; $\boldsymbol{\rho}$ and $\boldsymbol{\rho}'$ are the relative Jacobi coordinates of the third quark, respectively, prior to and after meson emission, $\boldsymbol{\rho} = (\mathbf{r}_1 + \mathbf{r}_2)/2 - \mathbf{r}_3$ and $\boldsymbol{\rho}' = (\mathbf{r}_1 + \mathbf{r}_2)/2 - \mathbf{r}_4$ (see the numbering of quarks in Fig. 2); and $\hat{O}^{(3)}(\boldsymbol{\rho}', \boldsymbol{\rho})$ is a nonlocal operator kernel,

$$\hat{O}^{(3)}(\boldsymbol{\rho}', \boldsymbol{\rho}) = \frac{1}{(4\pi b_K^2)^{3/2}}\exp\left(\frac{i}{2}\mathbf{k}(\boldsymbol{\rho}' - \boldsymbol{\rho})\right) \quad (2)$$
$$\times \exp\left(-\frac{1}{4b_K^2}(\boldsymbol{\rho}' - \boldsymbol{\rho})^2\right),$$

with b_K being the kaon radius. Our calculations revealed that the cross section is virtually independent of this quantity, and we can set $b_K = 0$ for a first approximation. The nonlocal operator then reduces to a delta function: $\hat{O}^{(3)}(\boldsymbol{\rho}', \boldsymbol{\rho}) = \delta^{(3)}(\boldsymbol{\rho}' - \boldsymbol{\rho})$. The amplitudes for the transitions $p \to K + \Lambda$ and $p \to K + \Sigma$ are calculated as the product of the respective matrix element of the operator in (1) and the number of quarks in a nucleon. The initial- and final-state wave functions are given by

$$|Y\rangle = |s^3[3]_X L = 0\rangle_{\mathrm{TISM}}|[1^3]_C, ([21]_S \circ [21]_F)[3]_{SF} : [1^3]_{CSF}\rangle, \quad (3)$$

where $|s^3[3]_X L = 0\rangle_{\mathrm{TISM}}$ is the radial part of the wave function in the translation-invariant shell model (TISM) (all three quarks are in the s state). The flavor parts of the wave functions for p, Λ, and Σ are

$$|[21]_F([2] \times [1])\rangle = -\frac{1}{\sqrt{3}}\left(\frac{u_1 d_2 + d_1 u_2}{\sqrt{2}}\right)u_3 \quad (4)$$

$$+\sqrt{\frac{2}{3}}u_1u_2d_3,$$

$$|[21]_F([1^2]\times[1])\rangle = \left(\frac{u_1d_2-d_1u_2}{\sqrt{2}}\right)u_3$$

for the proton (udu);

$$|[21]_F([2]\times[1])\rangle = \frac{1}{\sqrt{2}} \tag{5}$$
$$\times\left(\frac{u_1s_2+s_1u_2}{\sqrt{2}}d_3-\frac{d_1s_2+s_1d_2}{\sqrt{2}}u_3\right),$$

$$|[21]_F([1^2]\times[1])\rangle = \frac{1}{\sqrt{6}}$$
$$\times\left(\frac{u_1s_2-s_1u_2}{\sqrt{2}}d_3-\frac{d_1s_2-s_1d_2}{\sqrt{2}}u_3\right)$$
$$+\sqrt{\frac{2}{3}}\left(\frac{u_1d_2-d_1u_2}{\sqrt{2}}\right)s_3$$

for the Λ hyperon (uds); and

$$|[21]_F([2]\times[1])\rangle = -\frac{1}{\sqrt{6}} \tag{6}$$
$$\times\left(\frac{u_1s_2+s_1u_2}{\sqrt{2}}d_3+\frac{d_1s_2+s_1d_2}{\sqrt{2}}u_3\right)$$
$$+\sqrt{\frac{2}{3}}\left(\frac{u_1d_2+d_1u_2}{\sqrt{2}}\right)s_3,$$

$$|[21]_F([1^2]\times[1])\rangle = \frac{1}{\sqrt{2}}$$
$$\times\left(\frac{u_1s_2-s_1u_2}{\sqrt{2}}d_3+\frac{d_1s_2-s_1d_2}{\sqrt{2}}u_3\right)$$

for the Σ hyperon (uds).

Using expressions (3)–(6), we obtain the $p\to K+Y$ matrix element

$$\langle Y(\mu',f')K|3H^{(3)}_{u\to s+K^+}|p(\mu,f)\rangle \tag{7}$$
$$= 3\frac{f_{Kqq}}{(2\pi)^{3/2}(2\omega_K(\mathbf{k}))^{1/2}}i\frac{|\mathbf{k}|}{m_K}$$
$$\times\left[(\boldsymbol{\sigma}_{\mu\mu'}\cdot\hat{\mathbf{k}})\lambda_{ff'}\right]F_{KYN}(\mathbf{k}^2)\left(1+\frac{\omega_K(\mathbf{k})}{6m_{qs}}\right)\frac{1}{N},$$

where $N=\left(1+\frac{2}{3}x^2\right)^{3/2}$, $x=b_K/b_N$, with $b_N=0.6$ fm being the nucleon radius; (μ,f) and (μ',f') are the spin and flavor projections of the initial and final baryons, respectively; and

$$F_{KYN}(\mathbf{k}^2) \tag{8}$$
$$=\exp\left(-\frac{1}{6}\mathbf{k}^2b_N^2\left[1+\frac{1}{6}x^2\left(1+\frac{2}{3}x^2\right)^{-1}\right]\right)$$

is the form factor of the KYN vertex, $Y=\Lambda,\Sigma$.

The spin-averaged square of the spin–flavor part $\left[(\boldsymbol{\sigma}_{\mu\mu'}\cdot\hat{\mathbf{k}})\lambda_{ff'}\right]$ is

$$\overline{|\langle\Lambda K|(\boldsymbol{\sigma}\cdot\hat{\mathbf{k}})\lambda|p\rangle|^2} = \frac{1}{3}, \tag{9}$$

$$\overline{|\langle\Sigma K|(\boldsymbol{\sigma}\cdot\hat{\mathbf{k}})\lambda|p\rangle|^2} = \frac{1}{3}\cdot\frac{1}{27}. \tag{10}$$

Finally, the spin-averaged squared amplitude for the transition $P\to K+Y$ assumes the form

$$\overline{|J(p\to K+Y)|^2} = f^2_{KYN}\frac{4M_NM_Y}{m_K^2}\mathbf{k}^2 \tag{11}$$
$$\times\left(1+\frac{\omega_K(\mathbf{k})}{6m_{qs}}\right)^2\frac{1}{N^2}F^2_{KYN}(\mathbf{k}^2),$$

where $f_{K\Lambda N}=-\sqrt{3}f_{Kqq}$ and $f_{K\Sigma N}=(1/3)f_{Kqq}$. Thus, the microscopic model of a $^3P_0$ scalar quark–antiquark fluctuation leads to a specific value for the ratio of the $K\Lambda N$ and $K\Sigma N$ coupling constants:

$$f_{K\Lambda N}/f_{K\Sigma N} = -3\sqrt{3}. \tag{12}$$

This relation obeys $SU(3)$ symmetry and follows from the fact that, owing to the Pauli exclusion principle, the F/D coupling-constant ratio for the interaction of the baryon octet with the meson octet has a fixed value of $2/3$ in the quark model.

The total amplitude for the diagram in Fig. 1 has the form

$$J_\varkappa = \frac{J(p\to K+Y)}{k^2-m_K^2}e(k+k')\epsilon^{(\varkappa)}F_K(Q^2), \tag{13}$$

where e is the electron charge, k'_μ is the 4-momentum of the emitted (real) kaon, $\epsilon^{(\varkappa)}_\mu$ is the photon polarization 4-vector, and $F_K(Q^2)$ is the electromagnetic form factor for the kaon. Following [10], we took it in the form

$$F_K(Q^2) = \frac{a}{1+Q^2/b_1^2}+\frac{1-a}{(1+Q^2/b_2^2)^2}, \tag{14}$$

where Q^2 is the square of the 4-momentum of a virtual photon, $a=0.398$, $b_1=0.642$ GeV/c, and $b_2=1.386$ GeV/c.

The cross section for quasielastic kaon knockout from a proton was calculated by the formula

$$\frac{d\sigma}{dt} = \varepsilon\frac{d\sigma_L}{dt}+\frac{d\sigma_T}{dt}, \tag{15}$$

where ε is the degree of photon polarization, while the transverse and the longitudinal cross section are given by

$$\frac{d\sigma_i}{dt} = \frac{J_i^2}{32\pi W(W^2-M_N^2)|\mathbf{q}^*|}. \tag{16}$$

Table 1. Coupling constants $f_{K\Lambda N}$ and $f_{K\Sigma N}$ and their ratio

$f_{K\Lambda N}$	$f_{K\Sigma N}$	$\lvert f_{K\Lambda N}/f_{K\Sigma N}\rvert$	Reference
-3.16 ± 0.01	0.91 ± 0.01	3.47	[10]
-4.17 ± 0.75	1.18 ± 0.66	3.53	[11]
-2.38	0.27	8.81	[12]
-3.7 ± 0.7	1.1 ± 0.2	3.36	[13]
-1.73	0.33	5.2	This paper

Here, W is the total energy in the c.m. frame, $W^2 = (p_N + q)^2 = (k' + p_Y)^2$; $\mathbf{q}^*$ is the photon 3-momentum in the c.m. frame; and $i = T, L$ with $J_L = J_{\varkappa=0}$ and $J_T = (J_{\varkappa=+1} + J_{\varkappa=-1})/2$.

The squared radial part of the virtual-kaon wave function (momentum distribution) in the proton is

$$|R(\mathbf{k}^2)|^2 = \overline{|J(p \to K + Y)|^2} \times \frac{1}{(4\pi)^2 E_Y(\mathbf{k}) M_N \omega_K(\mathbf{k})}, \quad (17)$$

where $E_Y(\mathbf{k}) = \sqrt{M_Y^2 + \mathbf{k}^2}$ is the energy of the final baryon Y ($Y = \Lambda$ or Σ) and k_0 is the virtual-kaon energy in the "cloud"; it is calculated on the basis of energy conservation in the lower vertex of the pole diagram in Fig. 1—we have $k_0 = m_N - E_Y(\mathbf{k})$ in the laboratory frame, for example.

The spectroscopic factor (the number of kaons in a given channel) is equal to an integral of the squared wave function:

$$S_p^{KY} = \int |R(\mathbf{k}^2)|^2 k^2 dk. \quad (18)$$

3. RESULTS AND DISCUSSION

As was mentioned above, the microscopic $^3P_0$ model leads to the following expressions for the meson–baryon vertex constants: $f_{K\Lambda N} = -\sqrt{3} f_{Kqq}$ and $f_{K\Sigma N} = (1/3) f_{Kqq}$. The model gives no way to assess the absolute values of the coupling constants $f_{K\Lambda N}$ and $f_{K\Sigma N}$, since the quark constant f_{Kqq} is a free parameter; however, it unambiguously determines the ratio $|f_{K\Lambda N}/f_{K\Sigma N}| = 3\sqrt{3} \approx 5.2$. Table 1 displays available experimental data on the coupling constants $f_{K\Lambda N}$ and $f_{K\Sigma N}$, along with the results obtained in the present study. We extracted f_{Kqq} from experimental data on the differential cross section, assuming that the mechanism of quasielastic kaon knockout from the meson cloud completely determines the electroproduction cross section at small angles. However, a different mechanism according to which a kaon can be produced upon the deexcitation of the virtual vector meson $K^*(892)$ via photon emission in the same cloud (see below) contributes significantly to the transverse part of the cross section.

Table 2. Ratio R of the longitudinal and the transverse cross section in the reaction $H^1(e, e'K^+)\Lambda$

Q^2, $(\mathrm{GeV}/c)^2$	0.52	0.75	1.00	2.00
R	0.82 ± 0.18	0.96 ± 0.16	0.65 ± 0.29	0.56 ± 0.24

If the transverse contribution to the cross section could be disregarded, then, in order to reproduce experimental data, it would be necessary to choose a coupling-constant value in the range $f_{Kqq} = (2\text{–}2.8) f_{\pi qq}$, where the constant $f_{\pi qq}$ is normalized to the known value of the πNN coupling constant: $f_{\pi qq} = \frac{3}{5} f_{\pi NN}$, $f_{\pi NN} \approx 1$. It is clear that correct values of the coupling constants $f_{K\Lambda N}$ and $f_{K\Sigma N}$ can be extracted only from more detailed data on the longitudinal cross section.

Figure 3 shows the longitudinal cross section $d\sigma_L/dt$. Experimental data exist only for the sum (15) of the longitudinal and transverse cross sections. In addition, there are data on the total-cross-section ratio $R = \sigma_L/\sigma_T$ [14] for individual values of Q^2 (see Table 2).

The calculations performed in [4] revealed that the transverse part of the cross section for pion electroproduction at rather high Q^2 is almost completely determined by the contribution of vector (ρ) virtual mesons. Therefore, it is natural to expect that, in the case of kaon electroproduction, the main contribution to the cross section $d\sigma_T/dt$ comes from the process $p \to K^* + Y$ followed by the rearrangement $K^* \to K$.

The longitudinal cross section at rather high Q^2 is almost completely determined by the quasielastic contribution of pseudoscalar mesons. Therefore, it is necessary to separate the experimental values of the cross section into the longitudinal and the transverse component in order to estimate the constant f_{Kqq}. On the basis of the data in Table 2, we set $d\sigma/dt \approx 2 d\sigma_L/dt$ for a rough estimate. Figure 3 shows the data obtained precisely in this way. The model considered here makes it possible to obtain not only vertex constants but also analytic expressions for the form factors in meson–baryon vertices [Eq. (8)]. We note that the form factor (8) of the KYN vertex virtually coincides with the form factor calculated for the πNN

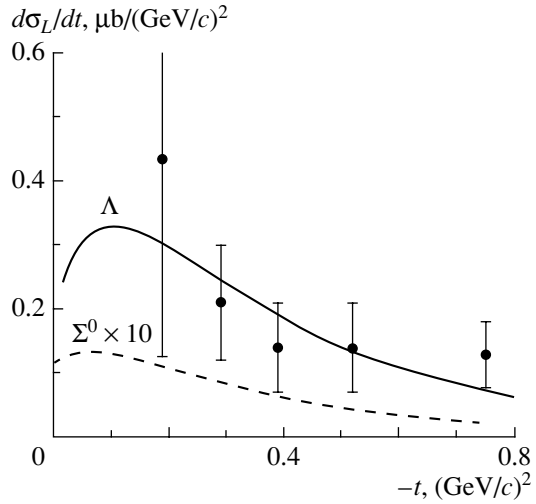

Fig. 3. Longitudinal cross section for kaon electroproduction at $Q^2 = 1.35$ (GeV/c)^2 and $W = 2.11$ GeV in the (solid curve) $p \to K + \Lambda$ and (dashed curve) $p \to K + \Sigma$ channels (the cross section for the channel $p \to K + \Sigma$ was magnified by a factor of 10) versus $-t$ (t is the square of the virtual-kaon 4-momentum). Experimental data from [8] for $d\sigma_T/dt + \epsilon d\sigma_L/dt$ in the $p \to K + \Lambda$ channel are used here with a factor of 0.5 merely as a rough estimate of the longitudinal cross section (see main body of the text).

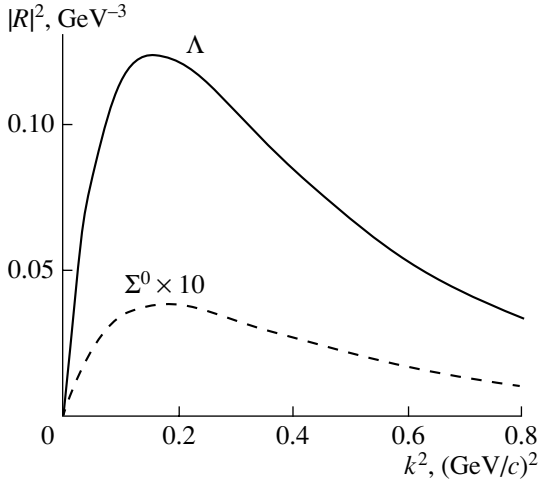

Fig. 4. Momentum distribution of kaons in the proton in the (solid curve) $p \to K + \Lambda$ and (dashed curve) $p \to K + \Sigma$ channels (the results for the $p \to K + \Sigma$ channel are magnified by a factor of 10).

vertex within the microscopic model proposed in [6], the only difference lying in the corrections proportional to powers of the parameter x, which is equal to b_K/b_N for the kaon and b_π/b_N for the pion. However, the calculations performed in [6] revealed that the form factor depends only slightly on these corrections. With the aid of expression (8) for the form factor, the momentum distribution of kaons in the proton in the two channels being considered can be calculated according to Eq. (17). The result is given in Fig. 4. The spectroscopic factors are equal to $S_p^{K\Lambda} = 0.076$ and $S_p^{K\Sigma} = 0.003$, respectively. The smallness of the ratio $S_p^{K\Sigma}/S_p^{K\Lambda} \approx 0.04$ follows from a large distinction between the coupling constants $f_{K\Lambda N}$ and $f_{K\Sigma N}$ that is predicted in the quark model [see Eq. (12)]. For the sake of comparison, the spectroscopic factor of the pion is $S_p^{n\pi} = 0.25$ [4].

Let us summarize our results once again. Within the microscopic model of a $^3P_0$ scalar quark–antiquark fluctuation, we have obtained the kaon form factor (momentum distribution) in the proton and the coupling-constant ratio $f_{K\Lambda N}/f_{K\Sigma N}$, which is in accord with data reported in [10]. We have used this form factor to calculate the longitudinal cross section for kaon electroproduction. More detailed experimental data on this cross section would enable one to refine the values of the coupling constants $f_{K\Lambda N}$ and $f_{K\Sigma N}$.

In conclusion, we characterize some possible lines of further investigations. In principle, it is necessary to extend the projection of the multiparticle wave function for the quark–gluon system *nucleon plus scalar $q\bar{q}$ fluctuation* (in the simplest case, this multiparticle system is the $q^4\bar{q}$ quark configuration, but it is reasonable to go over in the future to more advanced nonperturbative versions) onto $B + m$ channels, as is done in cluster physics in nuclei—namely, it is desirable to include, in addition to the $B\pi$ and YK channels, channels featuring virtually excited mesons π^*, ρ^*, K^*, etc., since, for example, the electron impact induces a transition of an orbitally excited meson $1^+(l = 1)$ to the ground state $0^-(l = 0)$, and so on. As a result, the microscopic picture of quasielastic meson knockout will become qualitatively richer. In order to assess the contribution of excited meson states, it would be helpful to use experience gained in applying Regge pole theory [5] to the analysis of pion and kaon electroproduction, where the contribution of the aforementioned states is treated at a phenomenological level. Such a synthesis may also be of importance for microscopically validating this theory, especially as it provides, by and large, a reliable description of channels like $N(e, e'\pi)N$ or $N(e, e'K)\Lambda$.

ACKNOWLEDGMENTS

This work was supported by the Russian Foundation for Basic Research (project no. 00-02-16117).

REFERENCES

1. M. A. Richovsky and T.-S. H. Lee, Phys. Rev. D **56**, 1644 (1997); S. R. Cotanch and R. A. Williams,

Nucl. Phys. A **631**, 487c (1998); Y. Oh, A. I. Titov, Sh. N. Yang, and T. Morii, Phys. Lett. B **462**, 23 (1999).
2. J.-M. Laget, Nucl. Phys. A **681**, 11c (2001).
3. H. Haberzettl, C. Bennhold, T. Mart, *et al.*, Nucl. Phys. A **695**, 237 (2001).
4. V. G. Neudatchin, N. P. Yudin, and L. L. Sviridova, Yad. Fiz. **60**, 2020 (1997) [Phys. At. Nucl. **60**, 1848 (1997)]; N. P. Yudin, L. L. Sviridova, and V. G. Neudatchin, Yad. Fiz. **61**, 1689 (1998) [Phys. At. Nucl. **61**, 1577 (1998)]; Yad. Fiz. **62**, 694 (1999) [Phys. At. Nucl. **62**, 645 (1999)]; V. G. Neudatchin, L. L. Sviridova, and N. P. Yudin, Yad. Fiz. **64**, 1680 (2001) [Phys. At. Nucl. **64**, 1600 (2001)].
5. M. Guidal, J.-M. Laget, and M. Vanderhaeghen, Nucl. Phys. A **627**, 645 (1997).
6. I. T. Obukhovsky, V. G. Neudatchin, L. L. Sviridova, and N. P. Yudin, Yad. Fiz. **66**, 338 (2003) [Phys. At. Nucl. **66**, 313 (2003)].
7. A. Le Yaouanc, Ll. Oliver, O. Péne, and J.-C. Raynal, *Hadron Transitions in the Quark Model* (Gordon and Breach, New York, 1988).
8. P. Brauel, T. Canzler, D. Cords, *et al.*, Z. Phys. C **3**, 101 (1979); C. J. Bebek, C. N. Brown, S. D. Holmes, *et al.*, Phys. Rev. D **17**, 1693 (1978).
9. I. T. Obukhovsky, A. Faessler, G. Wagner, and A. J. Buchmann, Phys. Rev. C **60**, 035207 (1999).
10. J. C. David, G. Fayard, G. H. Lamot, and B. Saghai, Phys. Rev. C **53**, 2613 (1996).
11. R. A. Adelseck and B. Saghai, Phys. Rev. C **42**, 108 (1990); R. A. Adelseck *et al.*, Phys. Rev. C **45**, 2030 (1992).
12. R. A. Williams *et al.*, Phys. Rev. C **46**, 1617 (1992).
13. J. de Swart, Rev. Mod. Phys. **35**, 916 (1963).
14. G. Niculescu *et al.*, Phys. Rev. Lett. **81**, 1805 (1998).

Translated by M. Kobrinsky

Physics of Atomic Nuclei, Vol. 66, No. 12, 2003, pp. 2189–2198. Translated from Yadernaya Fizika, Vol. 66, No. 12, 2003, pp. 2239–2249.

ELEMENTARY PARTICLES AND FIELDS
Theory

Measurement of Total Cross Sections for *pp* Interactions at Colliders by New Methods

A. A. Bogdanov, A. N. Vasiliev[1)], S. B. Nurushev[1)], A. Penzo[2)], M. F. Runzo, O. V. Selugin[3)], and M. N. Strikhanov*

Moscow Engineering Physics Institute (State University), Kashirskoe sh. 31, Moscow, 115409 Russia

Received June 19, 2002; in final form, December 26, 2002

Abstract—It is proposed to extract the total cross section for proton–proton (pp) interaction from the results obtained by measuring the analyzing power for elastic pp scattering in the region of Coulomb–nuclear interference. Contributions to the cross section are estimated that affect the accuracy in determining $\sigma_T(pp)$ and which originate from various sources, including single-spin-flip interactions. The applicability of the factor of merit to extracting $\sigma_T(pp)$ from experimental data is briefly discussed. It is concluded that, under some conditions, measurement of the analyzing power $A_N(t)$ may be a good approach to determining $\sigma_T(pp)$. © *2003 MAIK "Nauka/Interperiodica".*

INTRODUCTION

In this article, we discuss new methods for determining total cross sections for proton–proton (pp) interactions, $\sigma_T(pp)$, in experiments with polarized beams at colliders. The approach proposed in [1] is based on a relationship between $\sigma_T(pp)$ and the factor of merit, $M(t) = A_N^2(t)d\sigma/dt$ (where t is the invariant momentum transfer), which was introduced in polarimetry [2]. The approach proposed here is different from that and is based on the analyzing power $A_N(t)$, which is related to the total cross section. The methods developed here may prove to be appealing for the $pp2pp$ (R7) experiment, which will be performed at RHIC [3] and which is aimed at measuring three observables: $\sigma_T(pp)$, $d\sigma(t)/dt$, and $A_N(t)$; it is possible to apply the methods in question in this experiment.

In the present article, we give a detailed validation of new methods for measuring total cross sections. The ensuing exposition is organized as follows. Standard methods for measuring $\sigma_T(pp)$ in experiments with unpolarized beams at colliders are briefly described in Section 1 in order to illustrate the accuracies achieved in measuring $\sigma_T(pp)$ and $\sigma_T(p\bar{p})$. In Section 2, we present a new procedure that can be used to determine the total cross section both in unpolarized and in polarized beams at colliders. In Section 3, we give an example of using new approaches to extract the total cross section from data obtained in the E704 experiment at the Fermi National Accelerator Laboratory (FNAL). In Section 4, we discuss simulated data of the $pp2pp$ experiment and the expected corrections to $\sigma_T(pp)$ that originate from various sources. In Section 5, we estimate the contribution to $\sigma_T(pp)$ from the single-spin-flip amplitude. In the Conclusion, we summarize the results of the present investigation.

1. SURVEY OF STANDARD METHODS FOR MEASURING TOTAL CROSS SECTIONS AT COLLIDERS

Measurements of total cross sections at colliders (ISR, $Sp\bar{p}S$, Tevatron) were performed by four methods [4–12]. Given immediately below is a brief description of these methods.

1.1. Direct Method

This method is based on measuring the normalized yields $\dot{N}_T$ of secondary particles,

$$\dot{N}_T = \dot{N}^{\mathrm{el}} + \dot{N}^{\mathrm{inel}}, \qquad (1)$$

where $\dot{N}^{\mathrm{el}}$ and $\dot{N}^{\mathrm{inel}}$ are the normalized yields measured for, respectively, elastic and inelastic interactions by a detector of elastic interactions and a detector of inelastic interactions. The equipment including these detectors must cover the entire solid

[1)]Institute for High Energy Physics, Protvino, Moscow oblast, 142284 Russia.
[2)]Università di Trieste ed Istituto Nazionale di Fisica Nucleare, Sezione di Trieste, Strada Costiera 11, Miramare–Grignano, I-34014 Trieste, Italy.
[3)]Joint Institute for Nuclear Research, Dubna, Moscow oblast, 141980 Russia.
*e-mail: ~ASP9702@nm.ru

Table 1. Compilation of experimental data from measurements of σ_T in experiments with unpolarized beams at colliders

Experiment	$\sqrt{s}$, GeV	σ_T, mb				References
		direct method	indirect method	method independent of luminosity	normalization to Coulomb scattering	
		I	II	III	IV	
Tevatron, $\bar{p}p$						
E710	1800			71.71 ± 2.02		[4]
	1800	78.3 ± 5.9				[5]
CGF	546			61.26 ± 0.93		[6]
	1800			80.03 ± 2.24		[6]
	1800		72.0 ± 3.6			[7]
$Sp\bar{p}S$						
UA1	540		67.9 ± 5.9			[8]
UA4	541		63.0 ± 1.5			[9]
UA4/UA2	541		63.0 ± 2.1			[10]
UA4	546			61.9 ± 1.5		[11]
ISR						
pp	23.5	38.8 ± 0.25	39.01 ± 0.27	39.22 ± 0.55		[12]
	30.6	40.07 ± 0.24	40.38 ± 0.31	40.53 ± 0.62		[12]
	44.7	41.90 ± 0.24	41.45 ± 0.23	41.00 ± 0.43		[12]
	52.8	42.71 ± 0.35	42.38 ± 0.27	42.02 ± 0.47		[12]
	62.7	42.96 ± 0.38	43.07 ± 0.30	43.20 ± 0.54		[12]
	23.0				38.9 ± 0.7	[14]
	31.0				40.2 ± 0.8	[14]

angle of 4π. In actual practice, however, a vacuum tube and beam and detector parameters constrain the minimum accessible angle of the escape of secondary particles, $\theta_{\min}$. In view of this, measurements are performed down to this angle, whereupon the yields are extrapolated to zero angle in order to introduce corrections in σ_{obs} (by this symbol, we denote the observed cross section) for undetected events. In constructing this extrapolation, one has to use a phenomenological model for hadron amplitudes, and this is a disadvantage of the method being discussed.

Under the assumption that the integrated luminosity L of the collider used is known from an independent measurement, the total cross section can be determined as the ratio

$$\sigma_T = N_T/L_T, \tag{2}$$

where N_T and L_T are summed over the entire experimental time. The examples of direct measurements of σ_T in Table 1 (column I) were borrowed from [4, 12]. It can be seen that the highest precision in measurements of σ_T was achieved at ISR (0.5–1%) by applying a special technique for improving the quality of the beam used. The precision in measurements of σ_T at the Tevatron ($\pm 7.5\%$) was bounded by the errors in measurements of the luminosity.

1.2. Indirect Method

This method is based on the theorem according to which the differential cross section for elastic pp scattering in the forward direction, $(d\sigma^{\text{el}}/dt)_{t=0}$, is related to the total cross section σ_T by the equation

$$\left(\frac{d\sigma^{\text{el}}}{dt}\right)_{t=0} = \frac{\sigma_T^2(1+\rho^2)}{16\pi(\hbar c)^2}, \tag{3}$$

where ρ is the ratio of the real and imaginary parts of the nuclear non-spin-flip amplitude. It is assumed that the spin contribution to σ_T is negligible. In the region of nuclear diffractive scattering (at moderate invariant-momentum transfers t), the differential cross section $(d\sigma^{\rm el}/dt)$ is usually represented in the form

$$\frac{d\sigma^{\rm el}}{dt} = \left(\frac{d\sigma^{\rm el}}{dt}\right)_{t=0} e^{bt}, \qquad (4)$$

where b is the slope parameter. Therefore, $(d\sigma^{\rm el}/dt)_{t=0}$ must be determined through an extrapolation of $dN^{\rm el}(t)/dt$ for measured elastic events to the point $t = 0$; that is,

$$\frac{dN^{\rm el}(t)}{dt} = L\frac{d\sigma^{\rm el}}{dt} = L\left(\frac{d\sigma^{\rm el}}{dt}\right)_{t=0} e^{bt} = \frac{dN^{\rm el}(0)}{dt}e^{bt}, \qquad (5)$$

where

$$\frac{dN^{\rm el}(0)}{dt} = L\left(\frac{d\sigma^{\rm el}}{dt}\right)_{t=0}. \qquad (6)$$

From relations (3) and (6), we obtain

$$\sigma_T = \frac{1}{\sqrt{L}}\left[\frac{16\pi(\hbar c)^2}{(1+\rho^2)}\frac{dN^{\rm el}(0)}{dt}\right]^{1/2}. \qquad (7)$$

It follows that, knowing L and ρ from independent measurements, one can determine σ_T. The error of this method is due to the error in measuring the luminosity and is one-half as large as the error of the above direct method. This is the simplest method for determining σ_T. Examples in which this approach was employed are given in Table 1 (column II). Measurements at the Tevatron and $Sp\bar{p}S$ were performed with large errors because of an uncertainty of about $\pm 2\%$ in determining the luminosity. The most precise result was obtained in the UA4 experiment by thoroughly measuring beam parameters. The highest accuracy in determining σ_T was achieved at ISR.

1.3. Luminosity-Independent Method

In order to avoid measuring beam luminosities, the following technique was applied in [4, 6, 11, 12]. From relations (2) and (7), one can derive an expression for the total cross section in the form

$$\sigma_T = \frac{16\pi(\hbar c)^2}{(1+\rho^2)N_T}\frac{dN^{\rm el}(0)}{dt}, \qquad (8)$$

which does not involve the luminosity explicitly. In this method, it is necessary to employ detectors of two types, that for elastic and that for inelastic interactions. It is also assumed there that ρ is known. The results obtained by using this method are given in Table 1 (column III). It can be seen that the highest precision in measuring σ_T was achieved at ISR. The existing discrepancy of about 10% between the results of the measurements of σ_T in the E710 and CDF experiments at $\sqrt{s} = 1800$ GeV may be due to some hidden systematic error.

In all of the above three methods for measuring σ_T, it is necessary to extrapolate observables to zero angle. Data on inelastic scattering can be extrapolated by using a Gaussian function or an exponential dependence. In extrapolating elastic-scattering data, the following assumptions were made:

(i) The spin contribution is negligible.

(ii) At low t, the imaginary part of the nuclear amplitude is an exponential function of the invariant-momentum transfer.

(iii) The real and the imaginary part of the nuclear amplitude depend identically on t, whence it follows that ρ is independent of the momentum transfer.

The last two assumptions were questioned in [13].

1.4. Coulomb Scattering

This method, which is based on a theoretically reliable calculation of the differential cross section, makes it possible to avoid measuring luminosities. We have

$$\frac{d\sigma_{\rm C}(t)}{dt} = \frac{4\pi\alpha^2(\hbar c)^2}{t^2}F^4(t), \qquad (9)$$

where α is the fine-structure constant and $F(t)$ is the electromagnetic form factor for the proton. In order to apply this method, it is necessary to reach the Coulomb scattering region, which corresponds to the condition $|t| \simeq |t_0|$, where $|t_0| = 1.6 \times 10^{-3}\,({\rm GeV}/c)^2$ (at $\sigma_T = 40$ mb) is a special point where the Coulomb cross section is equal to the nuclear cross section. In response to variations in the initial momentum $p_{\rm in}$, the Coulomb scattering angle (in mrad) changes according to the law

$$\theta_0 = \frac{\sqrt{|t_0|}}{p_{\rm in}} = \frac{40\times 10^{-3}}{p_{\rm in}}. \qquad (10)$$

For ISR, the initial momentum is $p_{\rm in} = 15$ GeV/c and $\theta_0 \approx (40/15)\times 10^{-3} \approx 3$ mrad, which corresponds to a 3-cm deflection of the scattered proton from the beam axis at the end of the straight 10-m section of ISR. This method was applied in the experiment of Amaldi *et al.* [14] at two energies, $\sqrt{s} = 23$ and 31 GeV, at a distance of 10 m (at angles θ_0 smaller than 2 mrad, measurements by this method are impossible). Accordingly, measurements with the aid of this method could not be performed at ISR for a momentum of each beam below 15.4 GeV/c [14]. The results of the experiment in question are given in Table 1

(column IV). The precision attained in measuring σ_T was 2%. But in accordance with relation (10), this method cannot be applied at high energies without substantial modifications.

2. NEW APPROACHES TO MEASURING $\sigma_T(pp)$

In principle, any experiment where the total cross section is related in some way or another to measurable quantities can be used to determine σ_T. Below, we propose some new approaches to determining σ_T.

2.1. Collisions of Unpolarized Protons

Let us assume that two differential cross sections for elastic pp scattering can be measured independently to a high precision. The first is the Coulomb cross section

$$\frac{d\sigma_{\rm C}}{dt} = \pi |f_{\rm C}|^2, \tag{11}$$

where

$$f_{\rm C} = \pm \frac{2\alpha F^2(t)}{t}(\hbar c)\exp(\mp i\alpha\varphi). \tag{12}$$

Here, the upper (lower) sign corresponds to $\bar{p}p$ (pp) interaction; $F(t) = (1 + |t|/\Lambda^2)^{-2}$ is the dipole form factor for the proton with $\Lambda^2 = 0.71$ GeV^2; and φ is the Coulomb phase shift, which is given by

$$\varphi = \ln\frac{2}{|t|(b + 8/\Lambda^2)} - 0.5772. \tag{13}$$

The second is the cross section for elastic nuclear scattering,

$$\frac{d\sigma_n}{dt} = \pi |f_n|^2, \tag{14}$$

where

$$f_n = \frac{\sigma_T}{4\pi}(\rho + i)e^{-b|t|/2}. \tag{15}$$

Here, ρ is the ratio of the real and the imaginary part of the nuclear amplitude at $|t| = 0$ and b is the slope parameter.

We can extrapolate both cross sections, that in (4) and that in (9), to the point t_0, where they are equal to each other:

$$\frac{d\sigma_{\rm C}(t_0)}{dt} = \frac{d\sigma_n(t_0)}{dt}. \tag{16}$$

By using the above relations, we obtain

$$\frac{|t_0|e^{-b|t_0|/2}}{F^2(t_0)} = \frac{8\pi\alpha}{\sigma_T}. \tag{17}$$

At low $|t|$, we therefore have

$$\sigma_T \approx \frac{8\pi\alpha}{|t_0|}. \tag{18}$$

We are unaware of cases where relation (18) was used in experiments studying high-energy physics. In all probability, this is explained by difficulties encountered in measuring the Coulomb cross section at low $|t_0|$. It is assumed that lower values of t [about 2×10^{-4} (GeV/c)^2] can be reached in the $pp2pp$ experiment. In this case, it is possible to measure $d\sigma_{\rm C}/dt$ off the region of Coulomb–nuclear interference (for $|t| < |t_0|$). If so, this method can be applied at RHIC.

In the following, we will consider additional special features of the differential cross section for pp scattering that are possibly of use for obtaining the total cross section. It is well known that, in the region of Coulomb–nuclear interaction, the differential cross section for elastic pp scattering can be represented in the form

$$\frac{d\sigma^{\rm el}(t)}{dt} = \frac{d\sigma_{\rm C}}{dt} + {\rm Int} + \frac{d\sigma_n}{dt}, \tag{19}$$

where the first and the third term are given by (9) and (14), respectively, and Int stands for the interference cross section, which can be expressed as

$$\begin{aligned}{\rm Int} &= \mp 2{\rm Re}(f_{\rm C}^* f_n)\\ &= \mp\frac{\alpha F^2(t)\sigma_T}{t}e^{bt/2}\left[\rho\cos(\alpha\varphi) \pm \sin(\alpha\varphi)\right].\end{aligned}$$

The upper (lower) sign corresponds to pp ($\bar{p}p$) scattering.

From relation (19), one can determine three special points. The first of these, the point t_{in}, is that where the nuclear cross section is equal to the interference cross section:

$${\rm Int} = d\sigma_n/dt.$$

For the case of pp scattering, we therefore obtain

$$t_{in} = -\frac{16\pi\alpha(\hbar c)^2}{(1+\rho)^2\sigma_T}e^{bt_{in}/2}\left[\rho\cos(\alpha\varphi) + \sin(\alpha\varphi)\right].$$

Assuming that $bt \ll 1$ and taking into account the smallness of $\alpha\varphi$, we can obtain

$$t_{in} = -\frac{16\pi\alpha\rho}{(1+\rho)^2\sigma_T}(\hbar c)^2 = \frac{2\rho}{1+\rho^2}t_0.$$

At $\sqrt{s} = 541$ GeV ($\sigma_T = 63$ mb, $\rho = 0.135$), we arrive at $-t_{in} = 3.1 \times 10^{-4}$ (GeV/c)^2, while, at $\sqrt{s} =$ 19.4 GeV ($\sigma_T = 38$ mb, $\rho = -0.034$), the result is $-t_{in} = 1.3 \times 10^{-4}$ (GeV/c)^2. Thus, a very interesting situation arises in the case of elastic pp scattering. First, the method being considered is more easily realizable at high than at low energies because of the value of ρ. Second, the interference term is negative

at $t = t_{in}$ and therefore fully compensates the term that is responsible for nuclear scattering. As a result, only Coulomb scattering occurs at this point, and one can use this scattering to perform a normalization of the particle yield—that is, the absolute luminosity. There arises only one problem—in the $pp2pp$ experiment, it is planned to reach the value of $t_{\min} = 7 \times 10^{-4}$ $(\mathrm{GeV}/c)^2$, which is greater than the required value of t_{in}.

There is yet another special point ($t_{i\mathrm{C}}$), that at which the interference cross section is equal to the Coulomb cross section—that is, $\mathrm{Int} = d\sigma_{\mathrm{C}}/dt$; it is given by

$$t_{i\mathrm{C}} = \frac{4\pi\alpha F^2(t)(\hbar c)^2}{\sigma_T \rho} e^{bt_{i\mathrm{C}}/2}.$$

At low values of t, this expression reduces to the form

$$t_{i\mathrm{C}} = -\frac{4\pi\alpha(\hbar c)^2}{\sigma_T \rho} = \frac{1}{2\rho} t_0. \qquad (20)$$

At $\sqrt{s} = 541$ GeV, we obtain $-t_{i\mathrm{C}} = 4.2 \times 10^{-3}$ $(\mathrm{GeV}/c)^2$. This value can be accessible in the $pp2pp$ experiment. At the point $t_{i\mathrm{C}}$, there occurs only purely nuclear scattering, and this makes it possible to verify some hypotheses, such as the variation of the slope parameter with $|t|$ or oscillations of the differential cross section [13]. Upon the improvement of beam parameters and of the resolution power of the equipment used, we can hope that all of the above three approaches to determining the total cross sections for pp scattering will be used.

Let us introduce the function f_2 as

$$f_2(t) = t^2 \frac{d\sigma}{dt}. \qquad (21)$$

It has a maximum at the special point t_2 defined as

$$t_2 = \frac{8\pi\alpha\rho}{\sigma_T(1+\rho)^2} = \frac{\rho}{1+\rho} t_0, \qquad (22)$$

where t_0 is given by (18). The point t_2 is useful in that, at this point, one can perform an absolute normalization of the differential cross section to the Coulomb cross section. At the highest RHIC energy value, we have $-t_2 = 1.5 \times 10^{-4}\,(\mathrm{GeV/c})^2$. This is the smallest value among four special points. It is very difficult to reach t_2 in experiments since it is less than t_0 by an order of magnitude. The results of this section are summarized in Table 2.

In practice, t_{in} and $t_{i\mathrm{C}}$ can be found by applying the following procedure. The differential cross section $d\sigma^{\mathrm{meas}}/dt$ is measured by using available equipment under fixed experimental conditions. After that, the Coulomb differential cross section $d\sigma_{\mathrm{C}}/dt$ is calculated by means of Monte Carlo methods. The difference of these two quantities vanishes at the point t_{in}. The point $t_{i\mathrm{C}}$ can be found in a similar way.

Table 2. Special points of t in the cross section for elastic pp scattering [general formulas and numerical values in $(\mathrm{GeV}/c)^2$]

Point	Expression in terms of σ_T and ρ	Value at $\sqrt{s} \simeq 500$ GeV
$-t_0$	$\dfrac{8\pi\alpha(\hbar c)^2}{\sigma_T}$	1.1×10^{-3}
$-t_{in}$	$\dfrac{16\pi\alpha\rho(\hbar c)^2}{\sigma_T(1+\rho)^2}$	3.1×10^{-4}
$-t_{i\mathrm{C}}$	$\dfrac{4\pi\alpha(\hbar c)^2}{\sigma_T\rho}$	4.2×10^{-3}
$-t_2$	$\dfrac{8\pi\alpha\rho(\hbar c)^2}{\sigma_T(1+\rho)^2}$	1.5×10^{-4}

2.2. Collision of Polarized Protons

In the following, we discuss the possibility of extracting $\sigma_T(pp)$ from the results obtained by measuring the analyzing power $A_N(t)$ (our proposal) and the factor of merit $M(t)$ (proposal of Gauron *et al.* [1]). First of all, it is necessary to obtain analytic expressions for these quantities (this will be done in this section and those that follow). Further, we need experimental data on $M(t)$ [data on $A_N(t)$ either are available or will be obtained in the near future].

The simplest expression for $A_N(t)$ in the region of Coulomb–nuclear interference was first given in [15]. A more detailed expression that includes the parameter ρ and one- and two-spin interactions was recently presented in [16]. We employ the expression from [16], but we disregard all spin dependences, as is usually done in conventional procedures for measuring σ_T. In this approach, the expression for $A_N(t)$ has the form

$$A_N(t) = C_0 \times \frac{\sigma_T(1-\rho\alpha\varphi)(-t)^{3/2}}{1 + C_1(\rho+\alpha\varphi)\sigma_T|t| + C_2(1+\rho^2)\sigma_T^2|t|^2}, \qquad (23)$$

where

$$C_0 = (\mu_p - 1)/[8\pi\alpha m_p(\hbar c)^2] = 26.7735\ \mathrm{GeV}^{-3}\,\mathrm{mb}^{-1},$$
$$C_1 = -[4\pi\alpha(\hbar c)^2]^{-1} = -27.9972\ \mathrm{GeV}^{-2}\,\mathrm{mb}^{-1},$$
$$C_2 = [8\pi\alpha(\hbar c)^{-2}]^2 = 195.9609\ \mathrm{GeV}^{-4}\,\mathrm{mb}^{-2}$$

(μ_p and m_p are the proton magnetic moment and mass, respectively). Assuming that the parameter ρ is known from $d\sigma^{\mathrm{el}}/dt$, we can determine the total cross section σ_T as a parameter in a fit to experimental data.

The analyzing power has a maximum at the point $-t_A$ given by [16]

$$-t_A = -t_0 \qquad (24)$$

$$\times \left[\sqrt{3} - (\rho + \alpha\varphi) + \frac{8}{(\mu_p - 1)}(\rho I_5 - R_5)\right].$$

As is well-known, nucleon–nucleon scattering is determined by five complex-valued amplitudes, which are functions of the Mandelstam variables s and t. In the helicity representation, these are the amplitudes Φ_1 and Φ_3 corresponding to the scattering process not involving nucleon-spin flip, the amplitude Φ_5 corresponding to single-spin-flip scattering, and the amplitudes Φ_2 and Φ_4 corresponding to double-spin-flip scattering. Usually, an analysis is performed without including the amplitudes Φ_2 and Φ_4 because of their smallness. The non-spin-flip amplitudes are assumed to be equal to each other. The last term in the bracketed expression on the right-hand side of (24) corresponds to the single-spin contribution to the total cross section. Below, this term will be taken into account in calculating the single-spin contributions to $A_N(t)$ and σ_T. Using the results quoted in [16], we have also obtained an expression for the factor of merit; that is,

$$M(t) = \bar{C}_0 \frac{\sigma^2(1 - \rho\alpha\varphi)^2 e^{bt}|t|}{1 + C_1\sigma_T(\rho + \alpha\varphi)|t| + C_2\sigma_T^2(1 + \rho^2)t^2}, \quad (25)$$

where

$$\bar{C}_0 = (\mu_p - 1)^2/[16\pi m_p^2(\hbar c)^2] = 0.1867\ \text{GeV}^{-4}\ \text{mb}^{-1}.$$

The remaining parameters were defined previously. For $|t| \ll 1$, we have $\alpha\varphi \approx \alpha\varphi\rho \approx 0$. The factor of merit $M(t)$ has a maximum at the point t_M given by

$$-t_M = \frac{8\pi\alpha(\hbar c)^2}{\sigma_T\sqrt{1 + \rho^2}}. \quad (26)$$

Instead of the fitting procedure, one can therefore employ expression (26) to obtain σ_T. We can see that, over the energy range in which we are interested, t_M is not sensitive to changes in ρ.

3. DERIVATION OF $\sigma_T(pp)$ FROM DATA OF THE E704 EXPERIMENT

The E704 experiment involved the first measurement of the analyzing power $A_N(t)$ in the reaction

$$p\uparrow + p \to p + p, \quad (27)$$

at a primary polarized-proton-beam momentum of $p_{\text{in}} = 200$ GeV/c in the range $2 \times 10^{-3} \le |t| \le 4 \times 75 \times 10^{-2}$ (GeV/c)^2 [17]. The relevant experimental data are given in Table 3.

It is necessary to determine ρ at $\sqrt{s} = 19.4$ GeV. This parameter was measured at FNAL for $p_{\text{lab}} = 199$ GeV/c [18]. The result was $\rho = -0.034 \pm 0.014$. Upon substituting this value into (23) and constructing a fit to six experimental values of $A_N(t)$, it was found that

$$\sigma_T(pp) = 37.8 \pm 8.1\ \text{mb} \quad (28)$$

at $\chi^2 = 1.49$ per fives degrees of freedom (see Fig. 1*a*).

This result must be compared with the experimental value of $\sigma_T(pp) = 38.9 \pm 0.7$ mb, which was measured for $\sqrt{s} = 23.0$ GeV at ISR [14]. As can be seen from a comparison of the two values, there are limitations on the possibility of applying the new method. First, the statistics of E704 are insufficient for reaching the accuracy of the standard method—an increase in statistics by two orders of magnitude is required for the new method to be on par with the traditional one in accuracy. The second limitation is associated with the accuracy in measuring the beam polarization P_B. In the E704 experiment, it was found that $\Delta P_B/P_B = \pm 6.8\%$ [19], and this is an additional source of uncertainty in $\sigma_T(pp)$. The detector resolution Δt is a third source of uncertainties in determining $\sigma_T(pp)$. The E704 experimental facility had the following resolutions: $\Delta t/|t_{\min}| = 0.1$ (geometric resolution), $(\Delta t/|t_{\min}|)_{\text{ms}} \cong 0.07$ (resolution associated with multiple scattering), and $(\Delta t/|t_{\min}|) = 0.03$ (resolution associated with errors in momentum measurements). All these sources introduce an additional systematic error of about 14% in $\Delta\sigma_T(pp)$ in (28) and result in that the data from the E704 experiment cannot compete with the standard techniques.

In experiments of the E704 type, a considerable improvement of experimental accuracies in determining $\sigma_T(pp)$ may be achieved at RHIC by using a polarized jet target [20]. First, the target polarization P_T can be measured there to a precision higher than that in measuring beam polarization ($\Delta P_T/P_T \simeq 2\%$) [21]. Second, the statistics of A_N can be enlarged by two orders of magnitude owing to a high luminosity. Third, an accuracy of $\Delta t/|t_{\max}| < 5\%$ may be achieved at a recoil kinetic energy of $T_{\text{rec}} \cong 1$ MeV [which corresponds to $|t| \cong 2 \times 10^{-3}$ (GeV/c)^2] owing to the fact that a silicon detector of recoil nuclei has a high energy resolution of $\Delta T \approx 50$ keV in kinetic energy [22]. Thus, the difficulties listed above can be overcome at RHIC. Therefore, measurement of $A_N(t)$ in the region of Coulomb–nuclear interference in the fixed-target mode is quite appealing for testing the new method.

Let us consider the factor of merit $M(t)$. In contrast to $A_N(t)$, this quantity cannot be measured by a

Table 3. $A_N(t)$, $d\sigma^{\rm el}/dt$, and $M(t)$ at $\sqrt{s} = 19.4$ GeV

$-t$, $(\mathrm{GeV}/c)^2$	$A_N(t) \pm \Delta A_N(t)$	$d\sigma^{\rm el}/dt$, mb/$(\mathrm{GeV}/c)^2$	$M(t) \pm \Delta M(t)$, mb/$(\mathrm{GeV}/c)^2$
0.00288	0.0446 ± 0.0316	106.4 ± 2.3	0.212 ± 0.295
0.0083	0.0311 ± 0.0109	77.1 ± 1.7	0.0745 ± 0.0522
0.0175	0.0262 ± 0.0101	64.5 ± 1.2	0.0443 ± 0.0342
0.0273	0.0317 ± 0.0107	55.6 ± 1.1	0.0559 ± 0.0377
0.0368	0.0217 ± 0.0139	52.0 ± 1.0	0.0245 ± 0.0314
0.0475	0.0027 ± 0.0277	49.9 ± 0.8	0.0003 ± 0.0064

direct method. Therefore, it is necessary to determine the factor of merit as

$$M(t) = A_N^2(t)\frac{d\sigma^{\rm el}}{dt} \tag{29}$$

and to calculate the relevant uncertainty $\Delta M(t)$. We employ the experimental data on $d\sigma^{\rm el}/dt$ that were obtained at FNAL [18] (Table 3, third column). Comparing the relative errors in $A_N(t)$ and $d\sigma^{\rm el}dt$, we arrive at

$$\frac{\Delta M(t)}{M(t)} \approx 2\frac{\Delta A_N(t)}{A_N(t)}. \tag{30}$$

Taking $b = 12$ GeV^{-2} and setting ρ to the value identical to that which was used above, we construct a fit to the data (see Fig. 1*b*). The result is

$$\sigma_T = 22 \pm 40 \ \text{mb} \tag{31}$$

at $\chi^2 = 3.8$ per five degrees of freedom. At this accuracy, one can draw no conclusions concerning the value of σ_T. Therefore, the data on the analyzing power from the E704 experiment can only be used as a qualitative illustration of the applicability of the new method for extracting the total cross section. However, the accuracy in measuring $\sigma_T(pp)$ can be improved considerably by performing a similar experiment at RHIC with a jet target.

4. DERIVATION OF $\sigma_T(pp)$ FROM "SIMULATED DATA" OF THE $pp2pp$ EXPERIMENT AT RHIC

Measurement of the analyzing power $A_N(t)$ for elastic proton–proton scattering in the region of Coulomb–nuclear interference is one of the main objectives of the $pp2pp$ experiment at RHIC, special equipment being intended for this in the experiment. In simulating the experiment, the collision energy, the degree of beam polarization, and the luminosity were set to $\sqrt{s} = 500$ GeV, 70%, and 2×10^{29} cm^{-2} s^{-1}, respectively. In order to optimize left–right asymmetry with a vertically polarized beam, allowances were made for events lying in the azimuthal-angle region $\cos|\phi| < 1/\sqrt{2}$ (acceptance of the facility [3]). Under such conditions, 2.5×10^6 events were accumulated over 3.7 h. In order to simulate the left–right analyzing power, we used expression (23) at $\rho = 0$. The asymmetry $A_N(t)$ obtained as the difference of the number of events in the left and the right part of the detector is shown in Fig. 2*a*. The data in Table 4 were borrowed from [3].

We used the results of our simulation as experimental data and constructed a fit to them (solid curve in Fig. 2*a*). For the total cross section, this yielded

$$\sigma_T(pp) = 58.64 \pm 1.97 \ \text{mb}. \tag{32}$$

This value must be compared with experimental results obtained at *SppS* for $\sqrt{s} = 541$ GeV, $\sigma_T(\bar{p}p) = 63.0 \pm 1.5$ mb (UA4) [9], and at the Tevatron for $\sqrt{s} = 546$ GeV, $\sigma_T(\bar{p}p) = 61.26 \pm 0.93$ mb (CDF) [6]. Good agreement of the above results shows that the new method works rather well, becoming competitive with the standard method.

In order to extract $\sigma_T(pp)$ from the simulated data on proton–proton scattering, one can also use the factor of merit. For this, it is necessary to prepare experimental data on $M(t)$. The differential cross section for elastic proton–proton scattering at $\sqrt{s} = 541$ GeV can be obtained from the results of the UA4/UA2 experiment [10] under the assumption that the nuclear part of the cross section is equal to its Coulomb part, in which case the interference terms are equal in magnitude, but they have opposite signs. The results obtained in this way for $d\sigma^{\rm el}/dt$ are quoted in Table 4, along with the "experimental" data on $M(t)$. Using formula (25), we obtain

$$\sigma_T(pp) = 42.1 \pm 4.9 \ \text{mb}$$

at $\chi^2 = 1.42$ per degree of freedom (see Fig. 2*b*). This value is much less than the expected value of $\sigma_T(pp)$, and the error is twice as great as that in employing the method based on $A_N(t)$; nevertheless, the method of the factor of merit also makes it possible to determine

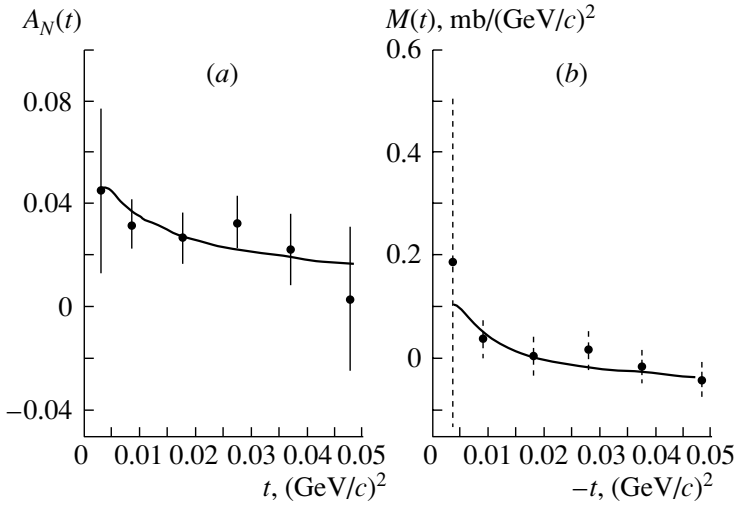

Fig. 1. (*a*) Analyzing power $A_N(t)$ according to measurements of the E704 Collaboration at $\sqrt{s} = 19.4$ GeV (points), along with a fit to these data (solid curve); (*b*) factor of merit $M(t)$ at the same energy (points), along with a similar fit (solid curve).

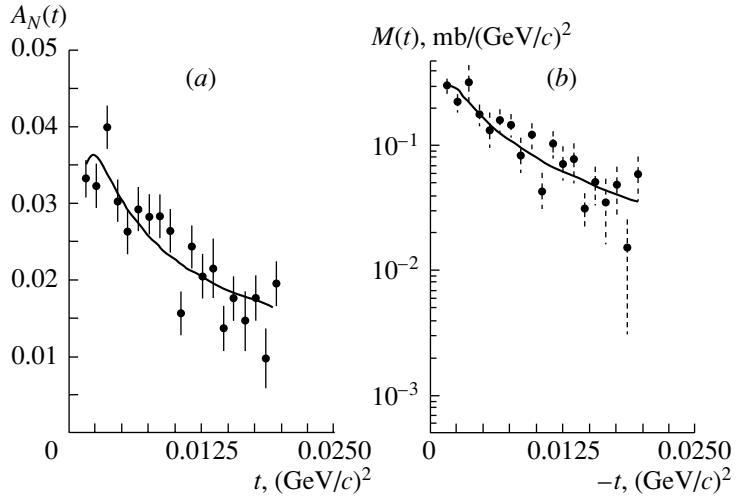

Fig. 2. (*a*) Simulated data on $A_N(t)$ for the *pp*2*pp* experiment at RHIC for $\sqrt{s} = 500$ GeV (points), along with a fit to these data (solid curve); (*b*) factor of merit $M(t)$ at the same energy (points), along with a similar fit (solid curve).

$\sigma_T(pp)$. It is only necessary to obtain more precise experimental data and to refine the formula for $M(t)$ by including terms disregarded above.

Systematic errors generate the main difficulties that must be overcome in applying the new approaches. The first of these errors is associated with the beam polarization P_B, which must be measured to a precision higher than $\Delta\sigma_T/\sigma_T$. This is because the quantities P_B and A_N are related by the equation

$$A_N = \frac{1}{P_B}\varepsilon, \tag{33}$$

where ε is the measured ("raw") asymmetry. Presently, the main task at RHIC is to attain a precision of $\Delta P_B/P_B = \pm 5\%$, and the same will hold for $\Delta A_N/A_N$. This constrains the accuracy in measuring $\sigma_T(pp)$, since the degree of beam polarization must be measured to a precision higher than 1% in order to determine the total cross section at RHIC by the new method.

The uncertainty Δt is determined by experimental conditions: (a) the error in measuring the angle between the beams (it is equal to 6 μrad, which leads to $\Delta t/t \approx 7\%$) and (b) the error in determining the momentum of scattered particles (it is equal to $\Delta p/p \approx 1.5\%$, which leads to $\Delta t/t \approx 3\%$).

Summing the squares of the above errors and taking the square root of the above sum, we find that their contribution to $\Delta\sigma_T/\sigma_T$ is about 9%. It is obvious that the experimental value must be still smaller.

Table 4. $A_N(t)$ (simulated values), $d\sigma^{\rm el}/dt$, and $M(t)$ at $\sqrt{s} = 500$ GeV

$-t$, $(\mathrm{GeV}/c)^2$	$A_N(t) \pm \Delta A_N(t)$	$d\sigma^{\rm el}/dt$, mb/$(\mathrm{GeV}/c)^2$	$M(t) \pm \Delta M(t)$, mb/$(\mathrm{GeV}/c)^2$
0.0015	0.034 ± 0.0025	275 ± 3.8	0.3179 ± 0.0467
0.0025	0.033 ± 0.003	216 ± 3.1	0.2352 ± 0.0429
0.0035	0.041 ± 0.003	199 ± 3.0	0.3345 ± 0.0492
0.0045	0.031 ± 0.003	192 ± 3.0	0.1845 ± 0.0358
0.0055	0.027 ± 0.003	187 ± 3.0	0.1363 ± 0.0304
0.0065	0.030 ± 0.003	184 ± 3.0	0.1656 ± 0.0332
0.0075	0.029 ± 0.003	181 ± 3.0	0.1522 ± 0.0316
0.0085	0.022 ± 0.003	178 ± 3.0	0.0862 ± 0.0235
0.0095	0.027 ± 0.003	175 ± 3.0	0.1276 ± 0.0284
0.0105	0.016 ± 0.003	172 ± 1.3	0.044 ± 0.0165
0.0115	0.025 ± 0.003	170 ± 1.3	0.1063 ± 0.0255
0.0125	0.021 ± 0.003	167 ± 1.3	0.0736 ± 0.0210
0.0135	0.022 ± 0.003	165 ± 1.2	0.0799 ± 0.029
0.0145	0.014 ± 0.003	163 ± 1.2	0.0319 ± 0.0137
0.0155	0.018 ± 0.003	160 ± 1.2	0.0518 ± 0.0173
0.0165	0.015 ± 0.004	158 ± 1.3	0.0356 ± 0.019
0.0175	0.018 ± 0.004	155 ± 1.3	0.0502 ± 0.0223
0.0185	0.01 ± 0.004	153 ± 1.3	0.0153 ± 0.0122
0.0195	0.02 ± 0.004	151 ± 1.3	0.0604 ± 0.0242

5. SPIN-FLIP CONTRIBUTION TO MEASUREMENT OF $\sigma_T(pp)$

In order to assess the spin-flip contribution to the total cross section $\sigma_T(pp)$, it is necessary to use data on $A_N(t)$ and $d\sigma^{\rm el}/dt$ from experiments at FNAL and to reconstruct the measured function

$$\psi(t) = \frac{m_p\sqrt{-t}}{\sigma_T} A_N(t) \frac{d\sigma^{\rm el}}{dt}. \qquad (34)$$

Experimental data for this function are given in Table 5.

In accordance with [16], the function $\psi(t)$ was taken in the simplified form

$$\psi(t) = -\alpha\left(\frac{\mu_p - 1}{2} - I_5\right) + \frac{\sigma_T}{4\pi(\hbar c)^2}(\rho I_5 - R_5)t. \qquad (35)$$

Using the numerical values of $\sigma_T = 38$ mb, $\rho = -0.034$, $\mu_p = 2.793$, and $\alpha = 1/137$, we reduce the expression for $\psi(t)$ at $\sqrt{s} = 19.4$ GeV to

$$\psi(t) = -0.00654 + 0.0073 I_5 + 7.7(0.034 I_5 + R_5)|t|, \qquad (36)$$

where I_5 and R_5 are the ratio of, respectively, the real and the imaginary part of the reduced amplitude Φ_5 for single-spin-flip scattering to the imaginary part of the non-spin-flip amplitude.

The results of a two-parameter fit to $\psi(t)$ are given in Fig. 3, the fitted values of the parameters in (36) being $I_5 = 1.63 \pm 0.31$ and $R_5 = -0.05 \pm 0.02$.

This value of I_5 is different from that quoted in [23], but this is immaterial for our estimates. The position

Table 5. Function $\psi(t)$ at $\sqrt{s} = 19.4$ GeV

$-t$, $(\mathrm{GeV}/c)^2$	$\psi(t)$
0.00288	0.0062863 ± 0.004454
0.0083	0.0053902 ± 0.0018892
0.0175	0.0055208 ± 0.0021282
0.0273	0.0071884 ± 0.0024264
0.0368	0.0053433 ± 0.0034227
0.0475	0.007248 ± 0.061125

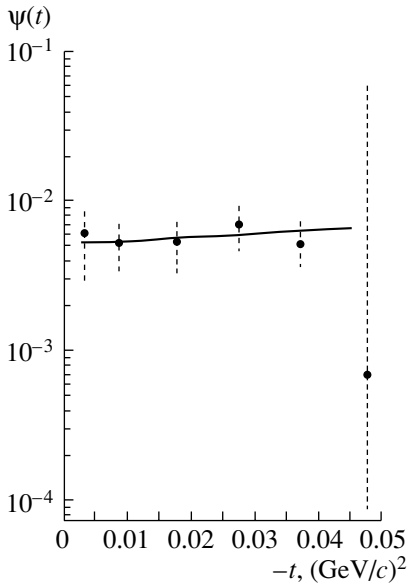

Fig. 3. Single-spin dimensionless function $\psi(t)$ versus $-t$ at $\sqrt{s} = 19.4$ GeV. The solid curve represents a two-parameter fit.

of the maximum changed by

$$\Delta t/t = \Delta_5 = \frac{8(\rho I_5 - R_5)}{(\mu_p - 1)(\sqrt{3} - (\rho + \alpha\varphi))}, \qquad (37)$$

with the result that $\sigma_T(pp)$ changes by the same value (about 4%). In order to determine $\sigma_T(pp)$, for example, to a precision of 1%, it is therefore necessary to measure I_5 and R_5 to a higher precision.

CONCLUSION

Our proposal to extract $\sigma_T(pp)$ from a measurement of the analyzing power for elastic proton–proton scattering in the region of Coulomb–nuclear interference is realistic in principle, but its implementation in practice involves serious experimental problems. Some limitations are associated with accuracy in measuring beam polarization (contribution to $\Delta\sigma_T/\sigma_T$ is about 5%) and in measuring the 4-momentum transfer t (contribution to $\Delta\sigma_T/\sigma_T$ is about 9%). In order to apply the above new methods, it is necessary to improve the accuracy in determining these parameters; otherwise, the new methods will not be able to compete with the standard procedures for measuring $\sigma_T(pp)$.

ACKNOWLEDGMENTS

We are grateful to V. Ejela, P. Gauron, V. Gurin, Yu.V. Kharlov, and B. Nicolescu for stimulating discussions on the problems considered in this article.

REFERENCES

1. P. Gauron, B. Nicolescu, and O. V. Selyugin, Phys. Lett. B **390**, 405 (1997).
2. K. Kuroda, AIP Proc. **95**, 618 (1983).
3. Experiment to Measure Total and Elastic *pp* Cross Section at RHIC, *BNL Proposal*, update version (Sept. 1995).
4. C. Avila *et al.*, Phys. Lett. B **446**, 179 (1999).
5. N. A. Amos *et al.*, Phys. Rev. Lett. **63**, 2784 (1989).
6. F. Abe *et al.*, Phys. Rev. D **50**, 5550 (1994).
7. S. White, Preprint Fermilab-Conf-91/268-E (1991).
8. G. Armson *et al.*, Preprint CERN-EP/83-7 (May 27, 1983).
9. C. Augier *et al.*, Phys. Lett. B **316**, 448 (1993).
10. C. Augier *et al.*, Phys. Lett. B **344**, 451 (1995).
11. M. Bozzo *et al.,* Phys. Lett. B **147B**, 392 (1984).
12. U. Amaldi *et al.*, Nucl. Phys. B **145**, 367 (1978).
13. P. Gauron, B. Nicolescu, and O. V. Selyugin, Phys. Lett. B **397**, 305 (1997).
14. U. Amaldi *et al.*, Phys. Lett. B **43B**, 231 (1973).
15. A. P. Vanzha, L. I. Lapidus, and A. V. Tarasov, Yad. Fiz. **16**, 1023 (1972) [Sov. J. Nucl. Phys. **16**, 565 (1973)].
16. N. H. Buttimore *et al.*, Phys. Rev. D **59**, 114010-1 (1999).
17. N. Akchurin *et al.*, Phys. Rev. D **48**, 3026 (1993).
18. D. Gross *et al.,* Phys. Rev. Lett. **41**, 217 (1978).
19. D. P. Grosnick *et al.*, Nucl. Instrum. Methods Phys. Res. A **290**, 269 (1990).
20. A. Penzo, in *Proceedings of the Workshop Polarized Protons at High Energies. Accelerator Challenges and Physics Opportunities, DESY, 1999*, p. 489.
21. C. Baumgarten, in *Proceedings of the 13th International Symposium on High Energy Spin Physics, Protvino, Russia, 1998,* p. 433.
22. K. Seth *et al.*, Phys. Lett. B **385**, 479 (1996).
23. N. Akchurin *et al.*, Phys. Rev. D **51**, 3944 (1995).

Translated by A. Isaakyan

Physics of Atomic Nuclei, Vol. 66, No. 12, 2003, pp. 2199–2207. Translated from Yadernaya Fizika, Vol. 66, No. 12, 2003, pp. 2250–2258.

ELEMENTARY PARTICLES AND FIELDS
Theory

Determination of Azimuthal Features of Jets without Measuring the Angle of the Reaction Plane

I. P. Lokhtin, L. I. Sarycheva, and A. M. Snigirev

Institute of Nuclear Physics, Moscow State University, Vorob'evy gory, Moscow, 119899 Russia
Received October 24, 2002; in final form, March 4, 2003

Abstract—A new method is proposed for determining the coefficient of elliptic anisotropy of jets in ultrarelativistic heavy-ion collisions. This method, which does not involve directly reconstructing the reaction plane, is a generalization of the method used in current experiments to measure the coefficient of elliptic anisotropy of particle fluxes. It is shown that, for the spectrum of hadronic jets, the method makes it possible to explore the azimuthal asymmetry caused by the rescattering of hard partons and by their energy losses in dense quark–gluon matter formed in the region of the initial overlap of nuclei in collisions at a nonzero value of the impact parameter—in particular, under the conditions of the CMS experiment at LHC. © *2003 MAIK "Nauka/Interperiodica".*

1. INTRODUCTION

Interest in studying azimuthal correlations in ultrarelativistic heavy-ion collisions has grown sharply in recent years (see, for example, [1]). One of the reasons for this is that the rescattering of hard partons and their energy losses in an azimuthally asymmetric volume of dense quark–gluon plasma may lead to anisotropy in the distribution of high-p_T hadrons at RHIC [1–3] and of jets at LHC [4, 5]. In the yield of jets from noncentral collisions of nuclei, the azimuthal asymmetry induced by the rescattering and the energy loss of hard partons produced in an asymmetric dense-matter volume formed in the region of the initial overlap of nuclei was earlier theoretically studied by our group in [4, 5]. Investigation of the azimuthal-angle distribution of jets seems promising from the experimental point of view since this does not require precisely measuring the initial energy of a jet (this would be a rather difficult challenge involving the dependence on the algorithm of searches for jets and on the size of the jet cone [6])—only a determination of the jet emission angle with respect to the angle of the reaction plane is necessary in this case.

The analysis in [4] revealed that, for noncentral Pb–Pb collisions at the LHC energy, it is possible in principle to find, on the basis of the HIJING Monte Carlo model [7], the angle of the reaction plane spanned by the beam-axis and impact-parameter directions. For jets of transverse energy in the region $E_T \geq 100$ GeV, the corresponding estimate obtained there for the coefficient v_2^{jet} (see below) of elliptic anisotropy varied between 0.01 and 0.16, depending on the mechanism of energy losses and on the angular size of a jet. Also, this estimate decreased somewhat with increasing jet energy.

In the present article, we would like to consider the possibility of calculating (measuring) the coefficient of elliptic anisotropy of jets without determining the angle of the reaction plane. In a sense, this is a development and a generalization of well-known methods proposed and summarized in [8–10], which are intended for measuring the coefficients of anisotropy of particle fluxes. The ensuing exposition is organized as follows. In Section 2, it is shown that the correlation between the azimuthal position of the axis of a jet and the azimuthal angles of particles not entering into the composition of this jet makes it possible to determine the coefficient of elliptic anisotropy of jets. In Section 3, we present formulas for calculating this coefficient in terms of higher order correlation functions. In Section 4, we compare the results obtained in [4] by precisely calculating the coefficient of elliptic anisotropy of jets on the basis of the known angle of the reaction plane and the result derived by determining this coefficient in terms of correlation functions. In the Conclusion, we summarize our basic results.

2. CORRELATION FUNCTIONS AND COEFFICIENT OF ELLIPTIC ANISOTROPY OF JETS

We begin by briefly recalling basic ideas of the methods proposed in [8, 9] and used in current experiments for measuring the coefficients of anisotropy of particle fluxes, irrespective of the determination of the angle of the reaction plane. In the case of elliptic

1063-7788/03/6612-2199$24.00

azimuthal asymmetry, the distribution of particles has the form

$$\frac{dN}{d\varphi} = \frac{N_0}{2\pi}[1 + 2v_2 \cos 2(\varphi - \psi_R)], \qquad (1)$$

$$N_0 = \int_{-\pi}^{\pi} d\varphi \frac{dN}{d\varphi},$$

where ψ_R is the azimuthal angle of the reaction plane, φ is the azimuthal angle of a particle, and N_0 is the number of particles in an event. Knowing ψ_R, we can calculate (determine) the coefficient of elliptic asymmetry, v_2, in terms of the mean cosine; that is,

$$\langle \cos 2(\varphi - \psi_R)\rangle = \frac{1}{N_0} \qquad (2)$$

$$\times \int_{-\pi}^{\pi} d\varphi \cos 2(\varphi - \psi_R)\frac{dN}{d\varphi} = v_2.$$

If the particles being considered are correlated only with the reaction plane, the coefficient of elliptic asymmetry can be determined in terms of the two-particle azimuthal correlation function as

$$\langle \cos 2(\varphi_1 - \varphi_2)\rangle = \frac{1}{N_0^2}\int_{-\pi}^{\pi} d\varphi_1 \qquad (3)$$

$$\times \int_{-\pi}^{\pi} d\varphi_2 \cos 2(\varphi_1 - \varphi_2)\frac{d^2N}{d\varphi_1 d\varphi_2}$$

$$= \frac{1}{N_0^2}\int_{-\pi}^{\pi} d\varphi_1 \int_{-\pi}^{\pi} d\varphi_2$$

$$\times \cos 2((\varphi_1 - \psi_R) - (\varphi_2 - \psi_R))\frac{dN}{d\varphi_1}\frac{dN}{d\varphi_2} = v_2^2,$$

and the evaluation (measurement) of this correlation function is independent of the angle ψ_R of the reaction plane.

It should be noted here that the disregard of other correlations is legitimate only if the coefficient v_2 of azimuthal anisotropy is much greater than $1/\sqrt{N_0}$, but, in fact, this condition is not always satisfied. In this connection, the recent article of Borghini *et al.* [11], who proposed a new method that relies on a cumulant expansion of multiparticle correlation functions and which makes it possible to measure azimuthal asymmetry up to values of about $1/N_0$, is worthy of special note. This method eliminates automatically the majority of systematic errors caused by the azimuthal asymmetry of the detectors used and may contribute to improving the accuracy of our approach (see Section 3).

It was shown in [4] that, in noncentral collisions, the distribution of jets with respect to the azimuthal angle φ can accurately be approximated by the dependence

$$\frac{dN^{\rm jet}}{d\varphi} = \frac{N_0^{\rm jet}}{2\pi}[1 + 2v_2^{\rm jet} \cos 2(\varphi - \psi_R)], \qquad (4)$$

$$N_0^{\rm jet} = \int_{-\pi}^{\pi} d\varphi \frac{dN^{\rm jet}}{d\varphi}.$$

Further, the coefficient of elliptic asymmetry of jets, $v_2^{\rm jet}$, is calculated (measured) in terms of the cosine averaged over events; that is,

$$\langle \cos 2(\varphi - \psi_R)\rangle_{\rm event} \qquad (5)$$

$$= \frac{1}{N_0^{\rm jet}}\int_{-\pi}^{\pi} d\varphi \cos 2(\varphi - \psi_R)\frac{dN^{\rm jet}}{d\varphi} = v_2^{\rm jet}.$$

In order to determine this averaged cosine, it is necessary to know the angle ψ_R of the reaction plane in each event.

If, however, we calculate the azimuthal correlation between the angle that determines the direction of the jet axis[1)] and the angles at which particles not belonging to the jet fly, the values of this cosine can be related to the ellipticity coefficients v_2 and $v_2^{\rm jet}$ as [12]

$$\langle \cos 2(\varphi_{\rm jet} - \varphi)\rangle_{\rm event} \qquad (6)$$

$$= \frac{1}{N_0^{\rm jet} N_0}\int_{-\pi}^{\pi} d\varphi_{\rm jet} \int_{-\pi}^{\pi} d\varphi \cos 2(\varphi_{\rm jet} - \varphi)\frac{dN^{\rm jet}}{d\varphi_{\rm jet}}\frac{dN}{d\varphi}$$

$$= \frac{1}{N_0^{\rm jet}}\int_{-\pi}^{\pi} d\varphi_{\rm jet} \cos 2(\varphi_{\rm jet} - \psi_R)\frac{dN^{\rm jet}}{d\varphi_{\rm jet}} v_2 = v_2^{\rm jet} v_2.$$

Using Eq. (3) and the intermediate result in (6), [upon averaging over particles, $\cos 2(\varphi_{\rm jet} - \varphi)$ reduces to $v_2 \cos 2(\varphi_{\rm jet} - \psi_R)$], we can easily derive the formula

$$v_2^{\rm jet} = \left\langle \frac{\langle \cos 2(\varphi_{\rm jet} - \varphi)\rangle}{\sqrt{\langle \cos 2(\varphi_1 - \varphi_2)\rangle}} \right\rangle_{\rm event}, \qquad (7)$$

which makes it possible to calculate (or to measure) the coefficient of elliptic asymmetry of jets without knowing the angle of the reaction plane. The angular

[1)] A different possibility consists in fixing the azimuthal position of a leading particle in a jet. In this case, the calculation of the correlation function will furnish information about the azimuthal anisotropy of particles having high transverse momenta, and this may also be of use in analyzing experimental data from RHIC.

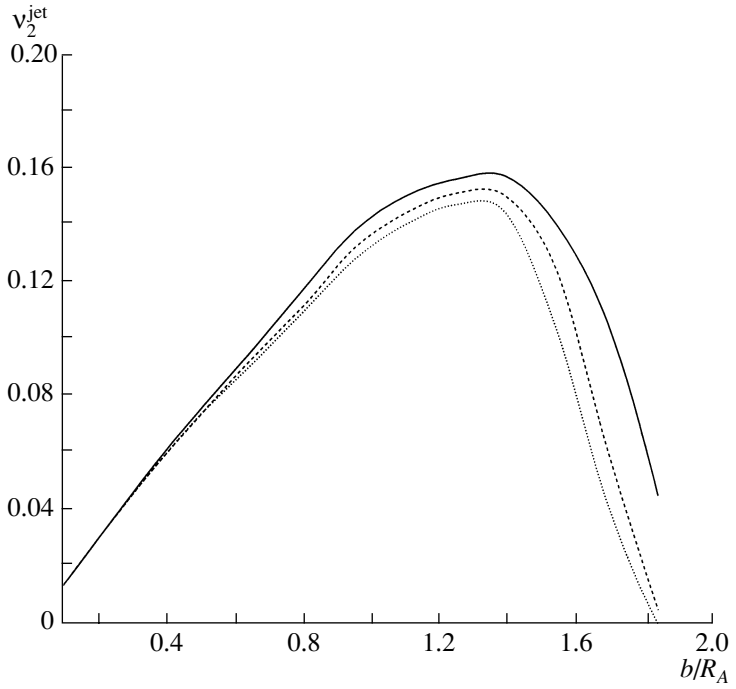

Coefficient of elliptic anisotropy of jets, v_2^{jet}, as a function of the impact parameter b: (solid curve) results of a "theoretical" calculation along with those obtained on the basis of the algorithm specified by Eq. (9) for two values of the charged-particle multiplicity per unit rapidity interval at $y^h = 0$ in central Pb–Pb collisions [$dN^{\pm}/dy^h =$ (dotted curve) 3000 and (dashed curve) 6000].

brackets $\langle\ \rangle$ denote averaging over particles not belonging to the jet in a given event. The brackets $\langle\ \rangle_{\text{event}}$ denote averaging over events.

This formula can be generalized by introducing particle momenta as weights; that is,

$$v_{2(p)}^{\text{jet}} = \left\langle \frac{\langle p_T(\varphi)\cos 2(\varphi_{\text{jet}} - \varphi)\rangle}{\sqrt{\langle p_{T1}(\varphi_1)p_{T2}(\varphi_2)\cos 2(\varphi_1 - \varphi_2)\rangle}} \right\rangle_{\text{event}}. \quad (8)$$

In this case, the angular brackets $\langle\ \rangle$ denote averaging not only over the angles of particles but also over their transverse momenta. Upon slightly modifying expression (8), we arrive at

$$v_{2(E)}^{\text{jet}} = \left\langle \frac{\langle E(\varphi)\cos 2(\varphi_{\text{jet}} - \varphi)\rangle}{\sqrt{\langle E_1(\varphi_1)E_2(\varphi_2)\cos 2(\varphi_1 - \varphi_2)\rangle}} \right\rangle_{\text{event}}, \quad (9)$$

where $E_i(\varphi_i)$ $(i = 1, 2)$ is the flux of energy in the segment i at an angle φ_i. Expression (9) enables one to determine the coefficient of elliptic asymmetry of jets under the conditions of calorimetric measurements of energy fluxes in the CMS experiment. Under these conditions, all cells of the calorimeter used are filled, and the elliptic anisotropy of jets can be determined by employing information about the energy fluxes in segments, whose azimuthal anisotropy is obviously correlated with the angle of the reaction plane in an event.

3. HIGHER ORDER CORRELATION FUNCTIONS

As was shown in [11], a basic advantage in employing correlation functions of higher rank is that the contribution of so-called nonflow correlations, which are not associated with the reaction plane, to the coefficient v_2 expressed in terms of multiparticle correlation functions is suppressed[2)] in relation to its definition in terms of the two-particle correlation function, the degree of suppression being proportional to an additional power of the particle multiplicity N_0 in an event.

By way of example, we indicate that, for the elliptic anisotropy of the particle flux, the fourth-order cumulant has the form [11]

$$c_2[4] = \langle\cos 2(\varphi_1 + \varphi_2 - \varphi_3 - \varphi_4)\rangle - \langle\cos 2(\varphi_1 - \varphi_3)\rangle\langle\cos 2(\varphi_2 - \varphi_4)\rangle - \langle\cos 2(\varphi_1 - \varphi_4)\rangle\langle\cos 2(\varphi_2 - \varphi_3)\rangle \quad (10)$$

[2)] This circumstance may play an important role in analyzing experimental data where the multiplicity of particles in an event is insufficiently high.

and, in the case where particles correlate only with the reaction plane [factorization of multiparticle distributions as in (3)], becomes

$$c_2[4] = -v_2^4. \tag{11}$$

If we now define the coefficient v_2 of azimuthal anisotropy in terms of the two-particle correlation function as

$$v_2 = \sqrt{\langle \cos 2(\varphi_1 - \varphi_2)\rangle}, \tag{12}$$

then, as was shown in [11], the contribution of nonflow correlations is of order $1/\sqrt{N_0}$. At the same time, their contribution to the coefficient v_2 defined in terms of the four-particle correlation function as

$$v_2 = (-c_2[4])^{1/4} \tag{13}$$

is of order $1/N_0^{3/4}$; that is, it is suppressed by the additional factor $1/N_0^{1/4}$. The corresponding analysis of current RHIC data that employs the four-particle correlation function (10) and relation (11) was already performed by the STAR Collaboration [13].

By using the derivation of Eq. (7) and the result presented in (11), we can obtain a formula for calculating (measuring) the coefficient of azimuthal anisotropy of jets in terms of correlation functions of higher rank, which are less sensitive to nonflow correlations. The result is

$$\begin{aligned} v_2^{\rm jet}[4] = \Big\langle \frac{1}{(-c_2[4])^{3/4}} \\ \times [-\langle \cos 2(\varphi_{\rm jet} + \varphi_1 - \varphi_2 - \varphi_3)\rangle \\ + \langle \cos 2(\varphi_{\rm jet} - \varphi_2)\rangle\langle \cos 2(\varphi_1 - \varphi_3)\rangle \\ + \langle \cos 2(\varphi_{\rm jet} - \varphi_3)\rangle\langle \cos 2(\varphi_1 - \varphi_2)\rangle] \Big\rangle_{\rm event}. \end{aligned} \tag{14}$$

We emphasize once again that, in the case where there are correlations only with the reaction plane, Eq. (14), as well as Eq. (7), reduces to an identity. In just the same way as was done in Section 2, the expression for the coefficient of azimuthal anisotropy can be generalized to the case of calorimetric measurements of energy fluxes. This yields

$$\begin{aligned} v_{2(E)}^{\rm jet}[4] = \Big\langle \frac{1}{(-c_{2(E)}[4])^{3/4}} [-\langle E_1(\varphi_1)E_2(\varphi_2)E_3(\varphi_3)\cos 2(\varphi_{\rm jet} + \varphi_1 - \varphi_2 - \varphi_3)\rangle \\ + \langle E_2(\varphi_2)\cos 2(\varphi_{\rm jet} - \varphi_2)\rangle\langle E_1(\varphi_1)E_3(\varphi_3)\cos 2(\varphi_1 - \varphi_3)\rangle \\ + \langle E_3(\varphi_3)\cos 2(\varphi_{\rm jet} - \varphi_3)\rangle\langle E_1(\varphi_1)E_2(\varphi_2)\cos 2(\varphi_1 - \varphi_2)\rangle] \Big\rangle_{\rm event}, \end{aligned} \tag{15}$$

where

$$\begin{aligned} c_{2(E)}[4] = \langle E_1(\varphi_1)E_2(\varphi_2)E_3(\varphi_3)E_4(\varphi_4)\cos 2(\varphi_1 + \varphi_2 - \varphi_3 - \varphi_4)\rangle \\ - \langle E_1(\varphi_1)E_3(\varphi_3)\cos 2(\varphi_1 - \varphi_3)\rangle\langle E_2(\varphi_2)E_4(\varphi_4)\cos 2(\varphi_2 - \varphi_4)\rangle \\ - \langle E_1(\varphi_1)E_4(\varphi_4)\cos 2(\varphi_1 - \varphi_4)\rangle\langle E_2(\varphi_2)E_3(\varphi_3)\cos 2(\varphi_2 - \varphi_3)\rangle. \end{aligned} \tag{16}$$

If the azimuthal position of the jet axis is correlated not only with the reaction plane, an attempt can be made to improve the accuracy of the method by using multiparticle correlation functions of a different type, those where averaging is performed over some subclasses of events rather than over all events. For example, one can consider subevents 1 and 2 in which jets are produced with rapidities $y > 0$ and $y < 0$, respectively. Evaluating the correlation function

$$\begin{aligned} c_2^{\rm jet}[4] \\ = \Big\langle \frac{1}{\sqrt{\langle \cos 2(\varphi_1 - \varphi_2)\rangle\langle \cos 2(\phi_1 - \phi_2)\rangle}} \\ \times [\langle \cos 2(\varphi_{\rm jet} - \varphi + \phi_{\rm jet} - \phi)\rangle \\ + \langle \cos 2(\varphi_{\rm jet} - \varphi - \phi_{\rm jet} + \phi)\rangle \\ - \langle \cos 2(\varphi_{\rm jet} - \varphi)\rangle\langle \cos 2(\phi_{\rm jet} - \phi)\rangle] \Big\rangle_{\rm event\ 1,2}, \end{aligned} \tag{17}$$

we find that, in the absence of nonflow correlations of product particles and under the condition that the azimuthal-angle distribution of jets in subevents is still described by expression (4), this correlation function becomes

$$c_2^{\rm jet}[4] = v_2^{\rm jet}(y > 0)\, v_2^{\rm jet}(y < 0). \tag{18}$$

In Eq. (17), φ and ϕ stand for the azimuthal angles of particles and jets in, respectively, $y > 0$ and $y < 0$ subevents. Accordingly, the angular brackets $\langle\ \rangle$ denote averaging over particles in subevents 1 and 2, while the angular brackets $\langle\ \rangle_{\rm event1,2}$ denote averaging over these subevents. A generalization of expression (17) to the case of calorimetric measurements of energy fluxes is obvious [it is similar to (9) and (15)];

for this reason, we do not write this result explicitly, nor do we provide examples of employing correlation functions of still higher rank.

4. SIMULATION AND NUMERICAL RESULTS

In order to illustrate the efficiency of the algorithm developed here and the possibility of performing a calorimetric measurement of the coefficient of elliptic asymmetry of jets, we compare the results of its precise calculation performed in [4] under the assumption that the angle of the reaction plane is known and the result obtained in terms of correlation functions [for the example of the simplest two-particle correlation function in expression (9)] within the following model.

Jets. The initial distribution of jets in nucleon–nucleon collisions within nuclei at $\sqrt{s} = 5.5$ TeV was generated with the aid of the PYTHIA model [14]. After that, these hard jets underwent rescattering and lost energy in gluon-rich plasma formed in the region of the initial overlap of lead nuclei in collisions at a nonzero value of the impact parameter. A detailed account of this is given in [4, 15, 16]. What is of importance for us here is that the azimuthal distribution of jets in noncentral collisions is well described by the elliptic dependence in (4). Within the model used, the effect of azimuthal anisotropy grows almost linearly with increasing impact parameter b (see figure), reaching a maximum at $b \sim 1.2R_A = 8.2$ fm (R_A is radius of the lead nucleus), whereupon the coefficient of elliptic anisotropy of jets begins to decrease (this is the region of b where the effect of a decrease in the jet-energy losses because of the reduction of the effective size of the dense region and because of the reduction of the initial medium energy density becomes critical and is not compensated by an increase in the degree of asymmetry of the volume). The p_T dependence of the coefficient of elliptic anisotropy—for particle fluxes, this dependence displays different types of behavior in hydrodynamic models [17] (a linear or a quadratic growth of v_2 with p_T) and in models where an elliptic flux results from the fragmentation of minijets losing energy in an asymmetric volume [3] (a decrease in v_2 with increasing p_T)—is yet another interesting feature of azimuthal anisotropy. In our model, the azimuthal anisotropy of jets becomes less pronounced with increasing jet energy E (the corresponding variation is smoother for collisions characterized by a higher degree of centrality); this can be explained by the reduction of the effect that the energy losses, which are weakly dependent on E, exert on the yield of jets with increasing primary energy. We have also taken into account kinematical cuts characteristic of the CMS facility [6]. Specifically, only pairs of jets such that each jet had a transverse energy in excess of 100 GeV and a rapidity in the region $|y^{\text{jet}}| < 1.5$ were selected, whereupon these two-string events were mixed with thermal events from Pb–Pb collisions.

Isotropic particle flux. The need for simulating nucleus–nucleus interactions at high energies led to creating microscopic Monte Carlo models (so-called generators of events) that are based either on perturbative calculations of parton cascades (HIJING [7, 18], PCM [19]) or on string phenomenology (FRITIOF [20], VENUS [21], QGSM [22, 23]). But the use of these generators in simulating heavy-ion collisions at the LHC energy consumes much machine time; at the same time, the results of such calculations are strongly model-dependent and, for the most part, underestimate the effect of azimuthal anisotropy (see, however, [23]). On the other hand, simple macroscopic hydrodynamic models are able to reproduce experimental data at the SPS [24–27] and RHIC [17] energies and can in principle be used for our purposes.

In thermal models [17, 26, 27], the spectrum of final hadrons,

$$E\frac{d^3N}{d^3p} = \int\limits_{\sigma} f(x,p)p^{\mu}d\sigma_{\mu}, \qquad (19)$$

is assumed to have the form of a superposition of a thermal distribution and a collective motion of a liquid, the collective motion obeying hydrodynamic equations; here, the invariant distribution function $f(x,p)$ is taken in the Bose–Einstein form for particles of integral spin and in the Fermi–Dirac form for particles of half-integer spin (p_μ is the 4-momentum of a hadron, and $E = p_0$ is its energy). Integration is performed over the hypersurface σ at the hadronic-liquid-decay temperature (so-called freezing temperature) $T = T_f$.

In the case of central collisions of nuclei ($b = 0$), cylindrically symmetric matter expands predominantly along the collision axis [28]; as to the transverse motion, it can be taken into account as a correction within simple models [24, 29, 30] (the validity of this approach was confirmed in [27] by directly constructing a numerical solution to relevant hydrodynamic equations). In describing the motion of the liquid, we use the variables τ, r, η, and Φ, where $\tau = \sqrt{t^2 - z^2}$, $r = \sqrt{x^2 + y^2}$, $\eta = \frac{1}{2}\ln\frac{t+z}{t-z}$, and $\tan\Phi = \frac{y}{x}$, instead of the Cartesian coordinates t, x, y, and z. For the sake of simplicity, we consider only pions, kaons, and protons, kaons and protons being assumed to be thermally suppressed because of their higher mass. In addition, it is assumed that the velocity profile in the transverse direction is linear,

$u_r = \sinh Y_T = \dfrac{dR}{d\tau}\dfrac{r}{R}$ (this follows from a solution to the continuity equation at a uniform density [24, 30]); the motion in the longitudinal direction is specified in accordance with the one-dimensional scaling solution $Y_L = \eta$ [28] (Y_T and Y_L are, respectively, the transverse and the longitudinal rapidity of collective motion, while R is the effective transverse radius of the system).

The following procedures were applied in performing a Monte Carlo simulation of thermal Pb–Pb events at the LHC energy [29].

(i) The 4-momentum p^*_μ of a hadron of mass m was generated at random in the rest frame of a liquid element in accordance with the isotropic Boltzmann distribution

$$f(E^*) \propto E^*\sqrt{E^{*2} - m^2}\exp(-E^*/T_f), \quad -1 < \cos\theta^* < 1, \quad 0 < \phi^* < 2\pi, \tag{20}$$

where $E^* = \sqrt{p^{*2} + m^2}$ is the energy of the hadron and the polar angle θ^* and the azimuthal angle ϕ^* specify the direction of its motion in the rest frame (in spherical coordinates) of the liquid element.

(ii) The spatial position of a liquid element and its local 4-velocity u_μ (in the system of cylindrical coordinates) were generated at random in accordance with phase space and the character of motion of the liquid; that is,

$$f(r) = 2r/R_f^2 (0 < r < R_f), \quad -\eta_{\max} < \eta < \eta_{\max}, \tag{21}$$

$$0 < \Phi < 2\pi, \quad u_r = \frac{r}{R_f}\sinh Y_T^{\max},$$

$$u_t = \sqrt{1 + u_r^2}\cosh\eta, \quad u_z = \sqrt{1 + u_r^2}\sinh\eta,$$

where R_f is the effective final transverse radius of the system and $\eta_{\max} = Y_L^{\max}$ and $Y_T^{\max}$ are model parameters that specify the maximum rapidities of the collective motion of the liquid in, respectively, the longitudinal and the transverse direction.

(iii) Further, a Lorentz transformation of the hadron 4-momentum (in Cartesian coordinates) was performed in such a way as to go over to the reference frame comoving with center of mass of the event being considered; that is,

$$p_x = p^*\sin\theta^*\cos\phi^* + u_r\cos\Phi\left[E^* + \frac{(u^i p^{*i})}{u_t + 1}\right], \tag{22}$$

$$p_y = p^*\sin\theta^*\sin\phi^* + u_r\sin\Phi\left[E^* + \frac{(u^i p^{*i})}{u_t + 1}\right],$$

$$p_z = p^*\cos\theta^* + u_z\left[E^* + \frac{(u^i p^{*i})}{u_t + 1}\right],$$

$$E = E^* u_t + (u^i p^{*i}),$$

where

$$(u^i p^{*i}) = u_r p^*\sin\theta^*\cos(\Phi - \phi^*) + u_z p^*\cos\theta^*. \tag{23}$$

In our calculations, we have also used the values of $dN^\pm/dy^h = 6000, 3000$ for the particle multiplicities per unit rapidity interval and the values of $T_f = 140$ MeV, $Y_L^{\max} = 5$, and $Y_T^{\max} = 1$ for the freezing parameters. In that case, the mean transverse momentum of hadrons is equal to 0.55 GeV for both values of the particle multiplicity per unit rapidity interval.

The slope of the p_T spectra of final hadrons is determined by the freezing temperature T_f and the maximum rapidity $Y_T^{\max}$ of the transverse collective motion of the liquid. The maximum rapidity $Y_L^{\max}$ of the longitudinal collective motion of the liquid affects the width of the distribution of hadrons with respect to the rapidity y^h. The spacetime dimensions of the freeze-out region depend on the proper time of freeze-out, τ_f, and on the effective final radius of the system, R_f, these parameters affecting primarily the absolute normalization of the spectra of final hadrons, which is fixed here by specifying the mean particle multiplicity per unit rapidity interval, $dN^\pm/dy^h$, in the final state.

Anisotropic particle flux. The simple hydrodynamic model proposed in [24, 29] yielded results that comply well with experimental data obtained by the NA35 [31] and NA49 [32] Collaborations at SPS and made it possible to develop more efficient methods [29] for separating thermal and hard QCD jets under the conditions of the CMS experiment at LHC. Under one simple assumption that the spatial transverse ellipticity of the freeze-out region,

$$\epsilon = \frac{\langle y^2 - x^2\rangle}{\langle y^2 + x^2\rangle}, \tag{24}$$

coincides with the ellipticity of the system formed in the region of the initial overlap of nuclei,

$$\epsilon_0 = \frac{b}{2R_A}, \tag{25}$$

the model can easily be generalized in such a way as to become appropriate for describing particle fluxes in noncentral collisions.

This scale invariance enables one to avoid introducing additional parameters and, at the same time, leads to an azimuthal anisotropy of the p_T spectrum of generated particles because the effective final radius

R_f in (21) now depends on the angle Φ:[3)]

$$R_f(b) = R_f(b=0)\min\left\{\sqrt{1-\epsilon_0^2\sin^2\Phi}+\epsilon_0\cos\Phi,\right.$$
$$\left.\sqrt{1-\epsilon_0^2\sin^2\Phi}-\epsilon_0\cos\Phi\right\}. \quad (26)$$

In developing this approach, the total multiplicity of thermal particles in an event was assumed to be proportional to the standard nuclear-overlap function $T_{AA}(b)$. As a matter of fact, initial-state nuclear effects of the shadowing or saturation type may lead to a weaker dependence of the multiplicities $dN^{\pm}/dy^h$ per unit rapidity interval on the impact parameter b (see, for example, [33]). It follows that, if the particle density in central collisions is fixed as a parameter, then we arrive at the most "pessimistic," minimal estimate of the mean multiplicity for noncentral collisions. Since the proposed method becomes more precise with increasing multiplicity, its weaker dependence on the impact parameter b will ensure a more accurate determination of $v_2^{\rm jet}$.

It is important to note that by no means do we pursue here the goal of describing the azimuthal p_T spectrum of thermal particles in detail or the goal of performing a comparison with current experimental data [one can reach agreement by considering, for example, ϵ_0 in (26) as a parameter]. The only point of importance for us here is that particles grouped in the way indicated above imitate well an anisotropic energy flux correlated with the reaction plane and enable us to test the efficiency of the recipe in (9) for measuring the coefficient of elliptic anisotropy of jets. (Yet, the problem of the azimuthal structure of energy fluxes under the conditions of the CMS experiment is of importance in and of itself and may be the subject of a further investigation.) This may be done either by refining our simple model on the basis of ideas that are similar to those developed in [34] (where the azimuthal asymmetry was due to the spatial ellipticity ϵ_s of the radiation region and to the azimuthal asymmetry of the collective velocity u_μ with a characteristic momentum ellipticity ϵ_f, ϵ_s and ϵ_f being model parameters) or by directly constructing a numerical solution to three-dimensional hydrodynamic equations [17].

Anisotropic energy flux. For the sake of definiteness, we have employed the parameters of the CMS facility at LHC [6]. By way of example, we indicate that the central, barrel, part of the facility covers the pseudorapidity range $|\eta| < 1.5$ and that the dimensions of the cells in the η–ϕ space of the electromagnetic and hadronic calorimeters are $\Delta\eta \times \Delta\phi = 0.0174 \times 0.0174$ and $\Delta\eta \times \Delta\phi = 0.0872 \times 0.0872$, respectively. In order to reproduce the experimental situation quite roughly (without allowance for detector effects, only the tightness of the calorimeters being assumed), we defined the energy fluxes $E_i(\varphi_i)$ as the sum of the energies of all particles generated in the way indicated above over the entire pseudorapidity range $|\eta| < 1.5$ within each of the 72 segments of the calorimeter that cover the whole azimuth ($72 \times 0.0872 = 2\pi$; $i = 1, ..., 72$).

Efficiency of the method. The results obtained in [4] by precisely calculating the coefficient of elliptic anisotropy of jets, $v_2^{\rm jet}$, as a function of the impact parameter b are displayed in the figure along with the results produced by the algorithm in (9) for the case where energy fluxes are simulated in the way described above. The estimations were performed at two values of the charged-particle multiplicity per unit rapidity interval at $y^h = 0$ in central Pb–Pb collisions: $dN^{\pm}/dy^h = 3000$ and 6000. It can be seen that the accuracy in determining $v_2^{\rm jet}$ is close to 100% for semicentral events ($b \le R_A$), but that it becomes much poorer for highly peripheral collisions ($b \sim 2R_A$), in which case a decrease in the multiplicity and in the azimuthal anisotropy leads to relatively large fluctuations of the energy deposition in calorimeter segments. It is worth noting here that the applicability of the hydrodynamic model to such peripheral collisions is questionable. Moreover, it is necessary in that case to take into account some other potentially important phenomena, such as boundary effects near the nuclear surface, the impact-parameter dependence of parton structure functions in nuclei, and a possible early transverse collective motion [35].

To conclude this subsection, we will discuss the effect of various factors on the result of determining $v_2^{\rm jet}$ with the aid of the algorithm proposed here. First of all, we note that the theoretical absolute value of the coefficient $v_2^{\rm jet}$ and its impact-parameter distribution are of course model-dependent. For example, the energy losses of jets and the corresponding azimuthal anisotropy are sensitive to the angular size of the jet cone [36–39]. This effect will be less pronounced for jets of finite angular size ($\theta_0 \neq 0$), since energy losses are considered here only at the parton level. The azimuthal anisotropy of jets may also decrease because of a possible sharp transverse collective expansion [35] in events characterized by large impact parameters. However, the relative error in determining $v_2^{\rm jet}$ is virtually independent of the

[3)] The geometry of noncentral symmetric ultrarelativistic collisions of nuclei and the model of hard-parton production and propagation through dense matter formed is described in detail elsewhere [15, 16].

absolute value of this coefficient. The reason for this is that, if use is made of fluxes, the relative error of the method based on Eq. (7) can be roughly estimated as the sum of two terms that are proportional to $(v_2^{\text{jet}} N_{\text{event}})^{-1}$ and $(v_2 N_0)^{-1}$. If the number of events is quite large ($N_{\text{event}} \gg 1$), as is indeed the case in our calculations, then the error is determined primarily by the term that is independent of v_2^{jet}. For the same reason, the relative error becomes large at small values of the coefficient of azimuthal anisotropy of particles and of their multiplicity. Under the condition $N_0 \gg N_{\text{segment}} \gg 1$ (in the calorimeter considered here, $N_{\text{segment}} = 72$), the same conclusion is also valid for the algorithm specified by Eq. (9), in which case use is made of energy fluxes.

In an actual experiment, the azimuthal distribution of particle fluxes and energies can be much more complicated because of the presence of other nonflow correlations, a limited accuracy in determining the impact parameter, a finite calorimeter resolution, and some other factors not considered above. In that case, an attempt at improving the accuracy of the method may rely on employing correlation functions of higher rank—such as those in (14) and (15)—or on averaging the quantities in question over some subevents, as is exemplified in (17).

5. CONCLUSION

In the case of jets, a methodological advantage of azimuthal observables is obvious: it is only necessary to reconstruct the azimuthal position of a jet without measuring its total energy. One of the possible methods is to analyze jet production versus the azimuthal angle, but this requires determining the angle of the reaction plane in each event. In the present article, we have proposed a method for measuring the coefficient of elliptic anisotropy of jets without directly reconstructing the reaction plane. The method is based on calculating correlations between the azimuthal direction of a jet and the azimuthal angles of particles that do not enter into the composition of this jet. For the example of a calorimetric measurement of energy fluxes, which is implementable in the CMS experiment, it has been shown that, under conditions close to those prevalent in an actual physical situation, the method is highly efficient even if use is made of the simplest two-particle correlation function in (9). It has been found that the method becomes more accurate with increasing multiplicity of product particles and with increasing azimuthal anisotropy of their flux (energy); also, the accuracy of the method can be improved by employing correlation functions of higher rank [such as those in (14), (15), and (17)], but it is virtually independent of the absolute value of the coefficient of elliptic anisotropy itself.

We believe that the algorithm proposed in this article will be of use in analyzing future experimental data from LHC and that it can also be employed in the current treatment of data from RHIC that concern the azimuthal anisotropy of high-transverse-momentum particles.

ACKNOWLEDGMENTS

We are grateful to G.M. Zinovjev, U. Wiedemann, S.A. Voloshin, S.V. Petrushanko, and V.V. Uzhinskii for stimulating discussions and N.P. Karpinskaya for assistance in the preparation of the manuscript.

REFERENCES

1. *Proceedings of the 15th Int. Conf. on Ultrarelativistic Nucleus–Nucleus Collisions, Quark Matter 2001 (QM 2001), Long Island, USA, 2001*; Nucl. Phys. A **698** (2002); *Proceedings of the 16th Int. Conf. on Ultrarelativistic Nucleus–Nucleus Collisions, Quark Matter 2002 (QM 2002), Nantes, France, 2002* (in press).
2. A. S. Galoyan and V. V. Uzhinskii, hep-ph/0007122.
3. X.-N. Wang, Phys. Rev. C **63**, 054902 (2001); M. Gyulassy, I. Vitev, and X.-N. Wang, Phys. Rev. Lett. **86**, 2537 (2001).
4. I. P. Lokhtin, S. V. Petrushanko, L. I. Sarycheva, and A. M. Snegirev, Yad. Fiz. **65**, 974 (2002) [Phys. At. Nucl. **65**, 943 (2002)].
5. I. P. Lokhtin, L. I. Sarycheva, S. V. Petrushanko, and A. M. Snigirev, hep-ph/0112180; in *Proceedings of Int. Conf. on Physics and Astrophysics of Quark–Gluon Plasma, Jaipur, India, 2001*.
6. G. Baur *et al.*, CERN CMS Note 2000/060 (2000).
7. M. Gyulassy and X.-N. Wang, Comput. Phys. Commun. **83**, 307 (1994).
8. S. A. Voloshin and Y. Zhang, Z. Phys. C **70**, 665 (1996); A. M. Poskanzer and S. A. Voloshin, Phys. Rev. C **58**, 1671 (1998).
9. S. Wang *et al.*, Phys. Rev. C **44**, 1091 (1991).
10. J.-Y. Ollitrault, Phys. Rev. D **46**, 229 (1992); **48**, 1132 (1993).
11. N. Borghini, P. M. Dinh, and J.-Y. Ollitrault, Phys. Rev. C **63**, 054906 (2001).
12. I. P. Lokhtin, L. I. Sarycheva, and A. M. Snigirev, Phys. Lett. B **537**, 261 (2002).
13. C. Adler *et al.* (STAR Collab.), nucl-ex/0206001.
14. T. Sjostrand, Comput. Phys. Commun. **82**, 74 (1994).
15. I. P. Lokhtin and A. M. Snigirev, Eur. Phys. J. C **16**, 527 (2000).
16. I. P. Lokhtin and A. M. Snigirev, Yad. Fiz. **64**, 1563 (2001) [Phys. At. Nucl. **64**, 1487 (2001)].
17. P. F. Kolb, J. Sollfrank, and U. Heinz, Phys. Rev. C **62**, 054909 (2000); P. F. Kolb *et al.*, Phys. Lett. B **500**, 232 (2001); P. Huovinen *et al.*, Phys. Lett. B **503**, 58 (2001); P. F. Kolb *et al.*, Nucl. Phys. A **696**, 175 (2001).

18. X.-N. Wang and M. Gyulassy, Phys. Rev. D **44**, 3501 (1991); **45**, 844 (1992).
19. K. Geiger, Phys. Rev. D **46**, 4965, 4986 (1992).
20. B. Andersson, G. Gustafson, and Hong Pi, Z. Phys. C **57**, 485 (1993); Hong Pi, Preprint LU TP 91-28.
21. K. Werner and P. Koch, Z. Phys. C **47**, 215 (1990).
22. N. S. Amelin, K. K. Gudima, and V. D. Toneev, Yad. Fiz. **51**, 1730 (1990) [Sov. J. Nucl. Phys. **51**, 1093 (1990)].
23. E. E. Zabrodin, C. Fuchs, L. V. Bravina, and A. Faessler, Phys. Lett. B **508**, 184 (2001).
24. I. P. Lokhtin and A. M. Snigirev, Phys. Lett. B **378**, 247 (1996).
25. Yu. M. Sinyukov, V. A. Averchenkov, and B. Lorstad, Z. Phys. C **49**, 417 (1991).
26. E. Schnedermann, J. Sollfrank, and U. Heinz, Phys. Rev. C **48**, 2462 (1993).
27. S. Muroya, H. Nakamura, and M. Namiki, Prog. Theor. Phys. Suppl. **120**, 209 (1995).
28. D. Bjorken, Phys. Rev. D **27**, 140 (1983).
29. N. A. Kruglov, I. P. Lokhtin, L. I. Sarycheva, and A. M. Snigirev, Z. Phys. C **76**, 99 (1997).
30. B. Kämpfer and O. P. Pavlenko, Z. Phys. C **62**, 491 (1994).
31. J. Bachler *et al.* (NA35 Collab.), Phys. Rev. Lett. **72**, 1419 (1994).
32. P. G. Jones *et al.* (NA49 Collab.), Nucl. Phys. A **610**, 188 (1996).
33. K. J. Eskola, K. Kajantie, and K. Tuominen, Phys. Lett. B **497**, 39 (2001); K. J. Eskola, P. V. Ruuskanen, S. S. Rasanen, and K. Tuominen, Nucl. Phys. A **696**, 715 (2001).
34. U. A. Wiedemann, Phys. Rev. C **57**, 266 (1998).
35. M. Gyulassy, I. Vitev, X.-N. Wang, and P. Huovinen, Phys. Lett. B **526**, 301 (2002).
36. R. Baier, Yu. L. Dokshitzer, A. H. Mueller, and D. Schiff, Nucl. Phys. B **531**, 403 (1998); Phys. Rev. C **58**, 1706 (1998).
37. I. P. Lokhtin and A. M. Snigirev, Phys. Lett. B **440**, 163 (1998).
38. U. Wiedemann, Nucl. Phys. B **588**, 303 (2000); Nucl. Phys. A **690**, 731 (2001).
39. M. Gyulassy, P. Levai, and I. Vitev, Nucl. Phys. B **571**, 197 (2000); Phys. Rev. Lett. **85**, 5535 (2000); Nucl. Phys. B **594**, 371 (2001).

Translated by A. Isaakyan

Physics of Atomic Nuclei, Vol. 66, No. 12, 2003, pp. 2208–2213. Translated from Yadernaya Fizika, Vol. 66, No. 12, 2003, pp. 2259–2265.

ELEMENTARY PARTICLES AND FIELDS
Theory

Limits on the Scalar-Leptoquark and Scalar-Gluon Masses from the Parameters S, T, and U in the Minimal Model Based on Four-Color Symmetry

A. V. Povarov* and **A. D. Smirnov****

Yaroslavl State University, Sovetskaya ul. 14, Yaroslavl, 150000 Russia

Received October 7, 2002; in final form, January 13, 2003

Abstract—The contributions to the parameters S, T, and U of radiative corrections from the doublets of scalar leptoquarks and scalar gluons are analyzed within the minimal model based on four-color symmetry of the Pati–Salam type. It is shown that current experimental data on the parameters S, T, and U admit the existence of relatively light scalar leptoquarks and scalar gluons (of mass lower than 1 TeV), the best fit to experimental data being attained at mass values not greater than 400 GeV. In particular, the existence of scalar leptoquarks of mass below 300 GeV is found to be compatible with data on the parameters S, T, and U at $\chi^2 < 3.1$ (3.2) for $m_H = 115$ (300) GeV as against $\chi^2_{\rm SM} = 3.5$ (5.0) in the Standard Model. The mass of the lightest scalar gluon is then predicted to be less than 850 (720) GeV. It is emphasized that the aforementioned doublets of scalar leptoquarks and scalar gluons can play a significant role in processes involving a t quark at LHC. © *2003 MAIK "Nauka/Interperiodica".*

1. INTRODUCTION

Searches for new physics beyond the Standard Model have become one of the lines of investigations in elementary-particle physics. One of the extensions of the Standard Model is based on four-color quark–lepton symmetry of the Pati–Salam type [1]. This model predicts the existence of vector leptoquarks V whose mass is bounded from below by 100 TeV or by some smaller value [2–7]. It also admits the existence of scalar leptoquarks [8, 9] and other particles.

Provided that the quark and lepton masses are generated via the Higgs mechanism, four-color symmetry also leads to the existence of scalar-leptoquark and scalar-gluon doublets [2, 3, 10], which, in the approach being considered, are responsible for the mass splitting of quarks and leptons, appearing to be some kind of partners to the standard Higgs doublet. There then arises the problem of deriving constraints on the scalar-leptoquark masses from available experimental data. Nonobservation of scalar leptoquarks in direct-production experiments sets a lower limit on their masses at about 250 GeV [11]. At these mass values, leptoquarks could manifest themselves in radiative corrections. The first estimates of the masses of the scalar-leptoquark doublets were obtained from an analysis of radiative corrections in terms of the parameters S, T, and U [12]. This analysis revealed that, in view of the possible mixing of their components of charge 2/3, the leptoquark masses may be as low as 1 TeV or even below this [13, 14]. In these estimates, it is assumed that the doublets of scalar gluons are degenerate in mass, so that their contributions to the parameters S, T, and U can be neglected.

In this study, we calculate and analyze the contributions to the parameters S, T, and U of radiative corrections from the doublets of scalar leptoquarks, along with the respective contributions of the doublets of scalar gluons, taking into account the mass splittings in the scalar-gluon doublets. We derive limits on the masses of scalar leptoquarks and scalar gluons from current experimental data [11] on the parameters S, T, and U. Some of the results discussed here were briefly mentioned in [15].

2. CONTRIBUTION OF SCALAR-LEPTOQUARK AND SCALAR-GLUON DOUBLETS TO THE PARAMETERS S, T, AND U

We consider the minimal model based on quark–lepton symmetry [2, 3]. In this model, the doublets of scalar leptoquarks $S^{(\pm)}_{a\alpha}$ and scalar gluons F_{ja} belong to the (15, 2, 1) multiplet $\Phi^{(3)}_{i,a}$ of the $SU_V(4) \times SU_L(2) \times U_R(1)$ group, where $a = 1, 2$ are the $SU_L(2)$ indices; $i = 1, 2, \ldots, 15$ are the $SU_V(4)$ indices; $\alpha = 1, 2, 3$; and $j = 1, 2, \ldots, 8$ are the $SU_c(3)$ (color) indices, the vacuum expectation value for this multiplet being denoted by η_3. The (15, 2, 1) multiplet

*e-mail: povarov@univ.uniyar.ac.ru
**e-mail: asmirnov@univ.uniyar.ac.ru

$\Phi_{i,a}^{(3)}$ and the (1, 2, 1) multiplet $\Phi_a^{(2)}$ (its vacuum expectation value is η_2) give rise to the masses of quarks and leptons, splitting them via the Higgs mechanism. A more detailed description of the scalar sector of the model under study is given in [14], along with some special points in the calculation of the scalar-doublet contributions to the parameters S, T, and U.

General expressions for the contributions of scalar leptoquarks to the parameters S, T, and U were obtained in [13, 14]. Here, we examine the particular case of the simplest mixing of scalar leptoquarks, neglecting the small parameter $\xi^2 = \frac{2}{3}g_4^2\eta_3^2/m_V^2 \ll 1$, where g_4 is the coupling constant associated with the $SU_V(4)$ group and m_V is the mass of the vector leptoquarks generated by this group. In this case, the doublets of scalar leptoquarks can be represented in the form

$$S^{(+)} = \begin{pmatrix} S_1^{(+)} \\ cS_1 + sS_2 \end{pmatrix}, \quad S^{(-)} = \begin{pmatrix} S_1^{(-)} \\ -s\overset{*}{S}_1 + c\overset{*}{S}_2 \end{pmatrix}. \tag{1}$$

Here, the upper components $S_1^{(+)}$ and $S_1^{(-)}$ have the electric charges of 5/3 and 1/3, respectively, while the lower components are combinations of the scalar leptoquarks S_1 and S_2 having a specific mass and the charge of 2/3; $c = \cos\theta$ and $s = \sin\theta$, where θ is the mixing angle in the simplest mixing scheme.

The contributions of the scalar-leptoquark doublets (1) to the parameters S, T, and U can then be derived by appropriately simplifying the general expressions obtained in [13, 14] and are given by

$$S^{(\mathrm{LQ})} = \frac{n_c}{12\pi}\left\{ - Y_+^{\mathrm{SM}}\left[c^2 \ln\frac{m_+^2}{m_1^2} + s^2 \ln\frac{m_+^2}{m_2^2}\right] \right. \tag{2}$$
$$- Y_-^{\mathrm{SM}}\left[s^2 \ln\frac{m_-^2}{m_1^2} + c^2 \ln\frac{m_-^2}{m_2^2}\right]$$
$$\left. + 4c^2s^2 f_2(m_1, m_2)\right\},$$

$$T^{(\mathrm{LQ})} = \frac{n_c}{16\pi s_{\mathrm{W}}^2 c_{\mathrm{W}}^2 m_Z^2} \tag{3}$$
$$\times \left\{ c^2\Big[f_1(m_+, m_1) + f_1(m_-, m_2)\Big] \right.$$
$$+ s^2\Big[f_1(m_+, m_2) + f_1(m_-, m_1)\Big]$$
$$\left. - 4c^2s^2 f_1(m_1, m_2)\right\},$$

$$U^{(\mathrm{LQ})} = \frac{n_c}{12\pi}\left\{ c^2\Big[f_2(m_+, m_1) + f_2(m_-, m_2)\Big] \right. \tag{4}$$
$$+ s^2\Big[f_2(m_+, m_2) + f_2(m_-, m_1)\Big]$$
$$\left. - 4c^2s^2 f_2(m_1, m_2)\right\},$$

where

$$f_1(m_1, m_2) = m_1^2 + m_2^2 - \frac{2m_1^2m_2^2}{m_1^2 - m_2^2}\ln\frac{m_1^2}{m_2^2}; \tag{5}$$

$$f_2(m_1, m_2) = -\frac{5m_1^4 + 5m_2^4 - 22m_1^2m_2^2}{3(m_1^2 - m_2^2)^2} \tag{6}$$
$$+ \frac{m_1^6 - 3m_1^4m_2^2 - 3m_1^2m_2^4 + m_2^6}{(m_1^2 - m_2^2)^3}\ln\frac{m_1^2}{m_2^2};$$

$n_c = 3; Y_\pm^{\mathrm{SM}} = 1 \pm 4/3$ are the hypercharges of the scalar leptoquarks $S^{(\pm)}$; $m_\pm = m_{S_1^{(\pm)}}$ and $m_{1,2} = m_{S_1,S_2}$ are the masses of the scalar leptoquarks; $c_{\mathrm{W}}^2 = 1 - s_{\mathrm{W}}^2$, s_{W} being the sine of the Weinberg angle; and m_Z is the Z-boson mass. In view of S_1–S_2 mixing, the contributions $T^{(\mathrm{LQ})}$ and $U^{(\mathrm{LQ})}$ are not positive definite; they can take negative values if m_+ and m_- lie between m_1 and m_2.

In general, the scalar-gluon doublets F_{ja} can be represented in the form

$$F_j = \begin{pmatrix} F_{1j} \\ (\phi_{1j} + i\phi_{2j})/\sqrt{2} \end{pmatrix}, \tag{7}$$

where the charged field F_{1j} and the neutral fields ϕ_{1j} and ϕ_{2j}, $j = 1, 2, \ldots, 8$, describe scalar gluons of specific mass (in general, the real part ϕ_{1j} and the imaginary part ϕ_{2j} of the lower component of the doublet F_j may be split in mass).

In the case of arbitrary mass splitting, the contributions of the scalar-gluon doublets (7) to the parameters S, T, and U are given by

$$S^{(F)} = -\frac{k_F}{24\pi}\left\{ \ln\frac{m_{F_1}^2}{m_{\phi_1}^2} + \ln\frac{m_{F_1}^2}{m_{\phi_2}^2} - f_2(m_{\phi_1}, m_{\phi_2})\right\}, \tag{8}$$

$$T^{(F)} = \frac{k_F}{32\pi c_{\mathrm{W}}^2 s_{\mathrm{W}}^2 m_Z^2}\left\{ f_1(m_{F_1}, m_{\phi_1}) \right. \tag{9}$$
$$\left. + f_1(m_{F_1}, m_{\phi_2}) - f_1(m_{\phi_1}, m_{\phi_2})\right\},$$

$$U^{(F)} = \frac{k_F}{24\pi}\{f_2(m_{F_1}, m_{\phi_1}) \tag{10}$$

$$+ f_2(m_{F_1}, m_{\phi_2}) - f_2(m_{\phi_1}, m_{\phi_2})\},$$

where $k_F = 8$ and the functions $f_1(m_1, m_2)$ and $f_2(m_1, m_2)$ are defined in (5) and (6), respectively. The contributions $T^{(F)}$ and $U^{(F)}$ are not positive definite: they are negative if m_{F_1} lies between m_{ϕ_1} and m_{ϕ_2} and are positive if $m_{\phi_1} = m_{\phi_2}$, in which case the contributions in (8)–(10) coincide with those obtained in [14]. At $m_{F_1} = m_{\phi_1} = m_{\phi_2}$, these contributions vanish.

3. SCALAR POTENTIAL AND MASSES OF SCALAR LEPTOQUARKS AND SCALAR GLUONS

In what follows, we assume that the masses of scalar leptoquarks and scalar gluons are generated by the scalar potential that describes their interaction with the standard Higgs doublet $\Phi_a^{(\mathrm{SM})}$, which is a superposition of the doublets $\Phi_{15a}^{(3)}$ and $\Phi_a^{(2)}$. In general, the terms of the scalar potential that contribute to the masses of scalar leptoquarks and scalar gluons can be represented in the form

$$V_m(\Phi^{(\mathrm{SM})}, S) = \sum_{+,-}\Big[m_\pm^{(0)2}(\overset{+}{S}{}^{(\pm)}S^{(\pm)}) + \beta_\pm(\overset{+}{\Phi}{}^{(\mathrm{SM})}\Phi^{(\mathrm{SM})})(\overset{+}{S}{}^{(\pm)}S^{(\pm)}) + \gamma_\pm(\overset{+}{\Phi}{}^{(\mathrm{SM})}S^{(\pm)})(\overset{+}{S}{}^{(\pm)}\Phi^{(\mathrm{SM})})\Big] + \Big[\delta_S(\overset{+}{\Phi}{}^{(\mathrm{SM})}S^{(+)})(\overset{+}{\Phi}{}^{(\mathrm{SM})}S^{(-)}) + \mathrm{h.c.}\Big], \tag{11}$$

$$V_m(\Phi^{(\mathrm{SM})}, F) = m_F^{(0)2}\sum_j(\overset{+}{F}_jF_j) + \beta_F(\overset{+}{\Phi}{}^{(\mathrm{SM})}\Phi^{(\mathrm{SM})})\sum_j(\overset{+}{F}_jF_j) + \gamma_F\sum_j(\overset{+}{\Phi}{}^{(\mathrm{SM})}F_j)(\overset{+}{F}_j\Phi^{(\mathrm{SM})}) + \Big[\delta_F\sum_j(\overset{+}{\Phi}{}^{(\mathrm{SM})}F_j)(\overset{+}{\Phi}{}^{(\mathrm{SM})}F_j) + \mathrm{h.c.}\Big], \tag{12}$$

where $m_\pm^{(0)2}$ and $m_F^{(0)2}$ are parameters that have dimensions of mass and $\beta_\pm$, $\gamma_\pm$, δ_S, β_F, γ_F, and δ_F are the dimensionless scalar-interaction coupling constants. Spontaneous symmetry breaking for the potential (11) gives rise to the mass matrix of the lower scalar leptoquarks $(S_2^{(+)}, \overset{+}{S}{}_2^{(-)})$ that has the form

$$M = \begin{pmatrix} M_{11} & M_{12} \\ M_{21} & M_{22} \end{pmatrix} = \begin{pmatrix} m_+^2 + \gamma_+\eta^2/2 & \overset{+}{\delta}_S\eta^2/2 \\ \delta_S\eta^2/2 & m_-^2 + \gamma_-\eta^2/2 \end{pmatrix}, \tag{13}$$

where $m_\pm^2 = m_\pm^{(0)2} + \beta_\pm\eta^2/2$ are the squares of the masses of the upper scalar leptoquarks and $\eta = \sqrt{\eta_2^2 + \eta_3^2}$ is the vacuum expectation value in the Standard Model.

Likewise, the masses of the scalar gluons are determined by the potential (12). The expression for the squares of the masses has the form

$$m_{\phi_1,\phi_2}^2 = m_{F_1}^2 + \gamma_F\eta^2/2 \pm \delta_F\eta^2, \tag{14}$$

where $m_{F_1}^2 = m_F^{(0)2} + \beta_F\eta^2/2$ is the square of the mass of the charged upper scalar gluon.

For real values of δ_S in (13), the masses of the scalar leptoquarks of electric charge 2/3 and the mixing angle are given by

$$m_{1,2}^2 = M_{11,22} \mp \Big[2M_{12}\cos\theta\sin\theta + (M_{11} - M_{22})\sin^2\theta\Big], \tag{15}$$

$$\tan 2\theta = -2M_{12}/(M_{11} - M_{22}). \tag{16}$$

For the ground state of the scalar fields to be stable, their scalar potential $V(\Phi^{(\mathrm{SM})}, S, F)$ must be positive definite; that is,

$$V(\Phi^{(\mathrm{SM})}, S, F) \equiv V_m(\Phi^{(\mathrm{SM})}, S) + V_m(\Phi^{(\mathrm{SM})}, F) + V_{\mathrm{SM}}(\Phi^{(\mathrm{SM})}) + \sum_{+,-}\lambda_\pm(\overset{+}{S}{}^{(\pm)}S^{(\pm)})^2 + \lambda_F\left(\sum_j(\overset{+}{F}_jF_j)\right)^2 + \sum_{+,-}\lambda_{S^{(\pm)}F}(\overset{+}{S}{}^{(\pm)}S^{(\pm)})\sum_j(\overset{+}{F}_jF_j) > 0, \tag{17}$$

where $V_{\mathrm{SM}}(\Phi^{(\mathrm{SM})}) = \lambda_{\mathrm{SM}}(\overset{+}{\Phi}{}^{(\mathrm{SM})}\Phi^{(\mathrm{SM})} - \eta^2/2)^2$ is the scalar potential in the Standard Model and $\lambda_{\mathrm{SM}} > 0$, $\lambda_\pm > 0$, $\lambda_F > 0$, and $\lambda_{S^{(\pm)}F} \geq 0$ are dimensionless coupling constants of scalar interactions. For the condition in (17) to be valid, it is necessary to require that the coupling constants in the potentials (11), (12), and (17) satisfy the inequalities

$$\beta_\pm > 0, \quad \beta_\pm + \gamma_\pm > 0, \quad |\delta_S| < \sqrt{(\beta_+ + \gamma_+)(\beta_- + \gamma_-)}, \tag{18}$$

$$\beta_F > -2\sqrt{\lambda_{\mathrm{SM}}\lambda_F}, \quad \beta_F + \gamma_F > 2|\delta_F| - 2\sqrt{\lambda_{\mathrm{SM}}\lambda_F}, \tag{19}$$

which must be taken into account in varying the parameters of the model.

In what follows, we consider

$$m_1, m_2, m_{\phi_2}, \gamma_+, \gamma_-, \delta_S, \gamma_F, \delta_F \qquad (20)$$

as adjustable parameters and determine the masses m_+, m_-, m_{ϕ_1}, and m_{F_1} and the mixing angle θ from Eqs. (13)–(16). The values obtained for these masses and for this mixing angle are then used to calculate the contributions in (2)–(4) and in (8)–(10) to the parameters S, T, and U from, respectively, the doublets of scalar leptoquarks and the doublets of scalar gluons. Note that perturbation theory is applicable only if the coupling constants appearing in the potentials (11), (12), and (17) are not overly great, which constrains the allowed domain of the masses and the mixing angle in (2)–(4) and (8)–(10). In the following, we assume that all coupling constants in expressions (11), (12), and (17) do not exceed in absolute value some preset value $\lambda_{\max}$ at which perturbation theory is still valid. In our numerical analysis, we restrict our consideration to values of $\lambda_{\max}$ in the range $\lambda_{\max} = 1.0$–4.0, this leading to reasonable values of the perturbation-theory parameter: $\lambda_{\max}/4\pi = 0.1$–$0.3$.

4. NUMERICAL ANALYSIS AND DISCUSSION OF THE RESULTS

In our numerical analysis of the contributions in (2)–(4) and (8)–(10) to the parameters S, T, and U from, respectively, the scalar-leptoquark doublet (1) and the scalar-gluon doublet (7), we use, for these parameters, the experimental values $S_{\text{new}}^{\text{expt}}$, $T_{\text{new}}^{\text{expt}}$, and $U_{\text{new}}^{\text{expt}}$ that are assumed to be determined by new physics. The latest experimental data [11] yield

$$\begin{aligned} S_{\text{new}}^{\text{expt}} &= -0.03 \pm 0.11(-0.08), \qquad (21)\\ T_{\text{new}}^{\text{expt}} &= -0.02 \pm 0.13(+0.09),\\ U_{\text{new}}^{\text{expt}} &= 0.24 \pm 0.13(+0.01), \end{aligned}$$

where the central values correspond to the Higgs boson mass of $m_H = 115$ GeV and the values given parenthetically are the respective shifts for $m_H = 300$ GeV.

By varying the parameters in (20), we minimize the functional of χ^2 defined as

$$\chi^2 = \frac{(S - S_{\text{new}}^{\text{expt}})^2}{(\Delta S)^2} + \frac{(T - T_{\text{new}}^{\text{expt}})^2}{(\Delta T)^2} + \frac{(U - U_{\text{new}}^{\text{expt}})^2}{(\Delta U)^2},$$

where $S = S^{(\text{LQ})} + S^{(F)}$, $T = T^{(\text{LQ})} + T^{(F)}$, and $U = U^{(\text{LQ})} + U^{(F)}$ are the sums of the contributions in (2)–(4) and (8)–(10) to the parameters S, T, and U from the scalar leptoquarks and scalar gluons and ΔS, ΔT, and ΔU are the experimental errors from (21).

In order to determine the effect of the scalar leptoquarks and scalar gluons on the parameters S, T, and U, we vary the masses of these particles without allowing them to fall below some lower limit $m_{\text{scalar}}^{\text{lower}}$:

$$m_1, m_2, m_\pm, m_{F_1}, m_{\phi_1}, m_{\phi_2} \geq m_{\text{scalar}}^{\text{lower}}. \qquad (22)$$

We sought a minimum of χ^2 with respect to variations in the adjustable parameters (20) under the condition in (22) and studied the resulting minimum value $\chi^2_{\min}$ as a function of the lower limit on the particle masses, $m_{\text{scalar}}^{\text{lower}}$, and the upper limit on the coupling constants, $\lambda_{\max}$.

For the case where there is no mixing of leptoquarks ($\theta = 0$), the minimum value $\chi^2_{\min}(m_{\text{scalar}}^{\text{lower}}, \lambda_{\max})$ as a function of the lower limit on the scalar-particle masses, $m_{\text{scalar}}^{\text{lower}}$, is shown in Figs. 1 and 2 for, respectively, $m_H = 115$ and 300 GeV at $\lambda_{\max} =$ (curve *1*) 1.0 and (curve *2*) 4.0. Our analysis reveals that $\chi^2_{\min}$ depends only weakly on θ, showing a shallow minimum at $\theta = 0$. For the Higgs boson mass of $m_{\text{H}} = 115$ (300) GeV, the horizontal line in Fig. 1 (Fig. 2) indicates the level of $\chi^2_{\text{SM}} = 3.5$ (5.0) at which zero values of the parameters S, T, and U in the Standard Model agree with the data in (21).

As can be seen from Figs. 1 and 2, the experimental data in (21) admit lower limits on the scalar-leptoquark and scalar-gluon masses within a broad range between large values at which the respective contributions to S, T, and U are small and values as small as 1 TeV or even below this. It is interesting to note that, both at $m_H = 115$ GeV and at $m_H = 300$ GeV, the agreement with the experimental data in (21) at lower masses of the scalar particles is better than in the Standard Model. At $m_H = 115$ GeV (Fig. 1), this improvement is observed for $m_{\text{scalar}}^{\text{lower}} < 400$ GeV, whereas, at $m_H = 300$ GeV, this is so over the entire region below 1 TeV (Fig. 2), the best fit in the latter case being attained for $m_{\text{scalar}}^{\text{lower}} < 400$ GeV as well. The predictions of the model involving light scalar leptoquarks of mass as small as 300 GeV ($\lambda_{\max} = 4.0$) agree with the data in (21) at a level of $\chi^2 < 3.1$ (3.2) for $m_H = 115$ (300) GeV, whereas the Standard Model predictions agree with these data at a level of $\chi^2_{\text{SM}} = 3.5$ (5.0). In this case, the mass of the lightest scalar gluon, m_{ϕ_2}, is expected to be below 850 (720) GeV.

The fact that, at $m_H = 300$ GeV, the leptoquark model describes the data better than the Standard Model over the range 400 GeV $\leq m_{\text{scalar}}^{\text{lower}} \leq 1$ TeV is due to significant contributions of the scalar leptoquarks and scalar gluons to the parameters S and

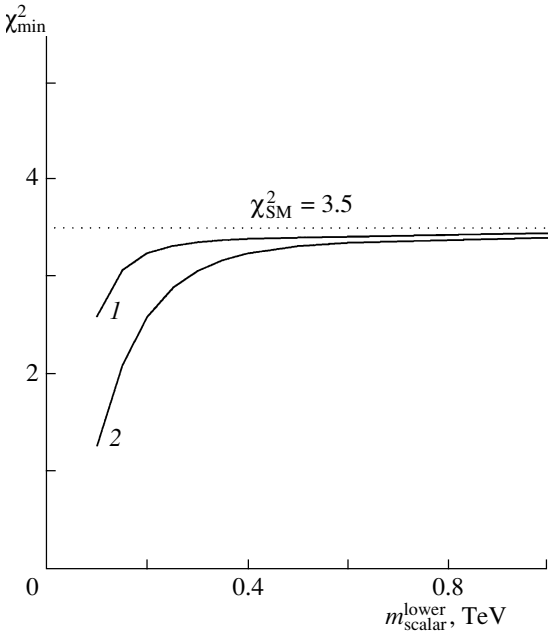

Fig. 1. Minimum value of χ^2, $\chi^2_{\min}(m^{\text{lower}}_{\text{scalar}}, \lambda_{\max})$, as a function of the lower limit on the scalar-leptoquark and scalar-gluon masses, $m^{\text{lower}}_{\text{scalar}}$, at the Higgs boson mass of $m_H = 115$ GeV for upper limits of $\lambda_{\max} =$ (curve *1*) 1.0 and (curve *2*) 4.0 on the coupling constant.

T, their contributions to the parameter U being negligible. At lighter scalar leptoquarks, the leptoquark contribution to the parameter U increases, being positive; concurrently, the leptoquark contributions to the parameters S and T cancel to a considerable extent the respective contributions of scalar gluons. Owing to this, the description of the data in (21) within the model under study becomes much better in the region $m^{\text{lower}}_{\text{scalar}} < 400$ GeV than the respective description within the Standard Model, this being so both at $m_H = 300$ GeV and at $m_H = 115$ GeV.

By way of example, we indicate that, at $\theta = 0$, the contributions of the scalar leptoquarks and scalar gluons having the masses

$$m_{S_1^{(+)}} = 330\ \text{GeV}, \quad m_{S_1^{(-)}} = 430\ \text{GeV}, \qquad (23)$$
$$m_{S_1} = 250\ \text{GeV}, \quad m_{S_2} = 250\ \text{GeV},$$
$$m_{F_1} = 850\ \text{GeV}, \quad m_{\phi_1} = 1040\ \text{GeV},$$
$$m_{\phi_2} = 770\ \text{GeV}$$

are given by

$$S^{(\text{LQ})} = -0.07, \quad T^{(\text{LQ})} = 2.03, \quad U^{(\text{LQ})} = 0.02,$$
$$S^{(F)} = 0.03, \quad T^{(F)} = -2.05, \quad U^{(F)} = -3 \times 10^{-3},$$
$$S = -0.04, \quad T = -0.02, \quad U = 0.02.$$

These values agree with (21) at $m_H = 115$ GeV at the level $\chi^2 = 2.9$ (the respective SM value $\chi^2 = 3.5$).

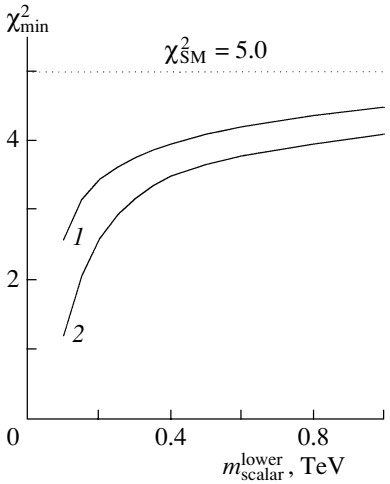

Fig. 2. As in Fig. 1, but for $m_H = 300$ GeV.

For

$$m_{S_1^{(+)}} = 430\ \text{GeV}, \quad m_{S_1^{(-)}} = 430\ \text{GeV}, \qquad (24)$$
$$m_{S_1} = 250\ \text{GeV}, \quad m_{S_2} = 250\ \text{GeV},$$
$$m_{F_1} = 650\ \text{GeV}, \quad m_{\phi_1} = 890\ \text{GeV},$$
$$m_{\phi_2} = 550\ \text{GeV},$$

we obtain

$$S^{(\text{LQ})} = -0.17, \quad T^{(\text{LQ})} = 3.39, \quad U^{(\text{LQ})} = 0.04,$$
$$S^{(F)} = 0.05, \quad T^{(F)} = -3.32, \quad U^{(F)} = -0.01,$$
$$S = -0.12, \quad T = 0.07, \quad U = 0.03.$$

At $m_H = 300$ GeV, these values agree with the data in (21) at a level of $\chi^2 = 2.9$, which is to be compared with the respective value of $\chi^2 = 5.0$ in the Standard Model.

The masses of the lightest scalar leptoquarks in (23) and (24) are chosen in the domain allowed by the constraints obtained from searches for scalar leptoquarks in direct production experiments. The most stringent constraint of this type comes from experiments that sought a direct production of pairs of scalar leptoquarks. For first-generation scalar leptoquarks, such experiments yield [11]

$$m_{\text{LQ}} > 225, 204, \text{ and } 79\ \text{GeV} \qquad (25)$$

under the assumption that the branching fraction for leptoquark decay into a quark and an electron is $B(eq) = 1, 0.5$, and 0, respectively.

Since the scalar-particle masses in the model under consideration are generated by the Higgs mechanism, the fermionic coupling constants of the scalar leptoquarks and the scalar gluons are proportional to the ratios of the fermion masses to the Standard Model vacuum expectation value η (general expressions for the interactions of the scalar doublets with fermions are given in [10]). The respective coupling

constants are small for all quarks, with the exception of the t quark, for which they are significant. For this reason, scalar leptoquarks decay predominantly via modes involving a t quark, the probability of first-generation-fermion production in leptoquark decay is small: $0 < B(eq) \ll 0.5$. Thus, the lower limit on the masses m_{S_1} and m_{S_2} of the lightest scalar leptoquarks must be close to the last value in (25), the scalar-leptoquark masses $m_{S_1^{(-)}}$ and $m_{S_1^{(+)}}$ then being consistent with the other constraints from direct searches for leptoquarks (this is so for the second and third generations inclusive).

It should also be noted that the existence of the light scalar leptoquarks is compatible with indirect constraints coming from decays of the type $K_L^0 \to \mu e$. Since the coupling of the scalar leptoquarks to the d and s quarks is small, the scalar-leptoquark contribution to the probability of the decay $K_L^0 \to \mu e$ is sufficiently small for the available stringent constraint $\mathrm{Br}(K_L^0 \to \mu e) < 4.7 \times 10^{-12}$ on the branching fraction for this decay mode to be satisfied even for relatively light scalar leptoquarks.

Experimental data on Z-boson decays give a lower limit of about 400 GeV on the scalar-leptoquark mass [16], provided that the leptoquarks are degenerate in mass.

Thus, both data on the direct production of scalar leptoquarks and indirect constraints on their masses coming from decays of the type $K_L^0 \to \mu e$ and Z-boson decays do not rule out at present the existence of relatively light scalar leptoquarks. Moreover, not only does our analysis of the parameters S, T, and U of radiative corrections admit the existence of such particles, but it also favors their lighter masses in the region $m_{\mathrm{scalar}}^{\mathrm{lower}} < 400$ GeV. In view of the aforementioned features of scalar-doublet interactions with fermions, it is of interest to seek scalar leptoquarks and scalar gluons in processes involving a heavy quark (predominantly, a t quark) at LHC.

5. CONCLUSION

Within the minimal model based on four-color symmetry and the Higgs mechanism of quark- and lepton-mass generation, we have performed an analysis of the contributions to the parameters S, T, and U of radiative corrections from scalar leptoquarks and scalar gluons.

It is shown that current experimental data on the parameters S, T, and U admit the existence of relatively light (lighter than 1 TeV) scalar leptoquarks and scalar gluons; moreover, the model involving very light leptoquarks (that is, of mass less than 400 GeV) provides a better fit to experimental data on the parameters S, T, and U than the Standard Model.

In particular, we have shown that the existence of scalar leptoquarks having masses in the region $m_{\mathrm{scalar}}^{\mathrm{lower}} < 300$ GeV is compatible with current data on the parameters S, T, and U at a level of $\chi^2 < 3.1$ (3.2) for $m_H = 115$ (300) GeV versus $\chi^2_{\mathrm{SM}} = 3.5$ (5.0) for the Standard Model fit. In this case, the mass of the lightest scalar gluon is expected to be below 850 (720) GeV.

Since the coupling of the doublets of scalar leptoquarks and scalar gluons to the t quark is not small, these particles can play a significant role in processes involving a t quark at LHC.

ACKNOWLEDGMENTS

This work was supported in part by the Russian Foundation for Basic Research (project nos. 00-02-17883, 02-02-06626).

REFERENCES

1. J. C. Pati and A. Salam, Phys. Rev. D **10**, 275 (1974).
2. A. D. Smirnov, Phys. Lett. B **346**, 297 (1995).
3. A. D. Smirnov, Yad. Fiz. **58**, 2252 (1995) [Phys. At. Nucl. **58**, 2137 (1995)].
4. R. Foot, Phys. Lett. B **420**, 333 (1998).
5. R. Foot and G. Filewood, Phys. Rev. D **60**, 115002 (1999).
6. T. L. Yoon and R. Foot, hep-ph/0105101; Phys. Rev. D **65**, 015002 (2002).
7. A. Blumhofer and B. Lampe, Eur. Phys. J. C **7**, 141 (1999).
8. W. Buchmüller, R. Rückl, and D. Wyler, Phys. Lett. B **191**, 442 (1987).
9. J. L. Hewett and T. G. Rizzo, Phys. Rev. D **56**, 5709 (1997).
10. A. V. Povarov and A. D. Smirnov, Yad. Fiz. **64**, 78 (2001) [Phys. At. Nucl. **64**, 74 (2001)].
11. D. E. Groom *et al.* (Particle Data Group), Eur. Phys. J. C **15**, 1 (2000); http://pdg.lbl.gov
12. M. E. Peskin and T. Takeuchi, Phys. Rev. D **46**, 381 (1992).
13. A. D. Smirnov, Phys. Lett. B **431**, 119 (1998).
14. A. D. Smirnov, Yad. Fiz. **64**, 367 (2001) [Phys. At. Nucl. **64**, 318 (2001)].
15. A. D. Smirnov, Phys. Lett. B **531**, 237 (2002).
16. J. K. Mizukoshi, O. J. P. Éboli, and M. C. González-García, Nucl. Phys. B **443**, 20 (1995).

Translated by R. Rogalyov

Physics of Atomic Nuclei, Vol. 66, No. 12, 2003, pp. 2214–2223. Translated from Yadernaya Fizika, Vol. 66, No. 12, 2003, pp. 2266–2275.

ELEMENTARY PARTICLES AND FIELDS
Theory

Searches for Self-Consistent Vacuum States of a Gluon Field

V. V. Vladimirsky

Institute of Theoretical and Experimental Physics,
Bol'shaya Cheremushkinskaya ul. 25, Moscow, 117259 Russia

Received September 23, 2002; in final form, February 7, 2003

Abstract—A theory of a non-Abelian gauge field is considered on the basis of an effective Lagrangian that possesses the property of asymptotic freedom. In this theory, the confinement–deconfinement phase transition has a nontrivial scenario according to which the two phases may exist in the same spacetime region. In the low-momentum region $|p^2| < \Lambda^2_{\mathrm{QCD}}$, we have a confining regime in the presence of a gluon condensate, while, in the high-momentum region $|p^2| \gg \Lambda^2_{\mathrm{QCD}}$, perturbative QCD holds. An iterative scheme for refining parameters of the effective Lagrangian is outlined. © *2003 MAIK "Nauka/Interperiodica".*

1. INTRODUCTION

In order to describe nonperturbative effects within QCD, it is desirable to have an appropriate model for the vacuum state of a gauge field. In developing such a scheme, it is necessary to rely on the Yang–Mills equations for the $SU(3)$ color group and, at the same time, to include, in the theory, the generally accepted concepts of a running coupling constant and of a nonzero expectation value of the squared gluon field (gluon condensate), $\langle F^2 \rangle > 0$. We will employ an effective Lagrangian in constructing a basic formalism and invoke, in describing a condensate, the model of a gluon field in non-Abelian configurations that is constant in time and space, additionally admitting chaotic fluctuations. The possibility that a condensate may arise in Yang–Mills theories owing to quantum corrections was first indicated by the authors of [1–3], who used the model of a covariantly constant field; as a matter of fact, this model reduces to an Abelian configuration of potentials: a constant field strength is achieved owing to a linear dependence of the potentials on coordinates. In the present study, we consider a different configuration: the potentials of the condensate are constant on average, but their components are noncommutative, which is the fact that leads to the emergence of a constant field strength (this is a mechanism that has no analogs in Abelian theories).

In a naive treatment, the constant-condensate model corresponds to the breakdown of gauge symmetry and Lorentz invariance, but, if states in which the field is shifted as $V^a_\mu \to A^a_\mu + w^a_\mu$, where A^a_μ is a constant field and w^a_μ is a small addition, are considered as stationary-phase points in an infinite-dimensional Fock space, this difficulty can be removed. Each solution associated with classical values of the vector V^a_μ must be considered together with all solutions that can be obtained from it by means of a gauge transformation. Integration over the color group then yields a state that possesses a gauge symmetry. The problem of restoring the invariance of such a vacuum under Lorentz transformations is more involved, since the Lorentz group is noncompact. If, however, an effective Lagrangian that leads to a spontaneous emergence of a condensate possesses the property of invariance under Lorentz transformations, then one solution goes over to another upon a change of the reference frame, so that the entire ensemble of admissible solutions can be considered to be invariant. As a matter of fact, the restoration of gauge symmetry does not require explicitly performing integration over the color group either. It is sufficient to postulate that, by a physical vacuum, one should mean the entire set of solutions of minimum energy that satisfy the requirement that the effective action be stationary. With these provisos, the physical vacuum treated as an ensemble of constant solutions possesses the following properties: $\langle F_{\mu\nu} \rangle = 0$ and $\langle F^2 \rangle \neq 0$. In the limit $w_\mu \to 0$, there are no transitions between individual components of the ensemble; each component can be separately considered as a formal solution featuring a spontaneous breakdown of symmetry, and this is quite convenient in intermediate calculations. In an actual system, where $w_\mu \neq 0$, transitions of course proceed, and it is owing to them that the system in question occurs in a color-singlet state.

From the aforesaid, it follows that the effective Lagrangian must be a scalar function of group invariants composed of field components and their derivatives. The linearized field equations must not have tachyon solutions. At the same time, we admit the dependence of the condensate (constant field components) on the

1063-7788/03/6612-2214$24.00

type of field being considered. In particular, we admit the dependence of the condensate on the gluon off-shellness in considering single-gluon excitations. For the sake of brevity, this construction will be referred to as a "floating condensate." Within this approach, there is of course a logical difficulty: the constant field of a condensate is not quantized, and it is not clear how the momentum of the propagating gluon may affect the magnitude of this field. A preliminary answer to this question is the following: in a physical vacuum, there are condensate fields of different strength, and the gluon chooses, among them, those that yield a minimum of energy at a given momentum.

The Yang–Mills Lagrangian [4] was obtained as the simplest Lagrangian that leads to a local gauge invariance; however, the formalism of quantum field theory admits a wider class of Lagrangians that satisfy this requirement. This class includes effective Lagrangians that can be obtained from the original Yang–Mills Lagrangian by including quantum corrections. In electrodynamics, this was demonstrated in [5]. An attempt at implementing a similar program for a non-Abelian theory is made here. In electrodynamics, a gauge field is strictly neutral, but, in a Yang–Mills theory, it carries a group charge. In the theory of a charged massless vector field, there are intrinsic inconsistencies: in a magnetic field, there arise instabilities (tachyons). The use of Lagrangians that lead to asymptotic freedom makes it possible to circumvent this difficulty and to obtain confinement. In contrast to what we have in electrodynamics, these modifications to the Lagrangian lead to radical changes in the properties of the theory.

In analyzing renormalizations within QCD, it is usually assumed that the effective coupling constant g remains finite in the infrared region. Here, use is made of an alternative scenario: as the gluon momentum decreases, g reaches infinity, whereupon there arises a condensate, which ensures confinement. In addition to a component that is constant in time and space, the condensate involves stochastic fluctuations.

The term "effective action" is treated below in a wider sense than is usually done: by it, we will imply a dimensionless scalar generating functional that determines correlation functions for vacuum fields. By the self-consistency of an effective action, we mean the following: treating it as a bare action functional, we determine quantum corrections, remove all divergences (both ultraviolet and infrared ones) by means of conventional renormalization procedures, and compare the resulting effective action with the original one. If, for a reasonable choice of a finite number of parameters, the results can be matched, the effective action is thought to be self-consistent. Forms that are used below for the effective action are nonlocal (more precisely, they are quasilocal), since the concept of asymptotic freedom does not fit in the usual field-theory formalism, where the parameters of the Lagrangian are fixed. Operators that represent the field and its derivatives may appear in the effective action not only in the form of polynomials but also in more intricate functional combinations.

The ensuing exposition is organized as follows. An iterative procedure for approaching a self-consistent effective action is given in Section 2. There, the possibility is also considered for removing instabilities of fluctuations of a non-Abelian vector field in a constant magnetic field (that is, for eliminating tachyons). Section 3 is devoted to refining the equations of motion that follow from the effective action and to studying their stability and the structure of the condensate. Quantum corrections are calculated in Section 4 for the simplest states. In Section 5, the proposed approach is generalized to the case of multigluon states. The results of the present study are discussed in Section 6.

2. BARE AND EFFECTIVE ACTION FUNCTIONALS

The classical equations for the gluon field,

$$D_\mu^{ac} F_{\mu\nu}^c = -J_\nu^a, \tag{2.1}$$

$$D_\mu^{ac} = \delta^{ac}\partial_\mu + g c^{abc} V_\mu^b, \tag{2.2}$$

$$F_{\mu\nu}^a = \partial_\mu V_\nu^a - \partial_\nu V_\mu^a + g c^{abc} V_\mu^b V_\nu^c, \tag{2.3}$$

can be obtained from the classical Lagrangian

$$S = -\frac{1}{4}\int d^4x F_{\mu\nu}^a F_{\mu\nu}^a = \int d^4x L^{(0)}, \tag{2.4}$$

where $F_{\mu\nu}^a$ is the field-strength tensor; D_μ^{ac} is a covariant derivative; J_ν^a is a current; g is a coupling constant; V_μ^a stands for the field potentials; $a, b, c = 1, 2, ..., 8$ are group indices of the $SU\{3\}$ group; and $\mu, \nu = 0, 1, 2, 3$ are Lorentz indices. If use is made of a conventional quantization scheme, it is necessary to introduce, in addition, gauge-fixing terms; the ghost Lagrangian L_{FP}; and a term that ensures coupling to matter currents or external currents, $J_\mu^a V_\mu^a$.

For a first step in constructing an effective Lagrangian, we employ the results presented in [6], where an effective Lagrangian was found in the one-loop approximation at zero field momentum. The present analysis relies on an iterative procedure that is not very common: on the basis of the equations that follow from the classical Yang–Mills Lagrangian $L^{(0)}$, one determines the quantum correction and the Lagrangian $L^{(1)}$ and, thereupon, treats $L^{(1)}$

as a classical Lagrangian, determining the next-approximation Lagrangian $L^{(2)}$ in the same way. Such approximations can be continued ceaselessly, but, even at the first steps, conditions for a phase transition to a confining state are realized, which is accompanied by the emergence of asymptotic freedom at high q^2. Upon going over from $L^{(0)}$ to $L^{(1)}$, the problem of tachyon branches in the Yang–Mills equations arises at nonzero values of the average field. The energy of a classical Yang–Mills field has the only minimum at $F^a_{\mu\nu} = 0$. As soon as one introduces external currents shifting the field value, the system develops an instability, with the result that there appear tachyons [7]. A totally different behavior of the system is possible if a nonzero average field emerges spontaneously upon a change in the Lagrangian at $J^a_\mu = 0$. By way of example, we indicate that, if the energy density in a stationary state, $-L^{(1)}$, has a minimum at $F^2 \neq 0$, the following relations hold in the vicinity of the minimum: $\partial L^{(1)}/\partial F^2 = 0$ and

$$-L^{(1)} \approx -\frac{1}{2}\left.\frac{\partial^2 L^{(1)}}{\partial (F^2)^2}\right|_{F^2=F^2_{\min}} (F^2 - F^2_{\min})^2 + \text{const}. \tag{2.5}$$

For $\partial^2 L^{(1)}/\partial (F^2)^2\big|_{F^2=F^2_{\min}} < 0$, we obtain a stable energy valley, so that tachyons do not arise. It is precisely the situation that results from a calculation of the one-loop effective Lagrangian [6].

The distinction between the stability of the external-current-induced shifted field and the stability of a spontaneously arising field can be traced by considering the following simple example. Suppose that the constant field component is specified by the potentials

$$A^1_1 = A^2_2 = A^3_3 = A, \tag{2.6}$$

the remaining being equal to zero, and that the fluctuations are given by

$$w^1_1 = -w^2_2 = w\cos kx_3, \quad w^1_2 = w^2_1 = w\sin kx_3. \tag{2.7}$$

The sum of the squares of spatial field components for the potentials $A^a_\mu + w^a_\mu$ has the form

$$\left(F^a_{ij}\right)^2 = 3A^4 + 2(2Ak + k^2)w^2 + w^4. \tag{2.8}$$

For $w \ll A$, there is a momentum region $(-2A < k < 0)$ where $(F^a_{ij})^2 < 3A^4$—that is, where the energy density of the classical Yang–Mills field is reduced. The equations that follow from the classical action functional (2.4) lead to the emergence of tachyons in this region. In the case of the Lagrangian in (2.5), there is no such reduction of the energy density, so that tachyons cannot arise there. The expansion of this Lagrangian in a power series in terms of the variable $w^a_\mu \sim w$ in the vicinity of the minimum $F^2_{\min} = 3A^4$ begins from w^4—that is, the quadratic term is absent. It follows that, for the fluctuations considered above, as well as for some other fluctuations, it is impossible to construct linearized equations and a conventional Green's function. In such a system, gluons do not propagate—there occurs confinement.

In all probability, the inclusion of multiloop diagrams of perturbation theory does not lead to qualitative changes in the situation: the dependence of L_{eff} on F^2 changes, but a stable minimum of the energy density survives.

Let us consider in greater detail the equations for the shifted fields $F^a_{\mu\nu} = B^a_{\mu\nu} + f^a_{\mu\nu}, V^a_\mu = A^a_\mu + w^a_\mu$ in the case of the effective Lagrangian $L(F^2, p^2)$; here, $F^2 = F^a_{\mu\nu}F^a_{\mu\nu}$, $\partial_\lambda B^a_{\mu\nu} = \partial_\lambda A^a_\mu = 0$, and p^2 is the square of the momentum of gluons (field fluctuations). We admit the dependence of $B^a_{\mu\nu}$ on p^2. For linearized equations, this is a conventional function of one variable. We expand $L(F^2, p^2)$ in a power series in terms of the variable $F^2 - B^2$ to the second-order term inclusive; that is,

$$L(F^2, p^2) \approx L(B^2, p^2) + L'(B^2, p^2)(F^2 - B^2) + \frac{1}{2}L''(B^2, p^2)(F^2 - B^2)^2, \tag{2.9}$$

where

$$L' = \left.\frac{\partial L}{\partial F^2}\right|_{F^2=B^2}, \quad L'' = \left.\frac{\partial^2 L}{(\partial F^2)^2}\right|_{F^2=B^2}.$$

Varying the Lagrangian, we arrive at the equation

$$L' D^{ac}_\mu F^c_{\mu\nu} + L'' D^{ac}_\mu F^c_{\mu\nu}(F^2 - B^2) = -4J^a_\nu. \tag{2.10}$$

Two regimes are distinguishable in solutions to this equation: these are the usual region $B^2 = 0$, $L' \neq 0$ (deconfinement) and the region $B^2 > 0$, where a condensate emerges spontaneously and where confinement occurs. In the last case, the equality $L' = 0$ and the inequality $L'' < 0$ inevitably hold. In the region of deconfinement, where $F^a_{\mu\nu} = f^a_{\mu\nu}$, the second term in Eq. (2.10) does not contribute in the linear approximation; therefore, the gluon propagator differs from the usual one only by the factor $-(4L')^{-1}$. Briefly, the situation can be characterized in the following way: upon introducing a constant external current in the classical Yang–Mills Lagrangian, the respective equations lose stability and become unrenormalizable. In a theory based on an effective Lagrangian, stability and renormalizability survive in the presence

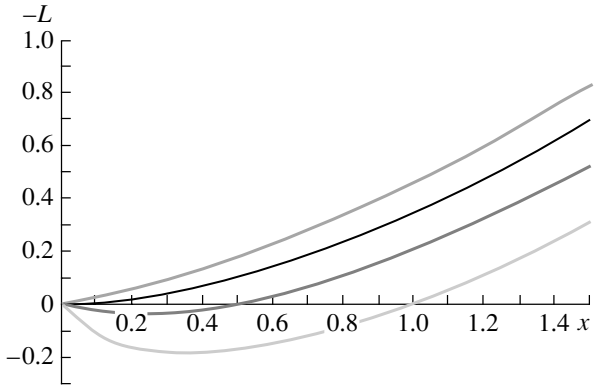

Fig. 1. Energy as a function of $x \sim F^2$ at various values of $y \sim p^4$: $y = 0, 0.5, 1.0, 1.5$ (from bottom to top).

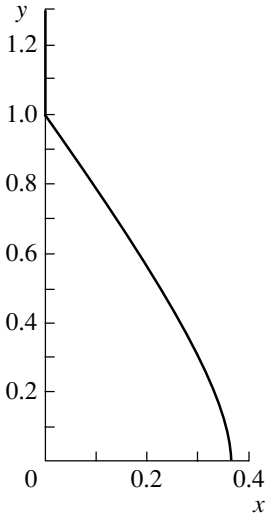

Fig. 2. Gluon-momentum dependence of $x \sim F^2$ for a floating condensate.

of an external current, but a spontaneous magnetization arises at low momenta. In view of this distinction between stability for the classical Yang–Mills Lagrangian and stability for an effective Lagrangian that exhibits the property of asymptotic freedom, it is better to choose a model effective Lagrangian as a starting point for an iterative process. For the input Lagrangian, one can take that which was proposed in [8] or a similar functional that leads to stable solutions.

Let us consider the model effective Lagrangian

$$L = -\frac{1}{4}F^2 t, \tag{2.11}$$

where the evolution variable has the simplest form

$$t = \frac{1}{2}\ln\frac{\gamma F^2 + q^4}{\Lambda^4} = \frac{1}{2}\ln(x+y). \tag{2.12}$$

Here, γ is a numerical factor (under the simplest assumptions, $\gamma = 4$), q is the gluon momentum, Λ is a dimensional parameter of the theory, and $x = \gamma F^2/\Lambda^4$ and $y = q^4/\Lambda^4$ are dimensionless variables. In the asymptotic region specified by the inequalities $y \gg 1$ and $y \gg x$, this Lagrangian leads to the usual dependence of α_s on q^2. In this approximation, the dependence of α_s on the sign of q^2 is not taken into consideration. This Lagrangian is consistent with dimensionality considerations and reduces to the well-known effective Lagrangians of the one-loop approximation in the limiting cases of $x \ll y$ and $y \ll x$. The factor γ reflects the distinctions between the dimensional constants defined in terms of the variables q^4 and F^2. The dependence of L on the variable x at various values of y is illustrated in Fig. 1. Different expressions for t are also possible, but we always assume that t is a function of invariant quantities. Formulas (2.11) and (2.12) provide a recipe for determining the density of an effective Lagrangian for a system formed by a constant condensate and one gluon of momentum q. An extension of this approach to multigluon states will be discussed in Section 5.

For the model Lagrangian in (2.11), we will now trace the confinement–deconfinement transition versus the parameter $y = q^4/\Lambda^4$. In the region $t > 0$, the minimum of the classical energy density, which is equal to $-L$, is attained at $F^2 = 0$, whence it follows that, at $y > 1$, the state in which $\langle F^a_{\mu\nu}\rangle = 0$ can be treated as the ground state—that is, a classical vacuum. If $y < 1$, the energy density reaches a minimum at a nonzero field strength, taking a negative value there. Rewriting L in terms of the dimensionless variables x and y as

$$L = -\frac{\Lambda^4}{8\gamma}x\ln(x+y), \tag{2.13}$$

we can easily find the relation between $x_{\min}$ and y. Indeed, the necessary condition for the existence of a nontrivial minimum of the energy density then has the form

$$\ln(x+y) + \frac{x}{x+y} = 0. \tag{2.14}$$

For $y > 1$, this condition has no solutions, but, for $0 \le y < 1$, there are solutions, which can be expressed as the dependence of $x_{\min}$ on y in the parametric form

$$x_{\min} = -z\ln z, \quad y = z - x_{\min}, \tag{2.15}$$

where the parameter z varies within the range $e^{-1} < z < 1$. The condition of stability of the minimum is satisfied. At $|q^2| = \Lambda^2$, the confinement–deconfinement transition is that of the second-order type: the energy density is continuous, but its derivatives undergo discontinuities. In particular, $\partial L/\partial F^2 = 0$ at $x = x_{\min}$ in the confining region, this corresponding

to an indefinitely large coupling constant; this relation ($\partial L/\partial F^2 = 0$) holds at the phase-transition point as well. At higher momenta corresponding to $y > 1$, we have $\partial L/\partial F^2 = -(1/8)\ln y$ at $x = 0$. Admitting the concept of a floating condensate—$B^2 = B^2(q^4)$—we can restrict ourselves to studying the effective Lagrangian in the vicinity of the point $x = 0$ for $y > 1$ and in the vicinity of the point $x = x_{\min}$ for $0 \le y \le 1$ (see Fig. 2) instead of examining it in the entire space of the variables x and y.

Presently, there are indications of the finiteness of the gluon coupling constant at the boundary of confinement [9]. In this case, a first-order phase transition seems more natural. Despite this circumstance, we will try to explore the possibility of obtaining self-consistent solutions on the basis of the Lagrangian specified by Eqs. (2.11) and (2.12), in which case there can occur the passage of the evolution variable t through zero and an indefinite growth of the coupling constant. If the coupling constant does not reach infinity, it is natural to expect within perturbation theory that, as one approaches the infrared limit, the function α_s^{-1} begins to decrease more slowly with increasing number of loops. The numerical investigation of this function to the four-loop level in [10] yielded an opposite result, and this provides an additional motivation for studying the scenario outlined in the present article above.

3. STABILITY, FIELD EQUATIONS, AND STRUCTURE OF THE CONDENSATE

For our purposes, it is not always necessary to fix the dependence of the evolution variable t on the dimensionless variables according to (2.12). This formula will be used in illustrative examples. Basic physical conclusions are controlled by the sign of t and by the values of the first two derivatives. It is assumed that t is a monotonically increasing function of each of the dimensionless arguments x and y; it is also assumed that this function is negative in the region specified by the inequalities $0 < x \ll 1$ and $0 < y \ll 1$, but that it becomes positive when the arguments or at least one of them is on the order of unity. Stability of the solutions being studied depends on the sign of the second derivative of xt with respect to x: if

$$\frac{\partial^2(xt)}{\partial x^2} = 2t_x + xt_{xx} > 0, \qquad (3.1)$$

the solutions in question are stable. For the effective Lagrangian, this circumstance makes it possible to perform a Legendre transformation, but this could not be done for the original Yang–Mills Lagrangian because of tachyon branches. In doing this, it is only necessary to take care that gauge-fixing terms would not violate stability.

Choosing the gauge of the background field as

$$L_{\mathrm{GF}} = -\frac{1}{2}t(\nabla_\lambda V_\lambda)^2, \qquad (3.2)$$

where $\nabla^{ac}_\lambda = \partial_\lambda\delta^{ac} + gc^{abc}A^b_\lambda$, we obtain the following equation in the linear approximation:

$$(t + xt_x)((\nabla^2)^{ac}\delta_{\mu\nu} + 2B^{ac}_{\mu\nu})w^c_\nu \qquad (3.3)$$
$$+ 2(2t_x + xt_{xx})\gamma\Lambda^{-4}$$
$$\times \nabla^{ac}_\nu(B^c_{\mu\nu}B^d_{\alpha\beta}(\nabla^{de}_\alpha w^e_\beta - \nabla^{de}_\beta w^e_\alpha)) = -J^a_\mu;$$

the quantities t, $t_x = \partial t/\partial x$, and $t_{xx} = \partial^2 t/\partial x^2$ must be taken at $x = 0$ if $y > 1$ and at the stationarity point of the action functional, $t + xt_x = 0$, if $0 < y < 1$. The constant Λ is normalized in such a way that $t(x, y) = 0$ at $x = 0$ and $y = 1$. Also, we have introduced the notation $B^{ac}_{\mu\nu} = gc^{abc}B^b_{\mu\nu}$. The current on the right-hand side of Eq. (3.3) is equal to the sum of a constant component and currents that generate fluctuations. In order to avoid confusion, it should be emphasized that use is made here of the background-field gauge rather than of the entire background-field formalism as formulated in [11], where the field components A_μ and w_μ are both treated within perturbation theory. In our approach, the simplicity of the classical component A_μ makes it possible to dispense with imposing the condition of smallness on it and to take exactly into account the effect of a constant condensate on gluons.

In the region where $y > 1$ and $x \approx 0$, we have the usual dynamics of gluon propagation, the only distinction between Eq. (3.3) and the conventional Yang–Mills equation consisting in the dependence of the coupling constant on q^2. Within this region, the square of the momentum is constrained by the inequality $|k^2| > \Lambda^2_{\mathrm{QCD}}$. This makes it possible to eliminate the emergence of tachyons in small fluctuations and to perform a Legendre transformation for a stochastic field. In accordance with (2.8), it is sufficient for this to constrain the magnitude of the constant potential component A by the inequality

$$4A^2 < \Lambda^2_{\mathrm{QCD}}. \qquad (3.4)$$

Since the equilibrium value of the potential is equal to zero in this region, the constraint in (3.4) does not prevent the use of standard perturbation-theory methods.

For $y < 1$, a totally different dynamics that is controlled by the second term in Eq. (3.3) arises in the vicinity of the point $x = x_{\min}$. On the left-hand side, there remains only the product of the fluctuating-magnetic-field term $\mathbf{f}^d_{\alpha\beta} = \nabla_\alpha w^d_\beta - \nabla_\beta w^d_\alpha$, which is linear in w^a_μ, and the constant field $\mathbf{B}^d_{\alpha\beta}$ of the condensate. For gluon dynamics in the confining region,

it is of importance that the term $\frac{1}{2}L''(F^2 - B^2)$ of the Lagrangian does not involve all of the fourth-order terms in the field—in particular, it does not involve the combination $\sim \mathbf{B}^2\mathbf{f}^2/\Lambda^4$. The only term that is quadratic in $\mathbf{f}$, $\sim(\mathbf{B}\cdot\mathbf{f})^2/\Lambda^4$, cannot be responsible for the propagation of gluons, if for no other reason than the absence of the electric field components and the time derivatives of the potential in it. The time dynamics of fluctuations is essentially nonlinear and, for $\mathbf{f} \ll \mathbf{B}$, is controlled by the $\mathbf{f}^4/\Lambda^4$ term. There are no tachyons for $y < 1$.

The condensate given by (2.6) can serve as a good example of solutions characterized by a nonzero square of the field strength. Among condensates of a different type (N_w according to the terminology adopted in [8, 6])—those in which the $SU(2)$ subgroup consists of the $SU(3)$ generators associated with the structure constants $\pm 1/2$—one can single out the condensate

$$A_1^7 = A, \quad A_2^5 = -A, \quad A_3^2 = A, \qquad (3.5)$$

the remaining components being equal to zero, which is symmetric under color permutations in the fundamental representation.

Neither of these condensate types possesses invariance under rotations in a conventional sense, but, in the case of a spatial rotation, it is always possible to indicate a global gauge transformation that returns the condensate to the original state owing to a rotation in the group space. Physically, this is equivalent to invariance under rotations.

Stability of solutions in the confining region is tightly related to the concept of a floating condensate. If there were no condensate for $y < 1$, a situation would arise in which the square of the running coupling constant would be negative. An imaginary coupling constant implies instability. Instead of this unsatisfactory picture, we obtain $t < 0, x > 0, t_x > 0$, and $t + xt_x = 0$ in the presence of a condensate; for passive degrees of freedom [$(Bf) = 0$], the effective value of the evolution variable, which determines the coupling constant, is equal to zero, while, for active degrees of freedom, which contribute to the product (Bf), it is controlled by the positive factor $2t_x + xt_{xx}$. The time derivatives of the potentials do not appear in the equations of motion either for active or for passive degrees of freedom. There is absolutely no gluon propagation. Active degrees of freedom differ from passive ones only by the contribution to the static energy of the vacuum. It should be recalled that, in the equations presented in this section, g means the coupling constant at the normalization point that is chosen for $y > 1$ (that is, off the confining region); for this reason, $g^2 > 0$, and the simplest choice of normalization is that for which $g = 1$.

In the confining region, the magnitude of the floating condensate, $\langle F^2\rangle$, is dependent on the square of the propagating-gluon momentum, k^2, and is determined by the relation

$$\partial L_{\text{eff}}/\partial F^2 = 0, \qquad (3.6)$$

the specific form of the k^2 dependence of L_{eff} having no effect on physical results, since gluons do not propagate in this region and since the relevant integrals with respect to the gluon momentum are taken over domains not intersecting this region of k^2. In practice, this circumstance makes it possible to treat the floating condensate as a unified gluon-field state in which the dependence of the Lagrangian density on $F^a_{\mu\nu}$ disappears. The condition in (3.6), which is necessary for the energy density to reach a minimum, does not determine the constant components of the potentials A_μ unambiguously. The space of admissible values of A_μ is not exhausted by the symmetric solutions specified by Eqs. (2.6) and (3.5)—in general, the absolute values of the spatial components do not coincide, $|A_1| \neq |A_2| \neq |A_3|$. The invariance of such condensates under rotations is restored by integration over the rotation group. If there are no, as we assume in this article, significant constraints, with the exception of the condition in (3.6), the floating condensate proves to be a strongly degenerate state.

Considering $L(A, w)$ as an effective Lagrangian, one should treat the quantity $-L(A, 0)$ as an analog of the potential energy (more precisely, potential-energy density). In the confining region, it becomes negative. At the same time, the vacuum energy density is equal to zero by definition; therefore, a state in which $A \neq 0$ and $w = 0$ cannot be a physical vacuum in the confining region—there, vacuum fluctuations for which $\langle w\rangle = 0$ and $\langle w^2\rangle > 0$ must inevitably be present. If the ergodic hypothesis is valid for vacuum fluctuations (as seems most probable), they can be described by introducing an effective temperature that is proportional to $|t|F^2_{\min}$. In doing this, it should be borne in mind that, in this section, the effective energy density is defined only for the *condensate plus one gluon* system, the evolution variable being dependent on the gluon momentum. A generalization to the case of multigluon states in considered in Section 5.

4. QUANTUM CORRECTIONS TO THE LAGRANGIAN

For the case of a field shifted as $V_\mu = A_\mu + w_\mu$, we will now recall a conventional scheme for calculating one-loop corrections to the Lagrangian [12]. In this scheme, the Lagrangian that involves a gauge-fixing term and ghosts is supplemented with the quantity $J_\nu V_\nu$, where the current J_ν is equal to the sum of the

constant term $J_\nu(0)$ and terms that are responsible for fluctuations, $j_\nu(q)e^{iqx}$.

The functional

$$e^{iW(J)} = \langle 0^+|0^-\rangle_J \tag{4.1}$$

depends on the currents $aJ_\nu(0)$ and $j_\nu(q)$, a being a numerical parameter. The mean field is defined by the relation

$$A_\mu = \left[\frac{\langle 0^+|V_\mu|0^-\rangle}{\langle 0^+|0^-\rangle}\right]_{\substack{a\to 0\\ j=0}}. \tag{4.2}$$

The effective action is obtained upon the Legendre transformation in the form

$$\Gamma(A_\mu) = W(J) - \int d^4x J_\mu(x)A_\mu(x). \tag{4.3}$$

In contrast to what we have in the theory of a one-component scalar field, the action functional of the mean field A_μ has, instead of isolated stationary-phase points, an entire set of solutions that correspond to a minimum of energy. The vacuum proves to be strongly degenerate: the set of A_μ values for $a = 0$ depends on the configuration of currents for $a \neq 0$. Moreover, the potentials A_μ depend on q^2, and this makes it possible to introduce asymptotic freedom in the calculations explicitly.

In calculating the one-loop contributions to the Lagrangian, the relevant integral with respect to the square of the gluon momentum is taken over the range $\Lambda^2 < q^2 < \infty$. Divergences arise at $q^2 = \infty$ and at $q^2 = \Lambda^2$.

We begin determining one-loop corrections by considering the simplest case of zero momentum in the loop. The contribution that is divergent at infinity is given by

$$\int \frac{d^4p}{(2\pi)^4} \times \left(-\frac{1}{2}\ln(\mathrm{Det}G/\mathrm{Det}G_0) + \ln(\mathrm{Det}D/\mathrm{Det}D_0)\right), \tag{4.4}$$

where G and D are the quadratic forms that determine the linearized equations of motion for gluons and ghosts with respect to the shift of the field according to $V_\mu = A_\mu + w_\mu$, while G_0 and D_0 are the values of G and D, respectively, at $A_\mu = 0$. Since there is no condensate in the asymptotic region, it is sufficient to determine that part of the contribution which diverges for $p \to \infty$ only at low fields, $A_\mu^2 \approx |B_{\mu\nu}| < \Lambda^2$.

From (3.3), it follows that

$$G/G_0 \to \left[-(\nabla^2\delta_{\mu\nu} + 2B_{\mu\nu})w_\mu + \frac{t_x\gamma}{t\Lambda^4}(\nabla_\mu B_{\mu\nu} + B_{\mu\nu}\partial_\mu)B_{\alpha\beta}(\nabla_\alpha w_\beta - \nabla_\beta w_\alpha)\right](-\partial^2)^{-1}\delta_{\mu\nu}w_\mu. \tag{4.5}$$

For ghosts, we merely have

$$D/D_0 = \nabla^2/\partial^2. \tag{4.6}$$

Under our assumptions, the second term in the bracketed expression in (4.5) is small, and the correction stemming from it does not change the structure of the original Lagrangian.

At the critical point $z = 0$, we have $y = 1$; for $y < 1$, the first term in (3.3) disappears, in which case the behavior of the relevant integrand is controlled by the second term. As a matter of fact, this is the region of strong coupling, where the calculation of one-loop diagrams may only provide estimates, which are helpful in obtaining deeper insight into the qualitative behavior of the action functional.

In assessing divergent integrals, we constrain the region of integration with respect to the momentum in order to perform an intermediate regularization. As a result, the integrals are calculated only in the vicinity of the stability line for $x \ll 1$ at $y > 1$, the confining region $0 < y < 1$ being eliminated, since gluons do not propagate there. Since the lower limit of integration with respect to the square of the momentum is equal to Λ^2, an expansion in inverse powers of the momentum can be performed in the relevant integral as in [6], the only difference being that the second term in (4.5) leads to a logarithmic divergence at the lower limit. The introduction of the corresponding counterterm leads to a change in the lower limit by a quantity that is proportional to B^2. As a result, we arrive at the contribution to the effective Lagrangian in the form

$$-\frac{11}{128\pi^2}g^2B^2\ln\frac{\Lambda^4 + \xi B^2}{M^4}, \tag{4.7}$$

where ξ is a numerical factor and M is the upper limit of integration with respect to the momentum. This quantum correction does not change the structure of the effective Lagrangian, only shifting the dimensional constant Λ. The main difficulty involved in the calculation of integrals of $\ln\mathrm{Det}G - \ln\mathrm{Det}G_0$ in the confining region is associated with a high degree of degeneracy of the matrices G and G_0. The arising indeterminate form of the $\ln(0/0)$ type can be evaluated for the particular case where the condensate is scaled as $B = \lambda^2 B^{(0)}$ and $A = \lambda A^{(0)}$, in which

case $\ln(0/0) = 0$, passive degrees of freedom dropping out completely. The remaining active (nondegenerate) degrees of freedom do not yield corrections to the Lagrangian for the reasons indicated in Section 3.

Summarizing the results obtained by determining the simplest quantum corrections, we can say that, at the level of the first nonvanishing approximations, the proposed effective Lagrangian has passed the self-consistency test.

5. MULTIPARTICLE STATES

In this section, methods for dealing with more complicated diagrams including the background field and an arbitrary number of gluons are formulated on the basis of the idea of multiargument renormalization [13]. An effective Lagrangian that is dependent on one additional variable, the Laplacian (squared momentum) of the gluon field, was considered in [13]. In this section, we immediately introduce a second invariant—the square of the field strength F^2—and this makes it possible to include the confining region in our consideration. In this connection, we would like to recall basic points of multiargument renormalization with the required extensions.

One introduces a shifted gluon field,

$$V_\mu = A_\mu + w_\mu, \quad F_{\mu\nu} = B_{\mu\nu} + f_{\mu\nu}. \tag{5.1}$$

The background field specified by A_μ and $B_{\mu\nu}$ is not subjected to quantization, but its optimum value is dependent on the fields involved in the process being considered. Physically significant quantities are assumed to be deeply degenerate with respect to the background field: B^2 and, possibly, some other invariants are significant, while the color and the direction of A_μ and $B_{\mu\nu}$ are immaterial, in just the same way as quantities that are associated with gauge arbitrariness. The quantity B^2 is not a universal characteristic of the gluon field and has a specific value of $B^2 = 0$ only in the case where all of the gluons being considered are off the confining region. A general treatment of multiparticle states requires considering B^2 as a floating condensate and establishing the algorithm of calculations at least at the level of recipes. For the quantized part of the field, it is convenient to use the Fourier expansion

$$V(x,x') = (2\pi)^{-4}\int dx V(k)\exp[ik(x-x')], \tag{5.2}$$

$$V(k) = \int d(x-x')V(x,x')\exp[ik(x-x')]. \tag{5.3}$$

The substitutions $gV \to V$ and

$$L \to -\frac{F^2}{4g^2} = -\frac{1}{4}tF^2 \tag{5.4}$$

make it possible to write all formulas at $g = 1$ and to go over from the renormalization of the coupling constant to a renormalization of fields. In introducing a new argument, F^2, in the evolution variable t, we retain basic hypotheses of multiargument renormalization: (i) the renormalization of propagators is determined by F^2 and by the square of the gluon momentum, and (ii) the renormalizion factor of a vertex is equal to the product of the renormalization factors of the fields appearing in this vertex and the momentum-transfer-dependent renormalization factor of the coupling constant. It is implied that the variable part of the field involved consists of the stochastic background-field component W_μ and the sum of gluons being studied, $w_\mu \to W_\mu + \Sigma_i w_i$, which have momenta k_i, and it is necessary to determine the fields A_μ and W_μ for each w_i individually, irrespective of other gluons. It should be emphasized that the recipes outlined above are based on an educated guess that must be confirmed by subjecting its corollaries to a self-consistency test. The evolution variable t is a factor in the effective Lagrangian. The relation $g^{-2} = t$ is valid only in the absence of a condensate—that is, in the deconfining region. In the confining region, the effective coupling constant is determined by means of the procedure described in Sections 2 and 3. The momentum arguments of t are determined by the following considerations. A three-vector vertex arises from the mixed term $\partial_\mu V^a_{1\nu} c^{abc} V^b_{2\mu} V^c_{3\nu}$ in the Lagrangian with the gluon momenta equal to $k_1 = -k_2 - k_3$; accordingly, the quantity $k_1^2 = (k_2 + k_3)^2$ will be an argument of t. In a four-vector vertex, there occurs momentum transfer from one pair of gluons to the other (there is no momentum transfer there from one gluon to the remaining three). The momentum argument is equal to the square of the momentum transfer from one pair of gluons to the other—that is, $(k_1 + k_2)^2 = (k_3 + k_4)^2$, $(k_1 + k_3)^2$, $(k_1 + k_4)^2$. In the deconfining region, one obtains Feynman rules for renormalized diagrams [13]. In general, the domain of integration with respect to momenta is partitioned into sectors in accordance with the number n_c of the momentum arguments that fall within the confining region, $n_c = 0, 1, 2, \ldots$. Since gluons do not propagate in the confining region, integration is performed only over the $n_c = 0$ sector in calculating radiative corrections. In this sector, there arises a logarithmically divergent contribution of one-loop diagrams (ultraviolet divergence). At the boundaries of other sectors ($n_c > 0$), there are infrared divergences.

By way of example, we consider a calculation of the polarization operator. Within perturbation theory, the running coupling constant is calculated in terms of multiplicative renormalization factors for propagators

and vertices (Z_3 and Z_1, respectively); that is,

$$g^2(p^2)/g_0^2 = Z_3^3/Z_1^2. \quad (5.5)$$

With the aid of gauge invariance, we can somewhat simplify the calculations by choosing the gauge where $Z_1 \equiv 1$. For this, it is sufficient to set the gauge factor to $\zeta = 17/9$ rather than to $\zeta = 1$, as is done in the Feynman gauge. The polarization operator $\Pi^{da}_{\alpha\lambda}$ receives contributions from two diagrams. These are the truncated gluon-field loop,

$$\begin{aligned}\frac{1}{2}\frac{g^2}{16\pi^2}\int c^{dbc}c^{abc}[&t_1^{-1/2}(p_{1\beta}\eta_{\gamma\alpha} - p_{1\gamma}\eta_{\alpha\beta}) \quad (5.6)\\ &+ t_2^{-1/2}(k_{2\gamma}\eta_{\alpha\beta} - k_{2\alpha}\eta_{\beta\gamma})\\ &+ t_3^{-1/2}(k_{3\alpha}\eta_{\beta\gamma} - k_{3\beta}\eta_{\gamma\alpha})]\\ &\times [t_1^{-\frac{1}{2}}(p_{1\mu}\eta_{\nu\lambda} - p_{1\nu}\eta_{\mu\lambda})\\ &+ t_2^{-\frac{1}{2}}(k_{2\nu}\eta_{\lambda\mu} - k_{2\lambda}\eta_{\mu\nu})\\ &+ t_3^{-\frac{1}{2}}(k_{3\lambda}\eta_{\mu\nu} - k_{3\mu}\eta_{\nu\lambda})]k_2^{-2}k_3^{-2}\\ &\times [\eta_{\beta\mu} - (1-\zeta)k_2^{-2}k_{2\beta}k_{2\mu}]\\ &\times [\eta_{\gamma\nu} - (1-\zeta)k_3^{-2}k_{3\gamma}k_{3\nu}]\frac{d^4k}{\pi^2 i},\end{aligned}$$

where $\eta_{\mu\nu} = \mathrm{diag}(1,-1,-1,-1)$ is the metric tensor, and the ghost loop,

$$\frac{g^2}{16\pi^2}\int c^{dbc}c^{abc}t_1^{-1}k_2^{-2}k_3^{-2}(k_2k_3)\frac{d^4k}{\pi^2 i}. \quad (5.7)$$

Calculating the scalar part $\Pi^{da}_{\lambda\lambda}$ of the polarization operator, we obtain its gluon component in the form

$$\begin{aligned}\Pi^{da}_{\lambda\lambda} = \frac{3\delta^{da}}{2}\frac{g^2}{16\pi^2}\int\frac{d^4k}{\pi^2 i}\{&6[\tau_{11}p^2 - \tau_{12}(pk_2) \quad (5.8)\\ &- \tau_{13}(pk_3) - \tau_{23}(k_2k_3) + \tau_{22}k_2^2 + \tau_{33}k_3^2]\\ &- (1-\zeta)[2\tau_{11}(p^2 + (pn_2)^2 + (pn_3)^2)\\ &- 6\tau_{12}(k_2n_3)(pn_3) - 6\tau_{13}(k_3n_2)(pn_2)\\ &+ \tau_{22}(k_2^2 + 2(k_2n_3)^2) + \tau_{33}(k_3^2 + 2(k_3n_2)^2)]\\ &+ (1-\zeta)^2\tau_{11}[(pn_2)n_3 - (pn_3)n_2]^2\}k_2^{-2}k_3^{-2}\end{aligned}$$

and its ghost component in the form

$$\Pi^{da}_{\lambda\lambda} = 3\delta^{da}\frac{g^2}{16\pi^2}\int\frac{d^4k}{\pi^2 i}\tau_{11}(k_2k_3)k_2^{-2}k_3^{-2}. \quad (5.9)$$

Here, we have introduced the notation $\tau_{jk} = (t_jt_k)^{-1/2}$, $n_j = k_j/\sqrt{k_j^2}$ and used the identity $c^{dbc}c^{abc} = 3\delta^{da}$ for the structure constants of the $SU(3)$ group; the vectors p, k_2, and k_3 are related by the conservation law $p_\lambda + k_{2\lambda} + k_{3\lambda} = 0$.

By extrapolating the Gell-Mann–Low equation to the strong-coupling region, we can express the first-order correction $t^{(1)}$ to the evolution parameter t of the Lagrangian in terms of the polarization operator as

$$\frac{dt^{(1)}}{d\ln p^2} = \frac{b}{16\pi^2}, \quad b = \frac{d\Pi_{\lambda\lambda}}{g^2 dp^2}. \quad (5.10)$$

An investigation of the ultraviolet divergence of the polarization operator leads to the following results: in addition to a logarithmic divergence, there arises terms featuring an integral logarithm of the upper limit, but this does not cause qualitative changes in the structure of the effective Lagrangian. A cutoff at the lower limit leads to the emergence of the new parameter $|k|_{\min} > \Lambda$, on which the dynamics of soft particles may depend. Two spheres of radius Λ are eliminated from the domain of integration with respect to the momentum; they intersect for $|p| < 2\Lambda$ and exist separately for $|p| > 2\Lambda$, a change in the regime of radiative corrections occurring at $|p| = 2\Lambda$. A similar change in the topology of the domain of integration takes place in higher orders of perturbation theory as well. As a result, the analyticity of perturbation-theory series is violated at $|k| = 2\Lambda, |k| = 3\Lambda, \ldots$. The question of whether these singularities may be compensated still remains open.

6. DISCUSSION

The asymptotic freedom of a non-Abelian theory and the confinement of color fields appear to be closely related to each other. An attempt at developing a formalism that would combine these two facets of QCD has been made above on the basis of renormalized diagrams. Since the language of diagrams is equivalent to the original operator language of quantum field theory [14], this description of quantum effects seems quite reasonable. One could refer to the effective action introduced above as a conditional one, assuming that it describes the behavior of all fields under the condition that there exist a few gluons and quarks of momentum k_i and p_i, respectively. In that case, the action functional would depend on all of the arguments k_i and p_i. The basic point of multiargument renormalization is that, in the deconfining region, one can take into account the interaction of each quark or gluon with an arbitrary number of other degrees of freedom, irrespective of other quarks or gluons singled out in this connection, whereby one reduces the interaction to renormalization of separate elements of Feynman graphs.

In QCD, which is a theory that features asymptotic freedom, there inevitably arises the question concerning the behavior of the running coupling constant in the infrared region. If the coupling constant

remains finite [9] and if there is no Landau pole in the infrared region, QCD does not differ qualitatively from conventional field theory developed for freely propagating fields. In this case, additional ad hoc assumptions are required for explaining confinement, but these have yet to be developed in detail. Here, we have discussed an alternative version where the coupling constant does in fact become infinite at $k^2 \approx \Lambda^2_{\rm QCD}$. But in this case, there arises a different problem: What occurs after the coupling constant has reached infinity? No comprehensive answer to this question has so far been deduced, but the following can be indicated as a preliminary scenario. For $k^2 < \Lambda^2_{\rm QCD}$, the $F^a_{\mu\nu} = 0$ field state (vacuum of perturbation theory) ceases to play the role of a stable vacuum state. The equality of the field to zero holds only on average, the expectation value of the field squared becoming positive. This description of the physical vacuum of a gluon field in terms of a floating condensate is similar to a phenomenological description of confinement as a state analogous to a superconducting state, the main distinction being that, in the case of floating-condensate formation, a spatial separation of the two phases does not necessarily occur: confinement and deconfinement are separated in momentum rather than in coordinate space. This picture is compatible with basic experimental facts. Indeed, quarks, and gluons are observed as jets in hard processes, but only color-singlet hadrons are observed in soft processes.

The possibility of spontaneous-condensate formation accompanied by a transition of the gluon field to a state where the effective Lagrangian is independent of the expectation value of the field squared, $\partial L_{\rm eff}/\partial\langle F^2\rangle = 0$, is a key point in the above scenario of confinement. A realization of (5.1) provides an example of such a state. Possibly, the representation of a condensate characterized by $\langle F^2\rangle > 0$ as the sum of vortex-like excitations for which an integral along a closed contour around the vortex axis corresponds to the center of the color group [15] will prove to be more promising. Also, we cannot rule out the possibility that degeneracy is so deep that it makes no sense to address the problem of describing the condensate in detail.

REFERENCES

1. G. K. Savvidi, Phys. Lett. B **71B**, 133 (1977).
2. S. G. Matinyan and G. K. Savvidi, Nucl. Phys. B **143**, 539 (1978).
3. I. A. Batalin, C. G. Matinyan, G. K. Savvidi, Yad. Fiz. **26**, 407 (1977) [Sov. J. Nucl. Phys. **26**, 214 (1977)].
4. C. N. Yang and R. L. Mills, Phys. Rev. **96**, 191 (1954).
5. W. Heisenberg and H. Euler, Z. Phys. **98**, 714 (1936); V. F. Weisskopf, K. Dan. Vidensk. Selsk. Mat. Fys. Medd. **14**, 1 (1936).
6. V. V. Vladimirsky and D. V. Peregudov, Yad. Fiz. **63**, 1534 (2000) [Phys. At. Nucl. **63**, 1455 (2000)].
7. T. N. Tudron, Phys. Rev. D **22**, 2566 (1980); A. V. Yung, Yad. Fiz. **41**, 1324 (1985) [Sov. J. Nucl. Phys. **41**, 842 (1985)].
8. V. V. Vladimirsky, Yad. Fiz. **59**, 2063 (1996) [Phys. At. Nucl. **59**, 1988 (1996)].
9. Yu. A. Simonov, Yad. Fiz. **58**, 113 (1995) [Phys. At. Nucl. **58**, 107 (1995)]; Yu. L. Dokshitzer, G. Marchesini, and B. R. Webber, Nucl. Phys. B **469**, 93 (1996); D. V. Shirkov and I. L. Solovtsov, Phys. Rev. Lett. **79**, 1209 (1997); D. V. Shirkov, Eur. Phys. J. C **22**, 331 (2001); A. V. Nesterenko and I. L. Solovtsov, Mod. Phys. Lett. A **16**, 2517 (2001).
10. P. A. Kovalenko and L. V. Laperashvili, Yad. Fiz. **62**, 1857 (1999) [Phys. At. Nucl. **62**, 1729 (1999)].
11. G.'t Hooft, Nucl. Phys. B **62**, 444 (1973); G.'t Hooft, Nucl. Phys. B **61**, 455 (1973); L. F. Abbott, Nucl. Phys. B **185**, 189 (1981); G. 't Hooft, Acta Univers. Wratislaviensis, No. 368; in *Proceedings of the 12th Winter School of Theoretical Physics in Karpacz, 1975,* Vol. 1, p. 347.
12. S. Coleman and E. Weinberg, Phys. Rev. D **7**, 1888 (1973).
13. V. V. Vladimirsky, Yad. Fiz. **65**, 330 (2002) [Phys. At. Nucl. **65**, 305 (2002)].
14. G.'t Hooft and M. Veltman, CERN 73-9 (Geneva, 1973).
15. G.'t Hooft, Nucl. Phys. B **138**, 1 (1978).

Translated by A. Isaakyan

Physics of Atomic Nuclei, Vol. 66, No. 12, 2003, pp. 2224–2232. Translated from Yadernaya Fizika, Vol. 66, No. 12, 2003, pp. 2276–2284.

ELEMENTARY PARTICLES AND FIELDS
Theory

Static Potential in a Baryon within the Method of Vacuum Correlation Functions

D. S. Kuzmenko

Institute of Theoretical and Experimental Physics,
Bol'shaya Cheremushkinskaya ul. 25, Moscow, 117259 Russia

Received November 4, 2002

Abstract—The static three-quark potential is calculated analytically for an arbitrary arrangement of quarks. The result is shown to be fully consistent with precise numerical simulations in lattice QCD. The results of this study have important applications in nuclear physics, since they make it possible to perform accurate analytic calculations of baryon spectra. © *2003 MAIK "Nauka/Interperiodica".*

1. INTRODUCTION

Good knowledge of the properties of nucleons is of paramount importance for obtaining deeper insight into nuclear processes. The static potential in a baryon plays a key role in calculating the spectra of baryons, as well as their wave functions and decays; therefore, its investigation is one of the important problems in nuclear physics. Moreover, investigation of such static potentials is of interest since it is related to two fundamental properties of strong interactions, color-charge confinement and the scale of fluctuations of confining gluon fields.

In the present study, the static potential in a baryon is calculated by the method of vacuum correlation functions [1], which is directly based on QCD and which is intended for dealing with the vacuum expectation values of correlation functions for gluon-field strengths.

Within the method of vacuum correlation functions, it is assumed that gluon fields play a double role in QCD. On one hand, gluons dynamically propagate in a vacuum, and this process can be described by perturbation theory at short distances. In particular, the interaction of quarks at short distances via one-gluon exchange leads to color Coulomb interaction between quarks. On the other hand, gluons form, in a vacuum, a nonpertubative condensate, which is a medium (background field) where perturbative gluons propagate.

Within the method of vacuum correlation functions, two-point correlation functions for gluon fields are parametrized in terms of scalar form factors [2]. The form factors of gluon fields decrease exponentially, which, in the case of mesons, leads to a linear growth of the potential and to the area law for the Wilson loop at long distances between a quark and an antiquark. It is well known that this behavior of the potential and of the Wilson loop implies the formation of a string that ensures color-charge confinement. The slope σ of the linear confining potential for a quark and an antiquark is a basic parameter in the method of vacuum correlation functions; it corresponds to the scale parameter in QCD, and its knowledge is sufficient for calculating the spectra of particles (in particular, mesons [3]) to within 5%. The magnitude of this parameter is determined phenomenologically by the slope of meson Regge trajectories.

The correlation length T_g for background gluon fields, which determines the rate of decrease in the form factors of the background fields, is another nonperturbative parameter in the method of vacuum correlation functions. This correlation length is small and insignificant in the case of mesons because, at short distances, quark–antiquark interaction is controlled by a perturbative field. In the case of baryons, however, the correlation length proves to be of importance for the interaction of background fields in the string-junction region, this interaction leading, as will be shown below in the present study, to an effective reduction of the slope of the baryon potential at short and intermediate distances between the quarks involved. In addition, the correlation length can also manifest itself in the dependence of the static potential on the arrangement of quarks at a given total length of the string. This effect will also be explored in this study.

Without taking into account sea quarks, the static three-quark potential was recently calculated in [4, 5] within lattice QCD to a rather high precision. In the present study, it will be shown that the potential

1063-7788/03/6612-2224$24.00

calculated by the method of vacuum correlation functions is in good agreement with lattice results.

Prior to proceeding to calculate the static potential, we will consider, in the next section, the baryon Wilson loop, which, in the case of static quarks, appears to be the baryon Green's function. We will express the vacuum expectation value of the Wilson loop in terms of the vacuum expectation values of two-point correlation functions for gluon-field strengths and parametrize them in accordance with the method of vacuum correlation functions; in this connection, we will also briefly discuss the results obtained by calculating the gluon condensate on the basis of sum rules. In Section 3, we describe the procedure used here to calculate the static potential and analyze special features of its behavior versus lattice data. In the Conclusion, we summarize our results and discuss prospects for their application.

2. BARYON WILSON LOOP AND ITS VACUUM EXPECTATION VALUE IN THE METHOD OF VACUUM CORRELATION FUNCTIONS

It is well known that the gauge-invariant state of a baryon where its quarks are at the points x, y, and z is described by the function

$$\Psi_B(x,y,z,Y) = \epsilon_{\alpha\beta\gamma}\Phi^{\alpha}_{\alpha'}(x,Y,C_1)\Phi^{\beta}_{\beta'}(y,Y,C_2) \times \Phi^{\gamma}_{\gamma'}(z,Y,C_3)q^{\alpha'}(x)q^{\beta'}(y)q^{\gamma'}(z), \quad (1)$$

where α, β, ... are color indices of the fundamental representation of the $SU(3)$ group;

$$\Phi^{\alpha}_{\beta}(x,y,C) = (P\exp ig\int\limits_C A_\mu dz_\mu)^{\alpha}_{\beta} \quad (2)$$

is the parallel transporter along the contour C connecting the points x and y [the symbol P in (2) means the ordering of color matrices along the trajectory of integration]; q and A are the operators of, respectively, the quark and the gluon field; and Y is the string-junction point. The baryon Green's function is defined as the vacuum expectation value

$$G_B(\bar{X},X) = \langle\Psi^{+}_B(\bar{X})\Psi_B(X)\rangle, \quad (3)$$

where $X \equiv x,y,z,Y$. If quarks are static, this Green's function is equal to the baryon Wilson loop $\mathcal{W}_B$, which is given by

$$\mathcal{W}_B = \left\langle \frac{1}{6}\epsilon_{\alpha\beta\gamma}\epsilon^{\alpha'\beta'\gamma'}\Phi^{\alpha}_{\alpha'}(C_1)\Phi^{\beta}_{\beta'}(C_2)\Phi^{\gamma}_{\gamma'}(C_3)\right\rangle. \quad (4)$$

The contours C_1, C_2, and C_3 and the direction of integration are shown in Fig. 1. The dotted line represents the string-junction trajectory, which is denoted by C_0.

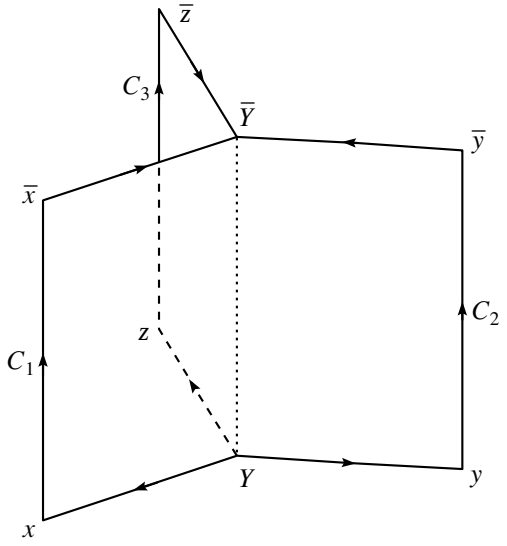

Fig. 1. Baryon Wilson loop.

It should be noted that this definition of the baryon Wilson loop is generally accepted. The static potential in the baryon and the Wilson loop are related as

$$V_B = -\lim_{T\to\infty}\frac{1}{T}\ln\mathcal{W}_B, \quad (5)$$

where T is the extension of the Wilson loop along the time axis.

Let us express the Wilson loop (4) in terms of correlation functions for the tensor of the gluon-field strength. For this, we recast the Wilson loop into the form

$$\mathcal{W}_B = \left\langle \frac{1}{6}\epsilon_{\alpha\beta\gamma}\epsilon^{\alpha'\beta'\gamma'}\Phi^{\alpha}_{\alpha'}(\tilde{C}_1)\Phi^{\beta}_{\beta'}(\tilde{C}_2)\Phi^{\gamma}_{\gamma'}(\tilde{C}_3)\right\rangle, \quad (6)$$

where $\tilde{C}_i = C_i \cup C_0$. Expression (6) is obtained by substituting into (4) the relation

$$\epsilon^{\alpha'\beta'\gamma'} = \epsilon^{\alpha''\beta''\gamma''}\Phi^{\alpha''}_{\alpha'}(C_0)\Phi^{\beta''}_{\beta'}(C_0)\Phi^{\gamma''}_{\gamma'}(C_0). \quad (7)$$

It should be noted that the last relation is valid in a generalized coordinate gauge where $\Phi^{\alpha}_{\alpha'}(C_0) = \delta^{\alpha}_{\alpha'}$ and, in general, depends on the choice of gauge, but expression (6) is a scalar of the $SU(3)$ color group; therefore, it does not depend on the choice of gauge. Since integration in (6) is performed along three closed rectilinear contours, the non-Abelian Stokes theorem [1] can be used for these contours of the baryon Wilson loop. As a result, we obtain

$$\mathcal{W}_B = \left\langle \frac{1}{6}\epsilon_{\alpha\beta\gamma}\epsilon^{\alpha'\beta'\gamma'}W^{\alpha}_{\alpha'}(S_1)W^{\beta}_{\beta'}(S_2)W^{\gamma}_{\gamma'}(S_3)\right\rangle, \quad (8)$$

where S_i are the minimal surfaces of the contours $\tilde{C}_i$ and

$$W^{\alpha}_{\alpha'}(S) = \mathcal{P}\exp\left(ig\int\limits_S d\sigma_{\mu\nu}(x)F_{\mu\nu}(x)\Phi(x,x_0)\right)^{\alpha}_{\alpha'} \quad (9)$$

is independent of the choice of the point x_0 if it lies on the surface S [1]. Let us now expand the exponential function in (9) as

$$W^{\alpha}_{\alpha'}(S) = \delta^{\alpha}_{\alpha'} + ig\int\limits_S d\sigma F^{\alpha}_{\alpha'} - \frac{g^2}{2} \quad (10)$$
$$\times\int\limits_S\int\limits_S d\sigma(1)d\sigma(2)F^{\alpha}_{\beta}(1)F^{\beta}_{\alpha'}(2) + \ldots,$$

where we have written explicitly only color indices and where the ellipsis stands for higher order terms of the expansion. Since the vacuum expectation value of the field-strength tensor is equal to zero, the Wilson loop has the form

$$\mathcal{W}_B = \frac{1}{6}\epsilon_{\alpha\beta\gamma}\epsilon^{\alpha'\beta'\gamma'}\left(\delta^{\alpha}_{\alpha'}\delta^{\beta}_{\beta'}\delta^{\gamma}_{\gamma'} - \delta^{\beta}_{\beta'}\delta^{\gamma}_{\gamma'}\frac{g^2}{2}\right. \quad (11)$$
$$\times\int_{S_1}\int_{S_1} d\sigma(1)d\sigma(2)F^{\alpha}_{\rho}(1)F^{\rho}_{\alpha'}(2)$$
$$\left.-\delta^{\gamma}_{\gamma'}g^2\int_{S_1}\int_{S_2} d\sigma(1)d\sigma(2)F^{\alpha}_{\alpha'}(1)F^{\beta}_{\beta'}(2)+\ldots\right),$$

where the ellipsis stands for the double integrals that are taken over S_2S_2, S_3S_3, S_1S_3, and S_2S_3 and which are of a form similar to that of the integrals written explicitly and for higher order correlation functions. Considering that $\epsilon_{\alpha\beta\gamma}\epsilon^{\alpha'\beta\gamma}F^{\alpha}_{\rho}F^{\rho}_{\alpha'} = 2\mathrm{tr}FF$ and $\epsilon_{\alpha\beta\gamma}\epsilon^{\alpha'\beta'\gamma}F^{\alpha}_{\alpha'}F^{\beta}_{\beta'} = -\mathrm{tr}FF$ and using (11), we obtain

$$\mathcal{W}_B = \exp\left\{-\sum_{i=1}^{3}\frac{1}{2}\int\limits_{S_i}\int\limits_{S_i} d\sigma(1)d\sigma(2)\right. \quad (12)$$
$$\times\left\langle\frac{g^2}{3}\mathrm{tr}F(1)F(2)\right\rangle$$
$$\left.+\sum_{i<j}\frac{1}{2}\int\limits_{S_i}\int\limits_{S_j} d\sigma(1)d\sigma(2)\left\langle\frac{g^2}{3}\mathrm{tr}F(1)F(2)\right\rangle\right\}.$$

Here and below, we do not take into account higher order correlation functions. We assume that they do not affect the expectation value of the Wilson loop. It will be seen that this assumption leads to the area law for the Wilson loop. It was shown in [6] that, in the approximation of two-point correlation functions, the static potentials of sources in various representations of the $SU(3)$ group obey Casimir scaling—that is, they are proportional to the corresponding Casimir operators. However, higher order correlation functions violate Casimir scaling. Since the property of Casimir scaling for the static potentials of sources in various representations was verified on a lattice to a high precision [7], it provides an argument in support of the validity of the bilocal approximation, where only two-point correlation functions are taken into account in the Wilson loop.

The cancellation of the contributions to the Wilson loop from higher order correlation functions is associated with the static properties of the QCD vacuum. It should be noted that the two-point correlation functions written above represent the first term of the cluster expansion used in the theory of fluctuations [8] to describe correlated stochastic processes. According to the fundamental identity of the cluster expansion, higher order correlation functions appear in (12) in the form of cumulants (an exact definition of cumulants can be found in [8], along with the proof of the fundamental identity), which, for almost independent points, decrease fast with increasing order. Thus, the inclusion of only two-point correlation functions is validated by fluctuation theory at distances longer than the correlation length for gluon fields. In the case of the $SU(N_c)$ gauge group, two-point correlation functions are parametrized, in accordance with the stochastic properties of four-dimensional Euclidean space, in terms of two scalar form factors D and D_1 as [2]

$$\frac{g^2}{N_c}\mathrm{tr}\left\langle F_{\mu_1\nu_1}(x)\Phi(x,x')F_{\mu_2\nu_2}(x')\Phi(x',x)\right\rangle \quad (13)$$
$$= (\delta_{\mu_1\mu_2}\delta_{\nu_1\nu_2} - \delta_{\mu_1\nu_2}\delta_{\mu_2\nu_1})D(z)$$
$$+\frac{1}{2}\left(\frac{\partial}{\partial z_{\mu_1}}(z_{\mu_2}\delta_{\nu_1\nu_2} - z_{\nu_2}\delta_{\nu_1\mu_2})\right.$$
$$\left.+\frac{\partial}{\partial z_{\nu_1}}(z_{\nu_2}\delta_{\mu_1\mu_2} - z_{\mu_2}\delta_{\mu_1\nu_2})\right)$$
$$\times D_1(z) \equiv \mathcal{D}_{\mu_1\nu_1,\mu_2\nu_2}(z),$$

where $z \equiv x - x'$. The form factors for the background fields are given by

$$D(z) = D(0)\exp\left(-\frac{|z|}{T_g}\right), \quad (14)$$
$$D_1(z) = D_1(0)\exp\left(-\frac{|z|}{T_g}\right).$$

The exponential behavior of the correlation functions in (14) is confirmed by lattice simulations [9, 10] at distances of $z \gtrsim 0.2$ fm. For the background fields, these lattice simulations yielded $T_g = 0.12$–0.2 fm for the correlation length [9, 10] and $D_1(0)/D(0) \lesssim 1/3$ for the form-factor ratio [9]. In the case of a static

quark and a static antiquark, the relation analogous to (12) has the form

$$\mathcal{W}_B = \exp\left\{ -\frac{1}{2}\int\limits_S\int\limits_S d\sigma(1)d\sigma(2) \times\left\langle \frac{g^2}{N_c}\mathrm{tr}F(1)F(2)\right\rangle\right\} \quad (15)$$

and, at long quark–antiquark distances, $R \gg T_g$, leads to the area law for the Wilson loop,

$$\langle\mathcal{W}\rangle^{\mathrm{biloc}} = \exp(-\sigma S), \quad (16)$$

the string tension σ being given by

$$\sigma = \frac{\pi}{2}\int\limits_0^\infty dz^2 D(z). \quad (17)$$

The string-tension value of $\sigma \approx 0.18\ \mathrm{GeV}^2$ can be determined phenomenologically from the slope of meson Regge trajectories [3]. It is worth noting that the value of $T_g \approx 0.12$ fm can be extracted from the gluelump spectrum calculated in [11] on the basis of the method of vacuum correlation functions by using the only nonperturbative parameter σ.

From (13) and (14), it follows that

$$\left\langle \frac{\alpha_s}{\pi}F^a_{\mu\nu}(x)F^a_{\mu\nu}(0)\right\rangle = \frac{18D(x)}{\pi^2}. \quad (18)$$

Among other things, this provides a relationship between the gluon condensate $\left\langle \frac{\alpha_s}{\pi}F^a_{\mu\nu}(0)F^a_{\mu\nu}(0)\right\rangle \equiv \left\langle \frac{\alpha_s}{\pi}F^2\right\rangle$ and the value of the form factor D at the origin. This value formally does not appear in the definition (17) of σ, but, if the behavior of $D(z)$ in (14) is valid at short distances inclusive (and this is what is assumed in the present article below), then $\sigma = \pi D(0)T_g^2$, whereby one can assess the gluon condensate: $\left\langle \frac{\alpha_s}{\pi}F^2\right\rangle = 18\sigma/(\pi^3 T_g^2) \approx 0.25\ \mathrm{GeV}^4$ if $T_g = 0.12$ fm.

The gluon condensate can also be evaluated with aid of the ITEP sum rules, which are described in the textbook of Ynduráin [12], where the interested reader can also find references to the original studies. In the sum rules, use is made of the operator-product expansion for currents, and the contribution of the gluon condensate appears in them through the combination $\langle\frac{\alpha_s}{\pi}G^2\rangle/Q^4$, the magnitude of the gluon condensate being assumed to be momentum-independent. By analyzing, with the aid of operator-product expansion, data on tau-lepton decay and the sum rules for charmonium, the gluon-condensates values of $\left\langle \frac{\alpha_s}{\pi}G^2\right\rangle = 0.006 \pm 0.012\ \mathrm{GeV}^4$ and $\left\langle \frac{\alpha_s}{\pi}G^2\right\rangle = 0.009 \pm 0.007\ \mathrm{GeV}^4$, respectively, were recently found in [13].

It can be assumed that the sum rules involve some effective condensate value that is equal to the correlation function $\left\langle \frac{\alpha_s}{\pi}F^a_{\mu\nu}(x_{\mathrm{eff}})F^a_{\mu\nu}(0)\right\rangle$ at the corresponding distance $x_{\mathrm{eff}} \neq 0$ between the points being considered. For $\left\langle \frac{\alpha_s}{\pi}G^2\right\rangle = 0.007\ \mathrm{GeV}^4$ and $T_g \approx 0.12$ fm, we have $x_{\mathrm{eff}} = T_g \ln\left(\left\langle \frac{\alpha_s}{\pi}F^2\right\rangle / \left\langle \frac{\alpha_s}{\pi}G^2\right\rangle\right) \approx 0.5$ fm; that is, the sum rules involve the gluon correlation function at the characteristic confinement radius. If one further assumes that two-point correlation functions are independent of the distance, in which case $D(x) = \mathrm{const}$, and performs integration in (17) up to characteristic hadron dimensions of $r_h = 1$ fm, then the estimate obtained for the gluon condensate from (17) and (18) is $\left\langle \frac{\alpha_s}{\pi}F^2\right\rangle \approx \sigma/r_h^2 \approx 0.007\ \mathrm{GeV}^4$, which is also consistent with the gluon-condensate value derived in [13].

Thus, the results produced by the sum rules can neither confirm nor disprove the parametrization used in the method of vacuum correlation functions [see Eq. (14)].

3. BARYON POTENTIAL

According to (5), (12), and (14), the baryon potential has the form

$$V_B = \lim_{T\to\infty}\frac{1}{2}\sum_{a=1,2,3}\int\limits_{S_a}\int\limits_{S_a} d\sigma^{(a)}_{\mu_1\nu_1}(x)d\sigma^{(a)}_{\mu_2\nu_2}(x') \times \mathcal{D}_{\mu_1\nu_1,\mu_2\nu_2}(x-x') - \frac{1}{2}\sum_{a<b}\int\limits_{S_a}\int\limits_{S_b} d\sigma^{(a)}_{\mu_1\nu_1}(x) \times d\sigma^{(b)}_{\mu_2\nu_2}(x')\mathcal{D}_{\mu_1\nu_1,\mu_2\nu_2}(x-x'), \quad (19)$$

where $d\sigma^{(a)}$ denotes integration over the surface S_a. It should be emphasized that the off-diagonal part of the potential (for $a \neq b$) differs by a factor of $-1/2 = -1/(N_c-1)$ from the corresponding quantity in [14, 15], where the authors made an error {see formula (24) in [14] and formula (46) in [15]}.

Since the surfaces of the Wilson loop are oriented along the time axis, only color-electric-field correlation functions contribute to the potential. Here, the surface integral in four-dimensional space reduces to a spatial curvilinear integral of the second kind and a single integral with respect to the time variable; that is,

$$F_{i4}d\sigma_{i4} = \mathbf{E}(l\mathbf{n}, x_4)\mathbf{n}dldx_4, \quad (20)$$

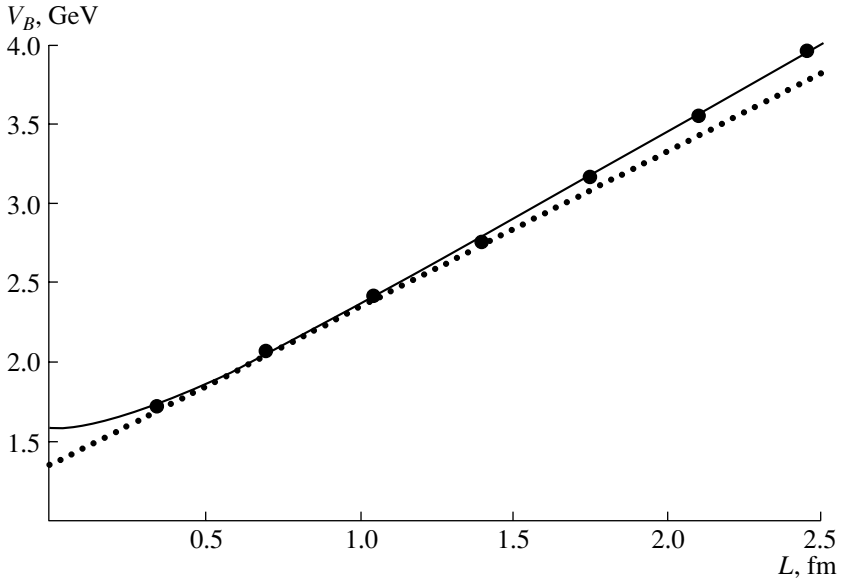

Fig. 2. Static nonperturbative potential of three quarks versus the minimum string length L within the method of vacuum correlation functions $[V_B(L/3)]$ at $\sigma = 0.22$ fm (solid curve) and in the lattice simulation from [4] at the lattice parameter of $\beta = 5.8$ (points). The dotted line is the tangent to the potential $V_B(L/3)$ at $L = 0.7$ fm. The size of the points corresponds to the error in the lattice calculations.

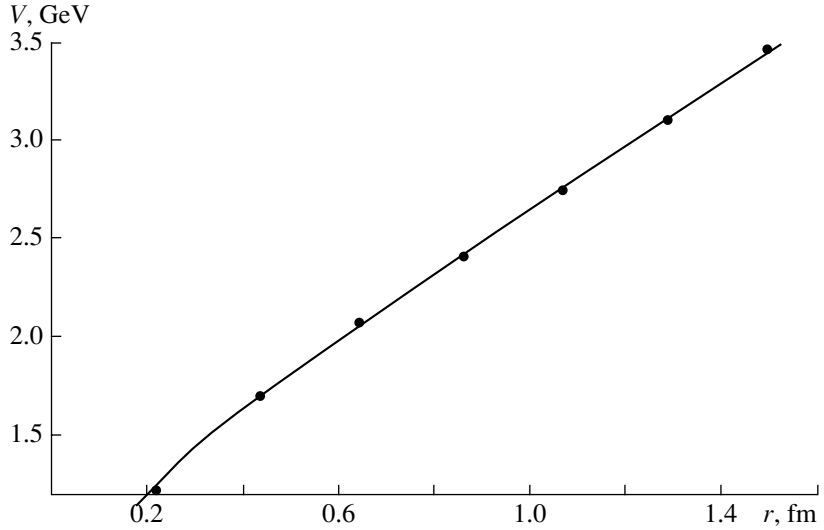

Fig. 3. Static baryon potential in an equilateral triangle versus the distance r between the quarks within the method of vacuum correlation functions $[V_{\text{pert}}(r) + V_B(r)]$ at $\alpha_s = 0.18$ and $\sigma = 0.18$ GeV^2 (solid curve) and in the lattice simulation from [5] at $\beta = 5.8$ (points). The size of the points corresponds to the error in the lattice calculations.

where $\mathbf{n}$ is the directing unit vector aligned with the straight line connecting the string junction with the corresponding quark. Making the change of variable $x_4 - x_4' = t$, we obtain

$$V_B(R_1, R_2, R_3) = \left(\sum_{a=b} - \sum_{a<b}\right) n_i^{(a)} n_j^{(b)} \tag{21}$$
$$\times \int_0^{R_a}\int_0^{R_b} dl dl' \int_0^{\infty} dt \mathcal{D}_{i4,j4}(z_{ab}),$$

where $z_{ab} = (l\mathbf{n}^{(a)} - l'\mathbf{n}^{(b)}, t)$, R_a is the distance from the string junction to the corresponding quark, and

$$\mathcal{D}_{i4,j4}(z) = \delta_{ij} D(z) + \frac{\partial}{\partial z_i} \frac{z_j D_1(z)}{2}. \tag{22}$$

Since the form factor D_1 is small and appears in (22)

under a derivative sign, we can disregard its contribution to the potential and assume that

$$n_i^{(a)} n_j^{(b)} \mathcal{D}_{i4,j4}(z) = \mathbf{n}^{(a)} \cdot \mathbf{n}^{(b)} D(z). \qquad (23)$$

In calculating the baryon potential, we must distinguish between quark configurations where the quarks involved form (i) triangles where each of the angles is smaller than $2\pi/3$ and (ii) triangles where one of the angles is larger than $2\pi/3$. In the first case, the minimal surface of the Wilson loop consists of three surfaces intersecting at angles of $2\pi/3$, as is shown in Fig. 1. In the second case, the Wilson loop consists of two surfaces, the position of the string junction being coincident with the position of the quark corresponding to the larger angle. In Eq. (21), we can then set $R_3 = 0$.

Let us first consider the equilateral-triangle configuration, in which case $R_1 = R_2 = R_3 \equiv R$. The baryon potential can then be represented as

$$V_B(R) = 3V_M(R) + V_{\rm nd}(R), \qquad (24)$$

where V_M is obtained upon performing double integration in (21) over the same surface, while $V_{\rm nd}$ is obtained upon the analogous integration over different surfaces. From Eqs. (14) and (21)–(23), we derive the relation

$$V_M(R) = 2D(0) \int_0^R dz_1 (R - z_1) \qquad (25)$$

$$\times \int_0^\infty dt \exp\left(-\frac{|z|}{T_g}\right) = \frac{2\sigma}{\pi}$$

$$\times \left\{ R \int_0^{R/T_g} dx x K_1(x) - T_g \left(2 - \frac{R^2}{T_g^2} K_2\left(\frac{R}{T_g}\right)\right)\right\},$$

where $\sigma = \pi D(0) T_g^2$ and K_1 and K_2 are the modified Bessel functions of the second kind. This potential determines the interaction of a static quark and a static antiquark at a distance R; that is, it is a static potential in a meson. It is worth noting that this potential and the gluon field calculated in a meson with the aid of a bound probe by the method of vacuum correlation functions [15] are related by the equation

$$\frac{dV_M(R)}{dR} = \frac{2\sigma}{\pi} \int_0^{R/T_g} dx x K_1(x) \equiv E_0(R), \qquad (26)$$

where $E_0(R)$ is the confining field that acts on the quark.

In the case of a nondiagonal potential, we have $\mathbf{n}^{(a)}\mathbf{n}^{(b)} = -1/2$ and

$$V_{\rm nd}(R) = \frac{2}{\sqrt{3}}\sigma T_g - \frac{3\sqrt{3}}{2\pi}\frac{\sigma R^2}{T_g} \qquad (27)$$

$$\times \int_{\frac{\pi}{6}}^{\frac{\pi}{3}} \frac{d\varphi}{\cos\varphi} K_2\left(\frac{\sqrt{3}R}{2T_g \cos\varphi}\right).$$

It is worthy of note that this potential is positive, growing from zero to $(2/\sqrt{3})\sigma T_g$, and that it is saturated for $R \gtrsim 0.6$ fm.

The behavior of the potential in (24) as a function of the minimum string length in a baryon, $L = R_1 + R_2 + R_3 = 3R$, is illustrated in Fig. 2, along with lattice data from [4]. It can be seen that the potential faithfully reproduces these lattice results. At long distances, $L \gtrsim 1.5$ fm, the potential grows linearly with a slope equal to σ. At characteristic hadron scales, the slope of the potential decreases, which is demonstrated in Fig. 2 by the tangent to the potential at the point $L = 0.7$ fm, where its slope is $\sim 0.9\sigma$. It is interesting to note that, for $L < 1.5$ fm, all points from the lattice simulation fit in the tangent quite well. In connection with the phenomenology of baryon spectra, the effect of the baryon-potential slope reduced in relation to the slope of the meson static potential was discussed in [16] more than fifteen years ago. Within the method of vacuum correlation functions, this effect was calculated analytically for the first time.

Let us analyze the potential calculated in [5] on the basis of lattice theory. For this purpose, we supplement the potential in (24) with the perturbative one-gluon-exchange color Coulomb potential

$$V_{\rm pert} = -\frac{3}{2}\frac{C_F \alpha_s}{r}, \qquad (28)$$

where $C_F = 4/3$ is the fundamental Casimir operator. The results are displayed in Fig. 3. It can be seen that our potential faithfully reproduces these independent results of numerical lattice simulations as well.

In the case of a triangle where the distances R_a from the quarks involved to the string junction are different and where the angles do not exceed $2\pi/3$, we have

$$V_B(R_1, R_2, R_3) = \sum_{a=1}^{3} V_M(R_a) + \sum_{a<b} V_{\rm nd}(R_a, R_b), \qquad (29)$$

where

$$V_{\rm nd}(R_a, R_b) = \frac{2\sigma T_g}{3\sqrt{3}} - \frac{\sqrt{3}\sigma}{4\pi T_g} \qquad (30)$$

$$\times\left\{R_a^2\int\limits_0^{\tilde\varphi_{ab}}\frac{d\varphi}{\cos^2\left(\varphi+\frac{\pi}{6}\right)}K_2\left(\frac{\sqrt{3}R_a}{2T_g\cos\left(\varphi+\frac{\pi}{6}\right)}\right)\right.$$
$$\left.+R_b^2\int\limits_{\tilde\varphi_{ab}}^{\frac{\pi}{3}}\frac{d\varphi}{\sin^2\varphi}K_2\left(\frac{\sqrt{3}R_b}{2T_g\sin\varphi}\right)\right\},$$

with $\tilde\varphi_{ab}=\arctan(\sqrt{3}/(1+2R_a/R_b))$.

If one of the angles of the triangle is larger than $2\pi/3$, then the string junction coincides in position with the quark at the vertex of this angle. We denote by α the angle complementary to this one and by r_1 and r_2 the distances from this vertex to the neighboring quarks. We then have $\mathbf{n}\cdot\mathbf{n}_2=-\cos\alpha$ and

$$V_B(r_1,r_2,\alpha)=V_M(r_1)+V_M(r_2)+V_{\rm nd}(r_1,r_2,\alpha), \tag{31}$$

where

$$V_{\rm nd}(r_1,r_2,\alpha)=\frac{2\alpha\cot\alpha}{\pi}\sigma T_g-\frac{\sigma\sin2\alpha}{2\pi T_g} \tag{32}$$
$$\times\left\{r_1^2\int\limits_0^{\tilde\varphi}\frac{d\varphi}{\sin^2(\alpha-\varphi)}K_2\left(\frac{r_1\sin\alpha}{T_g\sin(\alpha-\varphi)}\right)\right.$$
$$\left.+r_2^2\int\limits_{\tilde\varphi}^{\alpha}\frac{d\varphi}{\sin^2\varphi}K_2\left(\frac{r_2\sin\alpha}{T_g\sin\varphi}\right)\right\},$$

with $\tan\tilde\varphi=r_2\sin\alpha/(r_1+r_2\cos\alpha)$. It should also be noted that

$$V_{\rm nd}(r_1,r_2,\alpha)=V_{\rm nd}(r_2,r_1,\alpha),$$
$$V_{\rm nd}(r_1,r_2,\pi/3)=V_{\rm nd}(r_1,r_2),$$
$$V_{\rm nd}(R,R)=(1/3!)V_{\rm nd}(R).$$

In order to analyze the dependence of the potential on the arrangement of quarks, we consider its behavior in isosceles triangles for a fixed string length $L=R_1+R_2+R_3$ versus the angle at the vertex γ. At distances of $R_a\gtrsim0.5$ fm, it is legitimate to approximate the expression under study by using asymptotic formulas that follow from (25), (30), and (32). We then have

$$V_M(R)\approx\sigma R-\frac{4}{\pi}\sigma T_g, \tag{33}$$
$$V_{\rm nd}(R_a,R_b)\approx\frac{2\sigma T_g}{3\sqrt{3}},$$
$$V_{\rm nd}(r_1,r_2,\alpha)\approx\frac{2\alpha\cot\alpha}{\pi}\sigma T_g.$$

It follows that, at $\gamma=0$, in which case the positions of two quarks coincide, so that they are in the antitriplet of the $SU(3)$ color group, the baryon potential in an isosceles triangle reduces to a meson potential; that is,

$$V^L(\gamma=0)\approx\sigma L-\frac{4}{\pi}\sigma T_g. \tag{34}$$

If $0<\gamma<2\pi/3$, the string consists of three straight-line segments, in which case we have

$$V^L(0<\gamma<2\pi/3)\approx\sigma L+\left(-\frac{12}{\pi}+\frac{2}{\sqrt{3}}\right)\sigma T_g. \tag{35}$$

But if the string consists of two segments, then we have

$$V^L(\gamma\geq2\pi/3)\approx\sigma L \tag{36}$$
$$+\left(-\frac{8}{\pi}+\frac{2}{\pi}(\pi-\gamma)\cot(\pi-\gamma)\right)\sigma T_g.$$

From formulas (34)–(36), it follows that, as the angle γ increases from the value of $\gamma=0$, the potential decreases fast by the value

$$\Delta V_1=\left(\frac{8}{\pi}-\frac{2}{\sqrt{3}}\right)\sigma T_g\approx150\ \text{MeV} \tag{37}$$

and changes only slightly in the range $0\lesssim\gamma\lesssim2\pi/3$, whereupon it increases fast in the vicinity of the point $\gamma\approx2\pi/3$ by the value

$$\Delta V_2=\left(\frac{4}{\pi}-\frac{4}{3\sqrt{3}}\right)\sigma T_g\approx55\ \text{MeV} \tag{38}$$

and grows slowly in the range $2\pi/3\leq\gamma\leq\pi$ in such a way that

$$\Delta V_3\equiv V^L(\gamma\to\pi)-V^L\left(\frac{2\pi}{3}\right) \tag{39}$$
$$=\left(\frac{2}{\pi}-\frac{2}{3\sqrt{3}}\right)\sigma T_g\approx30\ \text{MeV},$$

where the numerical values are given for $\sigma=0.18\ \text{GeV}^2$ and $T_g=0.12$ fm. The baryon potential in an isosceles triangle for $L=1.8$ fm is shown in Fig. 4 as a function of the angle γ. It should be noted that the characteristic jumps of the potential are proportional to σT_g; that is, they are determined both by confinement and by correlations of stochastic nonperturbative fields. It would be of interest to obtain them independently within lattice QCD. The quark configurations considered in [4], where the angles satisfied the condition $\pi/20\lesssim\alpha<\pi/2$, provide no information about this dependence. In the region of small angles, simulations are complicated both by a strong effect of perturbative fields and by the finiteness of the lattice parameter. In order to examine this dependence, it is therefore necessary to consider configurations featuring large angles.

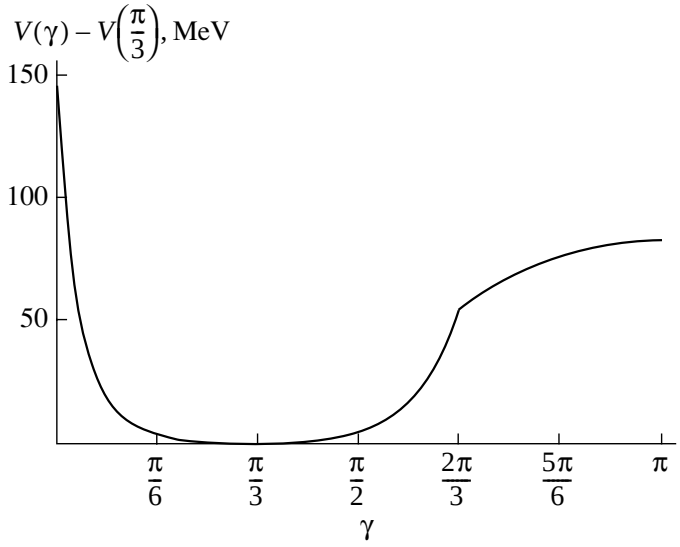

Fig. 4. Potential in an isosceles triangle for the total string length of $L = 1.8$ fm versus the angle at the vertex γ for $\sigma = 0.18$ GeV^2 and $T_g = 0.12$ fm.

It is also of interest to explore the effect of gluon-field interaction on the string shape in the string-junction region. This effect is determined by the energy in the string-junction region, that is, by the quantity

$$\tilde{V}^L(\gamma) = \frac{1}{2}\left(\sum_{a=1}^{3} V_M(R_a) - \sigma L\right) + \sum_{a<b} V_{\rm nd}(R_a, R_b). \tag{40}$$

In the case where the angle at the apex of the isosceles triangle satisfies the condition $2\pi/3 \le \gamma \le \pi$ and where the string length is fixed, this potential behaves in just the same way as the total potential $V^L(\gamma)$ since, in this region, the angular dependence is determined by the off-diagonal term exclusively. This means that the field in the string-junction region grows with increasing angle. The jump of $\tilde{V}$ at $\gamma = 0$ is

$$\Delta\tilde{V}_1 = \left(\frac{4}{\pi} - \frac{2}{\sqrt{3}}\right)\sigma T_g = 0.12\sigma T_g \approx 13\ \text{MeV}. \tag{41}$$

At $\gamma = 2\pi/3$, it is negative,

$$\Delta\tilde{V}_2 = \left(\frac{2}{\pi} - \frac{4}{3\sqrt{3}}\right)\sigma T_g = -0.13\sigma T_g \approx -15\ \text{MeV}; \tag{42}$$

that is, the energy decreases. It can be concluded that the field in the vicinity of the string junction depends on the arrangement of quarks insignificantly and that its magnitude at the string junction is close to the magnitude of the field in the string segments, possibly exceeding it. This conclusion is at odds with the field distributions obtained in [14, 15], where the authors made an error in input formulas (11)–(18) in [14] and (27) in [15], which should be associated with the distributions of fields in three interacting mesons for the case where three antiquarks occur at the same point.

4. CONCLUSION

The nonperturbative static potential in a baryon has been calculated analytically for an arbitrary arrangement of the quarks involved. The result obtained in this way provides a basis for accurately investigating the spectra of baryons—first of all, nucleons—and is of considerable importance for various applications in nuclear physics.

Two effects peculiar to the potential in a baryon have been examined. First, there is the effect of an increase in the slope of the nonperturbative potential with increasing total string length. It has been shown that the slope grows from zero to σ and that it is about 0.9σ at characteristic hadron scales. It has also been shown that the behavior of the potential as a function of the string length is fully consistent with the latest lattice results. Second, the dependence of the potential on the arrangement of quarks at a fixed value of the total string length has been studied for the first time. It has been revealed that the magnitude of this effect (potential difference) is proportional to the parameter σT_g; that is, it is determined by two nonperturbative phenomena, confinement and correlations of stochastic nonperturbative fields. The effect

is the most significant when the quarks form a triangle having a large angle. For configurations featuring a large angle, further investigation on a lattice would be of considerable interest since this would make it possible to verify the effect of the configuration dependence of the potential and to calculate the correlation length T_g precisely.

The error previously made in [14, 15] in using the method of vacuum correlation functions to calculate off-diagonal terms of the potential in an equilateral triangle—the necessary factor of $-1/2$ was absent in those studies—has been corrected in the present article. The error in the field distributions in a baryon that were calculated in [14, 15] has also been indicated.

ACKNOWLEDGMENTS

I am grateful to Yu.A. Simonov for numerous stimulating discussions. I am also indebted to T. Takahashi and Ph. de Forcrand for placing the numerical results of their lattice simulations at my disposal and to V.I. Shevchenko for discussions on some individual points of this study.

This work was supported by the Russian Foundation for Basic Research (project nos. 00-02-17836, 00-15-96786) and by INTAS (grant nos. 00-00110, 00-00366).

REFERENCES

1. A. Di Giacomo, H. G. Dosch, V. I. Shevchenko, and Yu. A. Simonov, hep-ph/0007223; Phys. Rep. **372**, 319 (2002).
2. H. G. Dosch, Phys. Lett. B **190**, 177 (1987); H. G. Dosch and Yu. A. Simonov, Phys. Lett. B **205**, 399 (1988); Yu. A. Simonov, Nucl. Phys. B **307**, 512 (1988).
3. A. Yu. Dubin, A. B. Kaidalov, and Yu. A. Simonov, Phys. Lett. B **323**, 41 (1994); Phys. Lett. B **343**, 310 (1995); Yu. S. Kalashnikova, A. V. Nefediev, and Yu. A. Simonov, Phys. Rev. D **64**, 014037 (2001).
4. T. T. Takahashi *et al.*, Phys. Rev. D **65**, 114509 (2002).
5. C. Alexandrou, Ph. de Forcrand, and O. Jahn, hep-lat/0209062.
6. Yu. A. Simonov, Pis'ma Zh. Éksp. Teor. Fiz. **71**, 187 (2000) [JETP Lett. **71**, 127 (2000)]; hep-ph/0001244; V. I. Shevchenko and Yu. A. Simonov, Phys. Rev. Lett. **85**, 1811 (2000).
7. G. S. Bali, Nucl. Phys. B (Proc. Suppl.) **83**, 422 (2000).
8. N. G. Van Kampen, *Stochastic Processes in Physics and Chemistry* (North-Holland, Amsterdam, New York, 1981; Vysshaya Shkola, Moscow, 1990).
9. M. Campostrini, A. Di Giacomo, and G. Mussardo, Z. Phys. C **25**, 173 (1984); A. Di Giacomo and H. Panagopoulos, Phys. Lett. B **285**, 133 (1992); A. Di Giacomo, E. Meggiolaro, and H. Panagopoulos, Nucl. Phys. B **483**, 371 (1997).
10. G. S. Bali, N. Brambilla, and A. Vairo, Phys. Lett. B **421**, 265 (1998).
11. Yu. A. Simonov, Nucl. Phys. B **592**, 350 (2001).
12. F. J. Ynduráin, *The Theory of Quark and Gluon Interactions* (Springer-Verlag, Berlin, 1999), p. 208.
13. B. V. Geshkenbein, B. L. Ioffe, and K. N. Zyablyuk, Phys. Rev. D **64**, 093009 (2001); B. L. Ioffe and K. N. Zyablyuk, hep-ph/0207183; Eur. Phys. J. C **27**, 229 (2003); B. L. Ioffe, hep-ph/0209313.
14. D. S. Kuzmenko and Yu. A. Simonov, Phys. Lett. B **494**, 81 (2000).
15. D. S. Kuz'menko and Yu. A. Simonov, Yad. Fiz. **64**, 110 (2001) [Phys. At. Nucl. **64**, 107 (2001)]; hep-ph/0010114.
16. S. Capstick and N. Isgur, Phys. Rev. D **34**, 2809 (1986).

Translated by A. Isaakyan

Physics of Atomic Nuclei, Vol. 66, No. 12, 2003, pp. 2233–2237. From Yadernaya Fizika, Vol. 66, No. 12, 2003, pp. 2285–2289.

ELEMENTARY PARTICLES AND FIELDS
Theory

Pion Damping Width from $SU(2) \times SU(2)$ NJL Model*

D. Blaschke, M. K. Volkov, and V. L. Yudichev

Joint Institute for Nuclear Research, Dubna, Moscow oblast, 141980 Russia

Received November 26, 2002; in final form, March 3, 2003

Abstract—Within the framework of the NJL model, we investigate the modification of the pion damping width in a hot pion gas for temperatures ranging from 0 to 180 MeV. The pion is found to broaden noticeably at $T > 60$ MeV. Near the chiral phase transition $T \sim 180$ MeV, the pion width is saturated and amounts to 70 MeV. The main contribution to the width comes from pion–pion collisions. Other contributions are found to be negligibly small. © *2003 MAIK "Nauka/Interperiodica".*

1. INTRODUCTION

In the atmosphere of growing interest in quark–gluon plasma, observations of dilepton (electron–positron pair) production in relativistic heavy-ion collisions draw more and more attention of physicists making efforts to investigate hadron physics in extreme conditions of temperature and density. Experimental data have already been taken, and some recent analyses on the dilepton production in Pb + Au (158 GeV/u) collisions are available, e.g., from the CERES Collaboration [1, 2].

Insofar as the description of hot and dense media directly from QCD is not yet available, simulation of such processes is an urgent problem. Recently, an attempt was made to account for the observed dilepton production rate [1, 2] using the simple Bjorken scenario of the spacetime evolution [3, 4] of an ultrarelativistic heavy-ion collision and the vector-dominance-model expression for the pion electromagnetic form factor [4]. In [4], it was concluded that the experimental dilepton spectrum could not be explained without assuming a modification of the ρ-meson mass and width in the medium.

Besides the ρ-meson mass and width modification, the same is expected for pions. Pions dominate in heavy-ion collisions and it is very important to study how their properties change with increasing temperature and density, especially when approaching a phase transition in hot matter. The behavior of the pion in extreme conditions has already been investigated in models of the NJL type [5–8] within the mean-field approximation, which is common in NJL [9, 10], but does not take into account collisions in the pion gas. However, as we show in our paper, collisions can give a significant contribution to the pion width in extreme conditions.

For light particles (like pions), the density increases with temperature approximately as T^3. Thus, one expects that the density is large near the supposed phase-transition temperature T_c, and collisions of particles occur at a much higher rate than in cold matter. Collisions lead to shorter lifetimes (or larger widths) of hadronic states in extreme environmental conditions. In terms of hadron correlators, an additional imaginary contribution to the hadron self-energy operator comes from collision integrals [11], thereby broadening all particles in the hadron gas. The resulting width is closely related to the process of returning a disturbed many-particle system to an equilibrium state: damping. Further, the width thus formed is called the damping width.

There are several approaches to calculate the collision integrals. In our work, we follow the prescription given by Kadanoff and Baym [11]. This way, the contribution to the hadron self-energy from collision integrals has a straightforward interpretation: its reciprocal is the average time between two consecutive collisions, the lifetime. To estimate the average lifetime of a hadron state, one needs to know cross sections for different collision processes averaged over the density of particles with the Bose amplification and Pauli suppression taken into account.

One can try to find the modified self-energy of a particle using a self-consistent functional formalism, as is described, e.g., by Hees and Knoll in [12]. However, in [12], the pion damping width was treated as an external parameter and was not fixed. Our purpose is to find an estimate for the pion damping width from a simple quark model and investigate possible implications of the pion broadening. We calculate cross sections in the framework of the bosonized NJL model with infrared cutoff [8]. The meson spectral functions are chosen to be of the Breit–Wigner form. Then, we iterate the equation for the width until a self-consistent solution is found.

*This article was submitted by the authors in English.

1063-7788/03/6612-2233$24.00

The structure of our paper is as follows. In Section 2, we introduce the pion damping width. In Section 3, the cross section of the process $\pi\pi \to \pi\pi$ is derived. The numerical results are given in Section 4. The discussion is given in the last section.

2. PION LIFETIME IN HOT MATTER

In vacuum, the lifetime of a particular state is determined by the probability of its decay into other states. Thus, a stable particle gains no width in vacuum at all, whereas in a dense medium a particle can strike another one and change its initial state. Thus, the lifetime of a particular state is determined by its collision rate. There are also inverse processes that can restore the decayed state due to the interaction of particles in the medium, and then one can find this state again. This process prolongs the lifetime of the state. Therefore, the average lifetime of a particular state is determined by the direct and inverse processes.

The in-medium hadron properties are usually investigated in terms of correlators. A two-point correlator can then be expressed through a spectral function that is just the correlator's imaginary part. For a stable particle, whose correlator has only one pole, the spectral function is simply a delta function, while, for a state whose energy is spread, the spectral function is a continuous function of energy and momentum.

As discussed in [11], the probability that, after putting a particle with momentum p in the gas at the time t and removing the particle with the same momentum at time t', one can find the gas in the same state as in the beginning decays as $e^{-\Gamma(t'-t)}$, where Γ is a constant determining the decay rate and is usually called the width. If one chooses the spectral function in the Breit–Wigner form

$$A(s) = \frac{1}{\pi}\,\frac{M\Gamma}{(s-M^2)^2 + M^2\Gamma^2}, \qquad (1)$$

where M is the mass of the state, the probability decays as $e^{-\Gamma(t'-t)}$ (see [11]). Here, the width is a measure of the dispersion of the state energy. In general, the width is a function of energy and momentum, and one would finally come to a set of functional equations for the width, which are difficult to solve. In our work, we approximate the pion width by a constant and obtain a simple equation to be solved by iteration. However, the width is supposed to depend on the temperature and density.

The pion damping width (or lifetime τ) can be calculated by the following formula from [11]:

$$\Gamma(p) = \tau^{-1}(p) = \Sigma^{>}(p) - \Sigma^{<}(p), \qquad (2)$$

where

$$\Sigma^{<}(p) = \int_{p_1}\int_{p_3}\int_{p_4} (2\pi)^4 \delta_{p_1,p;p_3,p_4} \times |\mathcal{T}|^2 G^{>}(p_1) G^{<}(p_3) G^{<}(p_4), \qquad (3)$$

$$\Sigma^{>}(p) = \int_{p_1}\int_{p_3}\int_{p_4} (2\pi)^4 \delta_{p_1,p;p_3,p_4} \times |\mathcal{T}|^2 G^{<}(p_1) G^{>}(p_3) G^{>}(p_4), \qquad (4)$$

in accordance with the notation given in [11]. Here, $\mathcal{T}$ is the process amplitude (this will be given in Section 3); $G_i^{>}(p) = [1 + n_i(\mathbf{p}, s_i, T)]A_i(p^2)$, and $G_i^{<}(p) = n_i(\mathbf{p}, s, T)A_i(p^2)$, with n_i being the boson occupation numbers

$$n_i(\mathbf{p}, s_i, T) = \left[\exp\left(\frac{\sqrt{\mathbf{p}^2 + s_i}}{T}\right) - 1\right]^{-1} \qquad (5)$$

and $A_i(p^2)$ being the spectral function of the ith state. We also use the notations $\int_{p_i} = \int d^4p_i/(2\pi)^4$ and $\delta_{p_1,p_2;p_3,p_4} = \delta(p_1 + p_2 - p_3 - p_4)$ in (3) and (4), omitting the subscript at p_2 to comply with the general definition of width (2); $p_2 = p$ is assumed throughout the rest of the paper. The integration is performed in the four-dimensional momentum space over the momenta p_1, p_3, p_4. The indices 1 and 2 correspond to the initial states, while 3 and 4 correspond to the final states. The width Γ is calculated for pion 2 resting in the heat-bath frame.

For the inverse lifetime of a pion, one thus obtains

$$\tau^{-1} = \Gamma = \int \frac{d^3\mathbf{p}_1}{(2\pi)^3} \int ds_1 v_{\rm rel} A_\pi(s_1) \times [n_\pi(\mathbf{p}_1, s_1, T)\sigma^{\rm dir*}(s; s_1, s_2) - (1 + n_\pi(\mathbf{p}_1, s_1, T))\sigma^{\rm inv*}(s; s_1, s_2)], \qquad (6)$$

where $v_{\rm rel}$ is the relative velocity of particles 1 and 2, and $\sigma^{\rm dir*}(s; s_1, s_2)$ and $\sigma^{\rm inv*}(s; s_1, s_2)$ are the averaged cross sections for the "direct" and "inverse" processes, respectively, with the probability of the final states to be off-mass-shell taken into account:

$$\sigma^{\rm dir(inv)*}(s; s_1, s_2) = \int ds_3 \int ds_4 A_\pi(s_3) \times A_\pi(s_4)\sigma^{\rm dir(inv)}(s; s_1, s_2, s_3, s_4) \qquad (7)$$

(for definitions of s and s_i, see (13) and (16) below).

What one needs then is the cross sections of the processes under investigation. The amplitudes of these processes can be calculated in an effective model of pion interaction. In the next section, we calculate the amplitudes and cross sections in the framework of the NJL model with infrared cutoff [8].

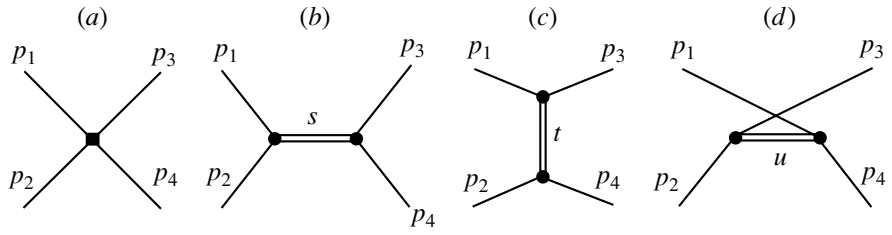

Fig. 1. Diagrams contributing to the $\pi\pi \to \pi\pi$ amplitude.

3. PION–PION SCATTERING AMPLITUDE AND CROSS SECTION FROM NJL MODEL

3.1. The $\pi\pi \to \pi\pi$ Amplitude

Let us consider scattering of π^0 on a pion from the medium: $\pi^0\pi^0 \to \pi^0\pi^0$, $\pi^0\pi^0 \to \pi^+\pi^-$, $\pi^0\pi^\pm \to \pi^0\pi^\pm$. We allow also for the lightest scalar–isoscalar resonance, the σ meson, as an intermediate state ($\pi\pi \to \sigma \to \pi\pi$), because of its importance shown in various investigations of pion–pion interaction [7, 9, 13, 14]. Here, we use an $SU(2) \times SU(2)$ chiral quark model of the NJL type [9, 10], where, using the bosonization procedure, one obtains the Lagrangian for pions and σ mesons. The part that contains three- and four-particle vertices has the form

$$\mathcal{L}_{\text{int}} = 2mg_\sigma\sigma^3 + 2mg_\pi\sqrt{Z}\sigma(2\pi^+\pi^- + (\pi^0)^2) - g_\pi^2\sigma^2\pi^2 - \frac{g_\pi^2 Z}{2}(4\pi^+\pi^-\pi^+\pi^- + 4\pi^+\pi^-(\pi^0)^2 + (\pi^0)^4) - \frac{g_\sigma^2}{2}\sigma^4. \quad (8)$$

Here, m is the constituent quark mass ($m = g_\pi f_\pi$; $f_\pi = 93$ MeV is the pion weak decay constant in vacuum). The constants g_π and g_σ describe the interaction of the pion and σ meson with quarks, respectively. They are related to each other by the equation

$$g_\pi = g_\sigma\sqrt{Z}. \quad (9)$$

The constant Z originates from π–a_1 transitions and is equal to

$$Z = \left(1 - \frac{6m^2}{M_{a_1}^2}\right)^{-1}, \quad (10)$$

where $M_{a_1}^2 = 1250$ MeV is the mass of a_1 meson. The values of the constituent quark mass and the constants g_π and g_σ were calculated in [8]. In vacuum, we have $m = 242$ MeV, $g_\pi = 2.61$, and $g_\sigma = 2.18$. Their values at finite temperatures and zero chemical potential were calculated in [8]; here, we use these results as input data in our calculations.

In our approach, the total amplitude of $\pi^0\pi^0 \to \pi^0\pi^0$ consists of a contact term and three resonant contributions in the scalar channel (see Fig. 1),

$$\mathcal{T}_{\pi^0\pi^0\to\pi^0\pi^0} = -24g_\pi^2 + 3\mathcal{T}_\sigma(s) + 3\mathcal{T}_\sigma(t) + 3\mathcal{T}_\sigma(u), \quad (11)$$

where

$$\mathcal{T}_\sigma(x) = \frac{4g_\pi^2 m^2}{M_\sigma^2 - x - iM_\sigma\Gamma_\sigma} \quad (12)$$

and s, t, u are kinematic invariants,

$$s = (p_1 + p_2)^2 = (p_3 + p_4)^2, \quad (13)$$

$$t = (p_1 - p_3)^2 = (p_2 - p_4)^2, \quad (14)$$

$$u = (p_1 - p_4)^2 = (p_2 - p_3)^2, \quad (15)$$

for which the following identity is satisfied:

$$s + t + u = s_1 + s_2 + s_3 + s_4; \quad s_i = p_i^2. \quad (16)$$

The momentum p_1 corresponds to the impacting pion, while p_2 relates to the pion resting in the heat bath. The momenta p_3 and p_4 are those for the particles produced after collision.

For the charged pions in the final state, the amplitudes contain two terms:

$$\mathcal{T}_{\pi^0\pi^0\to\pi^+\pi^-} = -8g_\pi^2 + 2\mathcal{T}_\sigma(s) \quad (17)$$

for the process $\pi^0\pi^0 \to \pi^+\pi^-$ (Figs. 1*a* and 1*b*);

$$\mathcal{T}_{\pi^0\pi^\pm\to\pi^0\pi^\pm} = -8g_\pi^2 + 2\mathcal{T}_\sigma(t) \quad (18)$$

for $\pi^0\pi^\pm \to \pi^0\pi^\pm$ (Figs. 1*a* and 1*c*).

In the medium, model parameters depend on temperature and density. In our work, as only mesons are considered, we restrict ourselves to the case of zero chemical potential, for which the temperature dependence of the model parameter has been obtained in [8]. We use these results in [8] as input data in our calculations.

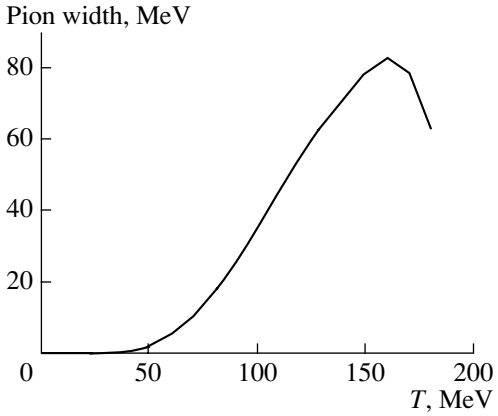

Fig. 2. Pion damping width as a function of T.

3.2. Cross Sections

The differential cross section for pion–pion scattering is determined by the equation

$$\frac{d\sigma^{\rm dir}}{dt} = \frac{|\mathcal{T}|^2(1+n_3)(1+n_4)}{64\pi s|\mathbf{p}_{1,\rm c.m.}|^2} \tag{19}$$

for the direct process and by

$$\frac{d\sigma^{\rm inv}}{dt} = \frac{|\mathcal{T}|^2 n_3 n_4}{64\pi s|\mathbf{p}_{1,\rm c.m.}|^2} \tag{20}$$

for the inverse process. Here, $\mathbf{p}_{1,\,\rm c.m.}$ is the momentum of pion 1 in the c.m. frame for pions 1 and 2; n_3 and n_4 are the occupation numbers of produced pions.

Having integrated over t in the interval defined by the lower and upper limits

$$t_{\rm min} = \left(\frac{s_1 - s_2 - s_3 + s_4}{2\sqrt{s}}\right)^2 - (|\mathbf{p}_{1,\rm c.m.}| + |\mathbf{p}_{3,\rm c.m.}|)^2, \tag{21}$$

$$t_{\rm max} = \left(\frac{s_1 - s_2 - s_3 + s_4}{2\sqrt{s}}\right)^2 - (|\mathbf{p}_{1,\rm c.m.}| - |\mathbf{p}_{3,\rm c.m.}|)^2, \tag{22}$$

we obtain the total cross section. The c.m. momenta of pions are determined by the equation

$$|\mathbf{p}_{i,\rm c.m.}| = \sqrt{E_{i,\rm c.m.}^2 - s_i}, \qquad i = 1,3, \tag{23}$$

where the energies $E_{i,\rm c.m.}$ are defined in the c.m. frame

$$E_{1,\rm c.m.} = \frac{s + s_1 - s_2}{2\sqrt{s}}, \tag{24}$$

$$E_{3,\rm c.m.} = \frac{s + s_3 - s_4}{2\sqrt{s}}. \tag{25}$$

To calculate the occupation numbers n_i in (19) and (20), one needs to know the energies of pion 3 and pion 4 in the heat-bath frame,

$$E_3 = \frac{s_2 + s_3 - t}{2\sqrt{s_2}}, \qquad E_4 = \frac{s_2 + s_4 - t}{2\sqrt{s_2}}. \tag{26}$$

In the case of pion–pion collisions, four processes contribute to the total cross section:

$$\sigma(\pi\pi \to \pi\pi) = \sigma(\pi^0\pi^0 \to \pi^0\pi^0) + \sigma(\pi^0\pi^0 \to \pi^+\pi^-) + 2\sigma(\pi^0\pi^+ \to \pi^0\pi^+). \tag{27}$$

The process $\pi^0\pi^+ \to \pi^0\pi^+$ occurs at the same rate as $\pi^0\pi^- \to \pi^0\pi^-$, so we do not calculate them separately; we just put the factor 2 before the last term in (27). To obtain the pion damping width, we substitute the obtained cross sections into Eqs. (6) and (7).

4. NUMERICAL RESULTS

Using the definition of the pion lifetime given in Section 2 and the cross sections determined in Section 3, we evaluate numerically the pion damping width at temperatures ranging from 0 to 180 MeV. The upper limit on the temperature scale corresponds to the expected transition from the phase with broken chiral symmetry to the symmetric phase. The resulting curves are shown in Fig. 2.

All calculations are performed for a neutral pion resting in the heat-bath frame. The pion self-energy is approximated by a constant.

As one can see from Fig. 2, the pion state already broadens noticeably in hot matter, as compared to the vacuum state, at $T \approx 60$ MeV. At $T = 160$ MeV, the pion–pion scattering accounts for about 80 MeV in the total width; this is the maximum value. Then, the curve in Fig. 2 turns down; this behavior of the damping width is caused by a noticeable decrease in the constant g_π after $T = 160$ MeV. The cross section is proportional to g_π^4, whose value falls by half at $T = 180$ MeV compared to $T = 160$ MeV. For temperatures from 160 to 180 MeV, this weakening of the pion–pion interaction overpowers the expected increase in collision integrals.

Besides the pion–pion scattering, we also estimated some other possible contributions to the pion width. They come from the following processes: $\pi\pi \to \sigma\sigma$, $\pi\sigma \to \pi\sigma$, $\pi\pi \to \sigma$, and $\pi\pi \to \bar{q}q$. All these contributions were calculated separately, i.e., with other modes switched off. (This gives the upper limit for a solution to the equation for width, because the collision integrals decrease if the spectral functions broaden.) They turned out to be small. At $T =$ 180 MeV (which is a little below $T_c = 186$ MeV [8]), $\pi\sigma \to \pi\sigma$ gives about 5 MeV, $\pi\pi \to \sigma\sigma$ about 1 MeV, and $\pi\pi \to \sigma$ even less than 1 MeV. The decays

to quarks contribute less than 7 MeV to the pion width. The smallness of these contributions was the reason for discarding them in our calculations, whose purpose is to make a qualitative estimate for the pion damping width.

5. DISCUSSION AND CONCLUSION

In the framework of the $SU(2) \times SU(2)$ NJL model, the pion damping width was calculated for the range of temperatures from 0 to 180 MeV. The definition for the damping width given in [11] was used. A self-consistent method, where the pion width does not depend on energy and momentum, was used to estimate the contributions to the pion damping width from pion–pion scattering in hot and dense matter. Upper limits for alternative contributions were estimated qualitatively. It was found that the pion–pion scattering is dominant, and other processes that give small contributions can be discarded.

In our investigation, we came to the conclusion that, in a hot gas, the pion spectral function broadens significantly while nearing the phase transition point. This may have many implications for various processes in hot and dense matter, where pions are involved. In particular, this can affect the dilepton production through pion–pion annihilation in heavy-ion collisions [4].

Of course, a more systematic and formal approach, like one suggested by Hees and Knoll [12], would be more preferable for a study of processes occurring in hot matter. Nevertheless, our approach, which stems from quantum statistical mechanics, has a clear physical interpretation, and it allowed us to make a prediction for the behavior of the pion damping width in hot matter. Furthermore, similar calculations can be done for other particles, e.g., for the σ and ρ mesons. The σ-meson width at those temperatures at which the direct decay $\sigma \to \pi\pi$ is suppressed and contributions from collision integrals to the σ-meson width become noticeable is of particular interest. Moreover, the diagrams with the σ pole play an important role in different processes occurring in hot matter.

ACKNOWLEDGMENTS

This work was supported by the Russian Foundation for Basic Research (project no. 02-02-16194) and Heisenberg–Landau program.

REFERENCES

1. G. Agakishiev *et al.* (CERES Collab.), Phys. Lett. B **422**, 405 (1998).
2. B. Lenkeit *et al.* (CERES Collab.), Nucl. Phys. A **661**, 23 (1999).
3. J. D. Bjorken, Phys. Rev. D **27**, 140 (1983).
4. H.-J. Schulze and D. Blaschke, Phys. Lett. B **386**, 429 (1996).
5. M. Asakawa and K. Yazaki, Nucl. Phys. A **504**, 668 (1989).
6. D. Ebert, Yu. L. Kalinovsky, L. Münchov, and M. K. Volkov, Int. J. Mod. Phys. A **8**, 1295 (1993).
7. T. Hatsuda and T. Kunihiro, Phys. Rep. **247**, 221 (1994).
8. D. B. Blaschke, G. R. G. Burau, M. K. Volkov, and V. L. Yudichev, Eur. Phys. J. A **11**, 319 (2001).
9. M. K. Volkov, Fiz. Élem. Chastits At. Yadra **17**, 433 (1986) [Sov. J. Part. Nucl. **17**, 186 (1986)].
10. D. Ebert, H. Reinhardt, and M. K. Volkov, Prog. Part. Nucl. Phys. **35**, 1 (1994).
11. L. P. Kadanoff and G. Baym, *Quantum Statistical Mechanics* (Benjamin, New York, 1962).
12. H. van Hees and J. Knoll, Nucl. Phys. A **683**, 369 (2000).
13. M. K. Volkov, A. E. Radzhabov, and N. L. Russakovich, Yad. Fiz. **66**, 1030 (2003) [Phys. At. Nucl. **66**, 997 (2003)]; hep-ph/0203170.
14. E. Quack, P. Zhuang, Yu. L. Kalinovsky, *et al.*, Phys. Lett. B **348**, 1 (1995).

Physics of Atomic Nuclei, Vol. 66, No. 12, 2003, pp. 2238–2244. From Yadernaya Fizika, Vol. 66, No. 12, 2003, pp. 2290–2296.

ELEMENTARY PARTICLES AND FIELDS
Theory

On the Relation between Effective Supersymmetric Actions in Different Dimensions*

E. T. Akhmedov[1)] and A. V. Smilga[2)]

Received November 18, 2002

Abstract—We make two remarks: (i) Renormalization of the effective charge in a four-dimensional (supersymmetric) gauge theory is determined by the same graphs and is rigidly connected to the renormalization of the metric on the moduli space of the classical vacua of the corresponding reduced quantum-mechanical system. Supersymmetry provides constraints for possible modifications of the metric, and this gives us a simple proof of nonrenormalization theorems for the original four-dimensional theory. (ii) We establish a nontrivial relationship between the effective $(0+1)$-dimensional and $(1+1)$-dimensional Lagrangians. (The latter represent conventional Kählerian σ models.) © *2003 MAIK "Nauka/Interperiodica".*

1. INTRODUCTION

Consider four-dimensional supersymmetric gauge theory placed in a small spatial torus T^3 of characteristic size L. We assume that the effective coupling constant of the theory is $g^2(L) \ll 1$ and perturbation expansion makes sense. For unitary and symplectic gauge groups G, the only classical vacua of this theory are given by constant gauge potentials A_k, $k = 1, 2, 3$, lying in the Cartan subalgebra of the group G.[3)] The low-energy dynamics of the model is determined by the effective Hamiltonian describing motion over the vacuum moduli space. Due to supersymmetry, the energy of a classical vacuum configuration remains zero after loop corrections are taken into account—no potential is generated.[4)] However, supersymmetry usually allows the existence of a nontrivial metric on the moduli space, in which case such a metric is generated after loop corrections are taken into account.

The loop corrections to the effective Hamiltonian were calculated first in [3] in the simplest case of $N = 1$ supersymmetric QED (SQED) with two chiral matter multiplets of opposite charges. In this case, the moduli space is represented by the constant gauge potentials A_k and their superpartners. Note that, for a field theory on T^3, the moduli space is compact, $0 \le A_k \le 2\pi/L$.

The original calculation was carried out in the Hamiltonian framework. The effective Hamiltonian is expressed in terms of A_k, $P_k = -i\partial/\partial A_k$, and the zero Fourier mode of the photino field $\psi_\alpha, \alpha = 1, 2$. It has the form

$$\frac{1}{e^2}H^{\text{eff}} = \frac{1}{2}f(\mathbf{A})P_k^2 f(\mathbf{A}) \qquad (1)$$
$$- \epsilon_{jkp}\bar\psi\sigma_j\psi f(\mathbf{A})\partial_p f(\mathbf{A})P_k - \frac{1}{2}f(\mathbf{A})\partial_k^2 f(\mathbf{A})(\bar\psi\psi)^2,$$

where e is the coupling constant, σ_i are the Pauli matrices, and

$$f(\mathbf{A}) = 1 - \frac{e^2}{4}\sum_{\mathbf{n}}\frac{1}{|\mathbf{A}L - 2\pi\mathbf{n}|^3} + \ldots \qquad (2)$$

(we have rescaled $A \to A/e$ compared with the normalization of [3]). In this formula, $\mathbf{n}$ is a vector belonging to the three-dimensional lattice, corresponding to the torus. The dots stand for possible higher loop corrections. Expression (2) is written for the theory where the charged fields are massless.

Note that the sum on the right-hand side of Eq. (2) diverges logarithmically at large $|\mathbf{n}|$. This is none other than the effective charge renormalization

$$e^2(L) = e_0^2\left[1 - \frac{e_0^2}{4\pi^2}\ln(\Lambda_{\text{UV}}L) + \ldots\right], \qquad (3)$$

where e_0 is the bare charge and Λ_{UV} is the ultraviolet cutoff. In the massive case and if the box is large enough, $\ln(\Lambda L)$ is replaced by $\ln(\Lambda/m)$, with m being the mass of the lightest particle in the theory. On the other hand, if we are dealing with dimensionally

*This article was submitted by the authors in English.

[1)]Institute for Theoretical and Experimental Physics, Bol'shaya Cheremushkinskaya ul. 25, Moscow, 117259 Russia.

[2)]SUBATECH, Université de Nantes, France.

[3)]This is not the case for higher orthogonal and exceptional groups [1], but these complications are beyond the scope of the present paper.

[4)]This is true only for nonchiral theories, the only theories considered in the present paper. In the theories with chiral matter content, the situation is more complicated [2].

1063-7788/03/6612-2238$24.00

reduced SQED, where all Fourier harmonics with $\mathbf{n} \neq 0$ are ignored, we obtain

$$f(\mathbf{A}) = 1 - \frac{e^2}{4|L\mathbf{A}|^3}. \quad (4)$$

It is obvious that the coefficients in Eq. (4) and in Eq. (3) are related.[5)] The knowledge of the β function allows one to determine the modification of the metric on the moduli space, and this is how the effective Hamiltonian for $N = 1$ non-Abelian theories was evaluated in recent paper [5]. The inverse is also true, however, and this is one of the main emphases of the present paper. We note that the β function of field theories can conveniently be calculated via modification of the metric in the quantum-mechanical limit, where all nonzero Fourier harmonics are ignored. Ideologically, this is the ultraviolet cutoff procedure brought to its extreme. One can call it ultraviolet chopoff.

As was mentioned, the result (1) was first obtained in the Hamiltonian framework using a systematic Born–Oppenheimer expansion for H^{eff}. There is, however, a simpler way to derive the same result: to evaluate the term $\propto \dot{\mathbf{A}} \cdot \dot{\mathbf{A}}$ in the effective Lagrangian in a slowly varying bosonic background $\mathbf{A}(t), \psi_\alpha = 0$. Other structures in the Lagrangian can be restored using supersymmetry. The plan of the paper is the following. In Section 2, we present one-loop calculations of the effective Lagrangian. We use the background-field method and demonstrate that the result is given by exactly the same graphs as the graphs determining the four-dimensional β function. As in the four-dimensional case, the contribution of the scalar determinant cancels out in the supersymmetric case, and we are left with the graphs describing fermion and gauge boson magnetic interactions.

Next, we go beyond one loop and prove in Section 3 nonrenormalization theorems for four-dimensional $N = 2$ and $N = 4$ super Yang–Mills (SYM) theories. Section 4 is not devoted to the β function, but addresses a related question of the connections between effective models in different dimensions. The Hamiltonian (1) represents a nonstandard σ model. The model enjoys $N = 2$ quantum-mechanical QM symmetry (it has two different complex supercharges), but is not a Kählerian model (Kählerian σ models are defined on even-dimensional target spaces, whereas the model (1) is defined on a three-dimensional conformally flat manifold). We show that the model (1) is related, however, to Kählerian models in a nontrivial way: to obtain a Kählerian model out of Eq. (1), one has to go back to the original four-dimensional field theory and consider it on an asymmetric torus, with the size of one of its sides much larger than the others.

2. ULTRAVIOLET CHOPOFF AND β FUNCTION

Let us consider for definiteness $N = 1$ four-dimensional $SU(2)$ SYM theory

$$\mathcal{L} = \frac{1}{g^2}\mathrm{Tr}\left(-\frac{1}{2}F_{\mu\nu}^2 + i\bar{\lambda}\not{D}\lambda\right), \quad (5)$$

where λ are Majorana fermions in the adjoint representation of $SU(2)$ and $D_\mu = \partial_\mu - i[A_\mu, \cdot]$. Put the system in a small spatial box and impose periodic boundary conditions. We would like to calculate quantum corrections to the effective action in the Abelian background field $A_\mu = C_\mu t^3$, $C_\mu = (0, C_i)$, $i = 1, 2, 3$. We assume that C_i varies slowly with time, but does not depend on spatial coordinates.[6)] The background fermionic fields (superpartners of C_μ) are taken to be zero at this stage.

The calculation can conveniently be done using the background gauge method [8]. We decompose the field in the classical (Abelian) background and quantum fluctuations,

$$A_\mu \to C_\mu t^3 + \mathcal{A}_\mu, \quad (6)$$

and add to the Lagrangian the gauge-fixing term

$$-\frac{1}{2g^2}(D_\mu^{\text{cl}}\mathcal{A}_\mu)^2, \quad (7)$$

where $D_\mu^{\text{cl}} = \partial_\mu - i\left[A_\mu^{\text{cl}}, \cdot\right]$. In what follows, we use the notation $A_\mu \equiv A_\mu^{\text{cl}} = C_\mu t^3$. The coefficient chosen in Eq. (7) defines the Feynman background gauge, which is simpler and more convenient than others. Adding (7) to the first term in Eq. (5) and integrating by parts in the action, we obtain for the gauge-field-dependent part of the Lagrangian

$$\mathcal{L}_{\mathcal{A}} = -\frac{1}{2g^2}\mathrm{Tr}\left(F_{\mu\nu}^2\right) + \frac{1}{g^2} \quad (8)$$

[5)] The procedure for getting the aforementioned relation is similar to the T-duality transformation on D branes in string theory (see, in particular, [4]). In fact, $N = 2$ SQED with doublet of hypermultiplets (plus free uncharged hypermultiplets) reduced to one dimension can be interpreted as the theory of a $D0$ brane in the vicinity of a $D4$ brane. The latter system was extensively studied [4]. In this work, we concentrate, however, on the $N = 1$, $d = 4$ systems, which have not been considered thus far in the string-theory framework.

[6)] The setup of the problem is basically the same as in [6, 7]. There are two differences: (i) We are considering the $N = 1$ rather than $N = 4$ theory and the corrections are not going to vanish. (ii) The authors of [6] did their calculation bearing in mind the geometric picture of scattered $D0$ branes, and their background was slightly more sophisticated than ours.

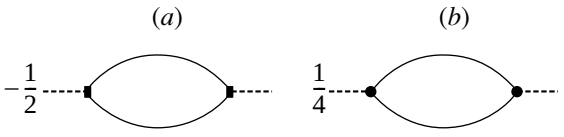

Fig. 1. One-loop renormalization of the kinetic term in SYM. Internal lines are Green's functions of the operator $(-D^2)$. The vertices involve the spin operator $J_{\alpha\beta}$ and are different for the gauge boson (a) and fermion (b) loops.

$$\times \mathrm{Tr}\left\{\mathcal{A}_\mu \left(D^2 g_{\mu\nu}\mathcal{A}_\nu - 2i\left[F_{\mu\nu}\mathcal{A}_\nu\right]\right)\right\} + \ldots,$$

where the dots stand for the terms of higher order in $\mathcal{A}_\mu$. The ghost part of the Lagrangian is

$$\mathcal{L}_{\mathrm{ghost}} = -2\mathrm{Tr}\left(\bar{c}D^2 c\right) + \text{higher order terms}, \quad (9)$$

where c is the ghost field.

Now, we can integrate over the quantum fields $\mathcal{A}_\mu$, c, and also over the fermions using the relation

$$(i\not{D})^2 = -D^2 + \frac{i}{2}\sigma_{\mu\nu}F_{\mu\nu},$$

$\sigma_{\mu\nu} = \frac{1}{2}[\gamma_\mu, \gamma_\nu]$. We obtain the effective action as follows:

$$S_{\mathrm{eff}} = -\frac{1}{2g^2}\int\limits_{T^3\times R} d^4x \mathrm{Tr}(F_{\mu\nu}^2) \quad (10)$$

$$+\log\left(\frac{\det^{\frac{1}{4}}\left(-D^2 I + \frac{i}{2}\sigma_{\mu\nu}\left[F_{\mu\nu},\cdot\right]\right)\det\left(-D^2\right)}{\det^{\frac{1}{2}}\left(-D^2 g_{\mu\nu} + 2i\left[F_{\mu\nu},\cdot\right]\right)}\right),$$

where I is a unit four-by-four matrix. We see that the fermion and gauge-field determinants involve, besides the term $-D^2$, which is also present in the scalar determinant, the term $\propto F_{\mu\nu}$ describing the magnetic moment interactions. An important observation is that, were these magnetic interactions absent, the contributions of the ghosts, fermions, and gauge bosons would just cancel and the effective action would not acquire any corrections. This feature is common for all supersymmetric gauge theories ($N = 1$, $N = 2$, $N = 4$; non-Abelian and Abelian). This fact is related to another known fact that, when the supersymmetric β function is calculated in the instanton background, only the contribution of the zero modes survives [9].

For nonsupersymmetric theories, also nonzero instanton modes provide a nonvanishing contribution in the β function. On the other hand, the contributions due to $\det(-D^2)$ in the effective action do not vanish in the nonsupersymmetric case.

To find the magnetic contributions, we have to calculate the graphs drawn in Fig. 1. The vertices there are proportional to $\epsilon^{abc}F_{\alpha\beta}J_{\alpha\beta}$ ($J_{\alpha\beta}$ being the spin operator in the corresponding representation) and the lines are Green's functions of the operator $-D^2$. Only the color components 1 and 2 circulate in the loops. They acquire the mass $|\mathbf{C}|$ in the Abelian background $C_i t^3$. One can be convinced that the gauge boson loop involves the factor -4 compared to the fermion one {the factor $\frac{1}{2} : -\frac{1}{4} = -2$ is displayed in Eq. (10) and Fig. 1 and another factor 2 comes from spin; see Eq. (16.128) in Peskin's book [8]}.

Let us calculate, say, the fermion loop. If all higher Fourier modes are "chopped off," $-D^2 \to -\partial_0^2 - \mathbf{C}^2$ and the corresponding contribution to the effective Lagrangian is

$$\frac{1}{4}\frac{1}{2}\cdot 2\dot{C}_j\dot{C}_k\mathrm{Tr}\{\sigma_{0j}\sigma_{0k}\} \quad (11)$$

$$\times\int\limits_{-\infty}^{\infty}\frac{d\omega}{2\pi}\frac{1}{\left(\omega^2+\mathbf{C}^2\right)^2} = \frac{\dot{\mathbf{C}}^2}{4|\mathbf{C}|^3}.$$

(The factor $1/4$ is the power of the determinant in Eq. (10), $1/2$ comes from the expansion of the logarithm, and 2 is the color factor.) Adding the gauge boson contribution and also the free bosonic term, we obtain

$$\frac{g^2}{L^3}\mathcal{L}_{\mathrm{bos}}^{\mathrm{eff}} = \frac{\dot{\mathbf{C}}^2}{2f^2(\mathbf{C})} \quad (12)$$

with

$$f(\mathbf{C}) = 1 + \frac{3g^2}{4L^3|\mathbf{C}|^3} + \ldots. \quad (13)$$

If higher Fourier modes are taken into account, we obtain in the exact analogy with Eq. (2)

$$f(\mathbf{C}) = 1 + \frac{3g^2}{4}\sum_{n_k}\frac{1}{\left[\sum_k (C_k L_k - 2\pi n_k)^2\right]^{3/2}} + \ldots, \quad (14)$$

where, bearing in mind further applications, we assumed that the sizes of the torus L_k, $k = 1, 2, 3$, do not coincide. The sum is logarithmically divergent at large n_k. The coefficient of the logarithm gives the β function of the $N = 1$ SYM theory. For sure, this could be expected in advance. What is not quite trivial, however, is that the calculation in the truncated theory is absolutely parallel to the well-known calculation in four dimensions [8]: in four dimensions, the corrections to the effective action are also given by the graphs in Fig. 1, and the gauge boson and the fermion contributions in the β function have the

respective coefficients $4:-1$.[7] We will see soon that this is specific for supersymmetric theories. In the nonsupersymmetric case, the β function can also be calculated with the chopoff technique, but the relevant graphs are different.

The bosonic effective Lagrangian (12) can be supersymmetrized using the superfield technique developed in [10]. The explicit expression in components was written in [5]:

$$\frac{g^2}{L_1L_2L_3}\mathcal{L} = \frac{1}{2f^2}\dot{C}^j\dot{C}^j + \frac{i}{2f^2}\left(\bar{\Psi}\dot{\Psi} - \dot{\bar{\Psi}}\Psi\right) \quad (15)$$
$$- \frac{\partial_i f}{f^3}\epsilon^{ijk}\dot{C}_j\bar{\Psi}\sigma_k\Psi + \frac{D^2}{2f^2} + \frac{D\partial_i f}{f^3}\bar{\Psi}\sigma_i\Psi$$
$$- \frac{1}{8}\partial^2\left(\frac{1}{f^2}\right)\left(\bar{\Psi}\right)^2(\Psi)^2,$$

where $\Psi = \psi f$, ψ and $\bar{\psi}$ being the canonically conjugated variables of Eq. (1), and D is the auxiliary field. The action corresponding to the Lagrangian (15) is invariant under the transformations

$$\delta_\epsilon C_k = \bar{\epsilon}\sigma_k\Psi + \bar{\Psi}\sigma_k\epsilon, \quad (16)$$
$$\delta_\epsilon\Psi_\alpha = -i(\sigma_k\epsilon)_\alpha\dot{C}_k + \epsilon_\alpha D,$$
$$\delta_\epsilon D = i\left(\dot{\bar{\Psi}}\epsilon - \bar{\epsilon}\dot{\Psi}\right),$$

where ϵ is a four-dimensional Weil fermion generating the SUSY transformations.

The chopoff procedure works also for nonsupersymmetric theories. Consider the simplest case of scalar QED. The one-loop correction to the effective Lagrangian is just

$$\delta\mathcal{L}_{\text{scalar QED}} = -i\log\det(-\partial_0^2 - A_k^2). \quad (17)$$

The double derivative term is given by the graph depicted in Fig. 2. We obtain

$$\delta\mathcal{L}_{\text{scalar QED}} = -(\mathbf{A}\cdot\dot{\mathbf{A}})^2\frac{\partial^2}{\partial\epsilon^2} \quad (18)$$
$$\times\int\limits_{-\infty}^{\infty}\frac{d\omega}{2\pi}\frac{1}{[\omega^2+\mathbf{A}^2][(\omega+\epsilon)^2+\mathbf{A}^2]}\bigg|_{\epsilon=0}$$
$$= \frac{(\mathbf{A}\cdot\dot{\mathbf{A}})^2}{8|\mathbf{A}|^5}.$$

Restoring the contribution of the higher Fourier modes, $\mathbf{A}\to\mathbf{A}-2\pi\mathbf{n}/L$, and performing the summation over $\mathbf{n}$, with averaging over directions $n_jn_k \equiv \frac{1}{3}\mathbf{n}^2\delta_{jk}$, we reproduce the known result for the one-loop β function in the scalar QED,

$$\frac{1}{e^2(L)}\bigg|_{\text{scalar QED}} = \frac{1}{e_0^2} + \frac{1}{24\pi^2}\ln(\Lambda_{\text{UV}}L). \quad (19)$$

Therefore, the chopoff method works also for nonsupersymmetric theories. Actually, it was applied before to pure Yang–Mills theory in [11]. There are three important distinctions, however:

(i) In the nonsupersymmetric case, the effective Lagrangian calculated in the Abelian background (6) involves besides the kinetic term also the potential part $\propto|\mathbf{C}|$. As a result, in the non-Abelian case, the true slow variables are not only Abelian, but all zero Fourier modes of the gauge potential, and the Born–Oppenheimer Lagrangian becomes more complicated.

(ii) A remark related to the previous one is that the metric in Eq. (18) is not conformally flat as it is in Eq. (12).

(iii) The graph in Fig. 2, which determines the correction to the effective Lagrangian in the QM limit, is quite different from the standard graph giving the β function in four dimensions. In particular, the former does not diverge in the ultraviolet in four dimensions.

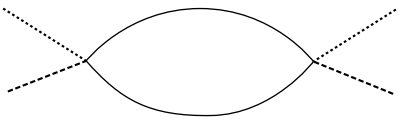

Fig. 2. Renormalization of the kinetic term in scalar QED in the QM limit. The dashed lines correspond to $\dot{\mathbf{A}}$ and the dotted lines correspond to $\mathbf{A}$.

3. NONRENORMALIZATION THEOREMS

In the dimensionally reduced $N=4$ SYM theory (alias maximally supersymmetric quantum mechanics, alias matrix model, alias the system of $D0$ branes), the corrections to the metric on the moduli space are absent. There are D-brane arguments in favor of this conclusion [12]; it was confirmed by explicit calculation [6] and finally proven using simple symmetry arguments [13]. To make the paper self-contained, we present here a somewhat refined version of these arguments.

In the maximally supersymmetric $SU(2)$ theory, the effective Lagrangian is written in terms of a nine-dimensional vector C_k and a real 16-component $SO(9)$ spinor λ_α. The Lagrangian must be invariant with respect to the supersymmetry transformations

$$\delta_\epsilon C_k = -i\epsilon\gamma_k\lambda, \quad (20)$$

[7] A remarkable fact is that one obtains the same ratio calculating the effective action in the instanton background field: the correct coefficient 6 in the β function is obtained as $8-2$, where "8" is the number of bosonic zero modes and "2" is half of the number of fermionic zero modes in the instanton background.

$$\delta_\epsilon \lambda_\alpha = \left(\gamma_k \dot{C}_k \epsilon\right)_\alpha + \left[M(C)\epsilon\right]_\alpha ,$$

where ϵ in this case is a real Grassmann spinor and γ_k are the nine-dimensional γ matrices, $\gamma_j\gamma_k + \gamma_k\gamma_j = 2\delta_{jk}$. They are all real and symmetric. The transformations (20) represent an analog of (16) with the auxiliary field expressed out by $M(C)$.

The commutator of two SUSY transformations with parameters ϵ_1 and ϵ_2 should amount to a time translation. A trivial calculation gives

$$[\delta_1, \delta_2] C_k = -2i\epsilon_2\epsilon_1 \dot{C}_k - i\epsilon_2\{\gamma_k M + M^T \gamma_k\}\epsilon_1, \tag{21}$$

and we conclude that

$$\gamma_k M + M^T \gamma_k = 0. \tag{22}$$

As was noted in [13], this implies that $M = 0$. Let us prove it. At the first step, note that any M satisfying (22) commutes with all generators $J_{kj} = \frac{1}{4}[\gamma_k, \gamma_j]$ of Spin(9). This means that, for any set λ belonging to the spinor representation of Spin(9), the set $M\lambda$ also forms a spinor representation. Hence, $M = \xi R$, where ξ is a real number and $R \in$ Spin(9). But R commutes with all generators of Spin(9) and should belong to the center of Spin(9), i.e., $M = \pm\xi I$. Then, (22) tells us that $\xi = 0$.

When proving this, we used implicitly the fact that the real spinor representation of $SO(9)$ is irreducible. If it could be decomposed in a direct sum of two other representations, we could choose M as diag$(\xi_1 z_1, \xi_2 z_2)$, with z_1 and z_2 belonging to the center of the group in the corresponding subspaces. Such M would not necessarily be proportional to I. This discussion is not purely academic. Actually, for Spin(3) and Spin(5), where real spinor representations are reducible, nontrivial matrices satisfying (22) exist.

The only structure not involving higher derivatives[8] and invariant with respect to the transformations (20) with $M = 0$ is

$$\frac{1}{2}\left[\dot{C}_k^2 + i\lambda\dot{\lambda}\right].$$

Nontrivial corrections to the metric are not allowed. Bearing in mind the discussion in the previous section, this simultaneously proves that the β function in $N = 4$ SYM theory vanishes exactly in all loops.

In the $N = 2$ case, the corrections to the metric survive, but the presence of four different complex supercharges dictates that the function $f^{-2}(\mathbf{C})$ ($\mathbf{C}$ is now a five-dimensional vector; in four dimensions, this corresponds to the gauge potential and a complex scalar) is not arbitrary, but should be a harmonic function, $\Delta^{(5)} f^{-2}(\mathbf{C}) = 0$ [15, 16]. The $O(5)$ invariance, which is manifested in the chopoff quantum-mechanical limit, tells us then that the only allowed form of the effective Lagrangian is

$$\mathcal{L}^{\text{eff}} = \frac{\dot{\mathbf{C}}^2}{2}\left(1 + \frac{\text{const}}{|\mathbf{C}|^3}\right); \tag{23}$$

i.e., all the corrections beyond one loop vanish. But this means also that multiloop corrections to the β function vanish in this case.

4. EFFECTIVE ACTION IN $(1+1)$ DIMENSIONS

Consider the gauge SYM theory with $SU(2)$ gauge group compactified on T^2 rather than on T^3. The low-energy dynamics is described by an effective $(1+1)$-dimensional field theory depending on two bosonic variables $C_{1,2}(z,t)$ and their fermionic superpartners. The effective Lagrangian represents in this case a supersymmetric Kählerian σ model.[9] The corresponding Kählerian manifold represents a two-torus dual to the spatial torus. The precise form of the metric can be determined by a simple one-loop calculation. It can be done along the same lines as in Section 2. Calculating the graphs in Fig. 1, we obtain for the correction to the effective Lagrangian density

$$\Delta\mathcal{L}^{d=2}_{\text{bos}} = -3(\partial_\alpha C_j)^2 \times \int_{-\infty}^{\infty} \frac{d^2p}{(2\pi)^2}\frac{1}{(p^2 + C_j^2)^2} = \frac{(\partial_\alpha C_j)^2}{4\pi C_j^2}, \tag{24}$$

where $\alpha = 0, 3$ and $j = 1, 2$. We obtain

$$\frac{g^2}{L^2}\mathcal{L}^{d=2}_{\text{bos}} = \frac{1}{2}(\partial_\alpha C_j)^2 \tilde{f}^{-2}(C_j), \tag{25}$$

where

$$\tilde{f}(C_j) = 1 + \frac{3g^2}{4\pi L^2 C_j^2}. \tag{26}$$

The fermion terms can be restored by supersymmetrizing. The full effective Lagrangian is

$$g^2\mathcal{L}^{d=2} = \int d^2\theta d^2\bar{\theta}\left[\bar{\Phi}\Phi - \frac{3}{4\pi}\ln\Phi\ln\bar{\Phi}\right], \tag{27}$$

where Φ is a chiral superfield with the lowest component $\phi = L(C_1 + iC_2)/\sqrt{2}$. When deriving (25), we neglected higher Fourier modes associated with compactified directions. This is justified if $|\phi| \ll 1$. (On

[8] Higher derivative terms, in particular, the term $\propto (\dot{C}_k\dot{C}_k)^2$ and its superpartners, are allowed. See [6, 14] for detailed discussion.

[9] This is a kind of folklore, but we did not see any explicit calculation in the literature.

the other hand, we have to keep $|\phi| \gg g$, otherwise higher loop corrections become relevant.) For $|\phi| \sim 1$, the higher Fourier modes should be taken into account, which can be easily done by substituting $C_j \to C_j - 2\pi n_j/L$ and performing the sum over integer two-dimensional n_j.

It is very instructive to explore the relationship between the effective $d = 2$ Lagrangian (27) and our nonstandard $(0+1)$-dimensional σ model (15). To begin with, let us study the geometric structure of the Lagrangian (15). To this end, we integrate out the auxiliary field D and express the Lagrangian in the form

$$\frac{g^2}{L_1L_2L_3}\mathcal{L} = \frac{1}{2}g_{jk}\dot{C}^j\dot{C}^k + \frac{i}{2}\left(\bar{\psi}\dot{\psi} - \dot{\bar{\psi}}\psi\right) \qquad (28)$$
$$+ i\omega_j^{ab}\dot{C}^j\bar{\psi}\sigma^{ab}\psi + \frac{1}{4}\left[f(\partial^2 f) - 2(\partial_j f)^2\right]\left(\bar{\psi}\right)^2(\psi)^2,$$

where we have raised the index of the vector C^j indicating its contravariant nature, $g_{jk} = f^{-2}\delta_{jk}$, $\psi = \Psi/f$, $\sigma^{ab} = \frac{i}{2}\epsilon^{abc}\sigma^c$ is the generator of rotations in the tangent space, and

$$\omega_i^{ab} = \delta_i^b\partial^a \log(f) - \delta_i^a\partial^b \log(f) \qquad (29)$$

is the spin connection on a conformally flat manifold with the natural choice of the dreibein, $e_j^a = f^{-1}\delta_j^a$.

We have succeeded in presenting the bifermion term in a nice geometric form. However, the 4-fermion term in Eq. (28) does not have an obvious geometric interpretation. In particular, its coefficient is not a three-dimensional scalar curvature.

To establish the relation of (28) to the Kählerian model, let us consider the original theory on an asymmetric torus $L_3 \gg L_1 = L_2 \equiv L$. The effective QM model is given by the Lagrangian (25) with $f(C_{1,2}, C_3)$ written in Eq. (14). If L_3 is very large, the range where C_3 changes is very small. In the limit $L_3 \to \infty$, C_3 is frozen to zero, but to perform this limit, we cannot just set $C_3 = 0$ in Eq. (14), but instead must average over C_3 within the range $0 \le C_3 \le 2\pi/L_3$ and simultaneously perform the summation over n_3. This amounts to calculating the integral

$$\frac{1}{f^2(C_3, C_{1,2})} \to 1 - \frac{3g^2}{2}$$
$$\times \sum_{n_j}\int \frac{da}{2\pi}\frac{1}{[\sum_{j=1,2}(LC_j - 2\pi n_j)^2 + a^2]^{3/2}},$$

which exactly gives the correction to the metric in Eqs. (25), (26).

The Lagrangian (28) involves also the kinetic term for the field C_3 and the term where $\dot{C}_3$ multiplies a bifermion structure. Performing the functional integral of $\exp\{iS\}$ over $\prod_t dC_3(t)$, we arrive at the expression

$$\mathcal{L} = \frac{1}{2}\tilde{g}_{jk}\dot{y}^j\dot{y}^k + i\bar{\chi}^a\left(\delta^{ab}\partial_t - \omega_j^{ab}\dot{y}^j\right)\chi^b \qquad (30)$$
$$+ \frac{1}{8}R\,(\bar{\chi})^2\,(\chi)^2,$$

where $y^j = Lc^j/g$, $\tilde{g}_{jk} = \tilde{f}^{-2}\delta_{jk}$, χ is related to ψ by a unitary transformation, ω_j^{ab} is the two-dimensional spin connection (29), and $R = 2[\tilde{f}\partial^2\tilde{f} - (\partial_j\tilde{f})^2]$ is the two-dimensional scalar curvature. The Lagrangian (30) coincides with the standard Lagrangian of the supersymmetric σ model [17] in the QM limit. The $(1+1)$ effective Lagrangian could be obtained if one takes into account the higher Fourier harmonics $\propto \exp\{izn/L_3\}$ of $C_j(z,t)$ and $\psi(z,t)$ in the background.

ACKNOWLEDGMENTS

A.V.S. is indebted to A.S. Losev and N.A. Nekrasov for illuminating discussions. E.T.A. acknowledges the warm hospitality extended to him at the University of Nantes, where this work was done. His work was partially supported by the Russian Foundation for Basic Research (project no. 01-02-17488) and INTAS (grant no. 00-390).

REFERENCES

1. E. Witten, J. High Energy Phys. **9802**, 006 (1998); A. Keurentjes, A. Rosly, and A. V. Smilga, Phys. Rev. D **58**, 081701 (1998); V. G. Kac and A. V. Smilga, hep-th/9902029; in *The Many Faces of the Superworld*, Ed. by M. A. Shifman (World Sci., 2000); A. Keurentjes, J. High Energy Phys. **9905**, 001, 014 (1999).
2. A. V. Smilga, Zh. Éksp. Teor. Fiz. **91**, 14 (1986) [Sov. Phys. JETP **64**, 8 (1986)]; B. Yu. Blok and A. V. Smilga, Nucl. Phys. B **287**, 589 (1987).
3. A. V. Smilga, Nucl. Phys. B **291**, 241 (1987).
4. J. Polchinski, hep-th/9611050.
5. A. V. Smilga, hep-th/0201048.
6. K. Becker and M. Becker, Nucl. Phys. B **506**, 48 (1997).
7. M. Douglas, J. Polchinski, and A. Strominger, J. High Energy Phys. **9712**, 003 (1997); E. Akhmedov, Phys. Rev. D **59**, 101901 (1999); hep-th/9812038.
8. L. F. Abbot, Nucl. Phys. B **185**, 189 (1981); M. Peskin, *An Introduction in Quantum Field Theory* (Addison-Wesley, Reading, 1995), p. 533.
9. V. A. Novikov *et al.*, Phys. Lett. B **217**, 103 (1989); M. A. Shifman and A. I. Vainshtein, hep-th/9902018; M. A. Shifman, *ITEP Lectures on Particle Physics and Field Theory* (World Sci., Singapore, 1999), Vol. 2, p. 485.

10. E. A. Ivanov and A. V. Smilga, Phys. Lett. B **257**, 79 (1991).
11. M. Lüscher, Nucl. Phys. B **219**, 233 (1983).
12. M. R. Duglas *et al.*, Nucl. Phys. B **485**, 85 (1997).
13. S. Paban, S. Sethi, and M. Stern, Nucl. Phys. B **534**, 137 (1998).
14. K. Becker *et al.*, Phys. Rev. D **56**, 3174 (1997); Y. Okawa and T. Yoneya, Nucl. Phys. B **538**, 67 (1999); R. Helling *et al.*, Nucl. Phys. B **559**, 184 (1999).
15. D.-E. Diaconescu and R. Entin, Phys. Rev. D **56**, 8045 (1997).
16. B. Zupnik, Theor. Math. Phys. **120**, 365 (1999).
17. D. Z. Freeman and P. K. Townsend, Nucl. Phys. B **250**, 689 (1985).